Modeling and Control of Longitudinal Single-Bunch Oscillations in Heavy-Ion Synchrotrons

Vom Fachbereich
Elektrotechnik und Informationstechnik
der Technischen Universität Darmstadt
zur Erlangung des akademischen Grades
eines Doktor-Ingenieurs (Dr.-Ing.)
genehmigte Dissertation

von

Dipl.-Ing. Dieter E. M. Lens

geboren am 22. Juli 1981 in Leuven, Belgien

Referent:	Prof. Dr.-Ing. J. Adamy
Korreferent:	Prof. Dr.-Ing. H. Klingbeil
Tag der Einreichung:	2. November 2011
Tag der mündlichen Prüfung:	20. Januar 2012

D17
Darmstadt 2012

Vorwort

Diese Arbeit enstand während meiner Tätigkeit als wissenschaftlicher Mitarbeiter am Fachgebiet Regelungstheorie und Robotik der Technischen Universität Darmstadt. Mein besonderer Dank geht an Professor Jürgen Adamy, der mir die Bearbeitung dieses besonderen Promotionsthemas ermöglicht hat. Seine Unterstützung, sein Vertrauen und die angenehmen Arbeitsbedingungen am Fachgebiet haben sehr zum Gelingen der Arbeit beigetragen.

Für die freundliche Übernahme des Korreferats möchte ich mich bei Professor Harald Klingbeil bedanken. Durch seine Initiative hatte ich das Glück, mich näher mit dem spannenden und vielseitigen Gebiet der Beschleunigertechnik befassen zu können. Die vielen fachlichen Diskussionen waren lehrreich und motivierend und haben meine Freude am wissenschaftlichen Arbeiten sehr gefördert. Des Weiteren möchte ich mich bei der Abteilung HF-Systeme der GSI bedanken, unter anderem bei Monika Mehler und Bernhard Zipfel für den Austausch und ihre Unterstützung.

Die vorliegende Arbeit wurde durch die Deutsche Telekom Stiftung im Rahmen eines Doktorandenstipendiums gefördert, wofür ich mich herzlich bedanken möchte, insbesondere bei Christiane Frense-Heck für die Betreuung während des Stipendiatenprogramms. Neben der finanziellen Unterstützung der Arbeit ermöglichte das Stipendium auch den Besuch von interessanten und abwechslungsreichen Seminaren und den Austausch mit Stipendiaten verschiedener Fachrichtungen.

In der Zeit am Fachgebiet Regelungstheorie und Robotik habe ich viele verschiedene Kollegen kennen und schätzen gelernt. Bei Birgit Heid, Sylvia Gelman und Susanne Muntermann möchte ich mich für die Unterstützung und den Rat bei Schwierigkeiten organisatorischer und technischer Art bedanken. Bei allen Kollegen möchte ich mich für zahlreiche Diskussionen und die schöne Zusammenarbeit bedanken und stellvertretend Boris Fischer, Kerstin Groß und Jochen Grieser hervorheben, die die Arbeit kritisch durchgesehen und damit wesentlich zur Verbesserung beigetragen haben. Auch möchte ich insbesondere Roland Kempf danken für seine Kurzeinführungen in Bereiche der Physik, die im Laufe eines Ingenieursstudiums zu kurz kommen. Bedanken möchte ich mich auch bei allen Studenten, die im Rahmen von studentischen Arbeiten mit Fragen und Ideen ihren Beitrag zur Arbeit geleistet haben.

Zu guter Letzt möchte ich mich bei meiner Frau Svenja, meiner Familie und meinen Freunden für ihre Unterstützung während meiner Studien- und Promotionszeit bedanken. Insbesondere der Rückhalt durch meine Frau Svenja war eine Hilfe, für die ich sehr dankbar bin.

Dieter Etienne Mia Lens, Darmstadt im März 2012

Contents

List of Symbols

The following tables are a selection of symbols that are important in more than one section of the thesis.

Abbreviations

RF	radio frequency	FFT	Fast Fourier Transform
FT	Fourier Transform	CoG	center of gravity
ref.	reference	rel.	relative
long.	longitudinal	w.r.t.	with respect to
R	subscript of ref. variables	PDE	partial differential equation
ODE	ordinary differential equation	MIMO	multi-input multi-output
LB	linear bucket	NB	nonlinear bucket
syn.	synchrotron	SB	stationary bucket
GSI	GSI Helmholtzzentrum für Schwerionenforschung GmbH		

Notation

i	imaginary unit $\sqrt{-1}$	$\lvert x \rvert$	absolute value of $x \in \mathbb{C}$
$f_{\boldsymbol{x}}$	gradient of f with respect to $\boldsymbol{x}$	$\binom{n}{m}$	binomial coefficient
$f(t)$	function in t	$f(n)$	discrete function, $t_n = n\, T_0$
$[a;\ b]$	interval including a and b	$\{a,\ b\}$	set with elements a and b
e^x	exponential function	e	elementary charge
$\mathbf{A}, \boldsymbol{x}$	matrix and vector	$\boldsymbol{f}(\boldsymbol{x})$	vector field
$[a \quad b]^{\mathrm{T}}$	vector $\in \mathbb{R}^2$	$\frac{\partial f}{\partial t}$	partial derivative
$\dot{x}(t)$	derivative w.r.t. t	$\mathbb{R}$	set of real numbers
s	Laplace variable	$\mathcal{O}\left(x^n\right)$	error term of order x^n

Coordinates

t	absolute time	z	longitudinal position
z_{R}	ref. long. position	$\Delta x,\ \Delta y$	transverse deviations w.r.t. R
Δz	long. deviation w.r.t. R	$\Delta p_x, \Delta p_y$	rel. momenta
Δp_z	rel. momentum	v_{R}	ref. long. velocity

φ, τ	RF phase and time lag w.r.t. the zero crossing of U_{gap}		
φ_{R}	ref. phase φ, p.25	$\Delta\varphi$	rel. phase $\varphi - \varphi_{\text{R}}$
τ_{R}	ref. time lag	$\Delta\tau$	rel. time lag $\tau - \tau_{\text{R}}$
δ	rel. impulse deviation	$\Delta\tilde{W}$	coordinate $\Delta W / \omega_{\text{RF}}$
Δw	normalized coordinate, p.29	(r, θ)	polar coordinates

Synchrotron and Beam Parameters

For all frequencies, the following relations hold:

$$\omega = 2\pi\, f = 2\pi / T.$$

Only the angular frequencies ω are summarized, the frequencies f and periods T follow accordingly.

h	harmonic number, integer	R	ref. point / trajectory
L_{R}	length of ref. orbit	L_{gap}	length of the cavity gap
Q	particle charge	m_0	rest mass of a particle
$B_{\text{R}}, B_{\text{max}}$	ref. and maximum magnetic flux density, dipole magnets		
r	curvature of dipole magnets	c	speed of light in vacuum
Q_{bunch}	charge of the bunch	k_{RF}	RF parameter $\in \{0, 1\}$
T_{cav}	cavity time constant	ω_{RF}	RF frequency
ω_{R}	ref. revolution frequency	ω_{syn}	synchrotron frequency, p.25
$\omega_{\text{syn,eff}}$	effective syn. frequency	ν_{syn}	synchrotron tune
ω_x	RF frequency in coordinate x	U_{gap}	gap voltage at the cavity
$\hat{U}_{1,\text{R}}$	ref. RF amplitude without modulation	$\hat{U}_1$	amplitude of gap voltage including RF feedback
Φ_{RF}	RF phase, p.9	U_{R}	ref. voltage, p.14
$\hat{U}_{1,\text{R,stat}}$	ref. RF amplitude, SB	ΔW_{acc}	energy gain in the cavity
W_{kin}	kinetic energy	W_{R}	total ref. energy
W	total energy	ΔW	energy deviation $W - W_{\text{R}}$
p_{R}	ref. momentum	γ	relativistic Lorentz factor
β	relativistic Lorentz factor	α_{p}	momentum compaction
η_{R}	phase slip factor	γ_{tr}	transition gamma

Modeling

$H(\boldsymbol{q}, \boldsymbol{p}, t)$	Hamiltonian	$V(\boldsymbol{q})$	potential function
$T(\boldsymbol{p})$	energy function	P, P_{sep}	integration constants, p.30
$\Delta\varphi_{\text{sep}\pm}$	separatrix intersections	$\Delta\varphi_{\pm}$	trajectory intersections
A_{bunch}	bunch area	A_{bucket}	bucket area
$A_{\text{bunch,stat}}$	bunch area in a SB	$A_{\text{bucket,stat}}$	bucket area in a SB

$A_{\text{bucket,stat}}$	bucket area, general case	$A_{\text{fill,stat}}$	bucket fill factor, p.34
$f(x,y,t)$	particle density distribution	f_{charge}	charge density distribution
λ_{charge}	charge density	$\lambda(x)$	line density
$\Lambda(\omega)$	FT of line density	$\Lambda_{\text{charge}}(\omega)$	FT of charge line density
$i_{\text{beam}}(x)$	RF beam current	$\bar{i}_{\text{beam}}$	DC beam current
$\hat{i}_{\text{beam}}$	peak beam current	$\overline{x}$	mean in x
σ_x^2	variance in x	$\sigma_{x,y}^2$	covariance in x and y
(x_0, y_0)	bunch center of gravity	Φ	bunch orientation angle
R_{1x}, R_{2x}	half axes of ellipsoidal bunch with uniform density	σ_{1x}, σ_{2x}	standard deviations, ellipsoidal & Gaussian density
R_x	bunch radius in x	m	single-bunch mode number
r_m	amplitude of mode m	$\hat{r}(\theta)$	bunch contour line function
$\theta_{m,0}$	phase of mode m	$\mathcal{D}_x$	bunch domain in x
ω_m	mode frequency	$\omega_{m,\text{hy}}$	hypothetical mode frequency
ω_1	dipole mode frequency	ω_2	quadrupole mode frequency
$B_{1,0}$	bunch CoG in x	$B_{0,1}$	bunch CoG in y
C_{n_x,n_y}	central moment	R_{n_x,n_y}	raw moment
$C_{2,0}$	variance in x	$E_{2,0}$	equilibrium of variance in x
E_2	same as $E_{2,0}$, but in the LB	E_{n_x,n_y}	equilibrium of C_{n_x,n_y}
$\Delta C_{n_x,n_y}$	deviation $C_{n_x,n_y} - E_{n_x,n_y}$	E_2, E_4	equilibria in the LB
I_2, I_4, I_6	invariants of motion	$a_1, b_1, \ldots$	functions of $E_{2,0}$
$\hat{k}$	Taylor series truncation parameter	$\mathbf{F}_{\text{T}}$	truncation matrix
		$\boldsymbol{f}_{\text{T,k}}$	truncation function
n_{model}	maximum moment order of the model state $\boldsymbol{x}$	$n_{\max}$	maximum order of the complete moment equations

Feedback and Simulation

ω_{samp}	sampling frequency	ω_{pass}	FIR filter parameter
T_{d}	time delay, feedback	c_k	Fourier coefficients of i_{beam}
A_k	beam harmonic amplitudes	φ_k	phases of harmonics of i_{beam}
$\Delta\varphi_{\text{gap}}$	phase shift of the gap voltage	φ_{f}	RF frequency deviation
u_ε	amplitude modulation, input	u_φ	phase modulation, input
u_1, u_2	inputs (4.27c)	χ_1, χ_2	frequency ratios $f_{\text{pass,m}}/f_m$
K_1, K_2	gains of feedback, p.132	N_{macro}	number of macro particles
N_{bin}	number of histogram bins	$\mathcal{C}(\mathbf{A},\mathbf{B})$	controllability matrix
λ_i	eigenvalues	T_0	basic simulation sample time

Abstract / Kurzfassung

This thesis contributes to the modeling and analysis of longitudinal radio frequency (RF) feedback systems in heavy-ion synchrotrons. Synchrotrons are ring accelerators with a constant reference orbit of the particle beam. They allow the acceleration of particles such as electrons, protons, and heavy ions to highest energies. The desired specifications for beam properties such as the quality, energy, and intensity drive the development of new accelerator components. Among other objectives, the stabilization of the beam before and during the acceleration is desirable to preserve the beam quality. The thesis deals with the modeling of longitudinal coherent oscillations of a bunched beam. The main focus is on the usability of the models for the analysis and design of digital RF feedback loops. The analysis of these models with methods from control theory leads to new insight into the possibilities of RF feedback with regard to the longitudinal beam stabilization. In particular it is shown that the nonlinearity of the beam dynamics plays a major role in the damping of coherent oscillations of higher order. An analysis of a specific RF feedback setup and the comparison with experimental data shows the practical relevance of the models.

Die vorliegende Arbeit liefert einen Beitrag zur Modellierung und Analyse von HF-Regelsystemen in Schwerionensynchrotrons. Synchrotrons sind Ringbeschleuniger, die sich durch einen konstanten Soll-Orbit des Teilchenstrahls auszeichnen. Mit ihrer Hilfe können unter anderem Elektronen, Protonen und schwere Ionen auf höchste Energien beschleunigt werden. Die gewünschten Anforderungen an Eigenschaften wie die Qualität, Energie und Intensität des Teilchenstrahls treiben die Entwicklung der Beschleunigerkomponenten voran. Unter anderem ist eine Stabilisierung des Strahls vor und während der Beschleunigung erwünscht, um die Strahlqualität zu erhalten. In der vorliegenden Arbeit werden longitudinale kohärente Oszillationen eines gebündelten Teilchenstrahls modelliert. Dabei liegt das Hauptaugenmerk auf der möglichen Verwendung der Modelle für die Analyse und den Entwurf von digitalen Hochfrequenz- bzw. HF-Regelkreisen. Die regelungstechnische Analyse dieser Modelle ermöglicht neue Erkenntnisse darüber, was HF-Regelungen für die longitudinale Strahlstabilisierung leisten können. Insbesondere wird gezeigt, dass die Nichtlinearität der Strahldynamik eine wichtige Rolle spielt bei der Dämpfung von Oszillationen höherer Ordnung. Eine Analyse einer konkreten HF-Regelungsstruktur und der Vergleich mit experimentellen Daten zeigen die praktische Relevanz der Modelle.

1 Introduction

After almost a century of steady development, particle accelerators belong to the most complex research facilities. For many fields of theoretic and applied science, they have become an indispensable tool. The research in this thesis is motivated by the planned accelerator center *Facility for Antiproton and Ion Research* (FAIR). This center expands the facilities of the *GSI Helmholtzzentrum für Schwerionenforschung GmbH*.[1)] The core of FAIR is a new double ring synchrotron with a circumference of 1100 meters and the existing facility with the synchrotron SIS18 will be used as a pre-accelerator for FAIR. A short overview of FAIR is given in [35], more information can be obtained from the FAIR homepage [1] or the technical design reports. Synchrotrons are ring accelerators that can accelerate charged particle beams up to highest energies. Typical for a synchrotron is the constant reference orbit of the particle beam. Figure 1.1 introduces the general setup of a synchrotron: the beam is first accelerated, for example by a linear accelerator. After the injection of the beam, a magnet lattice guides the beam on its orbit and in each turn, the beam is accelerated by radio frequency (RF) electric fields inside a cavity. Typically, the beam remains in the ring for more than 10^5 turns, before it is extracted for experiments or further acceleration.

The stability specifications for a synchrotron are ambitious. In the heavy-ion synchrotron SIS18, the particle beam covers distances of more than the circumference of the earth during the acceleration cycle, which lasts less than one second. The synchrotron is designed such that if particles deviate from the reference orbit with respect to longitudinal focusing, they will oscillate around this orbit. This is achieved by creating a potential well using electromagnetic fields. Along the orbit – in longitudinal direction – the potential well is established by a periodic RF voltage. In the transverse direction, perpendicular to the orbit, magnetic fields create the stabilizing potential and guide the beam.

However, no accelerator is ideal and there will be disturbances that act on the beam. Examples for such disturbances are noise in the RF voltage or errors in the magnetic fields. In addition, if the particle density is large enough, the particles in the beam will interact with the environment and with themselves. During the acceleration, the particle density is not homogeneously distributed along the ring circumference. Rather, the beam consists of a definite number of particle ensembles, called *bunches*, such that the particle density varies considerably along the longitudinal axis. This leads to effects such as the interaction of the beam with the RF cavity or the conducting beam pipe or interactions between different particle bunches. All these effects may lead to growing instabilities of the particle beam, destabilizing the beam, impairing the beam quality, and increasing beam losses. To prevent such instabilities, passive measures can be taken that reduce

[1)] Planckstraße 1, 64291 Darmstadt, Germany, URL: `www.gsi.de`

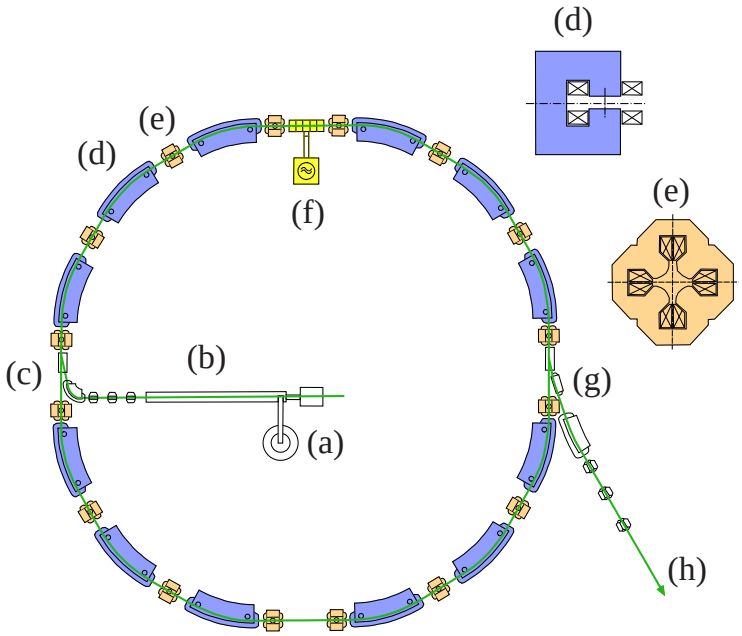

Figure 1.1: General setup of a synchrotron according to [137]. (a): particle source, (b): linear accelerator, (c): injection of the beam in the synchrotron ring, (d): dipole magnet, (e): quadrupole magnet, (f): accelerating RF cavity, (g): extraction of the beam, (h): experiment or further acceleration.

the interaction of the beam with its environment. In addition, active measures such as feedback systems are used to increase the stability of the beam.

Objectives

In this thesis, the focus is on the feedback of longitudinal single-bunch oscillations. These oscillations arise whenever the shape of a bunch is not consistent with the shape of the longitudinal RF potential. The longitudinal motion of a single particle in a synchrotron can be regarded as a relative oscillation around the moving reference position. This oscillation is called *synchrotron oscillation* and is desirable, as it enables the acceleration of a beam of particles with a certain energy spread. If the bunch shape is consistent with the RF potential, the overall bunch shape will be time-invariant, even though the individual particles perform the synchrotron oscillation. Conversely, any mismatch of the bunch shape will lead to single-bunch oscillations. The simplest longitudinal oscillation occurs if the bunch arrives too early or too late at the cavity. This will lead to relative longitudinal oscillations of the bunch center of gravity. Other mismatches in the bunch shape will lead to oscillations of the bunch length or more complex oscillations.

Longitudinal single-bunch oscillations can be damped using feedback systems, as has already been demonstrated in many synchrotron facilities. The feedback consists of a measurement of the beam current, a control algorithm, and a correction of the beam, as shown schematically in Figure 1.2. Typically, the correction is made by modulating the amplitude and phase of the total RF voltage, either by using the same cavities that are used for acceleration or by using dedicated kicker cavities. Many existing feedback systems are based on analog hardware and are thus not very flexible. At GSI, efficient new digital hardware enables the use of more flexible and sophisticated feedback algorithms.

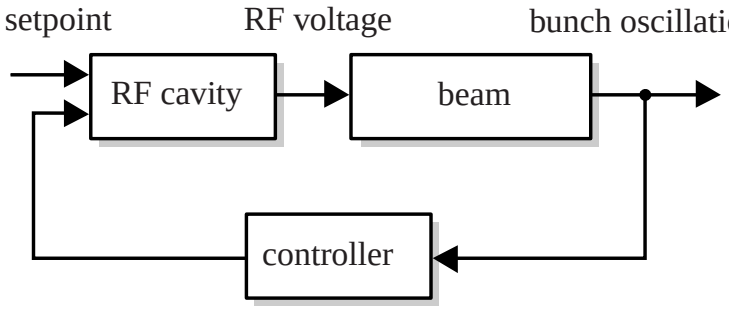

Figure 1.2: RF feedback of bunch oscillations.

With these possibilities, also new questions and challenges arise. The following of these challenges will be covered in this thesis for heavy-ion synchrotrons:

- How can single-bunch oscillations be modeled efficiently such that the resulting models can be used for a controller synthesis?
- How do the beam oscillations respond to the modulations of the RF amplitude and phase? What changes in beam shape are possible in principle?
- What can be said about the choice of the feedback algorithm and parameters? In which region is the feedback stable and how is the feedback performance?

Structure and Contribution of the Thesis

The unique contribution of this thesis is the modeling and analysis of longitudinal single-bunch oscillations from a control theoretic point of view. The contributions are: first, a new rigorous modeling procedure for single-bunch oscillations that allows for nonlinearities of the beam dynamics; second, the derivation of feedback models of single-bunch oscillations depending on the bunch size; and third, the analysis of the feedback properties of these models. Figure 1.3 shows the main topics of the thesis, the relations between these topics and the degree of innovation, i. e. of new results.

The thesis is structured as follows.

Chapter 2

Chapter 2 is a revision of the longitudinal single-particle dynamics as described in standard references and papers. Most of the theory of the chapter is well known, but there are two main reasons why it is included. First, the thesis is meant to be self-consistent for control engineers with a consistent notation of the physical variables. Many of the equations of this chapter are used in the subsequent chapters. Second, the derivations and also the equations of the beam dynamics differ from reference to reference. The contribution of Chapter 2 is also the attempt to compare and to evaluate these differences. The notation used in this thesis follows closely [57].

Chapter 3

Because the particles of a single bunch oscillate in general, it is possible that the bunch shape as a whole will oscillate. These coherent longitudinal bunch oscillations are defined

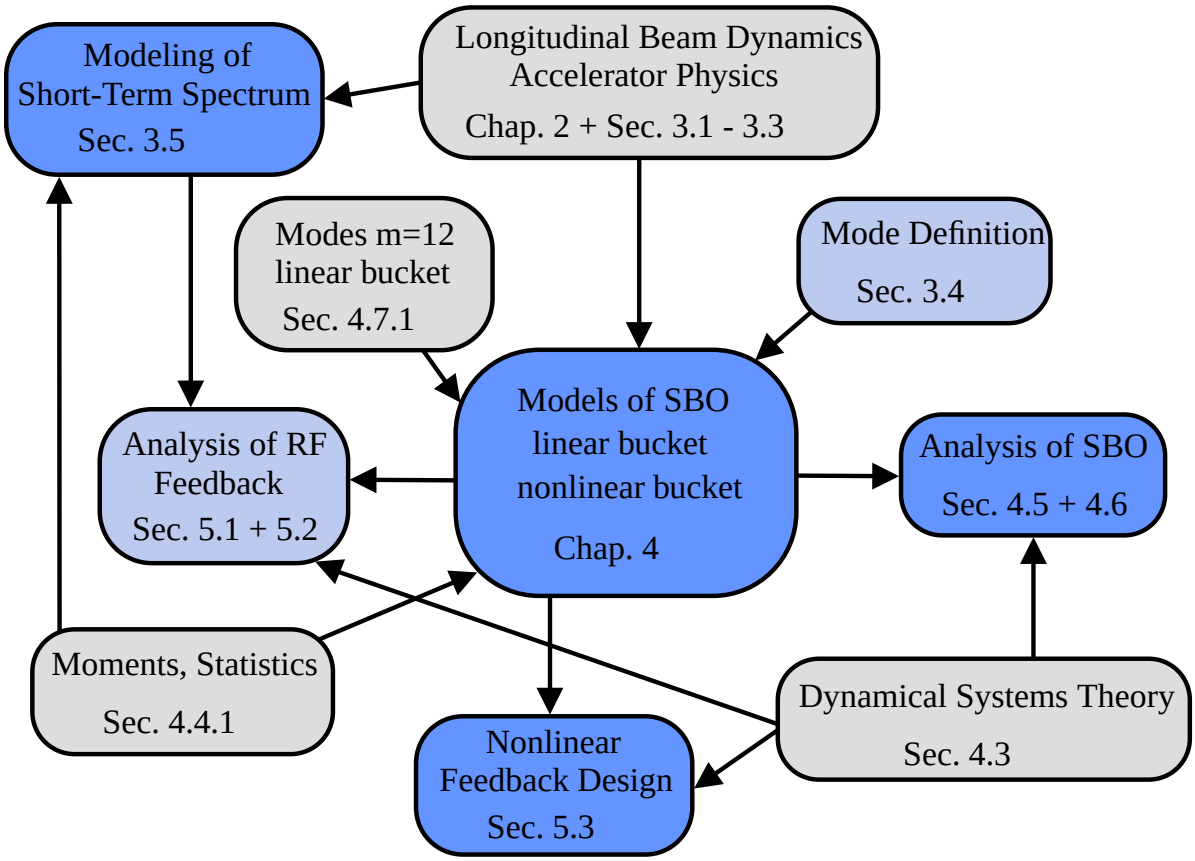

Figure 1.3: Contribution of the thesis. The colors signify existing theory (gray), partly new developments (light blue) and new results (blue). SBO: single-bunch oscillations.

and described in Chapter 3. After defining properties of particle bunches, the standard theory of bunch oscillations is reviewed. This theory proposes the decomposition of the longitudinal oscillations into orthogonal modes with a specific frequency. An important contribution of the thesis is presented in Section 3.5. In this section, formulas are derived that describe the relation between the bunch shape and its beam current spectrum for ellipsoidal bunches with uniform or Gaussian densities. These formulas are essential to the modeling of the measurement and detection of the bunch oscillations.

Chapter 4

Chapter 4 presents the main modeling result of the thesis. Several models are presented that describe the dynamics of the bunch shape with respect to the modulations of the RF voltage. The modeling approach is based on moments and can be applied for nonlinear RF potentials that can be approximated by finite polynomial series. The obtained models enable the use of state-space and nonlinear control methods in the time domain. The approach is superior to existing models in literature that are based on a linearization of the beam dynamics. It is shown that the nonlinearity of the RF potential plays an essential role for higher order coherent oscillations.

Chapter 5

Finally, in Chapter 5 the models are used to analyze RF feedback loops of the synchrotron

SIS18 at GSI. The analytic and simulation results are compared with measurement data of a beam experiment.

Many of the results and ideas of this thesis were developed in cooperation with the RF department at GSI. In particular, the definition of the bunch modes in Section 3.4.3 is based on the ideas of Dr. Harald Klingbeil and the modeling approach based on moments and the interpretation of the modeling results have greatly benefited from discussions with him. The beam experiment in Section 5.2 was realized by the ring RF group at GSI and the measurement results are courtesy of GSI.

In addition to the described topics, a simulation study was performed concerning the stability of a double-harmonic cavity setup under beam loading. The research questions in this study were different from the questions stated above and the results will not be included in this work, but can be found in [72, 73].

In the following, bunches with different bunch sizes will be considered, also small bunch sizes that may be unrealistic for real experiments. However, these considerations are used to illustrate the concepts and to check the analytical results for plausibility. As the scope of the modeling procedure is on feedback systems, the challenge of the modeling step is to include only the most relevant dynamics to obtain a model that is sufficiently accurate and as simple as possible. The question which level of model accuracy and complexity is appropriate cannot be answered in general, but will depend on the feedback structure and the specifications of the feedback task. Several simplifications will be made with respect to the beam dynamics and these have to be kept in mind. The comparison of the models with simulations and a beam experiment in Chapter 5 will be used to show the validity of the modeling assumptions.

2 Longitudinal Single Particle Dynamics

2.1 Introduction

A particle beam in a synchrotron ideally consists of a large amount of identical particles with equal rest mass and electrical charge. Classical methods to accelerate beams are electrostatic, linear, and circular accelerators. An overview of different accelerator types and their history can be found for example in [43, 71, 136, 137]. Electrostatic accelerators use high DC voltages that are generated for example with Cockroft-Walton multipliers. The maximum beam energy in these accelerators is limited by the maximum voltage. The use of radio frequency (RF) voltages and fields led to new accelerator types and enabled higher energies. The synchrotron was proposed independently by McMillan [92] and Veksler [131, 132] in 1945 as a new method to achieve high energy beams. An essential part of the development was the discovery of the *phase stability principle* [32, 71, 136, 137]. This principle enables the acceleration of particles which differ to a certain extent in phase and energy. Instead of DC voltages, periodic RF voltages are used in synchrotrons and a magnet lattice consisting of bending and focusing magnets forces the beam on a closed orbit. The main advantage is that the beam can be accelerated repeatedly by the same RF source. However, a necessary condition for the acceleration is the synchronization of the beam with the RF voltage [43]. Because of the energy spread of the beam, the particles have different velocities and without focusing, the beam will diverge longitudinally. The phase stability principle prevents this divergence and guarantees the longitudinal focusing of the beam. Figure 2.1 visualizes the direction of the longitudinal axis.

A consequence of the RF voltage is that the particle density of the beam is not equally distributed along the ring in the presence of the RF voltage. Rather, the particles of the beam are gathered in particle ensembles called *bunches* as shown in Figure 2.2. A particle in the bunch which matches the reference trajectory R perfectly will be accelerated such that its angular revolution frequency ω_R rises synchronously with the RF revolution frequency, i. e.

$$\omega_\mathrm{RF}(t) = h\omega_\mathrm{R}(t) \tag{2.1}$$

holds. The integer h is called the *harmonic number* and equals the maximum number of bunches. In the following, the particle on the reference trajectory will be referred to as the *reference particle* and its quantities will be denoted by the index R. It is not necessary and rather improbable that the beam indeed has a physical particle exactly at the reference, but this concept is convenient for modeling the dynamics and the reference particle may be regarded as a fictitious one. The particles of the bunch with a deviation in position or energy with respect to the reference particle perform the so-called *synchrotron oscillation*

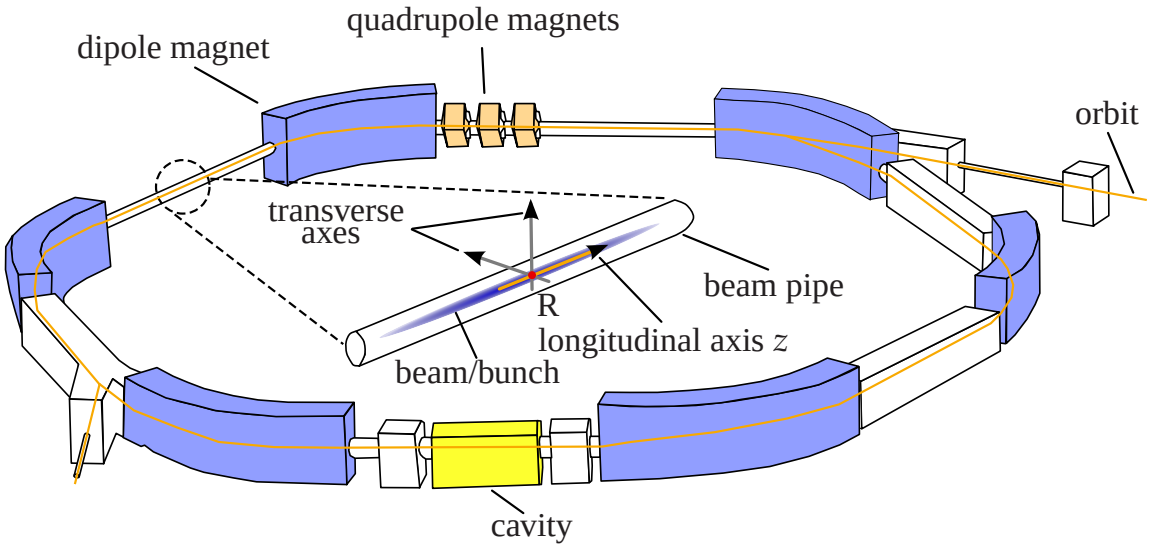

Figure 2.1: Scheme of a synchrotron and the longitudinal and transverse axes used to describe the beam. The number and position of the magnets is schematical. A detailed setup is given in Figure 1.1.

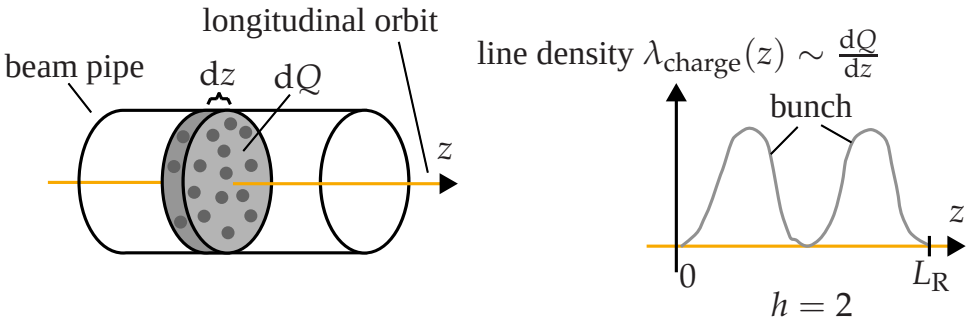

Figure 2.2: Typical line density for bunched beams. **Left**: The line density is defined as the amount of particles at the position z along the longitudinal orbit, it does not reveal anything about the density distribution in transverse directions. **Right**: A bunched beam with $h = 2$ bunches, L_R is the length of the ring.

which will be described in more detail in the next sections. Only the motion in the longitudinal phase space will be considered, i. e. the motion parallel to the reference (ideal) orbit. This motion is mainly dictated by the RF voltage. The motion in the transverse planes perpendicular to the orbit is governed by the magnetic lattice consisting of dipole, quadrupole, and optionally higher order magnets. This transverse motion will only be considered in terms of the so-called momentum compaction factor. This factor will account for the fact that off-momentum particles will have to cover a different distance in the ring for one turn. However, this is only the stationary component of the transverse motion, a dynamic coupling of longitudinal and transverse planes will not be considered. This is justified in almost all accelerator experiments, because the frequencies of the transverse

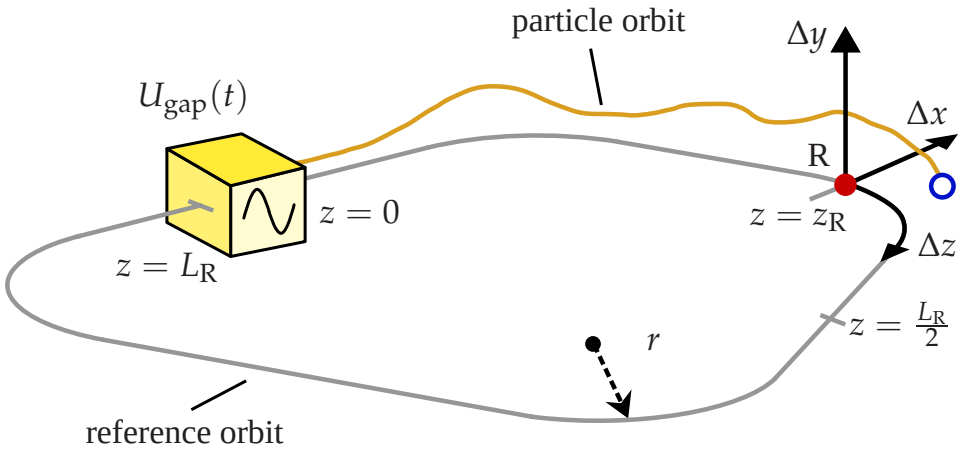

Figure 2.3: Absolute and relative coordinates. Moving reference R, absolute longitudinal position $z \in [0; L_{\mathrm{R}}[$ with length L_{R} of the reference orbit, transverse deviations Δx and Δy, longitudinal deviation Δz, curvature $r(z)$ of the reference orbit.

particle oscillations are larger by an order of two to three compared to the corresponding longitudinal frequencies. Because of this fact, transverse motion may be averaged over many turns, leading to the momentum compaction factor.

2.2 Synchrotron Oscillation

This section describes the theory of longitudinal motion of a particle in a synchrotron ring. Section 2.2.1 introduces the curvilinear coordinate system used in ring accelerators and Section 2.2.2 reviews the energy gain of particles in electromagnetic fields. Section 2.2.3 explains the general idea behind the synchrotron oscillation and Section 2.2.4 introduces the reference particle. After this, Sections 2.2.5 and 2.2.6 explain the derivation of the longitudinal equations of motion and Section 2.2.7 deals with the synchrotron oscillation. Finally, a discussion of the presented theory is given in Section 2.2.8.

2.2.1 Coordinate System in Beam Dynamics

The use of curvilinear coordinate systems has proved to be convenient to model the particle dynamics in accelerator rings [136]. In this case, only relative deviations with respect to the reference trajectory are considered. Figure 2.3 illustrates the typical choice of coordinates: the reference trajectory R is the origin of the coordinate system $(\Delta x, \Delta y, \Delta z)$. The absolute longitudinal position of the reference is $z_{\mathrm{R}}(t)$, its velocity is $\dot{z}_{\mathrm{R}} = v_{\mathrm{R}}(t)$. The reference trajectory $z_{\mathrm{R}}(t)$ is determined offline before the acceleration cycle of the beam. Section 2.2.4 describes this acceleration cycle in more detail. Along the ring, dipole magnets are used to guide the beam on the reference orbit with the curvature $r(z)$.

With the relative positions Δx, Δy, Δz and momenta Δp_x, Δp_y, Δp_z

$$\boldsymbol{x} = \begin{bmatrix} \Delta x & \Delta y & \Delta z & \Delta p_x & \Delta p_y & \Delta p_z \end{bmatrix}^{\mathrm{T}},$$

the dynamics of a single particle can be described in a 6-dimensional phase space. This phase space consists of two transverse planes $(\Delta x, \Delta p_x)$ and $(\Delta y, \Delta p_y)$ and one longitudinal plane $(\Delta z, \Delta p_z)$. As the particles in the beam have a certain momentum spread, the beam will diverge in transverse and longitudinal directions without focusing measures. In the transverse plane, quadrupole magnets focus the beam, whereas the RF voltage

$$U_{\mathrm{gap}}(t) = \hat{U}_1 \sin(\Phi_{\mathrm{RF}}(t)) \tag{2.2}$$

and thus the RF electrical field of the cavity provides acceleration and phase focusing in the longitudinal plane. The RF phase depends on the RF frequency as

$$\Phi_{\mathrm{RF}}(t) = \int_0^t \omega_{\mathrm{RF}}(t)\,\mathrm{d}t \;+\; \Delta\varphi(t), \tag{2.3}$$

where $\Delta\varphi$ is variation of the phase, for example due to a feedback system. Because the beam and the RF voltage should be synchronized, the RF frequency ω_{RF} is chosen as a multiple of the reference revolution frequency ω_{R}, cf. (2.1). where h is the harmonic number and the revolution frequency is

$$\omega_{\mathrm{R}}(t) = \frac{2\pi}{T_{\mathrm{R}}(t)} = \frac{2\pi v_{\mathrm{R}}(t)}{L_{\mathrm{R}}},$$

where L_{R} is the circumference of the ring along the reference orbit and T_{R} denotes the revolution period of the reference. The arrival time of the reference after turn k may be denoted by t_{k+1} and the time period for the reference to complete turn k by $T_{\mathrm{R}}(t_k)$, i. e. $t_{k+1} - t_k = T_{\mathrm{R}}(t_k)$. The synchronization condition (2.1) guarantees that the reference particle arrives repeatedly at the cavity at the same voltage $U_{\mathrm{gap}}(t_k) = U_{\mathrm{R}}$, because

$$\Phi_{\mathrm{RF}}(t_{k+1}) - \Phi_{\mathrm{RF}}(t_k) = \int_{t_k}^{t_{k+1}} \omega_{\mathrm{RF}}(t)\,\mathrm{d}t = \int_{t_k}^{t_{k+1}} \frac{2\pi h}{T_{\mathrm{R}}(t)}\,\mathrm{d}t \approx 2\pi h \frac{t_{k+1} - t_k}{T_{\mathrm{R}}(t_k)} = 2\pi h,$$

where the approximation is made under the assumption that ω_{RF} is ramped adiabatically, i. e. is almost constant during one turn. Also, this calculation for the reference particle sets $\Delta\varphi$ equal to zero, because the trajectory of the reference particle is predefined by the central control room. It is important to note that variations, disturbances, and feedback will affect all particles of the beam, but not the reference particle.

In the following, relative coordinates will be used rather than absolute coordinates such as t and Φ_{RF}. The definition of the relative coordinates is visualized in Figure 2.4. In the left image, the positions and velocities of the reference particle and a particle k are shown for a fixed time and are z_{R}, v_{R}, z_k, and v_k, respectively. Particle k is late with respect to the reference and will arrive later at the cavity. This is shown in the right image of

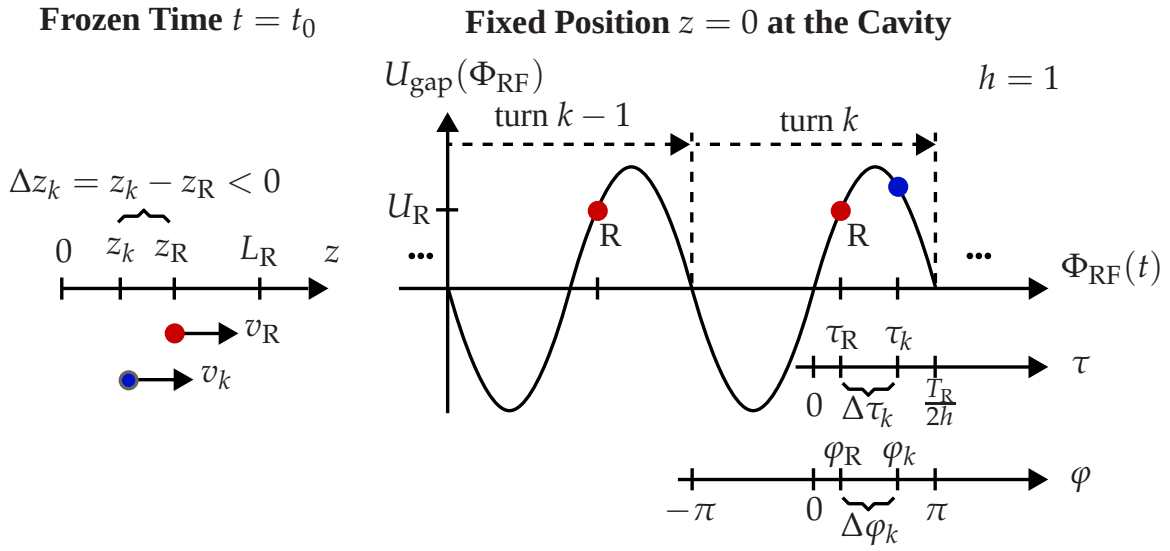

Figure 2.4: Relative and absolute coordinates. **Left**: longitudinal position z along the orbit for a fixed time t and a particle with a deviation $\Delta z_k < 0$. **Right**: gap voltage U_{gap} for $h = 1$ at the cavity, i. e. for a fixed position $z = 0$. The delayed particle has a positive time lag $\Delta\tau_k > 0$ and phase difference $\Delta\varphi_k > 0$ with respect to the reference (blue dot).

Figure 2.4. The relative time τ and the relative phase φ are measured with respect to the zero crossing of the gap voltage. The reference arrives at τ_R and the delayed particle at τ_k, resulting in a difference $\Delta\tau_k > 0$. The relative phase is related to the relative time by

$$\varphi = \omega_{RF}\,\tau, \qquad \Delta\varphi = \omega_{RF}\,\Delta\tau = \frac{2\pi h}{T_R}\Delta\tau. \tag{2.4}$$

The relative RF phase of the reference is denoted by φ_R. At each turn, the reference will arrive at the cavity when

$$U_R = \hat{U}_1 \sin(\varphi_R). \tag{2.5}$$

Usually, the velocity v_k is very similar to v_R and the approximation

$$\Delta z \approx -v_R\,\Delta\tau \tag{2.6}$$

holds.

The next sections will focus on the dynamics of the longitudinal plane. Thus, only the cavity and the magnetic field of the dipole magnets will be explicitly considered as components of the synchrotron. However, it is understood that quadrupole magnets and a large number of other components are necessary for the acceleration of the beam.

2.2.2 Relativistic Particles in Electromagnetic Fields

The force of an electromagnetic field on a charged particle is the Lorentz force

$$\boldsymbol{F}_L = Q\,[\boldsymbol{E} + \boldsymbol{v} \times \boldsymbol{B}]$$

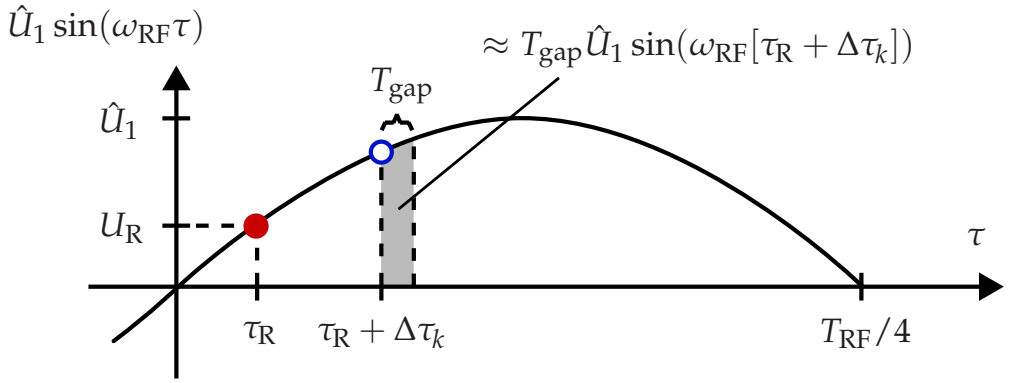

Figure 2.5: Transition and acceleration of a particle in the cavity. The approximation is valid for $T_{\mathrm{gap}} \ll T_{\mathrm{RF}}$.

with the particle charge Q, the electric field $\boldsymbol{E}$, the particle velocity $\boldsymbol{v}$ and the magnetic field $\boldsymbol{B}$ [54, 81, 136]. The Lorentz force is invariant under coordinate transformations and is also valid in this form for relativistic particles [57, 58]. In a synchrotron, the force due to the electric field is used to actually increase the energy of the particles. The electric fields are generated in the RF cavity and act on the particles only on a very small fraction of the ring circumference. The magnetic fields are generated in dipole and quadrupole magnets and are used to deflect and focus the particles. The order and position of the magnets is referred to as the magnet lattice. In a circular accelerator as the synchrotron, the magnet lattice is arranged such that the particles are forced on a closed reference orbit. In this way, the particles can be accelerated repeatedly in the RF cavity. The energy gain of a particle can be expressed as

$$\Delta W_{\mathrm{acc}} = \int \boldsymbol{F}_{\mathrm{L}}\,\mathrm{d}\boldsymbol{z} = \underbrace{Q\int \boldsymbol{E}\,\mathrm{d}\boldsymbol{z}}_{QV} + \underbrace{Q\int [\boldsymbol{v}\times\boldsymbol{B}]\cdot\boldsymbol{v}\,\mathrm{d}t}_{=0},$$

where $d\boldsymbol{z} = \boldsymbol{v}\,\mathrm{d}t$ was used. Only the electric field contributes to the energy gain. The term QV can be interpreted as the energy a particle with the charge Q gains if it passes through an effective voltage V. Thus, the unit of this energy gain is commonly given in electron volt and not in joule. The electron volt is equivalent to the energy gain of a single electron ($Q = -\mathrm{e}$) accelerated by an electric potential difference V of one Volt and equals

$$1\,\mathrm{eV} = 1.602 \cdot 10^{-19}\,\mathrm{J}.$$

In a synchrotron, a particle with the charge Q is only accelerated in one or more cavities. The gap of the cavity has the length L_{gap} and shall be placed at the position $z = 0$, cf. Figure 2.3. The electric field inside the cavity gap is proportional to the RF voltage $U_{\mathrm{gap}}(t)$ and is assumed to have only a nonzero component parallel to the orbit:

$$\boldsymbol{E}(t) = \frac{U_{\mathrm{gap}}(t)}{L_{\mathrm{gap}}} \cdot \boldsymbol{e}_z,$$

where $\boldsymbol{e}_z$ is the longitudinal unit vector. We will now consider the acceleration of a particle which can deviate from the reference. Its position z, velocity v, energy W, and arrival time τ at the cavity are, respectively,

$$z_k = z_\mathrm{R} + \Delta z_k, \quad v_k = v_\mathrm{R} + \Delta v_k, \quad W_k = W_\mathrm{R} + \Delta W_k, \quad \tau_k = \tau_\mathrm{R} + \Delta\tau_k, \tag{2.7}$$

with small deviations Δz_k, Δv_k, ΔW_k, and $\Delta\tau_k$. The energy gain of the particle is given by

$$\Delta W_\mathrm{acc} = Q \int_{z_1}^{z_2} \boldsymbol{E}\,\mathrm{d}\boldsymbol{z} = \frac{Q}{L_\mathrm{gap}} \int_{t_1}^{t_2} U_\mathrm{gap}(t)\boldsymbol{e}_z v(t)\boldsymbol{e}_z\,\mathrm{d}t \approx \frac{v_\mathrm{R}Q}{L_\mathrm{gap}} \int_{t_1}^{t_2} U_\mathrm{gap}(t)\,\mathrm{d}t,$$

where the approximation is made that $v_k \approx v_\mathrm{R}$ during the transition of the cavity. With the gap voltage defined by (2.2) and (2.3) and the assumption that ω_RF is approximately constant during the transition, the energy gain can be expressed in local coordinates as

$$\Delta W_\mathrm{acc} \approx \frac{v_\mathrm{R}Q\hat{U}_1}{L_\mathrm{gap}} \int_{\tau_\mathrm{R}+\Delta\tau_k}^{\tau_\mathrm{R}+\Delta\tau_k+T_\mathrm{gap}} \sin(\omega_\mathrm{RF}\tau)\;\mathrm{d}\tau \approx \frac{v_\mathrm{R}Q\hat{U}_1}{L_\mathrm{gap}} T_\mathrm{gap} \sin(\omega_\mathrm{RF}[\tau_\mathrm{R}+\Delta\tau_k]).$$

The approximation is justified by the fact that the cavity transition time T_gap is typically only a small fraction of the RF period T_RF as visualized in Figure 2.5. Finally, using (2.4) and $v_\mathrm{R}T_\mathrm{gap} \approx L_\mathrm{gap}$, the energy gain can approximately be described by

$$\boxed{\Delta W_\mathrm{acc} \approx Q\hat{U}_1 \sin(\omega_\mathrm{RF}[\tau_\mathrm{R}+\Delta\tau_k]) = Q\hat{U}_1 \sin(\varphi_\mathrm{R}+\Delta\varphi_k).} \tag{2.8}$$

2.2.3 Phase Stability Principle

The phase stability principle has been discovered in 1945 independently by McMillan and Veksler [92, 132]. It can be explained qualitatively as follows:[1)] A particle with a deviation $\Delta z_k > 0$ has a phase $\Delta\varphi_k < 0$ (cf. (2.4) and (2.6) and will arrive earlier at the cavity. As shown in Figure 2.6, the particle is decelerated with respect to the reference R by a negative voltage U_gap. After some turns, it will fall behind the reference and gain more energy due to the positive gap voltage. Altogether, this leads to a relative oscillation of the particle in longitudinal direction around the reference R called the *synchrotron oscillation*. The oscillation takes place in relative coordinates such as Δz_k and Δv_k as defined by (2.7). The resulting differences are small compared to their uniform components z_R and v_R. It should be emphasized that the synchrotron oscillation is desirable as it allows phase stability, i. e. the acceleration of particles with deviations in position and energy. The frequency of the synchrotron oscillation is called the *synchrotron frequency*

[1)] The reasoning is valid below the transition energy, which will be introduced later on. Above the transition energy, the reference R lies on the falling edge of the RF voltage and the situation is reversed.

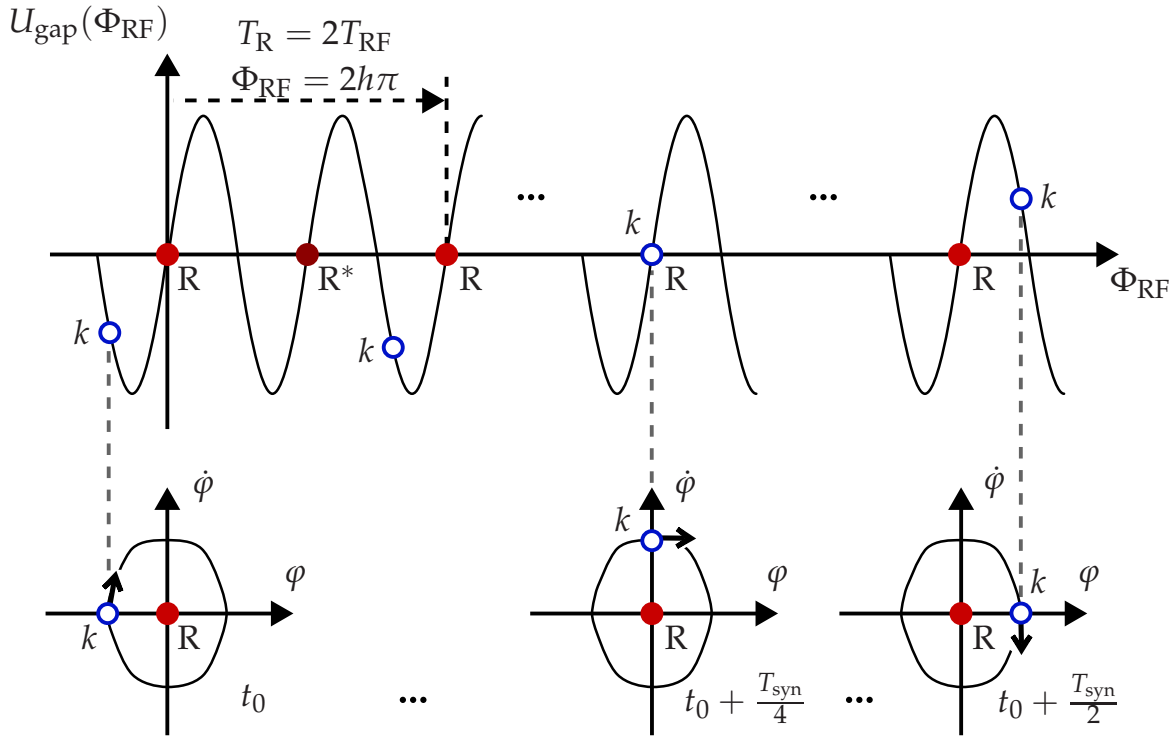

Figure 2.6: Phase focusing principle in the stationary case $\varphi_{\mathrm{R}} = 0$. **Top**: gap voltage U_{gap} at the cavity with $h = 2$, $\omega_{\mathrm{RF}} = 2\omega_{\mathrm{R}}$. This enables the space for $h = 2$ bunches with references R and R*. **Bottom**: synchrotron oscillation in relative coordinates φ and $\dot{\varphi}$. Particle k is advanced at t_0 and is decelerated with respect to R by U_{gap}. As soon as it is delayed, it is accelerated. This results in a synchrotron oscillation with period T_{syn}.

$\omega_{\mathrm{syn}} = 2\pi f_{\mathrm{syn}} = 2\pi/T_{\mathrm{syn}}$ and it typically is considerably smaller than the beam revolution frequency $\omega_{\mathrm{R}} = 2\pi f_{\mathrm{R}} = 2\pi/T_{\mathrm{R}}$. Typical values of the synchrotron frequency are

$$f_{\mathrm{syn}} = 10^{-3} \ldots 10^{-2} f_{\mathrm{R}}.$$

The *synchrotron tune*

$$\nu_{\mathrm{syn}} = \frac{T_{\mathrm{R}}}{T_{\mathrm{syn}}} = \frac{f_{\mathrm{syn}}}{f_{\mathrm{R}}} = 10^{-3} \ldots 10^{-2}$$

is defined as the number of synchrotron oscillations per turn.

2.2.4 Longitudinal Reference Trajectory

The energy gain of a particle has been expressed by (2.8). For the reference $\Delta\tau_k = \Delta\varphi_k = 0$ and the reference energy gain from turn $n-1$ to turn n is given by

$$\Delta W_{\mathrm{acc,R}} = W_{\mathrm{R}}(n) - W_{\mathrm{R}}(n-1) = QU_{\mathrm{R}}, \tag{2.9}$$

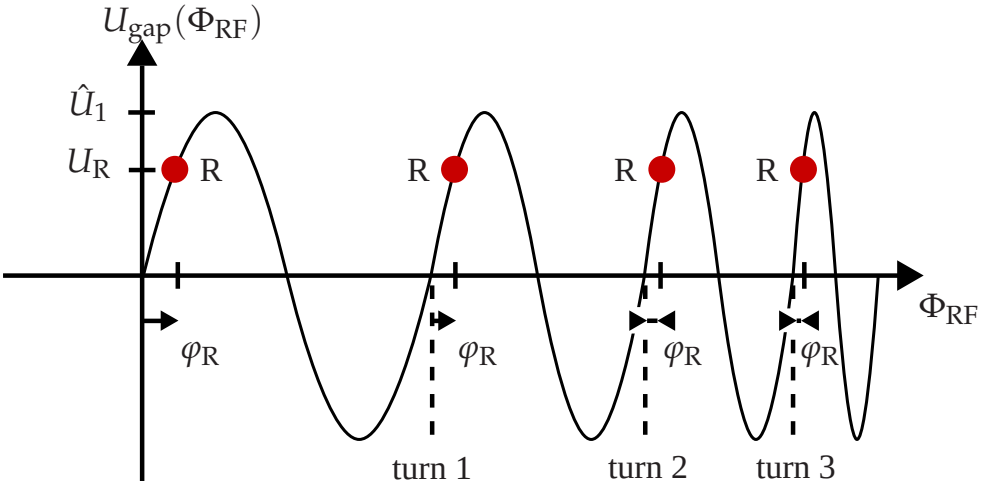

Figure 2.7: Synchronization of beam and RF voltage during acceleration with a constant acceleration voltage U_{R} and $h = 1$. The rate of acceleration is exaggerated.

where $W_{\mathrm{R}}(n)$ denotes the total particle energy during turn n and U_{R} is the reference voltage

$$\boxed{U_{\mathrm{R}} = \hat{U}_1 \sin(\omega_{\mathrm{RF}}\, \tau_{\mathrm{R}}) = \hat{U}_1 \sin(\varphi_{\mathrm{R}}).} \tag{2.10}$$

The phase φ_{R} is called *reference phase*. During acceleration, the reference energy W_{R} will increase and so will the revolution frequency f_{R}. As already stated, the beam and the RF voltage have to be synchronized for a successful acceleration (cf. (2.1)) and this implies an increase of the RF frequency f_{RF}. This is shown in principle in Figure 2.7. However, the rate of change of f_{R} is exaggerated, as a real acceleration cycle is normally close to an adiabatic process. The fact that several parameters have to be synchronously adapted to each other is the reason for the name *synchrotron*.

In practice, the magnetic field $B_{\mathrm{R}}(t)$ of the dipole magnets is predefined[2)] and the other synchrotron parameters follow synchronously. To keep the particles on the reference orbit, the Lorentz force $\boldsymbol{F}_{\mathrm{L}}$ has to balance the centripetal force $\boldsymbol{F}_{\mathrm{z}}$

$$|\boldsymbol{F}_{\mathrm{L}}| \stackrel{!}{=} |\boldsymbol{F}_{\mathrm{z}}| \quad \Rightarrow \quad Q v_{\mathrm{R}} B_{\mathrm{R}} \stackrel{!}{=} \frac{\gamma_{\mathrm{R}} m_0 v_{\mathrm{R}}^2}{r}$$

with the curvature r in the dipole magnets, the Lorentz factor or relativistic normalized reference energy γ_{R} and rest mass m_0. With the reference momentum $p_{\mathrm{R}} = m_0 \gamma_{\mathrm{R}} v_{\mathrm{R}}$ this leads to the synchrotron condition for a constant orbit for turn n

$$p_{\mathrm{R}}(n) = Q r B_{\mathrm{R}}(n). \tag{2.11}$$

Using the relativistic relations $\gamma = 1/\sqrt{1-\beta^2}$ and $\beta = v/c$, other quantities can be derived as functions of $B_{\mathrm{R}}(t)$. A short list of useful relativistic formulas can be found in

[2)] An essential reason is that the magnetic fields of the dipole magnets have a comparatively low response time.

Section B.1, these will be used in the following. If the magnetic field in turn n is given, this leads to the momentum $p_\mathrm{R}(n)$ of (2.11) and to the energy

$$W_\mathrm{R}(n) \overset{\text{(B.1)}}{=} m_0c^2\sqrt{1+\left[\frac{QrB_\mathrm{R}(n)}{m_0c}\right]^2}, \quad \gamma_\mathrm{R}(n) \overset{\text{(B.3)}}{=} \frac{W_\mathrm{R}(n)}{m_0c^2}, \tag{2.12}$$

and the velocity

$$v_\mathrm{R}(n) \overset{\text{(B.2)}}{=} c\frac{\frac{QrB_\mathrm{R}(n)}{m_0c}}{\sqrt{\left[\frac{QrB_\mathrm{R}(n)}{m_0c}\right]^2+1}}, \quad \beta_\mathrm{R}(n) = \frac{v_\mathrm{R}(n)}{c}.$$

The revolution period T_R, the revolution frequency f_R, and the RF frequency f_RF are given by

$$T_\mathrm{R}(n) = \frac{L_\mathrm{R}}{v_\mathrm{R}(n)}, \quad f_\mathrm{R}(n) = \frac{v_\mathrm{R}(n)}{L_\mathrm{R}}, \quad f_\mathrm{RF}(n) = hf_\mathrm{R}(n).$$

It is now possible to calculate the necessary $U_\mathrm{R}(n)$ to obtain the increase in energy. Inserting (2.9) in (2.12) yields

$$U_\mathrm{R}(n) = \frac{m_0c^2}{Q}\left[\sqrt{1+\left[\frac{QrB_\mathrm{R}(n)}{m_0c}\right]^2}-\sqrt{1+\left[\frac{QrB_\mathrm{R}(n-1)}{m_0c}\right]^2}\right]. \tag{2.13}$$

This calculation can also be performed in a continuous approximation: Assuming adiabatic acceleration, the rate of change in energy due to (2.9) can be expressed as

$$\dot{W}_\mathrm{R}(t) \approx \frac{\Delta W_\mathrm{acc}}{T_\mathrm{R}} = \frac{QU_\mathrm{R}(t)}{T_\mathrm{R}(t)}. \tag{2.14}$$

The reference energy $W_\mathrm{R}(t)$ is given by (2.12) as a function of $B_\mathrm{R}(t)$. The derivation with respect to t is

$$\dot{W}_\mathrm{R}(t) = \frac{c[Qr]^2B_\mathrm{R}(t)\dot{B}(t)_\mathrm{R}}{\sqrt{m_0^2c^2+[QrB_\mathrm{R}(t)]^2}}. \tag{2.15}$$

Comparing (2.15) and (2.14) leads after some calculation steps to the simple condition

$$U_\mathrm{R}(t) \approx L_\mathrm{R}r\dot{B}_\mathrm{R}(t). \tag{2.16}$$

A power series expansion of (2.13) leads in first order to the equivalent discrete result [57]

$$U_\mathrm{R}(n) \approx L_\mathrm{R}r\frac{B_\mathrm{R}(n)-B_\mathrm{R}(n-1)}{T_\mathrm{R}(n)}.$$

Thus, in the stationary case before (or after) acceleration, $\dot{B}_\mathrm{R} = 0$ implies $\varphi_\mathrm{R} = 0$, if $\hat{U}_1$ is nonzero. During acceleration, both $\hat{U}_1$ and φ_R can be varied to satisfy condition (2.16),

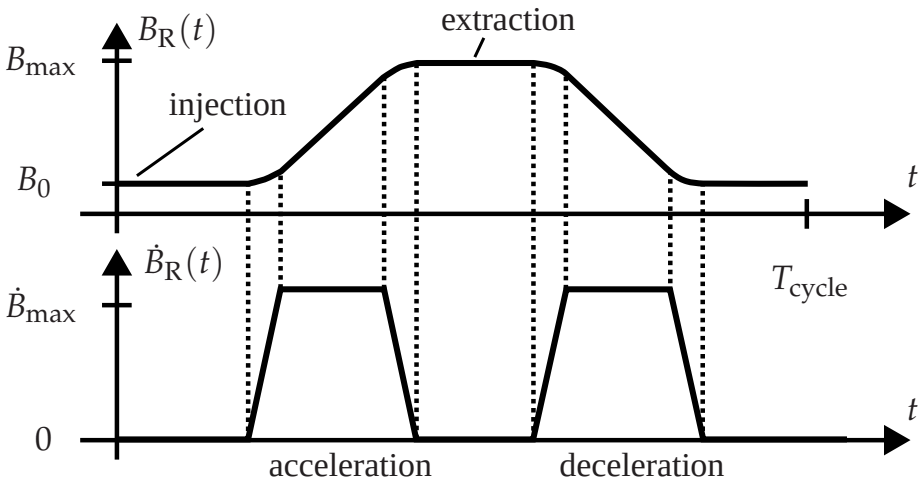

Figure 2.8: Typical acceleration cycle (not to scale).

as long as $\hat{U}_1$ is larger than the necessary voltage U_{R}. This additional degree of freedom is used to choose $\hat{U}_1$ such that the *bucket*[3)] area is kept constant, cf. [48] and Section 2.4. The reference phase φ_{R} is then chosen to satisfy (2.16).

Figure 2.8 shows a typical choice of $\dot{B}_{\mathrm{R}}$ and B_{R}. First, the beam is injected into the ring with the momentum $p_{\mathrm{R}}(0)$. The necessary magnetic flux density is obtained using (2.11) and equals

$$B_0 = B_{\mathrm{R}}(0) = \frac{p_{\mathrm{R}}(0)}{Qr}.$$

The minimum and maximum flux density $B_{\max}$ is determined by the type of dipole magnets. It is important to note that $\dot{B}_{\mathrm{R}}(t)$ should be a continuous function. This follows from (2.16). If $\dot{B}_{\mathrm{R}}(t)$ is discontinuous, this implies that $\varphi_{\mathrm{R}}(t)$ will be discontinuous. This would lead to a discontinuity in the reference trajectory and can induce beam oscillations. The period T_{cycle} of the acceleration cycle typically is of the order of

$$T_{\mathrm{cycle}} \approx 10^5 \ldots 10^6 \cdot T_{\mathrm{R}}.$$

This shows the importance of a longitudinal feedback system: small disturbances can sum up during thousands of turns and cause beam instabilities.

2.2.5 Discrete Equations and Mapping Algorithm

In this section, the discrete longitudinal equations of motion will be derived. The RF cavity generates a sinusoidal accelerating voltage and the particles in the ring are only accelerated when they enter the RF cavity, i. e. once a turn. This suggests a discrete modeling of the particle dynamics.

[3)] *Bucket* denotes the stable area in phase space and *bunch* denotes the particle ensemble. These terms will be specified in later sections.

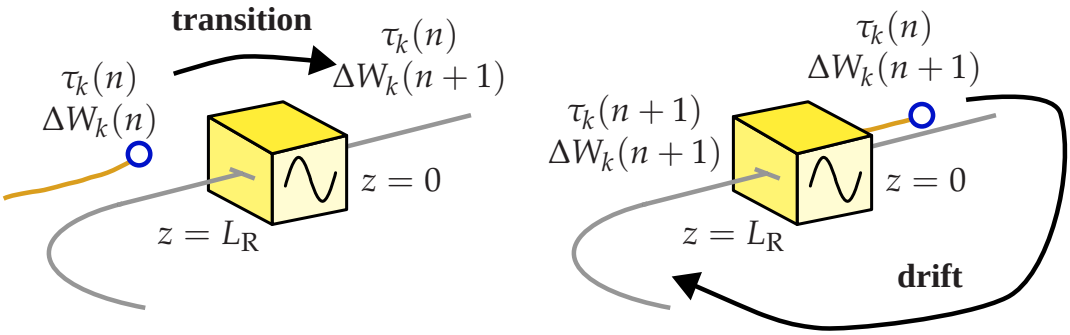

Figure 2.9: Mapping sequence of relative delay τ_k and relative energy ΔW_k.

To derive the discrete equations of longitudinal motion, we consider a particle k that has just completed turn n and has reached the cavity as shown in Figure 2.9. Its time of arrival at the cavity

$$\tau_k(n) = \tau_R(n) + \Delta\tau(n)$$

determines the voltage $U_{\text{gap}}(t)$ and thus the energy a specific particle gains. In principle, the voltage U_{gap} can be a general periodic function with an amplitude $\hat{U}_1$ that is greater than the reference amplitude $\hat{U}_{1,R}$ and a phase shift $\Delta\varphi_{\text{gap}}$

$$U_{\text{gap}}(\tau_k(n)) = \hat{U}_1(n)\sin(\omega_{RF}(n)\tau_k(n) + \Delta\varphi_{\text{gap}}(n)).$$

The amplitude and phase variations can be caused by a feedback system that is implemented to stabilize the beam, but they can also arise from imperfections and disturbances such as interactions with impedances in the ring.

The energy gain ΔW_{acc} of the particle and $\Delta W_{\text{acc,R}}$ of the reference are given by (2.8) and (2.9). After the transition of the cavity (cf. Figure 2.9), the energy deviation of the particle with respect to the reference has changed to

$$\boxed{\Delta W_k(n+1) = \Delta W_k(n) + Q\left[U_{\text{gap}}(\tau_k(n)) - U_R(n)\right],} \tag{2.17}$$

where it is assumed that the length of the cavity is so small that the voltage is almost constant while the particle is inside the cavity. In addition, a small cavity length implies that the phase $\varphi_k(n)$ does not change significantly. During the remaining part of the ring, the particle drifts and is guided by the magnetic fields. In an ideal accelerator, its energy would remain constant. However, due to *synchrotron radiation* and interactions with the vacuum tube (*wake fields*) and other devices along the ring (*impedances*), its energy may be disturbed [19, 20]. During one turn, the energy loss of a particle due to synchrotron radiation can be expressed by [137]

$$\Delta W_{\text{rad}} = \frac{Q^2}{3\varepsilon_0[m_0c^2]^4}\frac{W^4}{r} \sim \frac{W^4}{m_0^4}.$$

Due to the dependency on W and m_0, synchrotron radiation is relevant mainly for relativistic electron beams. In the case of proton and ion beams, synchrotron radiation is negligible for energies less than 1 TeV because of their larges masses, cf. [137]. Synchrotron radiation will be neglected in the following, as only protons and ions are considered.

Modeling of wake fields and impedances is necessary to simulate and analyze the beam behavior. However, wake fields and impedances will not be modeled explicitly in the following. Rather, they will be regarded as external disturbances acting on the phase and energy of the particles. The aim of this and the following chapter is to establish a mathematical model that is suitable for controller designs. If the controller design incorporates a certain robustness and the disturbances on the beam from wake fields, impedances and other sources are not too large, the controller will be able to suppress these disturbances and stabilize the beam.

With these assumptions, Equation (2.17) is the first equation of the longitudinal beam dynamics and the energy of the particle is assumed approximately constant as the particle drifts through the remaining part of the ring. During the drift, the arrival time τ_k will change depending on the difference in velocity of particle and reference, cf. Figure 2.9. At the end of turn $n+1$, i. e. just before the cavity, the new arrival time of particle k is

$$\tau_k(n+1) = \tau_k(n) + T_k(n+1) - T_\mathrm{R}(n+1), \tag{2.18}$$

where T_k is the period of particle k for one turn in the ring and T_R is the reference period. To find an expression for the period T_k, we consider the reference revolution period

$$T_\mathrm{R} = \frac{L_\mathrm{R}}{v_\mathrm{R}},$$

which depends on the reference orbit length L_R and the reference velocity v_R. The revolution period of the particle $T_k = T_\mathrm{R} + \Delta T_k$ can be expanded in a Taylor series around T_R as

$$T_k = T_\mathrm{R} + \Delta T_k = \frac{L_\mathrm{R} + \Delta L_k}{v_\mathrm{R} + \Delta v_k} = \frac{L_\mathrm{R}}{v_\mathrm{R}} + \frac{1}{v_\mathrm{R}}\Delta L_k - \frac{L_\mathrm{R}}{v_\mathrm{R}^2}\Delta v_k + \mathcal{O}(\Delta L_k^2, \Delta v_k^2),$$

where $\mathcal{O}(\Delta L_k^2, \Delta v_k^2)$ denotes the higher order terms. Neglecting the terms of second and higher order leads to

$$\frac{\Delta T_k}{T_\mathrm{R}} \approx \frac{\Delta L_k}{v_\mathrm{R} T_\mathrm{R}} - \frac{L_\mathrm{R}\Delta v_k}{T_\mathrm{R} v_\mathrm{R}^2} = \frac{\Delta L_k}{L_\mathrm{R}} - \frac{\Delta v_k}{v_\mathrm{R}}. \tag{2.19}$$

This equation shows the two mechanisms that lead to a deviation ΔT. First, a particle with a higher velocity ($\Delta v_k > 0$) will tend to circulate faster in the ring ($\Delta T_k < 0$). Second, a particle with a longer orbit ($\Delta L_k > 0$) will need longer for one turn ($\Delta T_k > 0$). Both effects depend on the energy of the particle, as will be shown in the following. For small deviations Δv_k, the approximation (cf. (B.6), Appendix B.1)

$$\frac{\Delta v_k}{v_\mathrm{R}} \approx \frac{1}{\gamma_\mathrm{R}^2 \beta_\mathrm{R}^2} \frac{\Delta W_k}{W_\mathrm{R}} \tag{2.20}$$

holds, i. e. the relative velocity deviation is proportional to the relative energy deviation. The orbit length deviation ΔL_k depends on the momentum of the particle. This follows from Equation (2.11), as the curvature $r \sim p$ is proportional to the momentum p. A larger momentum ($\Delta p_k > 0$) leads in general to a different curvature r and to a longer orbit. To calculate the dependency of Δp on ΔL, it is necessary to consider the geometry of the accelerator ring and the focusing forces in the transverse planes. These considerations can be summarized in the equation

$$\frac{\Delta L_k}{L_\mathrm{R}} = \alpha_\mathrm{p} \frac{\Delta p_k}{p_\mathrm{R}}, \tag{2.21}$$

where the *momentum compaction factor* α_p is a characteristic of the accelerator and a measure how compact the trajectories of particles with different momenta are focused in radial direction. If we take into account that approximation (B.6) is valid, i. e.

$$\frac{\Delta p_k}{p_\mathrm{R}} = \frac{1}{\beta_\mathrm{R}^2} \frac{\Delta W_k}{W_\mathrm{R}} \tag{2.22}$$

holds for small values of Δp, (2.19) can be written as

$$\frac{\Delta T_k}{T_\mathrm{R}} = \left[\alpha_\mathrm{p} - \frac{1}{\gamma_\mathrm{R}^2} \right] \frac{\Delta W_k}{\beta_\mathrm{R}^2 W_\mathrm{R}}.$$

The factor

$$\eta_\mathrm{R} = \alpha_\mathrm{p} - \frac{1}{\gamma_\mathrm{R}^2}$$

is called *phase slip factor*. At lower energies with $\gamma_\mathrm{R} \approx 1$, η_R is negative and a particle with a higher energy will reach the cavity earlier. At higher energies, η_R is positive and the effect of a longer orbit predominates, leading to a longer revolution period for faster particles. For a specific energy

$$\gamma_\mathrm{R} = \frac{1}{\sqrt{\alpha_\mathrm{p}}} =: \gamma_\mathrm{tr}$$

in between, η_R becomes zero and in a first-order approximation, the revolution period is T_R, even if the particle has a small energy deviation $\Delta W_k \ll W_\mathrm{R}$. This point is called *transition* and the corresponding energy is the *transition gamma* γ_tr. Thus, the phase slip factor can be written as

$$\boxed{\eta_\mathrm{R} = \gamma_\mathrm{tr}^{-2} - \gamma_\mathrm{R}^{-2}}$$

Using the above relations in Equation (2.18) leads to

$$\tau_k(n+1) = \tau_k(n) + \frac{\eta_\mathrm{R} T_\mathrm{R}}{\beta_\mathrm{R}^2 W_\mathrm{R}} (n+1) \Delta W_k(n+1). \tag{2.23}$$

The derivation of this equation uses (2.1), i. e. the fact that the RF frequency is an exact multiple h of the revolution frequency. In practice, there might be a frequency deviation $\dot{\varphi}_\mathrm{f}$, either intentionally due to a feedback correction or unwanted due to an error in the RF feedback of the cavity. Including this in (2.1) yields

$$\omega_\mathrm{RF}(t) = h\omega_\mathrm{R}(t) + \dot{\varphi}_\mathrm{f}(t). \tag{2.24}$$

In addition, this *cavity RF program* is sometimes extended to

$$\omega_\mathrm{RF}(t) = h\omega_\mathrm{R}(t) + \dot{\varphi}_\mathrm{f}(t) + \dot{\varphi}_\mathrm{R}(t) \tag{2.25}$$

to include a further term $\dot{\varphi}_\mathrm{R}$ [63, p.41]. This scheme can have an advantage over (2.24) for faster changes in φ_R since it assures that the RF voltage will keep up with the rate of change of the reference phase. With these programs (2.23) changes to

$$\boxed{\begin{aligned}\tau_k(n+1) \quad &= \tau_k(n) \;+\; \tfrac{\eta_\mathrm{R} T_\mathrm{R}}{\beta_\mathrm{R}^2 W_\mathrm{R}}(n+1)\Delta W_k(n+1) \;+ \\ &\quad + \tau_\mathrm{f}(n+1) - \tau_\mathrm{f}(n) \;+\; k_\mathrm{RF}\big[\tau_\mathrm{R}(n+1) - \tau_\mathrm{R}(n)\big],\end{aligned}} \tag{2.26}$$

where k_RF can be 0 or 1, depending on whether program (2.24) or (2.25) is used. The time lags due to the frequency deviation and the change of the reference are denoted by τ_f and τ_R, respectively.

Equations (2.17) and (2.26) establish the discrete nonlinear dynamics in the longitudinal phase space $(\tau, \Delta W)$. They are also referred to as *mapping equations*, as they can be used to map the state $(\tau_k, \Delta W_k)$ of a particle from turn n to turn $n+1$. Mapping equations are widely used in *macro particle tracking simulations* [85–89] to simulate the behavior of a beam of discrete particles $k = 1, \ldots, N_\mathrm{macro}$.[4)] The parameters T_R, η_R, β_R, and W_R are only constant if the beam is not accelerated, i. e. in the case of

$$U_\mathrm{R}(n) = 0.$$

This will be referred to as the *stationary case*. In the *acceleration case* U_R is positive and the reference energy increases each turn. Considering (2.9) leads to the additional equation for the reference energy

$$W_\mathrm{R}(n+1) = W_\mathrm{R}(n) + QU_\mathrm{R}(n). \tag{2.27}$$

The other parameters T_R, η_R, and β_R can be derived from this new energy value. The choice of $U_\mathrm{R}(n)$ is given by the acceleration cycle of the accelerator control room. As described in Section 2.2.4, U_R can be expressed as a function of the magnetic field $B_\mathrm{R}(n)$. It is thus sufficient to choose B_R as a function of time to define the complete acceleration cycle. All parameters of the longitudinal motion follow from this as shown in Section 2.2.4.

The mapping equations can also be extended for a ring with more than one cavity. In this case, the accelerating voltages of all the cavities in the ring can be added to an equivalent voltage amplitude $\hat{U}_1$, if the phases of the cavities are chosen appropriately [57]

[4)] *Macro* or *super* particle refers to the fact that each particle in the simulation represents several real particles, as the amount of simulated particles is usually smaller by a factor of 10^5 to 10^6 compared to a real beam.

or the mapping equations are used to map from one cavity to the next and have to be used several times for one revolution [63].

An important property of the derived mapping equations is that they preserve area in phase space. This is true for the stationary case $\varphi_R = 0$ and even for the acceleration case, as long as the change of the beam parameters is adiabatic [57]. This can be shown by computing the Jacobian matrix of (2.17) and (2.26), which is

$$\boldsymbol{J} = \begin{bmatrix} \frac{\partial \Delta W_k(n+1)}{\partial \Delta W_k(n)} & \frac{\partial \Delta W_k(n+1)}{\partial \tau_k(n)} \\ \frac{\partial \tau_k(n+1)}{\partial \Delta W_k(n)} & \frac{\partial \tau_k(n+1)}{\partial \tau_k(n)} \end{bmatrix} = \begin{bmatrix} 1 & Q U'_{\mathrm{gap}} \\ \frac{\eta_R T_R}{\beta_R^2 W_R} & 1 - \frac{\eta_R T_R}{\beta_R^2 W_R} Q U'_{\mathrm{gap}} \end{bmatrix}, \tag{2.28}$$

where U'_{gap} denotes the derivative of the gap voltage with respect to τ_k. The Jacobian determinant is $\det \boldsymbol{J} = 1$, thus these equations define an area preserving map. For the area preservation, it is essential that $\Delta W_k(n+1)$ is used in (2.26) instead of $\Delta W_k(n)$. This is similar to the use of a leap-frog scheme. The area preservation in the coordinates τ and ΔW has an important consequence; if an arbitrary region in the phase space $(\tau, \Delta W)$ with a certain amount of particles is selected at a given time or turn n, this region will then evolve during the following turns and may change its shape; the area of this region however will remain constant. This will be discussed in more detail in Section 3.

To simulate the longitudinal beam dynamics, it is usually more convenient to use the RF phase $\varphi = \omega_{\mathrm{RF}} \tau$ as a variable instead of the time lag τ. Multiplying (2.26) with $\omega_{\mathrm{RF}}(n+1)$ yields together with (2.17)

$$\begin{aligned} \Delta W_k(n+1) &= \Delta W_k(n) + Q\Big[U_{\mathrm{gap}}(\varphi_k(n)) - U_R(n)\Big], \\ \varphi_k(n+1) &= \frac{\omega_{\mathrm{RF}}(n+1)}{\omega_{\mathrm{RF}}(n)} \left[\varphi_k(n) - \varphi_f(n) - \varphi_R(n)\right] + \\ &\quad + \frac{2\pi h \eta_R}{\beta_R^2 W_R}(n+1)\Delta W_k(n+1) + \varphi_f(n+1) + k_{\mathrm{RF}}\, \varphi_R(n+1). \end{aligned} \tag{2.29}$$

These are the mapping equations in the phase space $(\varphi, \Delta W)$. The derived mapping equations are not area preserving since their Jacobian determinant is

$$\det \boldsymbol{J} = \frac{\omega_{\mathrm{RF}}(n+1)}{\omega_{\mathrm{RF}}(n)} = \frac{\beta_R(n+1)}{\beta_R(n)}.$$

Thus, it is quite common to use the coordinates $(\varphi_k, \Delta W_k/\omega_{\mathrm{RF}})$, because the mapping equations in these coordinates do preserve area in phase space.

The conclusion of the previous considerations is that the longitudinal dynamics for a single particle can be described by two discrete nonlinear equations with time-varying parameters. These equations describe a nonlinear oscillation called the *synchrotron oscillation* in the phase plane, as the next section will show. As the parameters of the synchrotron oscillation vary slowly with time, it is often possible to assume that the variation is *adiabatic* [110] and the parameters are approximately constant during one turn of the beam. Section B.3 summarizes the equations that are necessary to implement a longitudinal tracking algorithm.

2.2.6 Continuous Longitudinal Equations

The difference equations (2.17) and (2.26) can be written as continuous differential equations, if the assumption is made that the change of the variables τ and ΔW during one turn in the ring is not too large. In this case, the difference quotient can be approximated by the differential quotient

$$\frac{\tau_k(n+1) - \tau_k(n)}{T_\mathrm{R}} \approx \dot{\tau}_k(t).$$

This leads to the continuous equations

$$\Delta\dot{W}_k(t) = \frac{Q}{T_\mathrm{R}(t)}\left[U_\mathrm{gap}(\tau_k(t)) - U_\mathrm{R}(t)\right], \tag{2.30a}$$

$$\dot{\tau}_k(t) = \frac{\eta_\mathrm{R}(t)}{\beta_\mathrm{R}^2(t)W_\mathrm{R}(t)}\Delta W_k(t) + k_\mathrm{RF}\dot{\tau}_\mathrm{R}(t) + \dot{\tau}_\mathrm{f}(t). \tag{2.30b}$$

To begin with, the parameters T_R, η_R, β_R, and W_R are assumed to be constant and $\dot{\tau}_\mathrm{R}$ and $\dot{\tau}_\mathrm{f}$ are set to zero. The continuous equations then represent a Hamiltonian flow [71].

A dynamical system is called *Hamiltonian* if its equations of motion can be derived from a function $H(\boldsymbol{q}, \boldsymbol{p}, t)$ and Hamilton's equations of motion

$$\dot{q}_k = \frac{\partial H}{\partial p_k}, \qquad \dot{p}_k = -\frac{\partial H}{\partial q_k}, \tag{2.31}$$

where

$$\boldsymbol{q} = \begin{bmatrix} q_1 & \dots & q_k & \dots & q_N \end{bmatrix}^\mathrm{T}, \qquad \boldsymbol{p} = \begin{bmatrix} p_1 & \dots & p_k & \dots & p_N \end{bmatrix}^\mathrm{T},$$

are the *generalized coordinates* and *generalized momenta* of the system, respectively; H is the *Hamiltonian function* or *Hamiltonian*, and N are the degrees of freedom of the system. The space spanned by the q_k and p_k is called *phase space* and has the dimension $2N$. If the Hamiltonian H does not depend explicitly on the time t, the system is called *conservative* and the value of H is conserved, as the rate of change of H is

$$\frac{\mathrm{d}H}{\mathrm{d}t} = \underbrace{\frac{\partial H}{\partial t}}_{=0} + \sum_{k=1}^{N}\frac{\partial H}{\partial q_k}\dot{q}_k + \sum_{k=1}^{N}\frac{\partial H}{\partial p_k}\dot{p}_k = \sum_{k=1}^{N}\frac{\partial H}{\partial q_k}\frac{\partial H}{\partial p_k} + \sum_{k=1}^{N}\frac{\partial H}{\partial p_k}\left(-\frac{\partial H}{\partial q_k}\right) = 0.$$

The Hamiltonian is called *separable* if it has the form

$$H(\boldsymbol{q},\boldsymbol{p}) = V(\boldsymbol{q}) + T(\boldsymbol{p}),$$

where V is the *potential function* and T the *energy function*.

Equations (2.30) can be derived from Hamilton's equations

$$\dot{\tau}_k = \frac{\partial H}{\partial \Delta W_k}, \qquad \Delta\dot{W}_k = -\frac{\partial H}{\partial \tau_k}.$$

with the Hamiltonian

$$H(\tau_k, \Delta W_k) = \frac{\eta_\mathrm{R}}{2\beta_\mathrm{R}^2 W_\mathrm{R}} \Delta W_k^2 - \frac{Q}{T_\mathrm{R}} \int U_\mathrm{gap}(\tau_k) - U_\mathrm{R} \, \mathrm{d}\tau_k,$$

where the generalized coordinate is $q = \tau_k$ and the generalized momentum is $p = \Delta W_k$. This Hamiltonian is conservative and separable with the potential function

$$V(\tau_k) = -\frac{Q}{T_\mathrm{R}} \int U_\mathrm{gap}(\tau_k) - U_\mathrm{R} \, \mathrm{d}\tau_k.$$

For the single-harmonic voltage $U_\mathrm{gap} = \hat{U}_{1,\mathrm{R}} \sin(\omega_\mathrm{RF} \tau_k)$, the Hamiltonian is

$$\boxed{\begin{aligned} H(\tau_k, \Delta W_k) \quad &= \tfrac{Q}{T_\mathrm{R} \omega_\mathrm{RF}} \Big[\hat{U}_{1,\mathrm{R}} \left[\cos(\omega_\mathrm{RF}\, \tau_k) - \cos(\omega_\mathrm{RF}\, \tau_\mathrm{R}) \right] + \\ &\quad + U_\mathrm{R} \left[\omega_\mathrm{RF} \tau_k - \omega_\mathrm{RF} \tau_\mathrm{R} \right] \Big] + \tfrac{\eta_\mathrm{R}}{2\beta_\mathrm{R}^2 W_\mathrm{R}} \Delta W_k^2 \,, \end{aligned}} \tag{2.32}$$

where the integration constant is chosen such that $H(\tau_\mathrm{R}, 0) = 0$. The Hamiltonian is negative in the vicinity of $(\tau_\mathrm{R}, 0)$ below transition and positive above transition. The Hamiltonian flow preserves the area in phase space. This is consistent with the area conservation property of the discrete equations and their Jacobian in (2.28). In general, the parameters ω_R, η_R, β_R, and W_R vary slowly with time and the Hamiltonian becomes time dependent. If the variations are slow enough, the changes can however be regarded as adiabatic and the parameters as quasi-constant. The trajectories of the system may change slowly, but the area circumscribed by a specific trajectory in phase space will still be approximately conserved [110]. For a beam consisting of a large number of identical particles, this has the following consequence: the existence of a Hamiltonian implies that the phase space area occupied by the beam (*longitudinal emittance*) is an adiabatic invariant in $(\tau, \Delta W)$ coordinates [20, p.68]. The area preservation property and its consequences for a particle bunch will be discussed in more detail in Section 3.2.

The coordinates of a Hamiltonian may be changed by a canonical transformation [81]. Care must be taken that only canonically conjugate coordinates are used to preserve the area conservation property. Choosing inappropriate coordinates will result in conservation of phase space area in the wrong coordinates. In particular, for a Hamiltonian with one degree of freedom it is possible to choose a transformation

$$\tilde{q} = K(t) q, \qquad \tilde{p} = K(t)^{-1} p$$

where $K(t)$ is a factor that may be slowly time-dependent.

Table 2.1 lists common coordinate pairs for the longitudinal phase space. Not all possible pairs are canonically conjugate. Some transformations are only approximately valid, they are based on the relativistic relations in Appendix B.1, especially Equation (B.6). These transformations are valid for small deviations only, e. g. $\Delta p \ll p_\mathrm{R}$ and $\Delta v \ll v_\mathrm{R}$. The coordinates $(\varphi, \ \Delta W / \omega_\mathrm{R})$ are not strictly canonically conjugate, because ΔW is normalized by ω_R and not by $\omega_\mathrm{RF} = h \omega_\mathrm{R}$. But, because h is a constant factor, the simulation

Table 2.1: Coordinate transformations based on τ and ΔW. The given unit refers to area in phase space. CC: canonically conjugate, CAP: correct area preservation.

Coordinates and transformation	CC?	CAP?	Unit
$\tau, \quad \Delta W$	yes	yes	eVs
$\tau, \quad \Delta\gamma = \Delta W / m_0 c^2$	no	yes	s
$\Delta z \approx -\beta_\mathrm{R}(t) c\tau, \quad \Delta p_z \approx \Delta W / \beta_\mathrm{R}(t) c$	yes	yes	eVs
$\varphi = \omega_\mathrm{RF}(t)\,\tau, \quad \Delta W / \omega_\mathrm{RF}(t)$	yes	yes	eVs
$\varphi = \omega_\mathrm{RF}(t)\,\tau, \quad \Delta W / \omega_\mathrm{R}(t)$	no	yes	eVs
$\varphi = \omega_\mathrm{RF}(t)\,\tau, \quad \Delta W$	no	no	eVrad
$\varphi = \omega_\mathrm{RF}(t)\,\tau, \quad \delta = \Delta p / p_\mathrm{R} \approx \Delta W / \beta_\mathrm{R}^2(t) W_\mathrm{R}(t)$	no	no	rad

with these variables still leads to a correct conservation of phase space area in the coordinates $(\tau, \Delta W)$. It is interesting to note that the pair $(\Delta z, \Delta p_z)$, i. e. the physical position and momentum, is also canonically conjugate to $(\tau, \Delta W)$.

Because the phase space area in $(\tau, \Delta W)$ is preserved, the area in $(\varphi, \delta = \Delta p / p_\mathrm{R})$ will change according to

$$\omega_\mathrm{RF} \frac{1}{\beta_\mathrm{R}^2 W_\mathrm{R}} = \frac{2\pi h c}{L_\mathrm{R}} \frac{1}{\beta_\mathrm{R} W_\mathrm{R}} \sim \frac{1}{\beta_\mathrm{R} \gamma_\mathrm{R}}.$$

Thus, at the end of the acceleration cycle, the area occupied by the beam in the phase space (φ, δ) will be smaller. This is referred to as *adiabatic damping*.

For a RF cavity with a single harmonic the longitudinal motion of particle k in the phase space $(\varphi_k, \Delta\tilde{W}_k)$ with the new coordinate

$$\Delta\tilde{W}_k := \frac{\Delta W_k}{\omega_\mathrm{RF}}$$

can be written as

$$\Delta\dot{\tilde{W}}_k(t) = \frac{Q}{2\pi h} \left[\hat{U}_1(t) \sin(\varphi_k(t)) - U_\mathrm{R}(t)\right], \tag{2.33a}$$

$$\dot{\varphi}_k(t) - k_\mathrm{RF} \dot{\varphi}_\mathrm{R}(t) = \frac{\eta_\mathrm{R} \omega_\mathrm{RF}^2}{\beta_\mathrm{R}^2 W_\mathrm{R}} \Delta\tilde{W}_k(t) + \dot{\varphi}_\mathrm{f}(t). \tag{2.33b}$$

The variables $\hat{U}_1$ and φ_f can be used as input variables to implement a feedback loop. Equations (2.33) will be analyzed further in the next sections. The time dependency of the slowly varying parameters will be treated in the following in the framework of adiabatic motion. Only the RF amplitude $\hat{U}_1$ and the phase error φ_f will be allowed to make fast variations. These variables will be used in later chapters as inputs to control the beam. The reference particle is defined as the particle that exactly gains the energy U_R. For the reference RF amplitude $\hat{U}_1(t) = \hat{U}_{1,\mathrm{R}}(t)$, a corresponding reference phase can be

calculated: Rewriting the energy equation (2.33a) with $\Delta\dot{\tilde{W}}_k = 0$ for $\varphi_k = \varphi_\mathrm{R}$ yields the reference phase

$$\boxed{U_\mathrm{R} = \hat{U}_{1,\mathrm{R}} \sin(\varphi_\mathrm{R}) \quad \Rightarrow \quad \varphi_\mathrm{R}(t) = \arcsin\left(\frac{U_\mathrm{R}(t)}{\hat{U}_{1,\mathrm{R}}(t)}\right),} \tag{2.34}$$

where it is necessary to assume $U_\mathrm{R} \leq \hat{U}_{1,\mathrm{R}}$. In the following, the amplitude $\hat{U}_{1,\mathrm{R}}$ will denote the desired reference amplitude as given by the central control room. $\hat{U}_1$ will be used to denote the amplitude including beam control modulations.

2.2.7 Synchrotron Oscillation and Phase Stability

Equations (2.33a) and (2.33b) describe a nonlinear oscillation called the *synchrotron oscillation*. For small amplitudes the equations can be linearized around the working point

$$\varphi_k = \varphi_\mathrm{R}, \qquad \Delta\tilde{W}_k = 0.$$

Assuming $k_\mathrm{RF} = 1$ and $\hat{U}_1 = \hat{U}_{1,\mathrm{R}}$ and using $\Delta\varphi_k = \varphi_k - \varphi_\mathrm{R}$, differentiating (2.33b) and inserting (2.33a) and (2.34) yields

$$\Delta\ddot{\varphi}_k = \frac{Qh\omega_\mathrm{R}^2\eta_\mathrm{R}}{2\pi\beta_\mathrm{R}^2 W_\mathrm{R}}\hat{U}_{1,\mathrm{R}}\left[\sin(\Delta\varphi_k + \varphi_\mathrm{R}) - \sin(\varphi_\mathrm{R})\right] + \ddot{\varphi}_\mathrm{f}, \tag{2.35}$$

where $\Delta\varphi_k = \varphi_k - \varphi_\mathrm{R}$ is the small phase deviation. The Taylor-expansion of the nonlinear term on the right hand side at $\Delta\varphi_k = 0$ is

$$\sin(\Delta\varphi_k(t) + \varphi_\mathrm{R}) - \sin\varphi_\mathrm{R} = \cos\varphi_\mathrm{R}\ \Delta\varphi_k - \sin\varphi_\mathrm{R}\ \frac{\Delta\varphi_k^2}{2} + \ldots$$

and leads to the linear approximation

$$\Delta\ddot{\varphi}_k(t) + \omega_\mathrm{syn}^2\Delta\varphi_k(t) = \ddot{\varphi}_\mathrm{f}. \tag{2.36}$$

This is a linear harmonic oscillator with the solution

$$\varphi_k(t) = \hat{\varphi}\cos(\omega_\mathrm{syn}t + \Phi_{k,0}) \tag{2.37}$$

for $\ddot{\varphi}_\mathrm{f} = 0$ with the synchrotron frequency in the linear regime

$$\boxed{\omega_\mathrm{syn} = \frac{2\pi}{T_\mathrm{syn}} = \omega_\mathrm{R}\sqrt{\frac{Q\hat{U}_{1,\mathrm{R}}h\left[\gamma_\mathrm{R}^{-2} - \alpha_\mathrm{P}\right]\cos\varphi_\mathrm{R}}{2\pi\beta_\mathrm{R}^2 W_\mathrm{R}}},} \tag{2.38}$$

where the factor $[\gamma_\mathrm{R}^{-2} - \alpha_\mathrm{p}]\cos\varphi_\mathrm{R} = -\eta_\mathrm{R}\cos\varphi_\mathrm{R}$ should be nonnegative; with the proper choice of the operating point

$$\begin{cases} \cos\varphi_\mathrm{R} > 0 & \text{below transition, i. e. } \gamma_\mathrm{R} < \alpha_\mathrm{P}^{-1/2} \\ \cos\varphi_\mathrm{R} < 0 & \text{above transition, i. e. } \gamma_\mathrm{R} > \alpha_\mathrm{P}^{-1/2} \end{cases}$$

it is guaranteed that ω_{syn} is real and the resulting oscillation is stable. This condition is known as the *phase stability* or *phase focusing principle* [32, 71, 136, 137]. The phase stability enables the acceleration of particles with a momentum spread, because particles with small deviations from the reference trajectory are kept near the reference by this stable synchrotron oscillation.

With definition (2.38) the nonlinear differential equation can be written as

$$\Delta\ddot{\varphi}_k(t) = -\frac{\omega_{\mathrm{syn}}^2}{\cos\varphi_{\mathrm{R}}}\left[\sin(\Delta\varphi_k(t)+\varphi_{\mathrm{R}}) - \sin\varphi_{\mathrm{R}}\right] + \ddot{\varphi}_{\mathrm{f}}. \tag{2.39}$$

A similar calculation for $k_{\mathrm{RF}} = 0$ yields

$$\Delta\ddot{\varphi}_k(t) = -\frac{\omega_{\mathrm{syn}}^2}{\cos\varphi_{\mathrm{R}}}\left[\sin(\Delta\varphi_k(t)+\varphi_{\mathrm{R}}) - \sin\varphi_{\mathrm{R}}\right] + \ddot{\varphi}_{\mathrm{f}} - \ddot{\varphi}_{\mathrm{R}}. \tag{2.40}$$

2.2.8 Discussion of the Longitudinal Equations

A general way to derive the equations of longitudinal motion is to consider the relativistic Lagrangian for a charged particle, to define the electromagnetic fields that act on the particle, and to change to a Hamiltonian description of motion relative to the reference trajectory [90].

In the beam dynamics of a ring accelerator, deviations of the position and momenta are considered to simplify the obtained model. Thus a general Hamiltonian for the beam dynamics of a single particle

$$H(\Delta x,\, \Delta y,\, \Delta z,\, \Delta p_x,\, \Delta p_y,\, \Delta p_z;\; z;\; t)$$

depends on the position and momentum deviations, the absolute reference position z, and the time t. It describes the synchrotron and betatron motion of a charged particle in a circular accelerator [70]. Since the motion in the longitudinal phase space $(\Delta z,\, \Delta p_z)$ is usually considerably slower than the motion in the transverse phase spaces, the longitudinal part of the Hamiltonian can be obtained by averaging of the transverse motion. The Hamiltonian finally leads to continuous equations of longitudinal motion

$$\Delta\dot{z} = \frac{\partial H}{\partial \Delta p_z}, \qquad \Delta\dot{p}_z = -\frac{\partial H}{\partial \Delta z}.$$

In general the Hamiltonian will depend explicitly on the time t if the beam is accelerated. For example, the beam energy changes and this will influence the motion in the longitudinal phase space $(\Delta z, \Delta p_z)$. However, since the acceleration is usually slow, the assumption of *adiabaticity* is possible and leads to a conservative Hamiltonian [110].

A second approach is to regard the longitudinal motion as an inherently discrete process. The goal is then to find discrete equations that map the position and momentum of the particle from one turn to the next. The discrete approach was chosen in Section 2.2.5 to derive the discrete synchrotron equations.

As long as the synchrotron oscillation period T_{syn} is considerably longer than the revolution period T_{R}, both approaches lead to very similar results and the continuous equations can be discretized or derived from the discrete mapping equations. In both cases, the right choice of the longitudinal coordinates is essential to obtain correct results if the beam dynamics are simulated over a complete acceleration cycle.

To derive the longitudinal equations, some approximations had to be made in Section 2.2.5. In the following, these approximations and the obtained equations are discussed and compared with literature.

The first approximation made was the neglect of terms of higher order in Equation (2.19). This has the consequence that the following calculations are valid for small deviations only. This is also the case for (2.20) and (2.22). In principle, these approximations can be avoided [57], but this leads to a more complex equation in Δt compared to Equation (2.23).

A further approximation is that Definition (2.21) of the momentum compaction assumes that there is a linear dependency between the relative momentum and orbit length deviation. In general, the dependency is nonlinear and a general nonlinear relation

$$\frac{\Delta L}{L_{\mathrm{R}}} = f\left(\frac{\Delta p}{p_{\mathrm{R}}}\right)$$

of the momentum compaction could be assumed.

Typical relative momentum deviations $\Delta p / p_{\mathrm{R}}$ in synchrotrons have a magnitude of less than 10^{-3} and this is also an upper limit for the relative deviations in energy and velocity (cf. (B.7)). For this reason, the aforementioned approximations can be regarded as sufficiently accurate. It has to be noted that this would be different if the transition energy would be crossed. In this case, the frequency of the synchrotron oscillation becomes zero for all particles and nonlinear terms of the momentum compaction have to be taken into account [51, 126].

Different versions of the longitudinal equations exist, some are valid for certain accelerator classes only. An early literature survey on this topic can be found in [41]. In this survey, Hereward acknowledges that the process of acceleration in a synchrotron is in fact a discrete one. Another interesting reference is [9, p.24], where a ring accelerator is used as an example of inherently sampled systems. The early paper of Courant and Snyder [22] about the theory of the alternating-gradient synchrotron presents continuous longitudinal equations that are said to be accurate to first order in ΔW. These equations are in agreement with the derived (2.33a) and (2.33b) for $k_{\mathrm{RF}} = 0$. Courant and Snyder also include the additional frequency error term $\omega_1 = \dot{\varphi}_{\mathrm{f}}$. In [43, 136, 137], longitudinal differential equations are given that are equivalent to (2.39) and thus set $k_{\mathrm{RF}} = 1$. However, since during a normal acceleration cycle considerable care is taken to achieve an adiabatic process by assuring that φ_{R} changes only slowly, the difference due to k_{RF} is negligible in most cases.

The mapping equations (2.29) are almost equivalent to those used in the computer program ESME [85]. One difference is that in [85], the azimuthal angle $\theta_k = \varphi_k / h$ is used instead of φ_k. In addition, the equations in ESME do not need approximation (2.19) and are therefore exact mapping equations. However, they are only useful for simulation

purposes and are not readily accessible for further analytical calculations. And, as already stated, the difference due to (2.19) is usually negligible. Another computer simulation package for longitudinal dynamics is LONG1D [62, 63]. The mapping equations used in LONG1D use approximation (2.19) and are equivalent to (2.29) for $\varphi_\mathrm{f} = 0$ and $k_\mathrm{RF} = 1$.

The solutions of the discrete mapping equations and the continuous equations (2.30) are very similar for a large ratio $T_\mathrm{syn}/T_\mathrm{R} \gg 1$, i. e. for small synchrotron tunes $\nu_\mathrm{syn} = \omega_\mathrm{syn}/\omega_\mathrm{R} \ll 1$. For simulations with $T_\mathrm{syn}/T_\mathrm{R} < 100$, the discrete and continuous equations show a slightly different behavior [25], i. e. the discretization effects become visible. For example, the particle trajectories in phase space are tilted if discrete mapping equations are used [63]. As a consequence the particle trajectories are no longer exactly symmetric to the ΔW-axis. This effect is also reported in [62] and explained quantitatively in [61]. The effect is small, but should be considered if the synchrotron tune is small and a matched bunch is to be injected in the ring. If the tilt is not allowed for, this will result in filamentation and emittance growth.

2.3 Single Harmonic RF

2.3.1 Introductory Remarks

Due to the sinusoidal shape of the RF voltage, areas with similar stability properties are repeated periodically along the longitudinal axis. More specifically, h stable areas are formed along the synchrotron ring, where $h \in \mathbb{N}$ is the harmonic number. These stable areas are called *buckets*, as they can be used to capture bunches of particles and accelerate them. The particles of each bunch perform synchrotron oscillations around the stable fixed point of their bucket. The dynamics of these oscillations are described by (2.40) and have been analyzed thoroughly in literature. These longitudinal particle dynamics are similar to those of the nonlinear pendulum with periodic fixed points and areas in phase space of stable and unstable oscillations with an eye-shaped separatrix. The motion inside the separatrix corresponds to a librating pendulum with a small momentum whereas the motion outside corresponds to a rotating pendulum with a large momentum.

Although formulas for the particle trajectories can be found in literature, they are derived in the following for several reasons. First, the notations used in literature are heterogeneous and the formulas are spread over different references, and this thesis is intended to be self-contained for readers with a control engineering background. Second, a special normalization is needed to build models that can be used for control design. The third reason is that many of the derived formulas will be needed in the subsequent chapters.

2.3.2 Trajectory Properties

In the following, the index k of $\Delta\varphi_k$ will be omitted, as trajectories of a single particle are considered. For a subsequent controller design, it is convenient to choose the coordinates of the phase space in such a way that the resulting trajectories are circles, at least in the

linear regime of the bucket. This can be achieved by the longitudinal coordinates[5)]

$$\Delta\varphi = \varphi - \varphi_\mathrm{R}, \qquad \Delta w = -\frac{1}{\omega_\mathrm{syn}}\Delta\dot{\varphi}, \tag{2.41}$$

as this choice leads with (2.39) and $\varphi_\mathrm{f} = 0$ to the nonlinear dynamics

$$\Delta\dot{\varphi} = -\omega_\mathrm{syn}\Delta w, \tag{2.42a}$$

$$\Delta\dot{w} = \frac{\omega_\mathrm{syn}}{\cos\varphi_\mathrm{R}}\left[\sin(\varphi_\mathrm{R}+\Delta\varphi) - \sin\varphi_\mathrm{R}\right]. \tag{2.42b}$$

These dynamics are valid below and above transition and, due to the normalization of the coordinates, the direction of the flow is equal for both cases.

For small amplitudes $\Delta\varphi$, the approximation of first order is

$$\Delta\dot{\varphi} = -\omega_\mathrm{syn}\Delta w, \quad \Delta\dot{w} = \omega_\mathrm{syn}\Delta\varphi, \tag{2.43}$$

with the solution

$$\Delta\varphi(t) = \Delta\hat{\varphi}\cos(\omega_\mathrm{syn}t + \Theta_0), \quad \Delta w(t) = \Delta\hat{w}\sin(\omega_\mathrm{syn}t + \Theta_0).$$

The coordinate Δw is not canonically conjugate with respect to $\Delta\varphi$ and the phase space $(\Delta\varphi, \Delta w)$ can therefore not be used for particle tracking simulations if the beam is accelerated. Although the equations of motion are not canonical, a Hamiltonian will be constructed and used to analyze the system. The following calculations are with the implicit understanding that the equations and the Hamiltonian should only be used to analyze the beam dynamics during a short time of a few synchrotron periods T_syn or to design feedback controllers. They should not be used to simulate a complete acceleration cycle of the beam. The trajectories of the phase space $(\Delta\varphi, \Delta w)$ can be converted to the canonical phase space $(\Delta\tau, \Delta W)$ with

$$\Delta\varphi = \omega_\mathrm{RF}\,\Delta\tau, \qquad \Delta w = \frac{\omega_\mathrm{RF}[-\eta_\mathrm{R}]}{\omega_\mathrm{syn}\beta_\mathrm{R}^2 W_\mathrm{R}}\Delta W. \tag{2.44}$$

This follows from the definition of Δw and Equations (2.33b) and (2.38) with $k_\mathrm{RF} = 1$, $\dot{\varphi}_\mathrm{f} = 0$. With coordinate transformations of the form $\Delta\varphi = a\,\Delta\tau$ and $\Delta w = b\,\Delta W$, the Hamiltonian in the new coordinates is given by $\tilde{H} = abH$. For the special case of canonical transformations, $ab = 1$ and the Hamiltonian is preserved. With the original Hamiltonian $H(\tau,\Delta W)$ from (2.32), the Hamiltonian for the dynamics (2.42) is given by

$$\begin{aligned}\tilde{H}(\Delta\varphi, \Delta w) &= \frac{\omega_\mathrm{RF}^2[-\eta_\mathrm{R}]}{\omega_\mathrm{syn}\beta_\mathrm{R}^2 W_\mathrm{R}} H(\tau(\Delta\varphi), \Delta W(\Delta w)) = \tilde{T}(\Delta w) + \tilde{V}(\Delta\varphi) \\ &= -\frac{\omega_\mathrm{syn}}{2}\Delta w^2 - \frac{\omega_\mathrm{syn}}{\cos\varphi_\mathrm{R}}\left[\cos\varphi_\mathrm{R} - \Delta\varphi\sin\varphi_\mathrm{R} - \cos(\varphi_\mathrm{R}+\Delta\varphi)\right].\end{aligned} \tag{2.45}$$

[5)] The coordinate Δw is a normalized, dimensionless variable and is not an energy deviation.

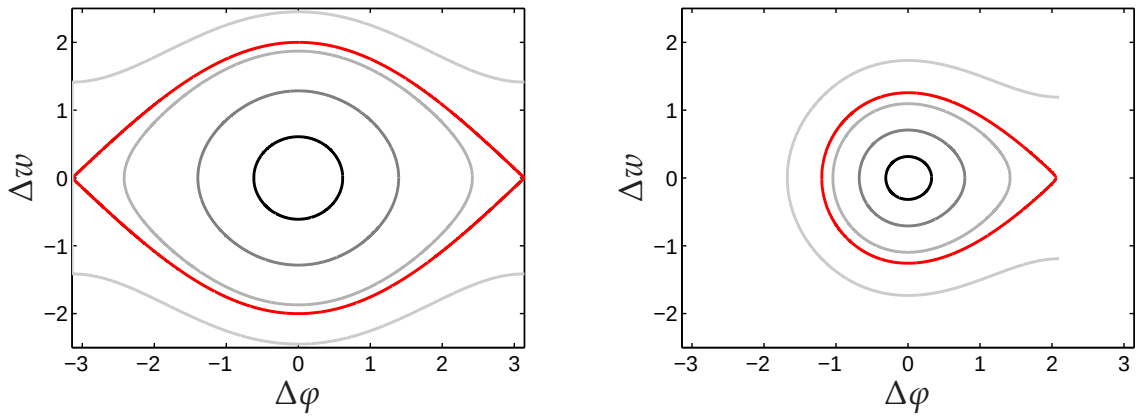

Figure 2.10: Trajectories in the longitudinal phase space $(\Delta\varphi, \Delta w)$ for a single bunch and different values $\tilde{H}$. The separatrix is highlighted in red in both diagrams and separates the stable bucket from the unstable oscillations. **Left**: stationary case $\varphi_R = 0°$ and $P \in \{0.37, 1.65, 3.5, 4, 6\}$. **Right**: acceleration with $\varphi_R = 30°$ and $P \in \{0.1, 0.5, 1.2, 1.58, 3\}$.

with the potential function $\tilde{V}(\Delta\varphi)$. The equation for a specific trajectory with given $\tilde{H}$ is obtained by solving for Δw:

$$\Delta w = \pm\sqrt{P - \frac{2}{\cos\varphi_R}\left[\cos\varphi_R - \Delta\varphi\sin\varphi_R - \cos(\varphi_R + \Delta\varphi)\right]} \tag{2.46}$$

with the constant $P = -2\tilde{H}/\omega_{syn} \geq 0$ below and above transition.

The potential $\tilde{V}$ strongly depends on φ_R. In the stationary case, we have $\varphi_R = 0$ and the accelerating reference voltage is $U_R = 0$. Figure 2.10 shows the trajectories in the phase space $(\Delta\varphi, \Delta w)$ for $\varphi_R = 0$ and $\varphi_R = 30°$. For small amplitudes, i. e. in the linear regime of the bucket, the trajectories are circles. This is also apparent from the linear approximation of the Hamiltonian $\tilde{H}$ for small $\Delta\varphi$

$$\tilde{H} \approx -\frac{\omega_{syn}}{2}[\Delta w^2 + \Delta\varphi^2] =: \tilde{H}_{lin}. \tag{2.47}$$

For larger amplitudes the trajectories flatten in the direction of Δw until they reach the separatrix. Outside the separatrix the dynamics are unstable.

In the following the intersections of the trajectories and separatrix with the axes $\Delta\varphi = 0$ and $\Delta w = 0$ will be calculated. The notation is shown in Figure 2.11. The separatrix is obtained for $P = P_{sep}$ and its intersections will be denoted by $\Delta\varphi_{sep+}$, $\Delta\varphi_{sep-}$, Δw_{sep+}, and Δw_{sep-}. Correspondingly, the intersections of the trajectory with $P < P_{sep}$ are denoted by $\Delta\varphi_+$, $\Delta\varphi_-$, Δw_+, and Δw_-.

To calculate the bucket height, the potential function $\tilde{V}(\Delta\varphi)$ is analyzed. The extremum in the interval $\Delta\varphi \in [-\pi - \varphi_R; \pi - \varphi_R]$ is obtained for $\Delta\varphi_{sep+}$ which is the

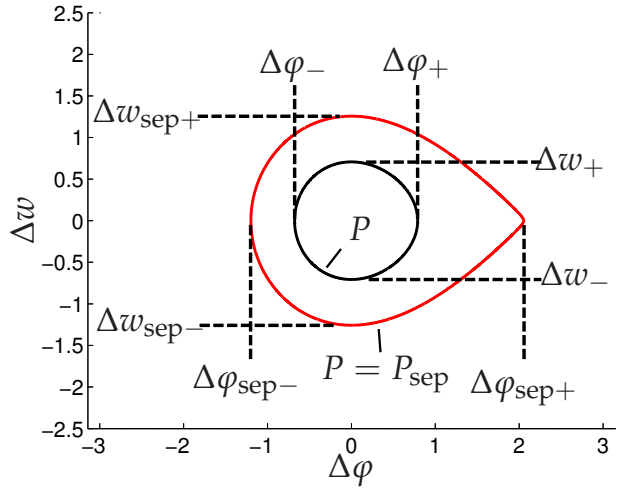

Figure 2.11: Definition of the intersections of a trajectory and the separatrix with the $\Delta\varphi$- and Δw-axis.

limit of the stable area. The condition $\mathrm{d}\tilde{V}/\mathrm{d}\Delta\varphi = 0$ leads to $\sin\varphi_\mathrm{R} = \sin(\varphi_\mathrm{R} + \Delta\varphi)$ and thus to the trivial solution $\Delta\varphi = 0$ and the solution

$$\Delta\varphi_{\mathrm{sep}+} = \pi - 2\varphi_\mathrm{R}. \tag{2.48}$$

The value of the Hamiltonian of the separatrix is obtained for $\Delta\varphi = \Delta\varphi_{\mathrm{sep}+}$ and $\Delta w = 0$:

$$\tilde{H}_\mathrm{sep} = \omega_\mathrm{syn}\left[[\pi - 2\varphi_\mathrm{R}]\tan\varphi_\mathrm{R} - 2\right] \quad \Rightarrow \quad P_\mathrm{sep} = 4 - 2[\pi - 2\varphi_\mathrm{R}]\tan\varphi_\mathrm{R}.$$

This leads to the values $P_\mathrm{sep} = 4$ for the stationary case and $P_\mathrm{sep} = 1.5816$ for the acceleration case with $\varphi_\mathrm{R} = 30°$ in Figure 2.10.

For a trajectory within the separatrix, the intersections can be calculated depending on P. However, for the models in the next chapters it will be more convenient to derive the values as functions of the amplitude

$$\Delta\varphi_+ \in [0;\ \Delta\varphi_{\mathrm{sep}+}] = [0;\ \pi - 2\varphi_\mathrm{R}].$$

For the intersection $(\Delta\varphi_+,0)$, Equation (2.46) leads to

$$P = \frac{2}{\cos\varphi_\mathrm{R}}\left[\cos\varphi_\mathrm{R} - \cos(\varphi_\mathrm{R} + \Delta\varphi_+) - \Delta\varphi_+\sin\varphi_\mathrm{R}\right]. \tag{2.49}$$

For the lower intersection $\Delta w = 0$ and $\Delta\varphi = \Delta\varphi_-$ we have

$$P = \frac{2}{\cos\varphi_\mathrm{R}}\left[\cos\varphi_\mathrm{R} - \cos(\varphi_\mathrm{R} + \Delta\varphi_-) - \Delta\varphi_-\sin\varphi_\mathrm{R}\right]. \tag{2.50}$$

Using (2.49) in (2.50) yields

$$\Delta\varphi_-\sin\varphi_\mathrm{R} + \cos(\varphi_\mathrm{R} + \Delta\varphi_-) = \Delta\varphi_+\sin\varphi_\mathrm{R} + \cos(\varphi_\mathrm{R} + \Delta\varphi_+). \tag{2.51}$$

This equation can be solved analytically only for the stationary case $\varphi_\mathrm{R} = 0$, in which case $\Delta\varphi_- = -\Delta\varphi_+$, i. e. the trajectories are symmetric to the axis $\Delta\varphi = 0$. In general the equation has to be solved numerically with the constraint $\Delta\varphi_- = -\Delta\varphi_+ < 0$ as a possible initial value.

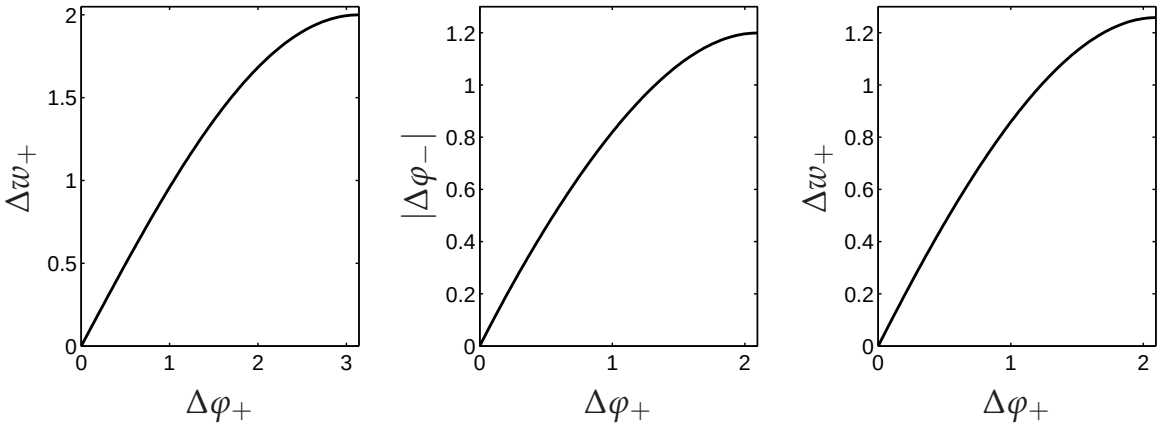

Figure 2.12: Intersections of the trajectories in coordinates $(\Delta\varphi, \Delta w)$. **Left**: Equation (2.54) and $\varphi_R = 0$. **Center**: Equation (2.51) and acceleration with $\varphi_R = 30°$. **Right**: Equation (2.53) and acceleration with $\varphi_R = 30°$.

Using $\Delta\varphi = 0$ and $\Delta w = \Delta w_+$ or $\Delta w = \Delta w_-$ in (2.46) yields

$$P = \Delta w_+^2 = \Delta w_-^2 \quad \Rightarrow \quad \Delta w_- = -\Delta w_+, \tag{2.52}$$

i. e. the trajectories are symmetric with respect to $\Delta w = 0$. Inserting (2.52) in (2.49) leads to

$$\Delta w_+ = \sqrt{\frac{2}{\cos\varphi_R}}\sqrt{\cos\varphi_R - \Delta\varphi_+ \sin\varphi_R - \cos(\varphi_R + \Delta\varphi_+)}. \tag{2.53}$$

The height of the seperatrix is obtained for $\Delta\varphi_+ = \Delta\varphi_{sep+} = \pi - 2\varphi_R$ and equals

$$\Delta w_{sep+} = \sqrt{4 - 2[\pi - 2\varphi_R]\tan\varphi_R}.$$

For the stationary case $\varphi_R = 0$, the simple equation

$$\Delta w_+ = \sqrt{2 - 2\cos(\Delta\varphi_+)} \tag{2.54}$$

is obtained and $\Delta w_{sep+} = 2$. Figure 2.12 shows the intersections for the stationary case with $\varphi_R = 0$ and the acceleration case with $\varphi_R = 30°$.

2.3.3 Bucket and Bunch Area

As mentioned before, the term *bucket* denotes the stable area in phase space and *bunch* denotes the particle ensemble. The trajectory equation in the bucket has already been

obtained in (2.46), inserting (2.49) yields the trajectory as a function of the maximum phase $\Delta\varphi_+$

$$\Delta w = \pm\sqrt{\frac{2}{\cos\varphi_\mathrm{R}}}\sqrt{\cos(\varphi_\mathrm{R}+\Delta\varphi)-\cos(\varphi_\mathrm{R}+\Delta\varphi_+)+[\Delta\varphi-\Delta\varphi_+]\sin\varphi_\mathrm{R}}.$$

Due to symmetry, the area circumscribed by the trajectory equals the integral

$$A_\mathrm{bunch}(\Delta\varphi_+,\varphi_\mathrm{R}) = 2\int_{\Delta\varphi_-}^{\Delta\varphi_+}\Delta w\left(\Delta\varphi,\Delta\varphi_+,\varphi_\mathrm{R}\right)\,\mathrm{d}\Delta\varphi, \tag{2.55}$$

with $\Delta\varphi_+ \in [0;\ \pi-2\varphi_\mathrm{R}]$ and $\Delta\varphi_-$ as a function of $\Delta\varphi_+$. The bucket area is obtained for $\Delta\varphi_+ = \Delta\varphi_{\mathrm{sep}+} = \pi - 2\varphi_\mathrm{R}$:

$$A_\mathrm{bucket}(\varphi_\mathrm{R}) = 2\int_{\Delta\varphi_{\mathrm{sep}-}}^{\Delta\varphi_{\mathrm{sep}+}}\Delta w\left(\Delta\varphi,\Delta\varphi_{\mathrm{sep}+},\varphi_\mathrm{R}\right)\,\mathrm{d}\Delta\varphi. \tag{2.56}$$

In the stationary case we have $\varphi_\mathrm{R}=0$, $\Delta\varphi_+ = -\Delta\varphi_-$, $\Delta\varphi_{\mathrm{sep}+}=\pi$, $P_\mathrm{sep}=4$, and the bunch area is

$$A_\mathrm{bunch,stat} = 2\int_{-\Delta\varphi_+}^{\Delta\varphi_+}\sqrt{2\left[\cos(\Delta\varphi)-\cos(\Delta\varphi_+)\right]}\,\mathrm{d}\Delta\varphi.$$

Using the relation $\cos(x) = 1-2\sin^2(x/2)$ and the substitution $\theta = \Delta\varphi/2$ yields

$$A_\mathrm{bunch,stat} = 8\int_{-\Delta\varphi_+/2}^{\Delta\varphi_+/2}\sqrt{\sin^2\left(\frac{\Delta\varphi_+}{2}\right)-\sin^2(\theta)}\,\mathrm{d}\theta.$$

As the integrand is an even function, it is sufficient to consider $\Delta\varphi_+ \in [0;\pi]$ and

$$\begin{aligned}A_\mathrm{bunch,stat} &= 16\sin\left(\frac{\Delta\varphi_+}{2}\right)\int_0^{\Delta\varphi_+/2}\sqrt{1-\frac{\sin^2(\theta)}{\sin^2(\Delta\varphi_+/2)}}\,\mathrm{d}\theta\\ &= 16\sin\left(\frac{\Delta\varphi_+}{2}\right)\,E\left(\frac{\Delta\varphi_+}{2},\csc\left(\frac{\Delta\varphi_+}{2}\right)\right),\end{aligned}$$

where $E(\varphi,\,k)$ is the incomplete elliptic integral of the second kind and $\csc(x) = \sin^{-1}(x)$. A short summary of important formulas for elliptic integrals is given in Section A.1. As $E(\pi/2,\,1)=1$, the size of the stationary bucket is

$$A_\mathrm{bucket,stat} = 16. \tag{2.57}$$

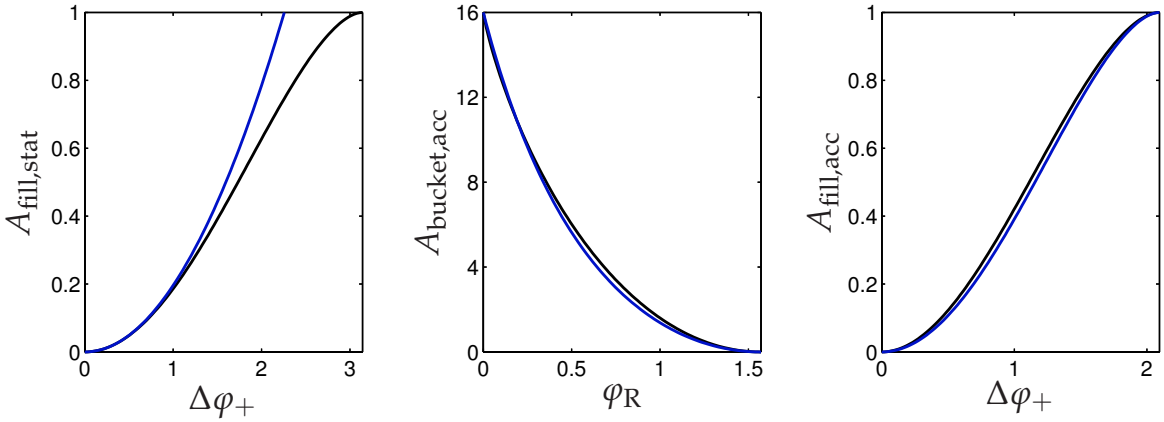

Figure 2.13: Left: stationary bucket fill factor $A_{\text{fill,stat}}$ (black) and approximation (2.59) for small bunches (blue). **Center**: bucket area for acceleration (black) and approximation (2.60) (blue). **Right**: bucket fill factor for acceleration (black) and approximation (2.61) (blue).

With (A.3) the special case $E(z, \csc(z))$ can be expressed as a combination of the complete elliptic integrals of the first and second kind $E(\,\cdot\,)$ and $K(\,\cdot\,)$ and the stationary bunch area can finally be expressed as a function of $\Delta\varphi_+$

$$A_{\text{fill,stat}}(\Delta\varphi_+) := \frac{A_{\text{bunch,stat}}}{A_{\text{bucket,stat}}} = E\left(\sin\frac{\Delta\varphi_+}{2}\right) - \cos^2\left(\frac{\Delta\varphi_+}{2}\right) K\left(\sin\frac{\Delta\varphi_+}{2}\right), \tag{2.58}$$

with the bucket fill factor $A_{\text{fill,stat}}$. For small bunches ($\Delta\varphi_+ \ll 1$) the trajectories are circles and the bunch area is approximately

$$A_{\text{bunch,stat}} \approx \pi\Delta\varphi_+^2. \tag{2.59}$$

For the acceleration case, the sizes of bucket and bunches must be calculated numerically. For example, $\varphi_R = 30^\circ$ yields $A_{\text{bucket,acc}} = 5.732$. However, the following useful approximation for the bucket size is given in [71]:

$$\frac{A_{\text{bucket,acc}}}{A_{\text{bucket,stat}}} \approx \frac{1-\sin\varphi_R}{1+\sin\varphi_R} = \frac{1-U_R/\hat{U}_1}{1+U_R/\hat{U}_1}. \tag{2.60}$$

Figure 2.13 shows the bucket and bunch areas for different configurations. The diagram on the left shows the bucket fill factor $A_{\text{fill,stat}}$ from (2.58) and the approximation (2.59). The approximation error is less than 10% for $\Delta\varphi_+ < 1.3$. The diagram in the center shows the bucket area as a function of the reference phase φ_R. The bucket area was obtained by numerical integration of (2.56). The second curve is the approximation from (2.60). The maximum relative error of the approximation is smaller than 17%. The bucket fill factor for acceleration with $\varphi_R = 30^\circ$ is shown in the right diagram. The curve

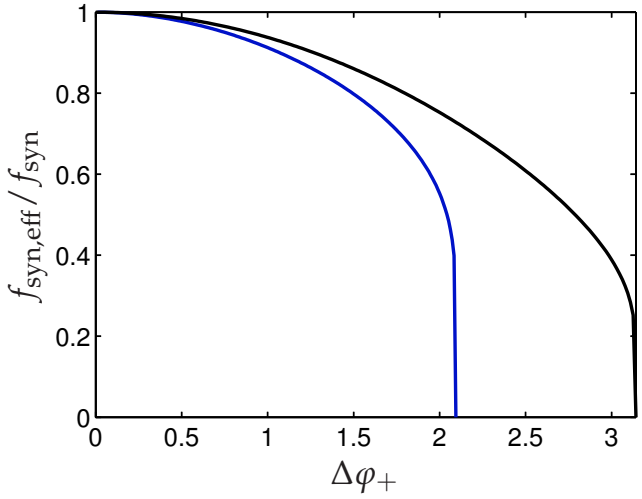

Figure 2.14: Nonlinear synchrotron frequency versus the maximum phase $\Delta\varphi_+$: stationary case (black) and acceleration with $\varphi_\mathrm{R} = 30^\circ$ (blue).

results from a numerical integration of (2.55), normalized with the solution of (2.56). The second curve is the approximation

$$A_{\mathrm{fill,acc}} = \frac{A_{\mathrm{bunch,acc}}}{A_{\mathrm{bucket,acc}}} \approx A_{\mathrm{fill,stat}} \left(\frac{\pi - 2\varphi_\mathrm{R}}{\pi} \, \Delta\varphi_+ \right), \tag{2.61}$$

which allows an excellent approximation, also for other values of $\varphi_\mathrm{R} \in [0; \frac{\pi}{2}[$.

In summary it can be concluded that it is possible to calculate the areas of bucket and bunch for the stationary case exactly with Equations (2.57) and (2.58) and for the acceleration case in good approximation with Equations (2.60) and (2.61), thereby avoiding the need for a numerical integration.

2.3.4 Nonlinear Synchrotron Frequency

An important property of the motion in the longitudinal phase space is the synchrotron frequency of the particles. It is well known that the synchrotron frequency depends on the oscillation amplitude $\Delta\varphi_+$. For larger amplitudes, the synchrotron frequency decreases, until it becomes zero at the separatrix. If a bunch comprising a large number of particles is considered, this leads to a spread in the synchrotron frequency and to effects known as *Landau damping* and *filamentation*. These effects will be considered in more detail in Chapter 3.

The synchrotron frequency in the linear regime, i. e. for small amplitudes, is given by (2.38) and is denoted by ω_syn. In the following, the more general synchrotron frequency in the nonlinear regime will be denoted by $\omega_{\mathrm{syn,eff}}(\Delta\varphi_+)$. It is a function of the maximum phase $\Delta\varphi_+$ of the trajectory. In addition the following relations hold:

$$f_{\mathrm{syn,eff}}/f_\mathrm{syn} = \omega_{\mathrm{syn,eff}}/\omega_\mathrm{syn} = T_\mathrm{syn}/T_{\mathrm{syn,eff}}.$$

There are different ways to derive the nonlinear synchrotron frequency [43, 57, 71]. One possibility is the multiplication of (2.40) with $2\Delta\dot{\varphi}/\omega_{\mathrm{syn}}^2$, which leads to

$$\frac{2\Delta\ddot{\varphi}\Delta\dot{\varphi}}{\omega_{\mathrm{syn}}^2} + \frac{2\Delta\dot{\varphi}}{\cos\varphi_{\mathrm{R}}}\left[\sin(\varphi_{\mathrm{R}}+\Delta\varphi) - \sin\varphi_{\mathrm{R}}\right] = 0,$$

and subsequent integration over t, yielding

$$\left[\frac{\Delta\dot{\varphi}}{\omega_{\mathrm{syn}}}\right]^2 - \frac{2}{\cos\varphi_{\mathrm{R}}}\left[\Delta\varphi\sin\varphi_{\mathrm{R}} + \cos(\varphi_{\mathrm{R}}+\Delta\varphi) - \cos\varphi_{\mathrm{R}}\right] = P$$

with the integration constant P. Because of $\Delta\dot{\varphi} = \frac{\mathrm{d}\Delta\varphi}{\mathrm{d}t}$, this equation can be rewritten as

$$\mathrm{d}t = \pm\frac{\mathrm{d}\Delta\varphi}{\omega_{\mathrm{syn}}\sqrt{P + \frac{2}{\cos\varphi_{\mathrm{R}}}\left[\Delta\varphi\sin\varphi_{\mathrm{R}} + \cos(\varphi_{\mathrm{R}}+\Delta\varphi) - \cos\varphi_{\mathrm{R}}\right]}}.$$

The synchrotron period follows with $T_{\mathrm{syn,eff}} = 2\pi/\omega_{\mathrm{syn,eff}} = 2\int_0^{T_{\mathrm{syn,eff}}/2}\mathrm{d}t$ and is obtained by integration of both sides, leading to

$$T_{\mathrm{syn,eff}} = 2\int_{\Delta\varphi_-}^{\Delta\varphi_+}\frac{\mathrm{d}\Delta\varphi}{\omega_{\mathrm{syn}}\sqrt{P + \frac{2}{\cos\varphi_{\mathrm{R}}}\left[\Delta\varphi\sin\varphi_{\mathrm{R}} + \cos(\varphi_{\mathrm{R}}+\Delta\varphi) - \cos\varphi_{\mathrm{R}}\right]}}.$$

Using (2.49) and $\omega_{\mathrm{syn}} = 2\pi/T_{\mathrm{syn}}$ leads to the ratio of the nonlinear to the linear synchrotron period

$$\frac{T_{\mathrm{syn,eff}}}{T_{\mathrm{syn}}} = \int_{\Delta\varphi_-}^{\Delta\varphi_+}\frac{\frac{\sqrt{\cos\varphi_{\mathrm{R}}}}{\pi\sqrt{2}}\mathrm{d}\Delta\varphi}{\sqrt{[\Delta\varphi-\Delta\varphi_+]\sin\varphi_{\mathrm{R}} + \cos(\varphi_{\mathrm{R}}+\Delta\varphi) - \cos(\varphi_{\mathrm{R}}+\Delta\varphi_+)}}. \quad (2.62)$$

In the stationary case it is possible to write the synchrotron period as an elliptic integral. The equation for $T_{\mathrm{syn,eff}}$ reduces to

$$\frac{T_{\mathrm{syn,eff}}}{T_{\mathrm{syn}}} = \frac{1}{\pi\sqrt{2}}\int_{-\Delta\varphi_+}^{\Delta\varphi_+}\frac{\mathrm{d}\Delta\varphi}{\sqrt{\cos(\Delta\varphi) - \cos(\Delta\varphi_+)}}.$$

Inserting the relation $\cos x = 1 - 2\sin^2(x/2)$, substituting $\theta = \Delta\varphi/2$ and considering that the integrand is an even function yields

$$\frac{T_{\mathrm{syn,eff}}}{T_{\mathrm{syn}}} = \frac{2}{\pi\sin\left(\frac{\Delta\varphi_+}{2}\right)}\int_0^{\Delta\varphi_+/2}\frac{\mathrm{d}\theta}{\sqrt{1-\frac{\sin^2\theta}{\sin^2\left(\frac{\Delta\varphi_+}{2}\right)}}} \overset{(A.1)}{=} \frac{2F\left(\frac{\Delta\varphi_+}{2}, \csc\left(\frac{\Delta\varphi_+}{2}\right)\right)}{\pi\sin\left(\frac{\Delta\varphi_+}{2}\right)},$$

where $F(\,\cdot\,)$ denotes the elliptic integral of the first kind as defined in Appendix A.1. This incomplete elliptic integral can be rewritten [57, 71]. Using Equation (A.2) leads to

$$\frac{T_{\mathrm{syn,eff}}}{T_{\mathrm{syn}}} = \frac{2}{\pi} K\left(\sin\frac{\Delta\varphi_+}{2}\right) \quad \Rightarrow \quad \frac{f_{\mathrm{syn,eff}}}{f_{\mathrm{syn}}} = \frac{\pi}{2K\left(\sin\frac{\Delta\varphi_+}{2}\right)}, \tag{2.63}$$

where $K(k)$ denotes the complete elliptic integral of the first kind. Figure 2.14 shows the synchrotron frequency for the stationary and for the acceleration case.

2.4 Acceleration Cycle

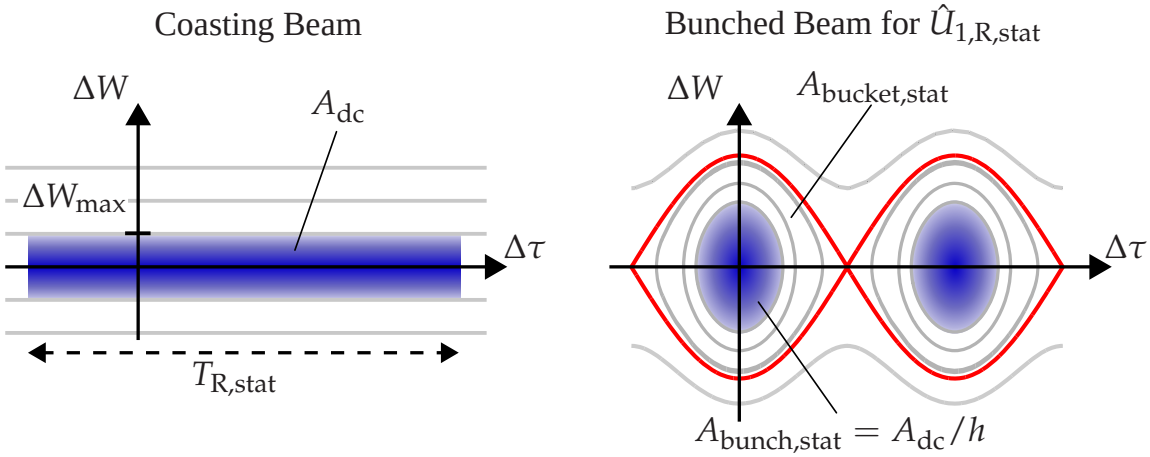

Figure 2.15: Bunching of a coasting beam. **Left**: coasting beam with area A_{dc} and $\hat{U}_1 = 0$. **Right**: bunched beam after increasing the voltage to $\hat{U}_1 = \hat{U}_{\mathrm{R,1,stat}}$.

There are two different scenarios of how a beam is injected into the synchrotron. The first possibility is to inject an already bunched beam into the ring. In this case the RF voltage of the ring is already switched on and special care has to be taken to ensure that the bunches are injected with a compatible phase and shape. Otherwise, filamentation will increase the emittance of the beam.

The second possibility is to fill the ring with a *coasting beam*, i. e. an unbunched stream of particles, while the RF voltage is almost zero. The beam can then be captured and bunched by ramping up the RF voltage amplitude slowly. If this is done slowly enough, the transition can be regarded as adiabatic and the emittances are approximately preserved. In this case, the necessary RF voltage amplitude can be calculated which is needed to obtain a certain bucket filling factor A_{fill}. In the following, this is demonstrated for a coasting beam with a homogeneous distribution. Specifications for the ramping in the accelerator chain SIS12/18 to SIS100 of GSI can be found in [48].

The bunching process of the beam is a stationary one ($\varphi_{\mathrm{R}} = 0$) and its quantities will be denoted by the additional index *stat* in the following. Assume as a coasting beam a bar

of particles in the phase space with a given momentum spread $[\Delta p/p_\mathrm{R}]_\mathrm{max}$ as shown in Figure 2.15. In coordinate ΔW, this is equal to the maximum energy spread

$$\Delta W_\mathrm{max} = \beta^2_\mathrm{R,stat} W_\mathrm{R,stat} \left[\frac{\Delta p}{p_\mathrm{R,stat}}\right]_\mathrm{max}$$

and because the length of the ring in coordinate $\Delta\tau$ is $T_\mathrm{R,stat}$, the area occupied by the coasting beam in the phase space $(\Delta\tau,\Delta W)$ is (cf. Figure 2.15)

$$A_\mathrm{dc} = T_\mathrm{R,stat} \cdot 2\Delta W_\mathrm{max} = 2T_\mathrm{R,stat}\beta^2_\mathrm{R,stat} W_\mathrm{R,stat} \left[\frac{\Delta p}{p_\mathrm{R,stat}}\right]_\mathrm{max}.$$

The area of a stationary bucket in coordinates $(\Delta\varphi, \Delta w)$ equals 16 and using (2.44) yields the bucket area in $(\Delta\tau,\Delta W)$

$$A_\mathrm{bucket,stat} = 16\frac{\omega_\mathrm{syn,stat}\beta^2_\mathrm{R,stat} W_\mathrm{R,stat}}{\omega^2_\mathrm{RF,stat}[-\eta_\mathrm{R,stat}]} = \frac{16}{h}\sqrt{\frac{Q\hat{U}_\mathrm{1,R,stat}\beta^2_\mathrm{R,stat} W_\mathrm{R,stat}}{2\pi h|\eta_\mathrm{R,stat}|\omega^2_\mathrm{R,stat}}}.$$

If necessary the fill factor $A_\mathrm{fill,stat} = A_\mathrm{bunch,stat}/A_\mathrm{bucket,stat}$ after the bunching is given, the necessary voltage $\hat{U}_\mathrm{1,R,stat}$ to achieve this can be calculated. Using the fact that the area A_dc is divided into h bunches, i. e. $A_\mathrm{bunch,stat} = A_\mathrm{dc}/h$, the voltage is

$$\hat{U}_\mathrm{1,R,stat} = \frac{\pi^3 h\beta^2_\mathrm{R,stat} W_\mathrm{R,stat}|\eta_\mathrm{R,stat}|}{8QA^2_\mathrm{fill,stat}} \left[\frac{\Delta p}{p_\mathrm{R,stat}}\right]^2_\mathrm{max}.$$

During acceleration the amplitude $\hat{U}_\mathrm{1,R}$ is usually adapted such that the bucket area is kept constant. If $\hat{U}_\mathrm{1,R}$ would not be changed, the bucket area would be increased during the acceleration and this would have to be an adiabatic transition to avoid emittance blow-up. The condition for a constant bucket area can be obtained with approximation (2.60) for the bucket area during acceleration

$$A_\mathrm{bucket,acc} \approx \frac{1 - U_\mathrm{R}/\hat{U}_\mathrm{1,R}}{1 + U_\mathrm{R}/\hat{U}_\mathrm{1,R}}\frac{16}{h}\sqrt{\frac{Q\hat{U}_\mathrm{1,R}\beta^2_\mathrm{R} W_\mathrm{R}}{2\pi h|\eta_\mathrm{R}|\omega^2_\mathrm{R}}}$$

and the condition for a constant bucket area $A_\mathrm{bucket,acc} \stackrel{!}{=} A_\mathrm{bucket,stat}$ leads to

$$\hat{U}_\mathrm{1,R}\left[\frac{\hat{U}_\mathrm{1,R} - U_\mathrm{R}}{\hat{U}_\mathrm{1,R} + U_\mathrm{R}}\right]^2 = \hat{U}_\mathrm{1,R,stat}\,\frac{|\eta_\mathrm{R}| W_\mathrm{R,stat}\beta^2_\mathrm{R,stat}\omega^2_\mathrm{R}}{|\eta_\mathrm{R,stat}| W_\mathrm{R}\beta^2_\mathrm{R}\omega^2_\mathrm{R,stat}}. \tag{2.64}$$

Solving this equation for $\hat{U}_\mathrm{1,R} > U_\mathrm{R}$ provides the necessary RF amplitude during the acceleration to keep the bucket area constant.

To start the acceleration, the reference magnetic field B_R that is provided by the central control system is raised and the frequency ω_RF is synchronously increased. This automatically changes the reference point φ_R, because a positive voltage $U_\mathrm{R} = \hat{U}_\mathrm{1,R}\sin\varphi_\mathrm{R}$ is now needed for a particle to catch up with the increasing frequency.

2.5 Conclusion

The chapter begins with a recapitulation of the longitudinal single-particle dynamics in heavy-ion synchrotrons. A derivation of the mapping equations has been presented and the synchrotron has been discussed. The theory is not new, but has been developed in a consistent way that is suitable for the later chapters. A comparison with the dynamics used in computer simulation packages ESME and LONG1D has shown that there are subtle differences depending on the assumptions made during the derivation of the longitudinal equations of motion. Next, continuous equations have been deduced from the mapping equations and the incoherent synchrotron oscillation of the individual particles has been described. This theory is described in more detail in references such as [71]. It has been reviewed to obtain a consistent notation in the thesis. The focus of the longitudinal motion has been on low-current beams; effects such as beam loading or space-charge (cf. [100] and [19]) were not included explicitly, but are regarded as disturbances acting on the RF feedback.

In the subsequent chapters, the following notation will be used:

- **Nonlinear bucket**: this will be used to signify that the respective analysis or simulation is based on the original nonlinear single-particle dynamics such as (2.35).
- **Linear bucket**: this implies that linearized dynamics are used, i. e. the RF potential is linearized as in (2.36).

3 Coherent Longitudinal Beam Oscillations

A particle beam in a synchrotron ring is an ensemble of a large number of particles. It is thus not only interesting to describe the single-particle dynamics, as has been done in the last chapter, but also to model the behavior and properties of the beam, in particular its shape. Section 3.1 reviews the concept of coherent bunch oscillations. Because the single-particle dynamics are Hamiltonian dynamics, Liouville's theorem applies, which is reviewed in Section 3.2. This also provides Liouville's equation that describes the evolution of the particle density in phase space. Important beam properties are introduced in Section 3.3 and a definition of the ideal bunch shape is given. Different density functions to describe small mismatches from this ideal shape are presented in Section 3.4. Finally, in Section 3.5 important relations are derived to describe the coherent bunch oscillations in the frequency domain.

3.1 Introduction

3.1.1 Sources of Disturbances

An ideal accelerator would have perfect guiding and accelerating fields and there would be no interactions between the beam and the surrounding walls of the beam pipe. For this ideal accelerator, there would be no need for any kind of feedback loop or correction. Particles with deviations from the reference would perform stable synchrotron oscillations in the longitudinal phase plane according to the phase stability principle. The equivalent in the transverse planes would be stable betatron oscillations. However, a charged particle beam in a real accelerator is exposed to several disturbances. Examples of such disturbances in the RF components are fluctuations and errors of higher order of the magnetic fields, noise in the frequency generator and ripple in the RF power amplifiers and phase and amplitude errors in the accelerating gap voltage [12].

In addition, for larger beam currents, the electromagnetic fields that are generated by the beam are no longer negligible and they will interact with the beam environment, i. e. with the surrounding walls of the vacuum chamber (i. e. the beam pipe) and accelerator components such as the accelerating cavity. A standard reference and introduction to these *collective effects* is [19]. Among others, there are three important effects that depend on the beam current.

First, the charged particle beam will induce so called *wake fields* due to the resistivity of the wall of the vacuum chamber or changes of its geometry. These wake fields may act back on the beam and destabilize it. The calculation of the wake fields is related to the concept of *impedances*, which are their counterpart in the frequency domain. Typically,

low impedances are desirable as they are equivalent to low induced voltages and thus low interactions of the beam with its surroundings.

A second effect in case of large beam currents is referred to as *space charge effects* [20, p.128], [136]. As the beam consists of particles with the same charge, the repulsing Coulomb forces between them will defocus the beam. This is relevant in particular for large particle densities and for low and medium beam energies. For large beam energies, the particle velocities are ultra-relativistic and the electric field around each particle is Lorentz contracted to a disc. Thus, the influence on the other particles of the bunch is weakened for high energies and space charge effects are relevant mainly for lower energies.

The third effect is called *beam loading* and occurs in resonant structures such as the RF cavity. The current of the beam induces a voltage inside these structures. This induced voltage is damped with a certain time constant which depends on the quality characteristics of the cavity. If a significant fraction of the induced voltage is still present when the same or the next bunch arrives at the cavity, this beam loading will have an impact on the beam stability.

In a circular accelerator such as the synchrotron, every disturbance can accumulate over many turns and lead to an inferior beam quality or in more severe cases to beam instabilities. In the machine design the described effects can be taken into account and the components of the accelerator can be optimized with respect to the stability of the beam. This passive approach leads to low impedances in the ring. However, there are also active measures to increase the beam stability: feedback control loops. In many cases, there is no alternative to feedback. For example, disturbances in the RF voltage can only be compensated by feedback. Furthermore, the beam itself has to be controlled by feedback, since there may be mismatches in the beam shape because of external disturbances or imperfections in the injection. These mismatches always lead to filamentation of the beam and to a dilution of the particle density, thus to a decreasing beam quality, as will be shown in this chapter.

The following sections will focus on beam shape mismatches in the longitudinal phase space and review the concept of longitudinal single-bunch oscillation modes.

3.1.2 Coherent Oscillations

As discussed in the previous chapter, the sinusoidal RF voltage creates h areas in the longitudinal direction called buckets. Inside these buckets the particles perform a stable synchrotron oscillation around the reference such that they can be accelerated. In the presence of a RF voltage, the beam is not uniformly distributed along the ring, but divided in particle ensembles called bunches. Not every bucket has to be filled with a bunch, but every bunch has to be inside a bucket, or else it will be lost during acceleration. The particle number of a bunch can vary by several orders of magnitude between different accelerators or experiments. Typical numbers are in the range of 10^9 to 10^{11} [48, 105] but can even be considerably higher [71]. If a rather low particle density is assumed, the interactions between the particles inside the bunch are negligible and the beam may be regarded as a collisionless plasma [80]. In this case the particles describe independent

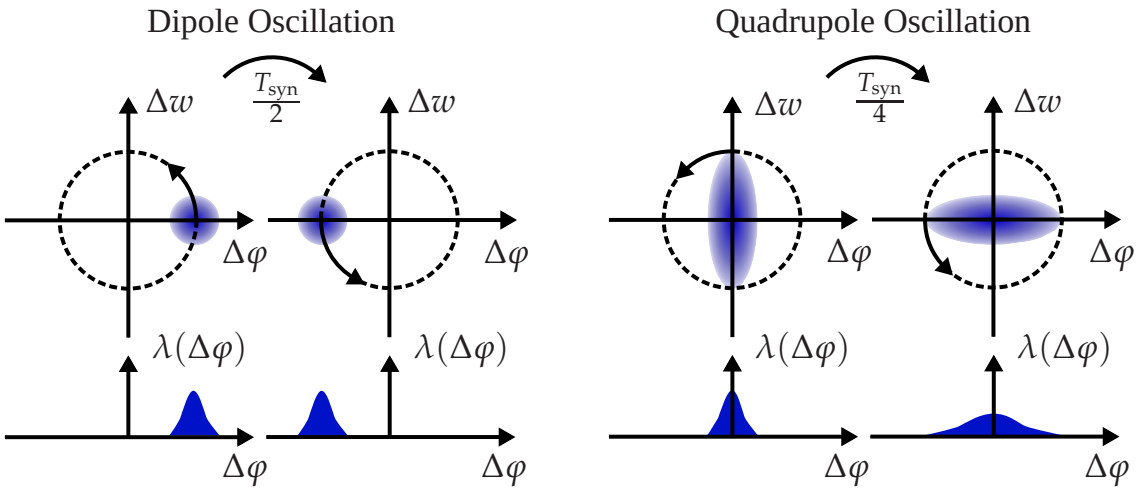

Figure 3.1: Phase space configurations and line densities for two beam shape oscillations. A small bunch is assumed, all particles have approximately the same synchrotron frequency. **Left**: coherent dipole oscillation at the time $t = 0$ and $t = T_{\mathrm{syn}}/2$. **Right**: coherent quadrupole oscillation at the time $t = 0$ and $t = T_{\mathrm{syn}}/4$.

synchrotron oscillations and the evolution of the bunch shape only depends on the initial configuration of the bunch. In the following, the oscillations of the bunch shape will be referred to as longitudinal single-bunch oscillations or simply as *coherent oscillations*.

A simple example of a coherent oscillation is a bunch whose particles have a similar phase. This is shown on the left of Figure 3.1. A linear bucket is assumed for the sake of simplicity. The initial particle bunch is off-center and after half a synchrotron period $T_{\mathrm{syn}}/2$, all particles have made half a synchrotron oscillation in phase space and thus the bunch shape is rotated by 180°. After one complete synchrotron period, the bunch returns to its initial configuration. This coherent oscillation is called *dipole mode* and its frequency is obviously ω_{syn}. The *line charge density distribution* or *line density* $\lambda(\Delta\varphi)$ is also shown in Figure 3.1, it is the projection of the phase space upon the axis $\Delta\varphi$ and proportional to the beam current of the bunch.[1)] The shape of the line density remains the same, only its center of gravity oscillates with the frequency ω_{syn}. A further coherent oscillation is the *quadrupole mode* as shown on the right of Figure 3.1. This configuration can be simply thought of as a bunch where every particle has a counterpart with a phase difference of the synchrotron oscilllation of 180°, in contrast to the dipole mode where all particles are in-phase. After $T_{\mathrm{syn}}/2$, this initial bunch distribution is repeated, leading to a coherent oscillation frequency of $2\omega_{\mathrm{syn}}$. The line density is centered, but oscillates in amplitude and width.

It is possible to construct an initial bunch configuration where there are no coherent oscillations at all. As a simple example, the particle density inside the bunch is assumed to be uniform, i. e. constant. If the bunch is small, the particle trajectories are approximately circles in the phase space. Thus, choosing the bunch as a centered circle will lead to a *matched bunch*, i. e. a bunch that will not perform any coherent oscillations, although

[1)] A more detailed description of the beam current follows in Section 3.3.3.

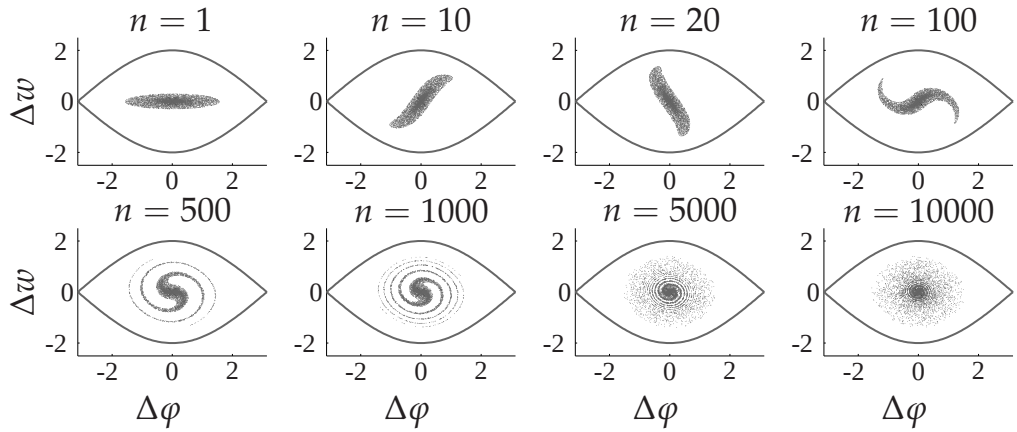

Figure 3.2: Filamentation of a mismatched bunch at turn n in the longitudinal phase space. This leads to a larger bunch area (emittance) and to a diluted particle density.

the particles perform synchrotron oscillations. If a more general density is assumed, it is plausible that the initial bunch has to be rotationally symmetric to be matched.

For larger bunches, the particle trajectories become considerably nonlinear and it is more difficult to find a matched configuration. But similar to the linear case, a necessary and sufficient condition is that the particle density must be constant. If this is fulfilled, the particles can move along the trajectories leaving the overall bunch density unchanged. There are two more differences for large bunches. First, there is a significant spread of synchrotron frequency among the particles of the bunch, resulting in a lower frequency of the coherent oscillations. Second, this frequency spread results in a filamentation of the bunch if any mismatch is present. This leads to a damping of the coherent oscillations called *Landau damping*. Figure 3.2 visualizes this damping for a seriously mismatched bunch. At first, the bunch performs a typical coherent quadrupole oscillation. After several synchrotron periods the bunch has filamented, the quadrupole mode disappears and the bunch is matched. The cost of this damping is a density dilution and a larger bunch area.

In a real bunch, the particle number is large and an approximation with a continuous density function is often justified. In the following sections, many analytical calculations will be based upon a density function $f(\Delta\varphi, \Delta w, t)$ that depends on the phase space coordinates and time. However, the particle number of a real bunch is always finite and this results in noise and fluctuations that can be measured. These fluctuations are exploited for example for stochastic beam cooling [16, 17, 42, 91, 96–98, 102, 129, 130].

The simulations in this work are *macro particle tracking* simulations. Similar to a real beam, a discrete number of particles is arranged in the phase space and simulated using the discrete mapping equations of the longitudinal beam dynamics. However, the particle number is only a small fraction compared to a real beam, thus each simulation particle is a macro particle representing a large number of real physical particles.

3.2 Hamiltonian Systems and Liouville's Theorem

Every system or flow that obeys Hamilton's equations for a conservative Hamiltonian (cf. (2.31), p.22) preserves the area in the $2N$ dimensional phase space. This is also known as *Liouville's theorem in Hamiltonian Dynamics* [110]. In this section, basic facts and their consequences for particle beams are reviewed. One way to prove Liouville's theorem uses the divergence theorem [24, 52, 57, 125, 134], other proofs rely on canonical transformations [65, 81]. In the following, a simple proof for the two dimensional longitudinal phase space is presented based on the divergence theorem. The generalization of the proof to the complete six dimensional phase space of longitudinal and transverse motion is similar. In general, Liouville's theorem is valid for the six dimensional phase space, but if the coupling between the transverse and longitudinal motion is negligible, it can be applied to the longitudinal phase plane [24].

A bunch with N particles obeying Hamilton's equations in the longitudinal phase space (q, p) with the Hamiltonian $H(q, p, t)$ can be described uniquely by N position and N momentum variables. Thus, the system has $2N$ degrees of freedom and the dimension $2N$. For large N it is reasonable to approximate the system with a particle density function $f(q, p, t)$. The particle number can then be obtained by an integration over the phase space. The density is usually normalized such that an integration over the complete phase space yields unity:

$$\int_{-\infty}^{\infty}\int_{-\infty}^{\infty} f(q, p, t)\,\mathrm{d}q\,\mathrm{d}p = 1.$$

Using the density function reduces the $2N$ coordinates to only two coordinates q and p since the information about the particle density is contained in f. Formally speaking, the $2N$ dimensional system is replaced by an infinite dimensional one. Another point of view is to regard the function f as the probability density and its integration over a certain region in phase space as the probability of a particle staying in this region. At each point (q, p) a velocity vector of the flow

$$\boldsymbol{v}(q, p, t) = \begin{bmatrix}\dot{q} & \dot{p}\end{bmatrix}^{\mathrm{T}} = \begin{bmatrix}\frac{\partial H}{\partial p} & -\frac{\partial H}{\partial q}\end{bmatrix}^{\mathrm{T}} \tag{3.1}$$

can be defined. Assume a start at time t_0 at an arbitrary point $(q_0,\ p_0)$ with the local density $f(q_0, p_0, t_0)$. Following the flow, the rate of change of the local density is obtained by the total derivative of f

$$\frac{\mathrm{d}f}{\mathrm{d}t} = \lim_{\Delta t \to 0}\left[\frac{f(q + \Delta q,\ p + \Delta p,\ t + \Delta t)\ -\ f(q, p,\ t)}{\Delta t}\right]$$

which can be expressed as

$$\frac{\mathrm{d}f}{\mathrm{d}t} = \frac{\partial f}{\partial t} + \frac{\partial f}{\partial q}\dot{q} + \frac{\partial f}{\partial p}\dot{p}. \tag{3.2}$$

Rewriting with the product rule yields

$$\frac{\mathrm{d}f}{\mathrm{d}t} = \frac{\partial f}{\partial t} + \frac{\partial(f\dot{q})}{\partial q} - f\frac{\partial \dot{q}}{\partial q} + \frac{\partial(f\dot{p})}{\partial p} - f\frac{\partial \dot{p}}{\partial p}. \tag{3.3}$$

Because the flow (3.1) is Hamiltonian,

$$\frac{\partial \dot{q}}{\partial q} + \frac{\partial \dot{p}}{\partial p} = \frac{\partial^2 H}{\partial p \partial q} - \frac{\partial^2 H}{\partial q \partial p} = 0$$

holds and introducing this equation in (3.3) cancels the third and fifth term on the right hand side and leads to

$$\frac{\mathrm{d}f}{\mathrm{d}t} = \frac{\partial f}{\partial t} + \frac{\partial(f\dot{q})}{\partial q} + \frac{\partial(f\dot{p})}{\partial p}. \tag{3.4}$$

The right hand side of (3.4) is a continuity equation; this can be shown as follows. We may consider a certain volume V in a general phase space. In case of the two dimensional phase space this is an area. The total change of the particle number inside this fixed volume can be calculated as

$$\frac{\mathrm{d}N_V}{\mathrm{d}t} = \lim_{\Delta t \to 0} \frac{1}{\Delta t} \left[\int_V f(q,\, p,\, t + \Delta t)\, \mathrm{d}V - \int_V f(q,\, p,\, t)\, \mathrm{d}V \right] = \int_V \frac{\partial f}{\partial t}\, \mathrm{d}V. \tag{3.5}$$

The last step of this equation assumes that the limit and integral can be interchanged (dominated convergence theorem). On the other hand, the particle number inside V can only change by the particle flux through its surface ∂V. The particle flux can be defined as the $\mathbb{R}^3 \mapsto \mathbb{R}^2$ function [57, 118]

$$\boldsymbol{J}(q,p,t) := f\, \boldsymbol{v} = \begin{bmatrix} f(q,p,t)\, \dot{q}(q,p,t) & f(q,p,t)\, \dot{p}(q,p,t) \end{bmatrix}^{\mathrm{T}}.$$

If we assume that neither particles are generated or annihilated inside V, the particle number changes only by

$$\frac{\mathrm{d}N_V}{\mathrm{d}t} = -\oint_{\partial V} \boldsymbol{J} \cdot \boldsymbol{n}\, \mathrm{d}A = -\int_V \nabla \boldsymbol{J}\, \mathrm{d}V,$$

where $\mathrm{d}A$ is an infinitesimal area element of ∂V, $\boldsymbol{n}$ is the normalized vector perpendicular to the surface ∂V and is pointing outwards of V, $\nabla(\,\cdot\,)$ is the divergence operator, and the last step uses the divergence theorem (Gauss-Ostrogradsky theorem) to write the surface integral as a volume integral. The minus sign is due to the fact that $\boldsymbol{n}$ points outwards of V. Comparing this result with (3.5) leads in differential form to the continuity equation of fluid dynamics

$$0 = \frac{\partial f}{\partial t} + \nabla \boldsymbol{J} = \frac{\partial f}{\partial t} + \frac{\partial(f\dot{q})}{\partial q} + \frac{\partial(f\dot{p})}{\partial p}$$

that is indeed (3.4) and Liouville's theorem can be written as

$$\frac{\mathrm{d}f(q,\,p,\,t)}{\mathrm{d}t} = 0.$$

One interpretation of this theorem is that the local particle density along a trajectory is preserved. This means that a certain region of the particle distribution in phase space can move and change its shape since the rate of change of the density at a fixed point (cf. (3.2))

$$\frac{\partial f}{\partial t} = -\frac{\partial f}{\partial q}\dot{q} - \frac{\partial f}{\partial p}\dot{p} \tag{3.6}$$

is not necessarily zero. The volume of the region in phase space is however preserved [44]. If q is a physical position and p a momentum, Equation (3.6) can be rewritten with $\dot{q} = p/\gamma m_0$ and $\dot{p} = F$ as the kinetic equation or *collisionless Boltzmann equation*, also called the *Vlasov equation* [139],

$$\frac{\partial f}{\partial t} + \frac{\partial f}{\partial q}\frac{p}{\gamma m_0} + \frac{\partial f}{\partial p}F(q,\,t) = 0,$$

where $F(q,\,t)$ is the force acting on the particles. The force depends on external electric and magnetic fields as well as on fields that are generated by the particles of the bunch. Considering this dependence leads to the Vlasov-Maxwell system of equations [68]. The Vlasov-Maxwell equations are a more general form to describe the dynamics of charged particle beams in accelerators but are valid for sufficiently diluted plasmas only. The assumption of a thin plasma assures that the Coulomb forces between the particles can be neglected and the approximation of the mean field can be used [80].

Liouville's theorem and the Vlasov equations are valid for the six dimensional phase space consisting of three spatial coordinates and their conjugate momenta. Under the assumption of a weak coupling between the transverse and longitudinal planes, the theory can also be applied to the two dimensional longitudinal phase space. This assumption will be made in the following.

The larger bunch area or the dilution of the phase space density due to filamentation or Landau damping discussed in Section 3.1.2 and visualised in Figure 3.2 do not conflict with Liouville's theorem. This is illustrated in Figure 3.3. If a bunch is matched, its shape matches the particle trajectories and both the bunch area and particle density f are constant. Due to a mismatch, the filamentation will start, leading to a distortion of the bunch shape. If a single point in the phase plane is followed along the flow, the density f will stay constant as stated by the theorem of Liouville. Also, the bunch area defined by the boundaries of the bunch will remain the same, although the area may be more difficult to compute. The dilution and the increase in area in Figure 3.2 are solely due to the fact that only a finite number of particles is used. After a long time, the filamentation is such that the original boundaries of the bunch are no longer distinguishable and in terms of the *effective* area and density, the beam quality deteriorates.

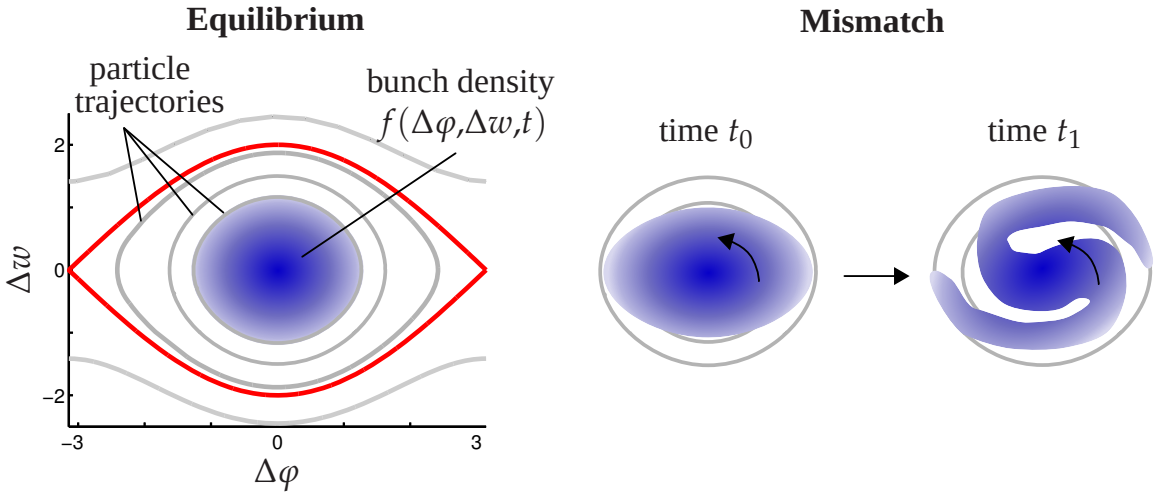

Figure 3.3: Filamentation and Liouville's theorem.

3.3 Properties of Bunched Beams

3.3.1 Particle Density Distributions

Different particle density distribution functions $f(\Delta\varphi, \Delta w)$ can be chosen to characterize a bunch in phase space [24]. The line density is the projection upon the $\Delta\varphi$ axis and can be calculated by integrating the density with respect to Δw

$$\lambda(\Delta\varphi) = \int_{-\infty}^{\infty} f(\Delta\varphi, \Delta w)\, \mathrm{d}\Delta w.$$

Different bunch types are given in Table 3.1. The density functions are chosen such that

$$\int_{-\infty}^{\infty}\int_{-\infty}^{\infty} f(\Delta\varphi, \Delta w)\, \mathrm{d}\varphi\, \mathrm{d}v = 1$$

holds. Note that the line density is normalized, i. e. it does not include the charge of the bunch. The charge density function f_{charge} and the charge line density λ_{charge} can be defined as

$$f_{\text{charge}}(\Delta\varphi, \Delta w) = Q_{\text{bunch}} f(\Delta\varphi, \Delta w), \qquad \lambda_{\text{charge}}(\Delta\varphi) = Q_{\text{bunch}}\lambda(\Delta\varphi), \tag{3.7}$$

where Q_{bunch} denotes the total charge of the bunch. Writing this in a more general way with the coordinate x, the charge density can be defined as

$$\int_{-\infty}^{\infty} \lambda_{\text{charge}}(x)\, \mathrm{d}x = Q_{\text{bunch}} \tag{3.8}$$

holds, i. e. the total area of the line charge density has to be equal to the charge of the bunch.

Table 3.1: Common bunch types and their line density. The bunches are centered and ellipsoidal. The line densities are defined on $\Delta\varphi \in [-R_1; R_1]$ and are zero elsewhere, except for the Gaussian case where f and λ can be defined over the complete length of the ring.

particle density function $f(\Delta\varphi, \Delta w)$	line density $\lambda(\Delta\varphi)$
uniform: $\frac{1}{\pi R_1 R_2}$ for $S = \frac{\Delta\varphi^2}{R_1^2} + \frac{\Delta w^2}{R_2^2} < 1$	elliptic: $\frac{2}{\pi R_1}\sqrt{1 - \frac{\Delta\varphi^2}{R_1^2}}$
elliptic: $\frac{3}{2\pi R_1 R_2}\sqrt{1 - S}$ for $S < 1$	parabolic: $\frac{3}{4R_1}\left[1 - \frac{\Delta\varphi^2}{R_1^2}\right]$
parabolic: $\frac{2}{\pi R_1 R_2}\left[1 - S\right]$ for $S < 1$	$\frac{8}{3\pi R_1}\left[1 - \frac{\Delta\varphi^2}{R_1^2}\right]^{3/2}$
Gaussian: $\frac{1}{2\pi\sigma_1\sigma_2}\mathrm{e}^{-\frac{1}{2}\left[\frac{\Delta\varphi^2}{\sigma_1^2} + \frac{\Delta w^2}{\sigma_2^2}\right]}$ for $\lvert\Delta\varphi\rvert < \pi$	Gaussian

In a macro particle tracking simulation, a phase space configuration of N_{macro} particles has to be chosen as an approximation of the presented density functions. However, standard algorithms usually provide only uniform or Gaussian pseudo random distributions. A numerical method that provides random values according to an arbitrary two-dimensional distribution $f(x, y)$ is given in [112]. The algorithm proceeds as follows [24]. A number N_{macro} of uniformly distributed triplets of random numbers (x_k, y_k, z_k) are generated. Only those triplets with $z_k < f(x_k, y_k)$ are chosen, the others are discarded. The pairs (x_k, y_k) of the remaining triplets are distributed according to $f(x, y)$.

3.3.2 Longitudinal Emittance

An important characteristic of the beam is its size in phase space. A smaller size for a given number of particles per bunch implies a higher particle density of the bunch and a higher beam quality, because more collision events in the experiment can be expected. The measure for the beam size is called the *beam emittance*. There exist diverse definitions for the emittance [69]. A common definition is the root mean square (RMS) emittance [43, 114]

$$\pi\varepsilon_{\mathrm{n}} = \pi\sqrt{\sigma_\tau^2\sigma_{\mathrm{W}}^2 - \sigma_{\tau,W}^4} \tag{3.9}$$

where σ_τ^2 and σ_W^2 are the variances of the beam in the longitudinal phase space coordinates $\Delta\tau$ and ΔW, respectively, and $\sigma_{\tau,W}^2$ is the covariance of the particle ensemble. Sometimes ε_{n} is also called *emittance* instead of $\pi\varepsilon_{\mathrm{n}}$. The variances can be estimated from a discrete

ensemble as

$$\sigma_x^2 = \frac{1}{N-1}\sum_{k=1}^{N}[x_k - \overline{x}]^2, \qquad \sigma_{x,y}^2 = \frac{1}{N-1}\sum_{k=1}^{N}[x_k - \overline{x}][y_k - \overline{y}]$$

with the center of gravity

$$\overline{x} = \frac{1}{N}\sum_{k=1}^{N} x_k, \qquad \overline{y} = \frac{1}{N}\sum_{k=1}^{N} y_k,$$

or from a continuous density function as

$$\sigma_x^2 = \int\int [x-\overline{x}]^2 f(x,y)\,\mathrm{d}x\,\mathrm{d}y, \qquad \overline{x} = \int\int x\, f(x,y)\,\mathrm{d}x\,\mathrm{d}y,$$

and further expressions accordingly. For a bunch with a uniform density and an elliptic shape the emittance $\pi\varepsilon_\mathrm{n}$ is proportional to the area in the longitudinal phase space

$$A_\mathrm{ell,uniform} = 4\pi\sqrt{\sigma_\tau^2\sigma_W^2 - \sigma_{\tau,W}^4}.$$

The emittance can also be defined as [67]

$$\pi\varepsilon_{\mathrm{n},2} = \pi\sqrt{[2\sigma_\tau]^2[2\sigma_\mathrm{W}]^2 - [2\sigma_{\tau,W}]^4} = 4\pi\varepsilon_\mathrm{n} = A_\mathrm{ell,uniform}.$$

This is equivalent to the definition (3.9) for 2σ, i. e. for two times the standard deviations.

The advantage of the defined emittances over the area calculation is that they can also be applied to non-uniform distributions and bunch shapes that are not elliptic. However, in these cases the physical interpretation of the emittance changes. For example, for a small bunch with a Gaussian distribution function the emittance $\pi\varepsilon_\mathrm{RMS}$ is the area circumscribed by a particle on the RMS trajectory. For large bunches the trajectories differ considerably from ellipses and a clear physical interpretation of the emittance is lost.

The subscript n of ε_n refers to the fact that this emittance is called *normalized* or *invariant*. Because the area in the phase space $(\Delta\tau, \Delta W)$ is conserved, the emittance is approximately conserved as well during acceleration. The conservation is only approximate, because the emittance is exactly equal to the bunch area for ellipsoidal shapes only. For more complicated shapes, the emittance is based on the RMS ellipse which can contain a lot of empty space. Figure 3.2 visualizes this. The initial bunch configuration has an ellipsoidal shape, a Gaussian density, and a low emittance. The emittance is equal to the bunch area. Because the bunch is not matched, there is a coherent quadrupole oscillation and the bunch filaments because of the synchrotron frequency spread. The bunch area itself remains constant during the simulation, but because of the complex bunch shape, a lot of empty space is included and the emittance increases. At the end of the simulation it is no longer possible to distinguish between the bunch and the empty spaces in between due to the finite number of particles. The effective bunch area is now considerably larger and equal to the emittance, the bunch is matched and its shape is approximately ellipsoidal. The mean particle density in the bunch has decreased. This process is a *dilution*

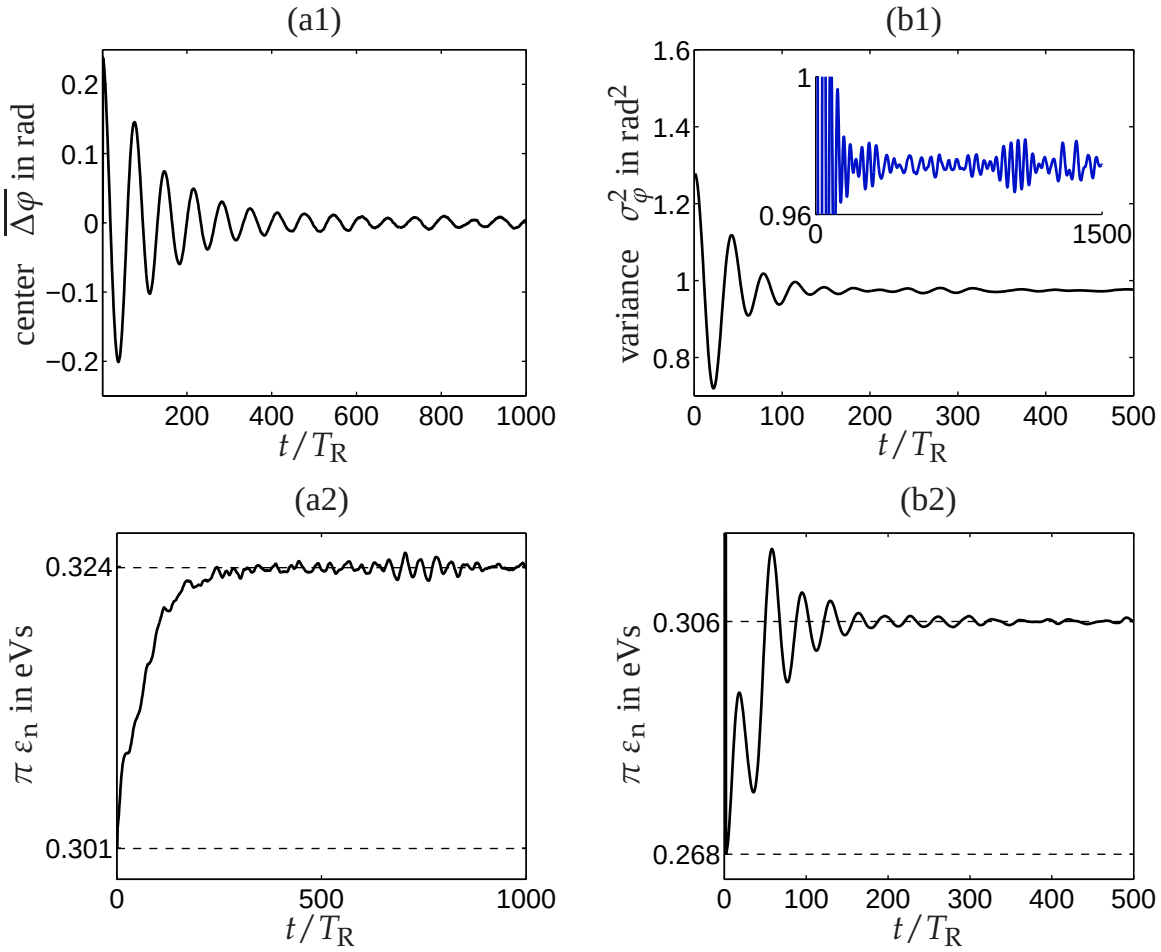

Figure 3.4: Landau damping and increase of the longitudinal emittance.

of the bunch density. The filamentation of the bunch leads to *Landau damping*: the coherent oscillation is damped until the mismatch of the bunch vanishes. These considerations show qualitatively that there is a link between the emittance and the disorder of the beam. Filamentation increases the disorder and the emittance. A formal treatment of the link between emittance and entropy for charged particle beams can be found in [69].

The increase of the effective bunch area is not a contradiction of Liouville's theorem as discussed in Section 3.2, since the theorem holds for particle densities with a Hamiltonian flow. In case of a filamented bunch with a finite number of particles, it is not possible to distinguish between the effective and the real bunch area. For a matched bunch however, the emittance is conserved.

The emittance is sometimes given in other coordinates, for example the phase deviation and relative impulse deviation

$$\Delta\varphi = \omega_\mathrm{RF}\Delta\tau = \frac{2\pi hc}{L_\mathrm{R}}\beta_\mathrm{R}\Delta\tau, \qquad \delta = \frac{\Delta p}{p_\mathrm{R}} = \frac{1}{\beta_\mathrm{R}^2\gamma_\mathrm{R}m_0c^2}\Delta W.$$

In this phase space, the area and the emittance

$$\pi\varepsilon \sim \frac{1}{\beta_\mathrm{R}\gamma_\mathrm{R}}$$

are not invariant and decrease during the acceleration. The emittance $\pi\varepsilon$ can be converted to the normalized emittance $\pi\varepsilon_\mathrm{n}$ by

$$\pi\varepsilon_\mathrm{n} = \beta_\mathrm{R}\gamma_\mathrm{R}\frac{m_0 c L_\mathrm{R}}{2\pi h}\pi\varepsilon$$

The unit of the normalized emittance $\pi\varepsilon_\mathrm{n}$ is eVs, whereas $\pi\varepsilon$ is given in rad.

A further emittance definition is the *elliptic emittance* which is defined as the area of an ellipse fitted in such a way that a predefined fraction of the particle ensemble is encircled. As an example, assume a Gaussian density with standard deviations σ_1 and σ_2. Using an ellipse with the half axes σ_1 and σ_2 will include 39.3% of the particles, whereas doubling the size of the ellipse will include 86.5% [43]. This is equivalent to the emittance $\pi\varepsilon_{\mathrm{n},2}$ based on 2σ.

Figure 3.4 shows how Landau damping increases the longitudinal emittance. In a first simulation[2)], a matched bunch receives a kick, i. e. the bunch center of gravity is shifted by $15^\circ = 0.26\,\mathrm{rad}$. Diagram (a1) shows how the oscillation amplitude decreases due to Landau damping, the increase of the longitudinal emittance is given in Diagram (a2). It has to be noted that this is no exact exponential damping. In particular, this is apparent in the close-up of Diagram (b1). Here, a voltage step leads to a mismatch of the bunch length and the variance oscillation is damped at the cost of an increasing emittance, cf. (b2). The close-up of (b1) shows that the oscillations returns in a recurrent way, although at small amplitudes. Also, the damping of the variance mismatch is stronger than the damping of the nonzero bunch center. In general, the exact shape of the Landau damping will depend on the bunch size und the type of density distribution.

In addition to the phase space area occupied by the beam, the number of particles in a bunch is an essential attribute of the beam. The *beam intensity* is defined as the number of particles per time unit and this is closely related to the beam current [43].

3.3.3 Line Density and Beam Current

The charge density distribution function of a bunch cannot be measured directly. What can be measured is the amount of charged particles that cross a certain point in the ring during a given time, because this corresponds to a current, the *beam current*, that can be observed with a pick-up monitor.

Figure 3.5 is now used to derive an expression for the beam current. First, assume a infinitesimal area with width $\mathrm{d}\Delta\varphi$ and height $\mathrm{d}\Delta w$ in phase space at the position

[2)] The simulations are performed with the same parameters as given in Table 5.2. The bunch has a Gaussian density distribution. For the damping of the bunch center of gravity, the initial bunch is matched for 10 kV with a variance of 0.92. For the damping of the bunch length, the bunch is matched for 5 kV with $E_{2,0} = 1.3$ and the voltage is raised stepwise to 10 kV.

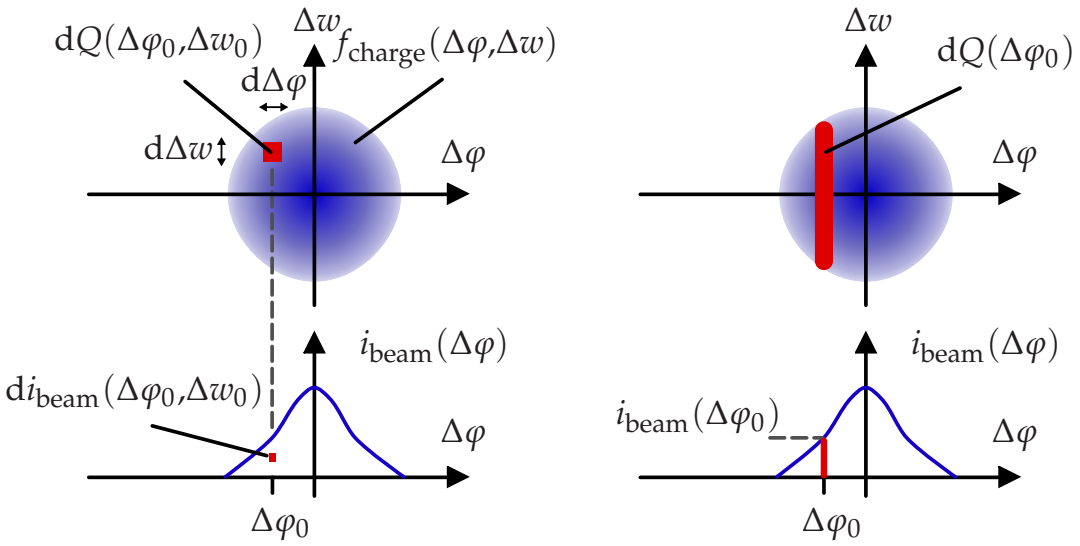

Figure 3.5: Calculation of the line density and beam current from the charge density function f_{charge}.

$(\Delta\varphi_0,\Delta w_0)$ as shown in the left drawing of Figure 3.5. This area contains particles with the total charge $\mathrm{d}Q$. This charge depends on the charge density function f_{charge} as

$$\mathrm{d}Q(\Delta\varphi_0,\Delta w_0) = f_{\text{charge}}(\Delta\varphi_0,\Delta w_0)\,\mathrm{d}\Delta\varphi\,\mathrm{d}\Delta w.$$

The particles in the considered area move and this leads to a current

$$\mathrm{d}i_{\text{beam}}(\Delta\varphi_0,\Delta w_0) = \frac{\mathrm{d}Q(\Delta\varphi_0,\Delta w_0)}{\mathrm{d}t(\Delta w_0)},$$

where $\mathrm{d}t$ is the time that the particles need to cross the pick-up monitor. This time depends on their velocity and thus the energy $W = W_{\mathrm{R}} + \Delta W$. The deviation ΔW follows from (2.44) and depends on Δw_0. The energy determines the revolution period $T(\Delta w_0)$ and revolution frequency $\omega(\Delta w_0)$ of the particles, and $\mathrm{d}t$ can be expressed as (cf. (2.4))

$$\mathrm{d}t(\Delta w_0) = \frac{T(\Delta w_0)}{2\pi h}\,\mathrm{d}\Delta\varphi = \frac{1}{h\omega(\Delta w_0)}\,\mathrm{d}\Delta\varphi.$$

Omitting the use of the specific point $(\Delta\varphi_0,\Delta w_0)$, the last equations lead to a current in phase space

$$\mathrm{d}i_{\text{beam}}(\Delta\varphi,\Delta w) = h\omega(\Delta w)\; f_{\text{charge}}(\Delta\varphi,\Delta w)\,\mathrm{d}\Delta w.$$

This current can be integrated over Δw to obtain the beam current

$$i_{\text{beam}}(\Delta\varphi) = \int \mathrm{d}i_{\text{beam}} = \int_{-\infty}^{\infty} h\omega(\Delta w)\; f_{\text{charge}}(\Delta\varphi,\Delta w)\,\mathrm{d}\Delta w.$$

If we assume that $\omega \approx \omega_\mathrm{R}$ for all particles of the beam, this can be simplified to

$$i_\mathrm{beam}(\Delta\varphi) \approx h\omega_\mathrm{R}\, \lambda_\mathrm{charge}(\Delta\varphi) = \omega_\mathrm{RF}\, \lambda_\mathrm{charge}(\Delta\varphi), \tag{3.10}$$

where λ_charge denotes the charge line density as defined in (3.7). In the following, it will be assumed that approximation (3.10) is valid and the approximation sign will be omitted. Equation (3.10) shows that, during acceleration, the beam current will increase with $\omega_\mathrm{RF}(t)$. In general, there will also be a change in beam current due to the time dependence of f_charge and λ_charge; for example, Landau damping decreases the density and thus the line density. An adiabatic increase in the RF voltage amplitude $\hat{U}_1$ has the opposite effect: the bunch will become narrower and higher in phase space and this increases the line density. The units of (3.10) are

$$[i_\mathrm{beam}] = \mathrm{A}, \quad [\omega_\mathrm{R}] = \frac{\mathrm{rad}}{\mathrm{s}}, \quad [\lambda_\mathrm{charge}] = \frac{\mathrm{As}}{\mathrm{rad}}.$$

Again, it may be beneficial to have the beam current (3.10) as a function of a general coordinate x. The charge line density $\lambda_\mathrm{charge}(x)$ is assumed to be nonzero only on the interval $\mathcal{D}_x =]-T_x/2; T_x/2]$, where T_x denotes the RF period. For $x = \Delta\varphi$ this period is 2π and for $x = \Delta\tau$ it equals T_RF. Due to (3.8), the beam current (3.10) can be written as

$$i_\mathrm{beam}(x) = \frac{T_x}{T_\mathrm{RF}}\, \lambda_\mathrm{charge}(x), \tag{3.11}$$

because this guarentees that the mean of i_beam over the interval $\mathcal{D}_x$ equals

$$\bar{i}_\mathrm{beam} := \frac{1}{T_x} \int_{-T_x/2}^{T_x/2} i_\mathrm{beam}(x)\, \mathrm{d}x = \frac{Q_\mathrm{bunch}}{T_\mathrm{RF}},$$

independent of the choice of x. Possible choices for x are given in Table 3.5. Note that in case of $x = \Delta\tau$ the beam current is $i_\mathrm{beam}(\Delta\tau) = \lambda_\mathrm{charge}(\Delta\tau)$.

The beam current signal i_beam is measured at a fixed location of the synchrotron. If the beam current is measured during several turns, the beam distribution function in the phase space can be recovered using only a few assumptions. A common method developed at CERN is called *longitudinal phase space tomography* [38, 39].

3.3.4 Matched Bunch

With the Vlasov equation it is now possible to express a more formal definition of matched bunches. A continuously differentiable density function $f(q = \Delta\varphi, p = \Delta w, t)$ is called a *matched* distribution if the density f at every point in the phase space remains constant and does not depend explicitly on time:

$$f(q, p, t) = f(q, p).$$

This is equivalent to

$$\frac{\partial f}{\partial t} = 0.$$

This simple condition guarantees that the shape of the particle bunch will remain constant, even if there is a flow of the particles inside the bunch. The line density and beam current of a matched bunch are also time-independent. A matched bunch is also called a *stationary* or *time invariant* particle distribution.

With Equation (3.6) the condition can be rewritten as

$$\frac{\partial f}{\partial \Delta\varphi}\Delta\dot{\varphi} = -\frac{\partial f}{\partial \Delta w}\Delta\dot{w}. \tag{3.12}$$

For very small bunches, the longitudinal motion is given in (2.43) and the density function has to satisfy

$$\frac{\partial f}{\partial \Delta\varphi}\Delta w = \frac{\partial f}{\partial \Delta w}\Delta\varphi.$$

Applying this condition to a Gaussian density function at time $t = 0$

$$f(\Delta\varphi, \Delta w, t = 0) = \frac{1}{\pi\sigma_1\sigma_2}\mathrm{e}^{-\frac{1}{2}\left[\Delta\varphi^2/\sigma_1^2 + \Delta w^2/\sigma_2^2\right]}$$

leads to the condition $\sigma_1 = \sigma_2 = \sigma$. Using this result and the polar coordinates

$$\begin{cases} r^2 = \Delta\varphi^2 + \Delta w^2 \\ \tan\theta = \frac{\Delta w}{\Delta\varphi} \end{cases}, \qquad \begin{cases} \Delta\varphi = r\cos\theta \\ \Delta w = r\sin\theta \end{cases}, \tag{3.13}$$

the resulting density function can be written as a function of r and $\tilde{H}_{\mathrm{lin}}$ (cf. (2.47))

$$f(r,\theta) = f(r) = \frac{1}{2\pi\sigma^2}\mathrm{e}^{-r^2/2\sigma^2} = f(H) = \frac{1}{2\pi\sigma^2}\mathrm{e}^{\tilde{H}_{\mathrm{lin}}/\sigma^2\omega_{\mathrm{syn}}}. \tag{3.14}$$

It is apparent that the density function has to be rotationally symmetric to represent a matched bunch. However, this is only valid for very small bunches or linear motion such as (2.43), because only in the special case of the linearized Hamiltonian (2.47), the trajectories are circles.

As a general necessary and sufficient condition for a stationary particle distribution, Hofmann and Pedersen state that the phase space density $f(\Delta\varphi,\Delta w)$ can be written as a function of the Hamiltonian H [45]. This can be shown as follows: Equation (3.12) can be reformulated as

$$\begin{bmatrix} \frac{\partial f}{\partial \Delta\varphi} & \frac{\partial f}{\partial \Delta w} \end{bmatrix} \cdot \begin{bmatrix} \Delta\dot{\varphi} \\ \Delta\dot{w} \end{bmatrix} = f_{\boldsymbol{x}} \cdot \dot{\boldsymbol{x}} \stackrel{!}{=} 0.$$

This implies that the gradient $f_{\boldsymbol{x}}$ of the density function should be perpendicular to the direction of the flow $\dot{\boldsymbol{x}}$ at every point in the phase plane. This is possible only if the contour

Table 3.2: Different stationary distributions. The Hamiltonian H is chosen such that $H(0,0) = 0$ and H_b is the value on the boundary of the bunch. f_0 and σ are positive and real numbers. As the Hamiltonian can be positive or negative depending on the direction of the flow, the absolute value $|H|$ is used.

Distribution	Particle Density Function
uniform	$f(H) = \begin{cases} f_0 & \lvert H\rvert \le \lvert H_\mathrm{b}\rvert \\ 0 & \text{else} \end{cases}$
elliptic	$f(H) = \begin{cases} f_0\sqrt{\lvert H_\mathrm{b}\rvert - \lvert H\rvert} & \lvert H\rvert \le \lvert H_\mathrm{b}\rvert \\ 0 & \text{else} \end{cases}$
Gaussian	$f(H) = f_0 \mathrm{e}^{-H/2H_\mathrm{b}}$

lines of f are identical with the trajectories of the motion. As the flow is Hamiltonian, a trajectory is a contour line of the Hamiltonian for a constant value H_1. Thus, for the correspondent contour line of f, the value of the Hamiltonian is also H_1 and constant. This implies that the density f only depends on the value of the Hamiltonian and f can be written as a function of H

$$f(\Delta\varphi, \Delta w) = f\left(H(\Delta\varphi, \Delta w)\right) = f(H)$$

as was also the case for the linear example in (3.14). Different stationary distributions are given in Table 3.2. The uniform and elliptic distributions have a density function f that is not continuously differentiable on the boundary of the bunch. However, their boundary $H = H_\mathrm{b}$ can be considered as a limit of the contour lines inside the bunch and it just as well has to be equal to a contour line of the Hamiltonian.

A Gaussian density function for the separable nonlinear Hamiltonian (2.45) can be expressed as the product of two exponential functions

$$f(\Delta\varphi, \Delta w) = f_0\, \mathrm{e}^{-\tilde{H}/2\tilde{H}_\mathrm{b}} = f_0\, \mathrm{e}^{-\tilde{T}(\Delta w)/2\tilde{H}_\mathrm{b}}\, \mathrm{e}^{-\tilde{V}(\Delta\varphi)/2\tilde{H}_\mathrm{b}}, \tag{3.15}$$

where $\tilde{H}_\mathrm{b} < 0$ is a constant. For very small $|\tilde{H}_\mathrm{b}|$, this density function can be approximated by (3.14).

3.4 Longitudinal Bunch Oscillations in the Time Domain

3.4.1 Mismatches of a Bunch

Usually, a bunch in a synchrotron ring will have small or large mismatches from the ideal matched distribution. These mismatches can for example result during the injection of the beam in the ring. If the beam is already bunched before it is injected in the ring, the bunch shapes have to be consistent with the buckets created by the RF voltage in the ring. Any deviation will result in a mismatch of the bunch. Even if the beam is injected as a coasting

Table 3.3: Mode numbers of longitudinal coherent beam oscillations for coasting and bunched beams [108].

Coasting Beams	Bunched Beams
n = azimuthal mode number $= 1,2,3,\ldots\infty$	n = coupled bunch mode number $= 0,1,2,\ldots(M-1)$ m = phase plane periodicity, within-bunch mode number $= 1$ (dipole), 2 (quadrupole), 3 (sextupole), $\ldots$ q = radial mode number

beam and is captured slowly by increasing the RF amplitude adiabatically, mismatches may happen during the capturing or thereafter during the acceleration. The disturbances described in Section 3.1.1 will create mismatches. These mismatches are usually damped by Landau damping as shown in Section 3.1.2, but this increases the emittance of the beam and deteriorates the beam quality. In addition, if the mechanisms or instabilities that drive the mismatches are faster than Landau damping, the bunch will eventually leave the bucket and will be lost.

Because of these reasons, a feedback system that is able to stabilize the bunch at the ideal matched shape is desirable. In general, it is not possible to measure the density in the phase plane and the mismatch directly. However, every mismatch will result in coherent oscillations of the beam: The bunch shape and the beam current will not be stationary and the resulting oscillations can be measured. To design a feedback system it is thus necessary to describe these coherent oscillations.

There are two possible modeling approaches. First, the oscillations can be described in the phase plane and time domain, this is the subject of this section. Second, the oscillations of the beam current can be observed in the frequency domain. This will be covered in the subsequent section.

In general, a beam consists of several bunches. Each bunch of the beam can perform coherent oscillations, these are called *single-bunch oscillations*. In addition, the bunches can oscillate against each other in the bunch train. This is referred to as *coupled-bunch oscillations*. The next sections and chapters will focus on single-bunch oscillations. It will be assumed that each bunch can be measured and controlled separately from the other bunches. Therefore, only a single bunch will be considered.

3.4.2 Longitudinal Oscillation Modes

The first classification of longitudinal bunched beam oscillations can be traced back to the theory of Sacherer [31, 109, 115–117]. A general framework exists for coasting and bunched beams to describe the coherent beam oscillations in the longitudinal and transverse planes [108]. In this framework, modes and mode numbers are defined to classify

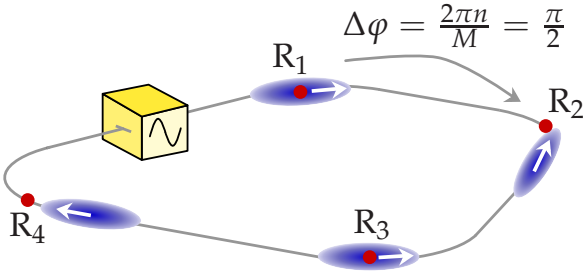

Figure 3.6: Illustration of the longitudinal coupled bunch mode number $n = 1$ for $M = 4$ bunches. Bunch $k \in \{1,2,3,4\}$ oscillates with $\sin(\varphi(t) + k\frac{2\pi n}{M})$. The arrows indicate the velocity of the relative bunch oscillation.

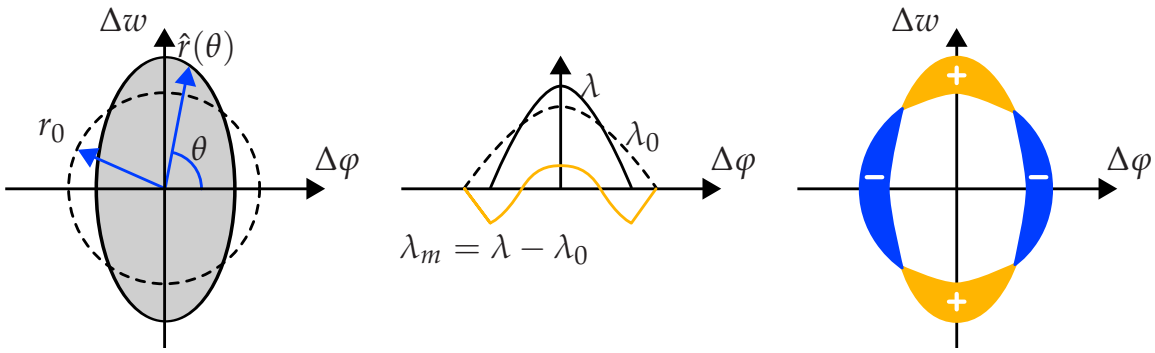

Figure 3.7: Within-bunch mode $m = 2$. **Left**: phase plane $(\Delta\varphi, \Delta w)$ and polar coordinates (r, θ), radius r_0 of the stationary distribution (dashed). **Center**: line density λ (solid), stationary line density λ_0 (dashed), and difference λ_m (orange). **Right**: modulation of the phase plane density for $m = 2$.

coherent oscillations. The oscillation modes can be considered as a basis of linearly independent functions that can be used to construct any possible oscillation.

Table 3.3 shows the longitudinal mode numbers for coasting and bunched beams. For bunched beams, there are the three mode numbers n, m, and q. The coupled bunch mode number n is used to classify the coupled bunch oscillations and the number of possible modes is equal to the number of bunches in the ring M. The mode number n defines the phase shift of oscillation between two adjacent bunches in the ring, as visualized in Figure 3.6. For example, for $n = 0$, all bunches in the ring oscillate in phase. The dynamics of the bunches can be coupled by impedances or wake fields and this can lead to a *coupled bunch instability*.

The within-bunch mode number m specifies the periodicity of a bunch density modulation in the phase plane with respect to the azimuth θ. Figure 3.7 shows the configuration of mode $m = 2$ in the phase plane $(\Delta\varphi,\Delta w)$, its line density as a superposition of a stationary λ_0 and oscillating λ_m, and the modulation of phase space density with respect to a stationary distribution. The first four modes, *dipole mode* $m = 1$, *quadrupole mode* $m = 2$, *sextupole mode* $m = 3$, and *octupole mode* $m = 4$, are shown in Figure 3.8 for linear longitudinal dynamics, i. e. without filamentation. The mode m is a density modulation that repeats itself after the fraction $1/m$ of the synchrotron period and thus has a frequency of m times the synchrotron frequency:

$$T_{\text{mode},m} = T_{\text{syn}}/m, \qquad \Rightarrow \qquad f_m = m f_{\text{syn}}.$$

From Figure 3.8, it can also be observed that the line density of mode m has m nodes, i. e. it has m intersections with the matched line density.

Finally, the framework also includes the radial mode number q to specify the modulation of the density with respect to the radius r of polar coordinates in the longitudinal phase plane. In the following, the coupled bunch mode number n and the radial mode number q will be ignored, as the main focus will be on the design of a feedback system for within-bunch modes m.

3.4.3 Analytical Definition of Within-Bunch Modes

The presented definition of the modes is not unique. So far, the mode m was said to be a modulation with respect to the azimuth θ such that the frequency in the phase plane is mf_{syn} and the modes $m = 1,\ldots,\infty$ are orthogonal, i. e. a mode cannot be constructed by a combination of any other modes. A possible analytical definition of mode m for a uniform distribution is [56]

$$f(r,\theta) = \begin{cases} f_0 & \text{for } (r,\theta) \in \mathcal{B} \\ 0 & \text{else} \end{cases}, \quad \mathcal{B} = \left\{ (r,\theta) \in \mathbb{R}^2 \,:\, r < R_0 \hat{r}(\theta) \right\}. \tag{3.16}$$

with the polar coordinates (r, θ) in the phase plane as shown in Figure 3.7, the radius of the stationary distribution R_0, and the boundary function

$$\hat{r}(\theta) = 1 + r_m \sin\left(m[\theta - \theta_{m,0}]\right).$$

In the linear regime of the bucket, the bunch rotates with ω_{syn} and this can be taken into account by $\theta_{m,0}(t) = \omega_{\mathrm{syn}} t$. This shows that the mode repeats itself after $t = T_{\mathrm{syn}}/m$ and the mode frequency is $m\omega_{\mathrm{syn}}$. It is now possible to construct more general boundary functions by taking the sum of all modes and the new boundary is

$$\hat{r}(\theta) = 1 + \sum_{m=1}^{\infty} r_m \sin\left(m[\theta - \theta_{m,0}]\right). \tag{3.17}$$

This is a Fourier series of the function $\hat{r}(\theta)$ and allows almost arbitrary bunch shapes. However, an important constraint is $\hat{r}(\theta) > 0$ and realistic bunches will have small mismatches with $r_m \ll 1$. This approach can also be used for other distribution functions. For a Gaussian distribution, the definition of the modes can be chosen as

$$f(r,\theta) = f_0 \, \mathrm{e}^{-r^2 \big/ 2\sigma_0^2 \hat{r}^2(\theta)}. \tag{3.18}$$

This leads to contour lines $r \sim \hat{r}(\theta)$ of the Gaussian density distribution with shapes defined by (3.17).

Besides the above explicit definition of the modes, it is also common to define the modes as deviations from the stationary distribution. This is shown in Figure 3.7 for mode $m = 2$ and $\theta_{m,0} = \pi/4$: the line density λ in the center can be regarded as a stationary line density λ_0 with a modulation λ_m. In the phase space (right image)

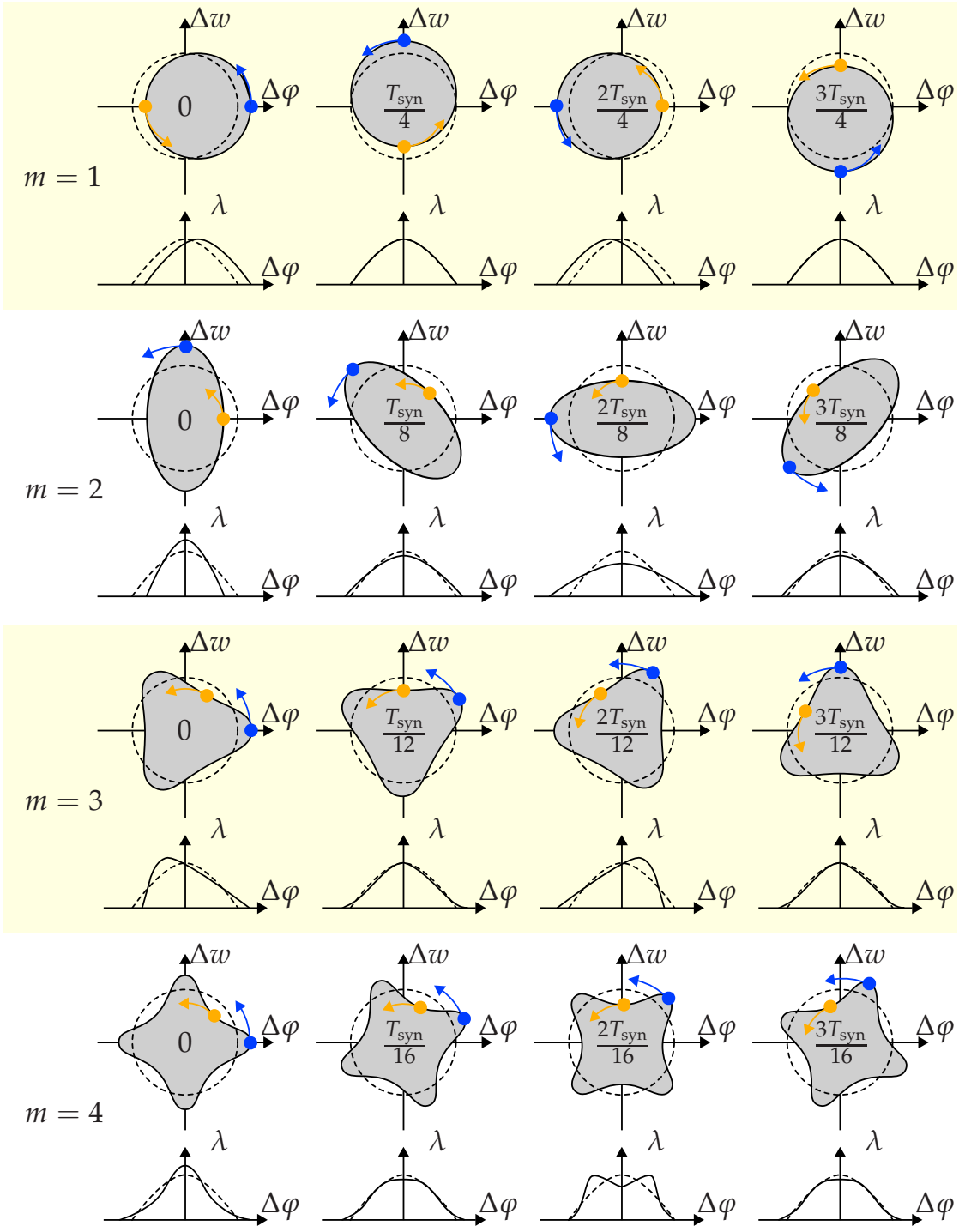

Figure 3.8: The phase plane and line density configuration for the first four single-bunch oscillation modes: dipole ($m = 1$), quadrupole ($m = 2$), sextupole ($m = 3$), and octupole mode ($m = 4$). The dashed circle is the matched shape in the phase plane and the matched line density λ. The time t of each configuration is given inside the bunches. The frequency of each mode is $m f_{\mathrm{syn}}$, because mode m is repeated after T_{syn}/m. Two particles (orange and blue) are shown to visualize the linear flow, i. e. the flow of the linear model.

the density modulation with respect to the stationary density f_0 is shown and depends mainly on the azimuth θ. This approach is convenient to examine a stationary beam that is perturbed by a small mode. For example, the frequency components of λ_m simply add to the stationary spectrum of λ_0. This approach is however less appropriate for the modeling of a feedback system, since the feedback acts on the complete density and not only on its deviation.

The presented mode definitions are so far valid for small bunches in the linear regime of the bucket only, because they rely on the fact that the trajectories near the origin are circles. A possible extension is to use the stationary distribution (3.15) for the nonlinear regime and define the modulated density

$$f(r,\theta) = f_0 \, \mathrm{e}^{-H(r,\theta)\big/2H_\mathrm{b}\hat{r}^2(\theta)}.$$

For a stationary bucket $\varphi_\mathrm{R} = 0$ and the Hamiltonian (2.45), the density can be rewritten with the polar coordinates (3.13) as

$$f(r,\theta) = f_0 \, \mathrm{e}^{-\left[r^2\sin^2\theta+2-2\cos(r\cos\theta)\right]\big/2\left[\frac{-2H_\mathrm{b}}{\omega_\mathrm{syn}}\right]\hat{r}^2(\theta)}.$$

Similar definitions can be made for uniform and other distributions.

3.5 Longitudinal Bunch Oscillations in the Frequency Domain

There are two important reasons why the frequency domain is commonly used to analyze beam oscillations. First, it is convenient to observe the beam spectrum using a spectrum analyzer. Second, the interactions of the beam with its environment are usually frequency-dependent, thus it is necessary to analyze the frequency components of the beam current. The calculation of the beam current spectrum can essentially be done in two different ways. If the coherent oscillations are small and the Landau damping is negligible, the beam current signal will repeat itself at the latest after one synchrotron period T_syn. The spectrum over this period will be time independent and it will be referred to as the *long-term spectrum*. For a feedback control however, this measurement is too slow, since coherent oscillations should be damped as soon as they arise. For control purposes, the beam current signal of a bunch should be measured during a single or a few revolution T_R. This *short-term spectrum* will be time dependent for non-stationary bunches and can be used as an input variable for control algorithms.

The convention of the Fourier transform used in the next sections and some necessary formulas are given in Appendix A.3.

3.5.1 Long-Term Spectrum of Bunched Beams

In this section the spectrum for the special case $h = 1$ is considered, because only single-bunch oscillations are of interest in this thesis. More general derivations can be found in [19, 30, 121, 136].

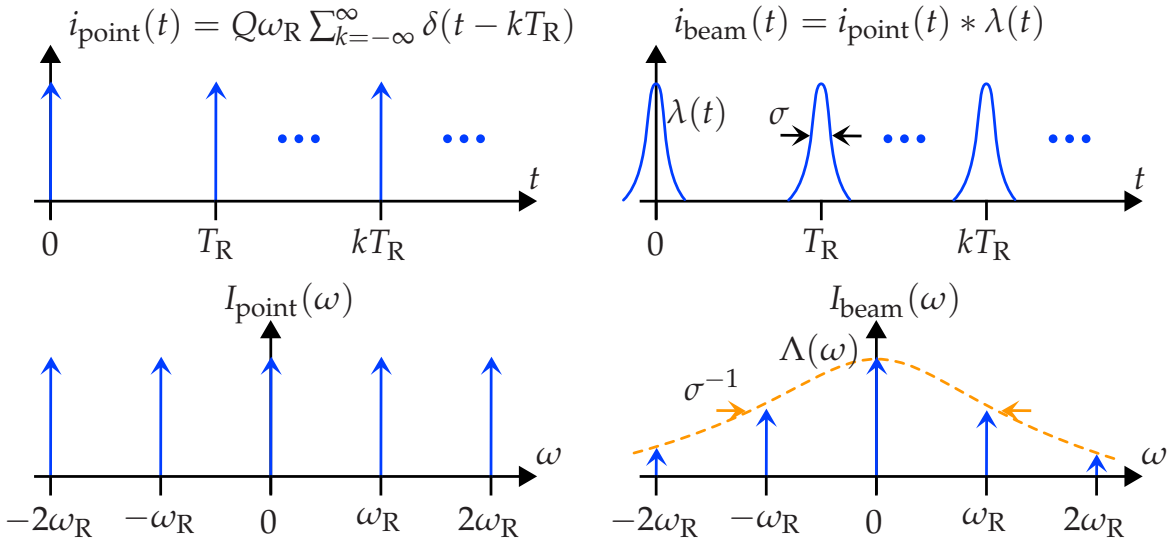

Figure 3.9: Top left: beam current of a single particle with the revolution time T_R. **Bottom left**: spectrum of single particle. **Top right**: stationary distribution $\lambda(t)$ with a finite bunch length. **Bottom right**: spectrum for a finite bunch length.

To begin with, a single particle or a point bunch with the charge Q in the ring is considered. The particle is assumed to be exactly on the reference trajectory with the reference energy and is thus not performing any oscillation. The time is chosen such that it crosses the pick-up monitor at $t = 0$. The particle will return periodically at the pick-up monitor with period T_R and the beam current can be modeled as a series of Dirac delta functions

$$i_{\text{point}}(t) = Q\omega_R \sum_{k=-\infty}^{\infty} \delta(t - kT_R)$$

as shown in the top left image of Figure 3.9. The spectrum of this signal follows from (A.10) and is also a series of delta functions

$$I_{\text{point}}(\omega) = Q\omega_R^2 \sum_{k=-\infty}^{\infty} \delta(\omega - k\omega_R) \tag{3.19}$$

with nonzero frequency components at multiples of ω_R as shown in the bottom left image of Figure 3.9.

A point bunch is not a very realistic example, so a stationary bunch with a finite length and the longitudinal line density $\lambda(t)$ for $t \in]-T_R/2; T_R/2]$ is now assumed. This can easily be derived from the previous case if the convolution[3)]

$$i_{\text{beam}}(t) = i_{\text{point}}(t) * \lambda(t) = \int_{-\infty}^{\infty} \lambda(\tau)\, i_{\text{point}}(t - \tau)\, \mathrm{d}\tau = Q\omega_R \sum_{k=-\infty}^{\infty} \lambda(t - kT_R)$$

[3)] In the following formula, τ is a variable for the convolution integral and not the coordinate τ of the longitudinal beam dynamics.

Table 3.4: Spectral density of uniform and Gaussian line densities. The Gaussian spectral density is approximately valid for $\sigma < T_\mathrm{R}/2\pi$.

Line Density $\lambda(t)$	Spectral Density $\Lambda(\omega)$	$\Lambda(0)$
uniform: $\begin{cases} \frac{1}{l_\mathrm{b}} & \text{for } t \in [-\frac{l_\mathrm{b}}{2}\,;\,\frac{l_\mathrm{b}}{2}] \\ 0 & \text{else} \end{cases}$	$\frac{\sin(\omega l_\mathrm{b}/2)}{\omega l_\mathrm{b}/2}$	1
Gaussian: $\begin{cases} \frac{1}{\sqrt{2\pi}\sigma}\mathrm{e}^{-\frac{1}{2}\frac{t^2}{\sigma^2}} & \text{for } t \in [-\frac{T_\mathrm{R}}{2};\frac{T_\mathrm{R}}{2}] \\ 0 & \text{else} \end{cases}$	$\approx \mathrm{e}^{-\frac{1}{2}\sigma^2\omega^2}$	1

is used [56, 60]. The resulting beam current is shown in the top right image of Figure 3.9. The only necessary assumption for this calculation is that adjacent bunches do not overlap, i. e. $\lambda(t)$ is zero outside the interval $t \in]-T_\mathrm{R}/2; T_\mathrm{R}/2]$. The convolution in time domain corresponds to the simple multiplication in frequency domain,

$$I_\mathrm{beam}(\omega) = I_\mathrm{point}(\omega)\;\Lambda(\omega) = Q\omega_\mathrm{R}^2 \sum_{k=-\infty}^{\infty} \Lambda(k\omega_\mathrm{R})\delta(\omega - k\omega_\mathrm{R}),$$

where $\Lambda(\omega)$ is the spectral density of the line density as defined by the Fourier transform (A.6), p.165. The spectrum remains a series of δ-functions, but these functions are modulated with $\Lambda(k\omega_\mathrm{R})$. Table 3.4 shows the spectral densities for uniform and Gaussian line densities. Taking the limits $l_\mathrm{b} \to 0$ and $\sigma \to 0$ leads in both cases to the special case of point bunches with the spectrum (3.19). For finite[4] bunch lengths, the higher frequency components are scaled or rather damped by Λ, cf. Figure 3.9, bottom right. A bunch with a larger length σ will have a narrower spectrum Λ and its spectral lines of higher frequencies will be less important. This is apparent from Table 3.4: The spectral density of a Gaussian density is also Gaussian, but with standard deviation σ^{-1}.

To be able to construct a non-stationary bunch, it is necessary to consider the more general case that the particle performs synchrotron oscillations. In turn k, the particle will then arrive with a time delay $\tau(k)$. For small amplitudes $\hat{\tau}$ of the synchrotron oscillation, the oscillation is linear and the time delay at turn k follows from the linear synchrotron oscillation (2.37) for the coordinate $\tau = \varphi/\omega_\mathrm{RF}$ and the arrival time $t = kT_\mathrm{R}$ and can thus be expressed by

$$\tau(k) = \hat{\tau}\cos\left(\omega_\mathrm{syn} k T_\mathrm{R} + \Phi_0\right). \tag{3.20}$$

The beam current of the oscillating particle is

$$i_\mathrm{point}(t) = Q\omega_\mathrm{R} \sum_{k=-\infty}^{\infty} \delta\left(t - kT_\mathrm{R} - \hat{\tau}\cos\left(\omega_\mathrm{syn} k T_\mathrm{R} + \Phi_0\right)\right). \tag{3.21}$$

[4] Here, finite is used as the opposite of the limit $\sigma \to 0$ of infinitesimal point bunches.

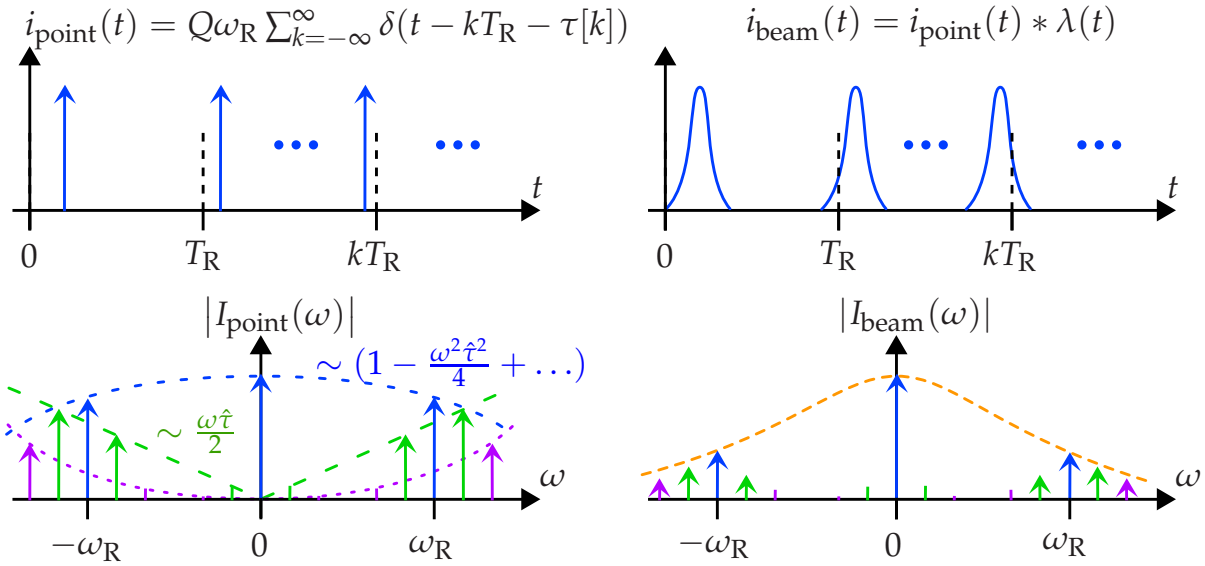

Figure 3.10: Top left: beam current of a single oscillating particle. **Bottom left**: spectrum of single particle. **Top right**: dipole oscillation of distribution $\lambda(t)$ with a finite bunch length. **Bottom right**: spectrum for finite bunch length. The magnitudes of the spectral lines are chosen randomly to clarify the principle shapes. Due to the oscillation, side bands appear.

This current is shown schematically in the top left diagram of Figure 3.10. Strictly speaking, this equation contains a simplification, since the frequency ω_R is valid for the reference particle only. An oscillating particle with an energy deviation also has a slightly different angular frequency. However, this difference is usually small and will be neglected in the following.

If T_{syn} is an integer multiple of T_R, the signal i_{point} repeats itself after $t = T_{\text{syn}}$ and $k = T_{\text{syn}}/T_R$ and a Fourier series can be derived [56, 60] without any approximations. This Fourier series can then be transformed into the frequency domain. Classical approaches to calculate the spectrum are given amongst others in [121] and [136]. However, these two references present results that differ slightly and the approaches do not seem to be completely consistent. In [136], the arrival time (3.20) is chosen slightly different as

$$\tau(k) \approx \tau(t) = \hat{\tau}\cos(\omega_{\text{syn}}t + \Phi_0).$$

This approximation changes the obtained spectrum, particularly the magnitude of side bands of higher order, but the principal shape is maintained. In [121], the same equation as (3.21) is used and transformed directly into the frequency domain with a Fourier transform. Transforming the series (3.21) elementwise with (A.7) yields

$$I_{\text{point}}(\omega) = Q\omega_R \sum_{n=-\infty}^{\infty} \mathrm{e}^{-\mathrm{i}\omega n T_R}\, \mathrm{e}^{-\mathrm{i}\omega\hat{\tau}\cos(\omega_{\text{syn}} n T_R + \Phi_0)}.$$

The second exponential function on the right hand side can be expanded as a Taylor series. Rewriting this series using $\cos^2 x = (1+\cos(2x))/2$ yields

$$1 - \frac{\omega^2\hat{\tau}^2}{4} \; - \; \mathrm{i}\omega\hat{\tau}\cos(\omega_{\mathrm{syn}} n T_{\mathrm{R}} + \Phi_0) \; - \; \frac{\omega^2\hat{\tau}^2}{4}\cos(2\omega_{\mathrm{syn}} n T_{\mathrm{R}} + 2\Phi_0) \; + \; \ldots$$

and with $\mathrm{e}^{\mathrm{i}x} + \mathrm{e}^{-\mathrm{i}x} = 2\cos(x)$ and (A.9), the beam current can be rewritten as

$$\begin{aligned}\frac{I_{\mathrm{point}}(\omega)}{Q\omega_{\mathrm{R}}^2} = &\left[1 - \frac{\omega^2\hat{\tau}^2}{4} + \ldots\right] \sum_{k=-\infty}^{\infty} \delta(\omega + k\omega_{\mathrm{R}}) - \\ &- \mathrm{i}\frac{\omega\hat{\tau}}{2}\mathrm{e}^{\mathrm{i}\Phi_0} \sum_{k=-\infty}^{\infty} \left[\delta(\omega - \omega_{\mathrm{syn}} + k\omega_{\mathrm{R}}) + \delta(\omega + \omega_{\mathrm{syn}} + k\omega_{\mathrm{R}})\right] \; + \\ &+ \frac{\omega^2\hat{\tau}^2}{8}\mathrm{e}^{\mathrm{i}2\Phi_0} \sum_{k=-\infty}^{\infty} \left[\delta(\omega - 2\omega_{\mathrm{syn}} + k\omega_{\mathrm{R}}) + \delta(\omega + 2\omega_{\mathrm{syn}} + k\omega_{\mathrm{R}})\right] + \ldots\end{aligned}$$

This approximation of the spectrum shows that due to the synchrotron oscillation, new lines or side bands appear next to the comb of lines at the rotation harmonics $k\omega_{\mathrm{R}}$ of (3.19). In [121], the Bessel function sum is additionally employed to obtain the exact spectrum. These derivations show that there is a double infinite number of side bands, spectral lines appear at

$$\omega = k\omega_{\mathrm{R}} + m\omega_{\mathrm{syn}}, \qquad k, m \; = -\infty, \ldots, -1, 0, 1, \ldots, \infty.$$

In addition, the magnitudes at the rotation harmonics $k\omega_{\mathrm{R}}$ decrease depending on $\omega\hat{\tau}$. The bottom left image of Figure 3.10 shows the principle shape of the spectrum. The magnitudes of the side bands are not symmetric and can be even larger than the magnitude of the spectral lines at the rotation harmonics. A more general result is obtained if an exact and closed-form expression of the spectral lines is derived [56, 60].

The top right image of Figure 3.10 shows the coherent dipole mode $m = 1$ of a bunch with a finite length. Its spectrum is again obtained simply by a multiplication with the spectrum of the line density Λ and the structure of side bands is preserved. Only for very small values of $\omega\hat{\tau} \ll 1$, the side bands of order $m > 1$ are negligible. This shows that there is no one-to-one correspondence of coherent modes m and the spectral lines of the side bands [60].

The calculation of the spectrum of higher order modes $m > 1$ is not as simple as the dipole case, because the shape of the bunch is no longer stationary. It is thus necessary to assume a bunch with many oscillating particles and to take the sum of the spectra of the individual particles. Because the number of particles is large, it is possible to approximate this sum as an integration over a density distribution. However, the calculation gets extremely complicated and an analytic solution for higher order modes $m > 1$ does not seem to exist.

As already mentioned, the particles in a bunch will have frequencies that differ slightly from ω_{R}, this was neglected in (3.21). If it is taken into account, the spectral lines smear out, i. e. the δ-functions turn into continuous and finite spectral densities [30]. For larger

Table 3.5: Possible coordinates for the short-term spectrum calculation.

Coordinates	x	y	T_x	ω_x	Domain $\mathcal{D}_x$
RF phase	$\Delta\varphi$	$\Delta w = -\frac{\Delta\dot{\varphi}}{\omega_{\text{syn}}}$	2π	1	$]-\pi, \pi]$
Time lag	$\Delta\tau$	$-\frac{\Delta\dot{\tau}}{\omega_{\text{syn}}}$	$T_{\text{RF}} = \frac{T_{\text{R}}}{h}$	ω_{RF}	$]-\frac{T_{\text{RF}}}{2}, \frac{T_{\text{RF}}}{2}]$

bunches, the linear calculation of (3.20) is no longer valid. The synchrotron oscillation is nonlinear and there is a synchrotron frequency spread leading to Landau damping. If Landau damping is large, the current signal is clearly not periodic and the interpretation of the spectrum is lost.

3.5.2 Short-Term Spectrum of Ellipsoidal Bunches

The long-term spectrum presented in the previous section is important for beam observations but often too slow to be used for beam corrections. In RF feedback loops, the beam current signal during one turn is usually measured and decomposed into its frequency components by a Fast Fourier Transform (FFT). To model this *short-term spectrum*, two different bunch density functions are analyzed in this section: a Gaussian and a uniform density distribution with elliptic bunch shapes. The line density signal of these bunches is calculated analytically and developed in a Fourier series. The results show that the amplitude and phase of the first harmonic can be used to calculate meaningful parameters of the bunch position and shape.

It is assumed that the bunch can be approximately described by the density function $f(x, y)$ in the longitudinal phase plane (x, y). The coordinates are not further specified; the coordinates are however assumed to be chosen such that the trajectories in the linear regime of the bucket are circles. The beam may consist of h bunches, but each bunch is measured separately. The time between two successive bunches will be denoted by T_x and this also defines the domain of one single bunch. Possible coordinate candidates are given in Table 3.5.

Uniform Density First, an ellipsoidal bunch with a uniform density is considered. It is desirable to have a fairly general definition of the bunch and a possible construction is shown in Figure 3.11. On the left, a simple ellipsoidal boundary is given, defined by the boundary function $b_1(\boldsymbol{x}) = \boldsymbol{x}^{\mathrm{T}}\mathbf{S}\boldsymbol{x} - 1 = 0$ with $\boldsymbol{x} = [x\ y]^{\mathrm{T}} \in \mathbb{R}^2$. This bunch can be rotated (center) and translated (right) by the maps $\boldsymbol{x} \mapsto \mathbf{R}_\Phi \boldsymbol{x}$ and $\boldsymbol{x} \mapsto \boldsymbol{x} - \boldsymbol{r}$. The shape, rotation, and translation matrices are

$$\mathbf{S} = \begin{bmatrix} R_{1x}^{-2} & 0 \\ 0 & R_{2x}^{-2} \end{bmatrix}, \qquad \mathbf{R}_\Phi = \begin{bmatrix} \cos\Phi & \sin\Phi \\ -\sin\Phi & \cos\Phi \end{bmatrix}, \qquad \boldsymbol{r} = \begin{bmatrix} x_0 \\ y_0 \end{bmatrix}$$

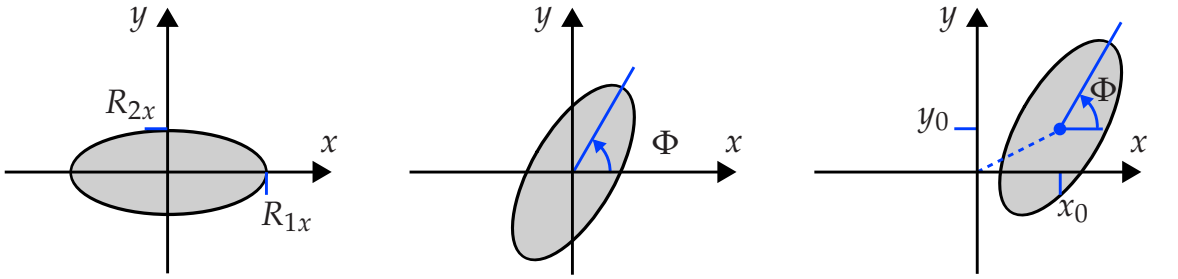

$\boldsymbol{x}^{\mathrm{T}}\mathbf{S}\boldsymbol{x} \leq 1$ $\quad$ $\boldsymbol{x}^{\mathrm{T}}\mathbf{R}_{\Phi}^{\mathrm{T}}\mathbf{S}\mathbf{R}_{\Phi}\boldsymbol{x} \leq 1$ $\quad$ $[\boldsymbol{x}-\mathbf{r}]^{\mathrm{T}}\mathbf{R}_{\Phi}^{\mathrm{T}}\mathbf{S}\mathbf{R}_{\Phi}[\boldsymbol{x}-\mathbf{r}] \leq 1$

Figure 3.11: Construction of a general ellipsoidal bunch with a uniform density and both arbitrary orientation and center of gravity. The vector $\boldsymbol{x} = [x\ y]^{\mathrm{T}} \in \mathbb{R}^2$ defines the position in the phase plane, Φ is the orientation, $\mathbf{R}_{\Phi}$ a rotation matrix, $\mathbf{S}$ contains the half-axes R_{1x} and R_{2x}, and $\boldsymbol{r}$ is a translation vector.

with the half-axes R_{1x} and R_{2x} and the angle Φ. The bunch is defined by the set

$$\mathcal{B}_{\mathrm{u}} = \left\{ \boldsymbol{x} = \begin{bmatrix} x \\ y \end{bmatrix} \in \mathbb{R}^2 \ : \ (\boldsymbol{x}-\boldsymbol{r})^{\mathrm{T}}\mathbf{R}_{\Phi}^{\mathrm{T}}\mathbf{S}\ \mathbf{R}_{\Phi}(\boldsymbol{x}-\boldsymbol{r}) \leq 1 \right\} \tag{3.22}$$

with the boundary function

$$\begin{aligned} s_{\mathrm{u}}(\boldsymbol{x}) &= [\boldsymbol{x}-\boldsymbol{r}]^{\mathrm{T}}\mathbf{R}_{\Phi}^{\mathrm{T}}\mathbf{S}\ \mathbf{R}_{\Phi}[\boldsymbol{x}-\boldsymbol{r}] \\ &= \frac{a^2[y-y_0]^2 + b^2[x-x_0]^2 - 2c[x-x_0][y-y_0]}{a^2b^2 - c^2} \end{aligned} \tag{3.23}$$

and the abbreviations

$$\begin{aligned} a &= \sqrt{R_{1x}^2\cos^2\Phi + R_{2x}^2\sin^2\Phi} \qquad b = \sqrt{R_{1x}^2\sin^2\Phi + R_{2x}^2\cos^2\Phi} \\ c &= \left[R_{1x}^2 - R_{2x}^2\right]\cos\Phi\sin\Phi \qquad \Rightarrow \qquad a^2b^2 - c^2 = R_{1x}^2R_{2x}^2 \end{aligned}$$

The defined bunch is static, but a time dependency can be introduced if x_0, y_0, and Φ are regarded as functions of time. For example, a linear synchrotron oscillation of the bunch is obtained by

$$\begin{aligned} x_0(t) &= \tilde{x}_0\cos(\omega_{\mathrm{syn}}t) + \tilde{y}_0\sin(\omega_{\mathrm{syn}}t) \\ y_0(t) &= \tilde{x}_0\sin(\omega_{\mathrm{syn}}t) + \tilde{y}_0\cos(\omega_{\mathrm{syn}}t) \\ \Phi(t) &= \Phi_0 + \omega_{\mathrm{syn}}t \end{aligned} \tag{3.24}$$

The constant parameters $\tilde{x}_0$, $\tilde{y}_0$, and Φ_0 are initial values of this oscillation.

The density of the bunch is chosen to be uniform:

$$f(x,y) = \begin{cases} \frac{1}{\pi R_{1x}R_{2x}} & \text{for } (x,y) \in \mathcal{B}_{\mathrm{u}}, \\ 0 & \text{else,} \end{cases} \tag{3.25}$$

with the set $\mathcal{B}_\mathrm{u}$ from (3.22). The line density of this bunch is

$$\lambda(x) = \int_{-\infty}^{\infty} f(x,y)\,\mathrm{d}y = \begin{cases} \frac{1}{\pi R_{1x} R_{2x}} \left[\overline{y}(x) - \underline{y}(x)\right] & \text{for } x \in \mathcal{D}_x, \\ 0 & \text{else,} \end{cases}$$

where $\overline{y}(x)$ and $\underline{y}(x)$ are the upper and lower boundary values of y with respect to x. Solving the boundary function $s_\mathrm{u}(x,y) = 1$ of (3.23) for y yields after some calculation steps the upper and lower boundary values

$$\left\{ \begin{array}{c} \overline{y}(x) \\ \underline{y}(x) \end{array} \right\} = y_0 + \frac{c}{a^2}[x - x_0] \quad \left\{ \begin{array}{c} + \\ - \end{array} \right\} \quad \sqrt{b^2 - \frac{c^2}{a^2}} \sqrt{1 - \frac{[x-x_0]^2}{a^2}}$$

inside the domain

$$\mathcal{D}_x = \{x \in \mathbb{R} \,:\, \underline{x} = x_0 - a \le x \le x_0 + a = \overline{x}\} \tag{3.26}$$

with the upper and lower boundary values $[\underline{x}\,;\,\overline{x}]$. This results in the line density

$$\lambda(x) = \begin{cases} \frac{2}{\pi a} \sqrt{1 - \frac{[x-x_0]^2}{a^2}} & \text{for } x \in \mathcal{D}_x, \\ 0 & \text{else.} \end{cases} \tag{3.27}$$

This signal can be Fourier transformed to obtain the spectral density

$$\Lambda(\omega) = \int_{-\infty}^{\infty} \lambda(x)\, \mathrm{e}^{-\mathrm{i}\omega x}\,\mathrm{d}x = \int_{\underline{x}}^{\overline{x}} \lambda(x)\, \mathrm{e}^{-\mathrm{i}\omega x}\,\mathrm{d}x.$$

A summary of the notations used for the Fourier transform are given in Appendix A.3.1. The substitution $\tilde{x} = [x - x_0]/a$ leads to

$$\Lambda(\omega) = \frac{2}{\pi} \mathrm{e}^{-\mathrm{i}\omega x_0} \int_{-1}^{1} \sqrt{1 - \tilde{x}^2}\, \mathrm{e}^{-\mathrm{i}\omega a \tilde{x}}\,\mathrm{d}\tilde{x}.$$

This integral is a standard integral for the Bessel function J_1 of the first kind:

$$\int_{-1}^{1} \sqrt{1 - \tilde{x}^2}\, \mathrm{e}^{-\mathrm{i}\omega \tilde{x}}\,\mathrm{d}\tilde{x} = \begin{cases} \frac{\pi}{2} & \omega = 0, \\ \frac{\pi J_1(\omega)}{\omega} & \omega \neq 0. \end{cases}$$

Finally, the spectrum can be written as

$$\Lambda(\omega) = \begin{cases} 1 & \omega = 0, \\ \frac{2J_1(\omega a)}{\omega a}\, \mathrm{e}^{-\mathrm{i}\omega x_0} & \omega \neq 0. \end{cases}$$

The beam current is proportional to the line charge density as stated in (3.11), p.53, and the spectral density of the beam current is given by

$$I_{\text{beam}}(\omega) = \frac{T_x}{T_{\text{RF}}}\,\Lambda_{\text{charge}}(\omega) = \frac{T_x}{T_{\text{RF}}} Q_{\text{bunch}}\,\Lambda(\omega), \tag{3.28}$$

where $\Lambda_{\text{charge}} = Q_{\text{bunch}}\Lambda$ is the Fourier transform of the line charge density λ_{charge}. A real measurement of the beam current is usually followed by a FFT or a filter to obtain the amplitude and phase values of the harmonics of the signal. If the measured beam current is continued periodically such that it becomes periodic with period T_x and frequency ω_x, a Fourier series can be calculated, provided the bunches do not overlap. According to (A.11) of Appendix A.3.3, the complex Fourier coefficients are then simply

$$c_k = \frac{1}{T_x} I_{\text{beam}}(\omega = k\omega_x) = \bar{i}_{\text{beam}} \cdot \begin{cases} 1 & k = 0, \\ \frac{2J_1(k\omega_x a)}{k\omega_x a}\, \mathrm{e}^{-\mathrm{i}k\omega_x x_0} & k \neq 0. \end{cases} \tag{3.29}$$

with the mean current or DC current of the bunch

$$\bar{i}_{\text{beam}} = |c_0| = \frac{A_0}{2} = \frac{Q_{\text{bunch}}}{T_{\text{RF}}}.$$

The amplitude and phase values of the harmonics are, cf. Appendix A.3.1,

$$A_k = 2|c_k|, \qquad \varphi_k = \measuredangle c_k. \tag{3.30}$$

For the considered uniform density, they are

$$A_k = 4\bar{i}_{\text{beam}} \frac{J_1\,(k\,a\,\omega_x)}{k\,a\,\omega_x}, \qquad \varphi_k = -k\,\omega_x\,x_0. \tag{3.31}$$

The units of R_{1x} and R_{2x} are equal to the unit of coordinate x, the phase φ_k is measured in radian and the amplitude A_k is measured in ampere.

The beam current follows with (3.27) and equals

$$i_{\text{beam}}(x) = \frac{T_x}{T_{\text{RF}}}\,\lambda_{\text{charge}}(x) = \begin{cases} \bar{i}_{\text{beam}} \frac{4}{\omega_x a} \sqrt{1 - \frac{[x-x_0]^2}{a^2}} & \text{for } x \in \mathcal{D}_x, \\ 0 & \text{else.} \end{cases}$$

for one bunch and, if continued periodically with period T_x, it can be rewritten according to (A.5) as

$$i_{\text{beam}}(x) = \bar{i}_{\text{beam}} \;+\; \sum_{k=1}^{\infty} A_k \cos(k\omega_x x + \varphi_k). \tag{3.32}$$

Gaussian Density Similar calculations can be performed for a Gaussian density function. A general Gaussian density function including a translation and rotation is given by

$$f(x,y) = \begin{cases} \frac{1}{2\pi\sigma_{1x}\sigma_{2x}}\, \mathrm{e}^{-\frac{1}{2}[\boldsymbol{x}-\boldsymbol{r}]^{\mathrm{T}}\mathbf{R}_{\Phi}^{\mathrm{T}}\mathbf{S}\mathbf{R}_{\Phi}[\boldsymbol{x}-\boldsymbol{r}]} & \text{for } x \in \left]-\frac{T_x}{2},\, \frac{T_x}{2}\right], \\ 0 & \text{else.} \end{cases} \tag{3.33}$$

with vectors and matrices

$$\boldsymbol{r} = \begin{bmatrix} x_0 \\ y_0 \end{bmatrix}, \qquad \mathbf{R}_{\Phi} = \begin{bmatrix} \cos\Phi & \sin\Phi \\ -\sin\Phi & \cos\Phi \end{bmatrix}, \qquad \mathbf{S} = \begin{bmatrix} \sigma_{1x}^{-2} & 0 \\ 0 & \sigma_{2x}^{-2} \end{bmatrix}.$$

The shape of a contour line of this Gaussian profile is elliptic and σ_{jx} are the standard deviations of the two-dimensional density distribution $f(x,y)$. The reason why f is not defined on the complete phase plane is that only one bunch is considered and adjacent bunches should not overlap.

With the abbreviations

$$a = \sqrt{\sigma_{1x}^2\cos^2\Phi + \sigma_{2x}^2\sin^2\Phi} \qquad b = \sqrt{\sigma_{1x}^2\sin^2\Phi + \sigma_{2x}^2\cos^2\Phi}$$
$$c = \left[\sigma_{1x}^2 - \sigma_{2x}^2\right]\cos\Phi\sin\Phi \qquad \Rightarrow \qquad a^2b^2 - c^2 = \sigma_{1x}^2\sigma_{2x}^2$$

the density can be rewritten as

$$f(x,y) = \frac{1}{2\pi\sqrt{a^2b^2-c^2}}\, \mathrm{e}^{-\frac{1}{2}\left[a^2[y-y_0]^2+b^2[x-x_0]^2-2c[x-x_0][y-y_0]\right]\Big/\left[a^2b^2-c^2\right]}$$

for $x \in \left]-\frac{T_x}{2}\,;\,\frac{T_x}{2}\right]$. The line density of this bunch is obtained by integrating over y, taking into account the integral

$$\int_{-\infty}^{\infty} \mathrm{e}^{-\frac{1}{2}\tilde{y}^2/m}\, \mathrm{d}\tilde{y} = \sqrt{2\pi m}.$$

This leads to the line density

$$\lambda(x) = \begin{cases} \frac{1}{\sqrt{2\pi}\,a}\, \mathrm{e}^{-\frac{1}{2}[x-x_0]^2/a^2} & \text{for } x \in \left]-\frac{T_x}{2},\, \frac{T_x}{2}\right], \\ 0 & \text{else.} \end{cases}$$

The spectral density is

$$\Lambda(\omega) = \frac{1}{\sqrt{2\pi}\,a} \int_{-T_x/2}^{T_x/2} \mathrm{e}^{-\frac{1}{2}[x-x_0]^2/a^2}\, \mathrm{e}^{-\mathrm{i}\omega x}\, \mathrm{d}x.$$

For

$$\sigma_{1x}, \sigma_{2x} < 1 \text{ and } x_0 \ll T_x/2, \tag{3.34}$$

the line density is negligible outside the integration interval and the approximation $T_x \to \infty$ for the integration limits can be made to simplify this integral. Finally, this leads with

$$\int_{-\infty}^{\infty} \mathrm{e}^{-\frac{1}{2}\tilde{x}^2/m}\, \mathrm{e}^{-\mathrm{i}\omega\tilde{x}}\, \mathrm{d}\tilde{x} = \sqrt{2\pi m}\, \mathrm{e}^{-\frac{1}{2}\omega^2 m}$$

to the approximation

$$\Lambda(\omega) \approx \mathrm{e}^{-\mathrm{i}\omega x_0}\, \mathrm{e}^{-\frac{1}{2}a^2\omega^2}.$$

To obtain the phase and amplitude of the harmonics, Equations (3.28), (3.29), and (3.30) can again be used. The mean current or DC current of the bunch is again

$$\bar{i}_{\mathrm{beam}} = \frac{Q_{\mathrm{bunch}}}{T_{\mathrm{RF}}}.$$

With (3.11), the beam current yields

$$i_{\mathrm{beam}}(x) = \begin{cases} \bar{i}_{\mathrm{beam}} \frac{\sqrt{2\pi}}{\omega_x\, a}\, \mathrm{e}^{-\frac{1}{2}[x-x_0]^2/a^2} & \text{for } x \in \left]-\frac{T_x}{2}, \frac{T_x}{2}\right], \\ 0 & \text{else.} \end{cases}$$

The phase and amplitude values of the harmonics are

$$A_k \approx 2\bar{i}_{\mathrm{beam}}\, \mathrm{e}^{-\frac{1}{2}[k\, a\, \omega_x]^2}, \qquad \varphi_k \approx -k\, \omega_x\, x_0. \tag{3.35}$$

In the following, the approximation signs will be omitted, but it has to be kept in mind that the derived results are based on ellipsoidal Gaussian distributions for which assumptions (3.34) hold.

3.5.3 Bunch Position and Length

In the last section, the phase and amplitude values of the beam current were derived depending on parameters of the density function f. But how do the A_k and φ_k depend on the bunch position and length, i. e. on the two parameters that are important for coherent dipole and quadrupole oscillations? The bunch position will be defined as the first moment or center of gravity

$$B_{1,0} := \int_{-\infty}^{\infty}\int_{-\infty}^{\infty} x\, f(x,y)\, \mathrm{d}x\, \mathrm{d}y \tag{3.36}$$

and the bunch length as the second central moment or variance

$$C_{2,0} := \int_{-\infty}^{\infty}\int_{-\infty}^{\infty} [x - B_{1,0}]^2 \; f(x,y)\,\mathrm{d}x\,\mathrm{d}y. \tag{3.37}$$

For the uniform bunch density (3.25), the bunch position and length are

$$B_{1,0} = x_0, \qquad C_{2,0} = \frac{1}{4}\left[R_{1x}^2\cos^2\Phi + R_{2x}^2\sin^2\Phi\right] = \frac{a^2}{4}. \tag{3.38}$$

In case of a matched bunch in a linear bucket, $R_{1x} = R_{2x} = R_x$ is the radius of the bunch and the variance is $C_{2,0} = R_x^2/4$. The standard deviation $\sqrt{C_{2,0}}$ equals half the radius.

With approximation (3.34), the bunch position and length calculation for the Gaussian bunch density (3.33) yields

$$B_{1,0} = x_0, \qquad C_{2,0} \approx \sigma_{1x}^2\cos^2\Phi + \sigma_{2x}^2\sin^2\Phi = a^2. \tag{3.39}$$

The matched case for a linear bucket is now $\sigma_{1x} = \sigma_{2x} = \sigma_x$; this is also the standard deviation of the bunch distribution. Comparing (3.38) and (3.39) shows that a uniform bunch with half-axes

$$R_{1x} = 2\sigma_{1x}, \qquad R_{2x} = 2\sigma_{2x} \tag{3.40}$$

has the same variance $C_{2,0}$ as a Gaussian bunch with standard deviations σ_{1x} and σ_{2x}.

By means of (3.38) and (3.39), the results of Section 3.5.2 can be written in a compact way. Table 3.6 summarizes these dependencies of the beam current and the amplitude and phase values on the bunch center of gravity and variance for the coordinate choice $x = \Delta\varphi$.

Equation (3.35) for A_k is appealing from an analytical point of view, since it can be easily inverted. This yields equations to calculate the center of gravity and variance, if phase and amplitude of a harmonic k are known:

$$B_{1,0} = -\frac{\varphi_k}{k\omega_x}, \qquad C_{2,0} \approx \frac{2}{k^2\omega_x^2}\ln\left(\frac{A_0}{A_k}\right). \tag{3.41}$$

Here, use was made of the fact that A_0 equals $2\bar{i}_{\mathrm{beam}}$. The special case $k = 1$ and $x = \Delta\varphi$ leads to

$$B_{1,0} \approx -\varphi_1, \qquad C_{2,0} \approx 2\,\ln\left(\frac{A_0}{A_1}\right). \tag{3.42a}$$

Of course, the proposed density functions f are only ideal models for a real bunch. A real bunch will never be exactly Gaussian or even uniform in its distribution. However, the longitudinal density of many bunches in proton and heavy-ion synchrotron rings is reported to be approximately Gaussian or parabolic. An additional complication is that the density distribution is not accessible for a direct measurement. The distribution can be reconstructed offline after the experiment, but online approaches require much effort

Table 3.6: Results for the short-term spectrum for ellipsoidal bunches with a uniform or Gaussian density function and coordinates $x = \Delta\varphi$. The moments $B_{1,0}$ and $C_{2,0}$ are assumed to be given in the variable $\Delta\varphi$.

Uniform density and $x = \Delta\varphi$:

$$i_{\text{beam}}(\Delta\varphi) = \frac{2\bar{i}_{\text{beam}}}{\sqrt{C_{2,0}}}\sqrt{1 - \frac{[\Delta\varphi - B_{1,0}]^2}{C_{2,0}}} \tag{3.43a}$$

$$A_k = 4\bar{i}_{\text{beam}}\frac{J_1\left(k\sqrt{4C_{2,0}}\right)}{k\sqrt{4C_{2,0}}}, \qquad \varphi_k = -k\,B_{1,0} \tag{3.43b}$$

Gaussian density and $x = \Delta\varphi$:

$$i_{\text{beam}}(\Delta\varphi) \approx \frac{\bar{i}_{\text{beam}}\sqrt{2\pi}}{\sqrt{C_{2,0}}}\,\mathrm{e}^{-[\Delta\varphi - B_{1,0}]^2/2C_{2,0}} \tag{3.44a}$$

$$A_k \approx 2\bar{i}_{\text{beam}}\,\mathrm{e}^{-\frac{1}{2}k^2C_{2,0}}, \qquad \varphi_k \approx -k\,B_{1,0} \tag{3.44b}$$

at the moment. Despite these difficulties, the equations for the Gaussian case seem to be suitable for an approximate estimation even for non-Gaussian distributions. Before this is demonstrated by simulation results, the derived equations are discussed for small bunches. It turns out that for the limit of very small bunches, the equations for the uniform and the Gaussian case become identical. This is conclusive, because both densities converge to a Dirac function for very small bunches. For small $R_x \ll 1$, property (A.4) for Bessel functions of the first kind can be used and A_k of (3.31) can be approximated by

$$A_k \approx 2\bar{i}_{\text{beam}}\left[1 - \frac{1}{2}k^2\omega_x^2\,C_{2,0}\right] \qquad \Rightarrow \qquad C_{2,0} \approx \frac{2}{k^2\omega_x^2}\left[1 - \frac{A_k}{2\bar{i}_{\text{beam}}}\right].$$

The linearisation for $\sigma_x \ll 1$ of the exponential function of (3.35) of the Gaussian density leads to the same result. The conclusion is that for small bunches, the formulas of the Gaussian density can also be used for bunches with uniform distributions. This will lead to an error in the estimated bunch variance $C_{2,0}$, but the error is bounded and increases with increasing bunch size. It is thus interesting to note that the error is smallest for $A_k = A_1$, since A_k depends on $kC_{2,0}$ and a larger k has the same effect on the error as a larger bunch size. For $C_{2,0} \to 0$, the amplitudes converge to $A_k \to 2\bar{i}_{\text{beam}}$, the result for a Dirac density function.

As the uniform and the Gaussian case can be regarded as the two extreme cases of realistic density functions of Table 3.1, the following simulation results demonstrates that (3.41) has a certain robustness against variations from the ideal Gaussian density function.

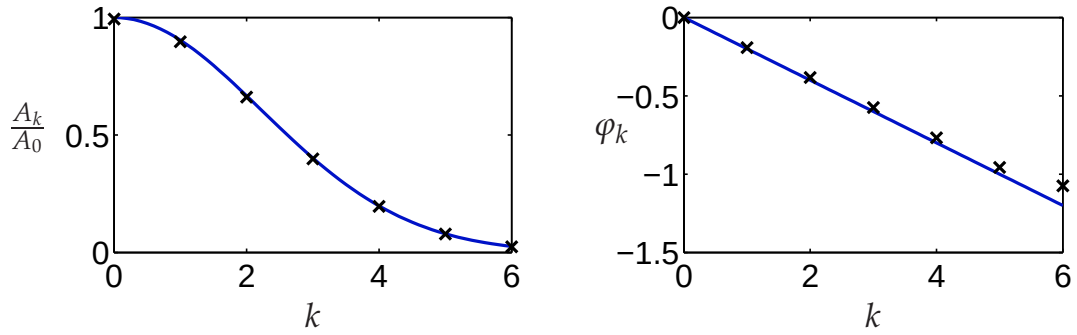

Figure 3.12: Beam current spectrum of a simulated particle bunch for a Gaussian density and $\sigma_\varphi = 0.5$, $\Delta\varphi_0 = 0.2$. Amplitude and phase values from the simulation ($\times$) and from (3.35) (blue).

3.5.4 Simulation Results of Short-Term Spectrum

Simulations with macro-particle bunches are now used to evaluate the theory of the last sections. In these simulations, the bunch consists of a number N_{macro} of macro particles. The particles are distributed according to the uniform or Gaussian densities (3.25) and (3.33) with $x_0 = 0$. The used coordinates are $\Delta\varphi$ and Δw. The line density and beam current are calculated by means of a histogram; the x-axis is divided in equally spaced bins and the number of particles in each bin is counted to obtain the histogram. The histogram values are collected in a vector and processed by a FFT algorithm. The resulting FFT coefficients are then converted to amplitude and phase values A_k and φ_k.

The number of bins N_{bin}, i. e. the number of divisions on the interval $\mathcal{D}_x$, and the number of macro particles N_{macro} are increased until a further increase in both numbers does not lead to a significant change of the simulation result. Typical numbers are between 100 and 500 for N_{bin} and between 10^3 and $2 \cdot 10^5$ for N_{macro}. For smaller bunches, the necessary number of bins tends to be larger to obtain a reasonable smooth beam current signal. Compared to uniform densities, Gaussian densities require a larger number of macro particles. This is due to the fact that the uniform density is obtained by a regular arranged pattern in the phase plane, whereas the bunch particles with a Gaussian density are initially distributed in a statistical manner in these simulations. It is also possible to have regularly distributed Gaussian bunches, this has been analyzed in [11].

Figure 3.12 compares the beam current spectrum obtained by the FFT in a multi-particle simulation with the calculated spectrum for a Gaussian bunch density. The simulation was performed with $2.25 \cdot 10^4$ particles and a histogram with 150 bins. Figure 3.13 shows the reconstruction of the beam current according to the sum of (3.32), if only the first N_h harmonics are used. In this example, the sum of the first 6 harmonics is already close to the ideal shape of (3.44a).

The spectrum values A_k and φ_k can be used to calculate the first and second moments of the bunch using (3.41). To compare these FFT-based calculations with their real values, the first and second moments of the bunch are needed. Because the bunch consists of a discrete number of particles, Equations (3.36) and (3.37) are approximated in the

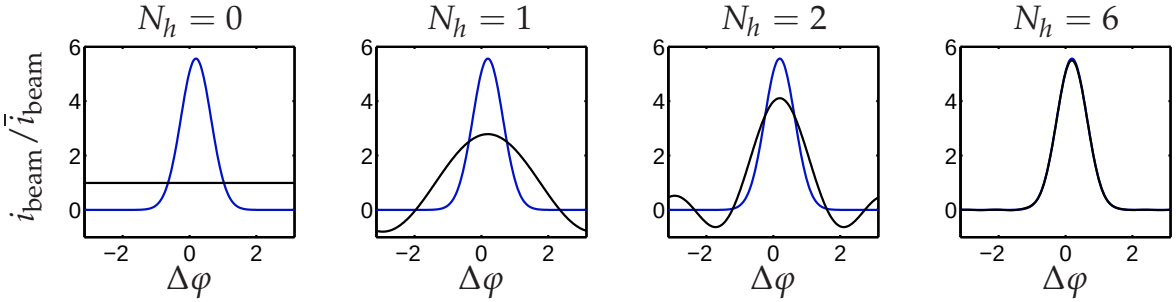

Figure 3.13: Reconstruction of the beam current with its harmonics in a tracking simulation: sum of the first N_h harmonics (black) and the ideal Gaussian beam current of (3.44a) (blue) and $\sigma_\varphi = 0.5$.

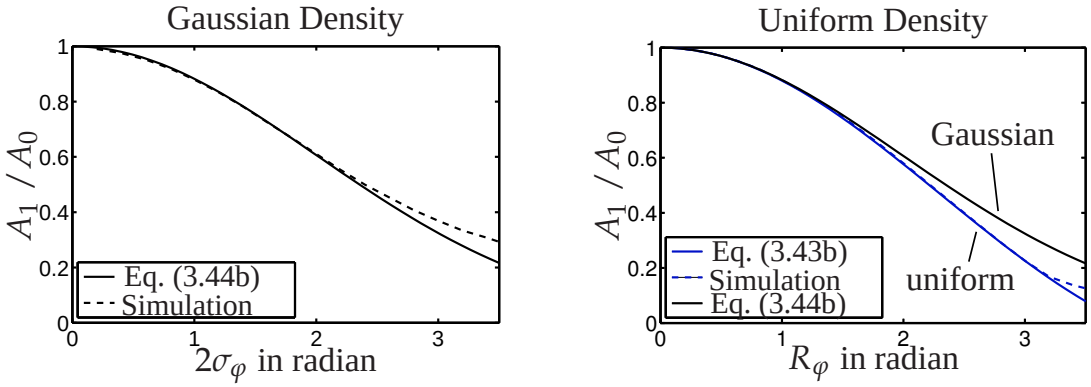

Figure 3.14: Comparison of the calculated short-term spectrum with simulation results.

simulation by the sums[5)]

$$B_{1,0} \approx \frac{1}{N}\sum_{n=1}^{N} x_n, \qquad C_{2,0} \approx \frac{1}{N}\sum_{n=1}^{N}\left[x_n - \frac{1}{N}\sum_{j=1}^{N} x_j\right]^2, \tag{3.45}$$

where N is the number of particles and x_n is the x-position of particle n in the phase plane.

Figure 3.14 shows the amplitude A_1 of the first harmonic versus the bunch size. The amplitude is calculated numerically in a macro particle simulation with Equations (3.43b), (3.44b), and $k = 1$. Because of (3.40), uniform bunches with R_x are compared to Gaussian bunches with $2\sigma_x$. The left image shows the results for an ellipsoidal bunch with a Gaussian density and standard deviations $\sigma_{1\varphi} = \sigma_{2\varphi} = \sigma_\varphi$. The amplitude A_1 is normalized with $A_0 = 2\bar{i}_{\text{beam}}$. The value of A_1 calculated with (3.43b) agrees very well with the simulation up to $\sigma_\varphi \approx 1$. For larger bunch sizes $\sigma_\varphi > 2$ assumption (3.34) is no longer valid and a small difference between the simulation result and Equation (3.44b)

[5)] The point of view is as follows: The particle bunch is assumed to be a realization of an underlying particle density distribution with parameters such as $B_{1,0}$ and $C_{2,0}$. These parameters are not exactly known, but can be estimated by the given sums.

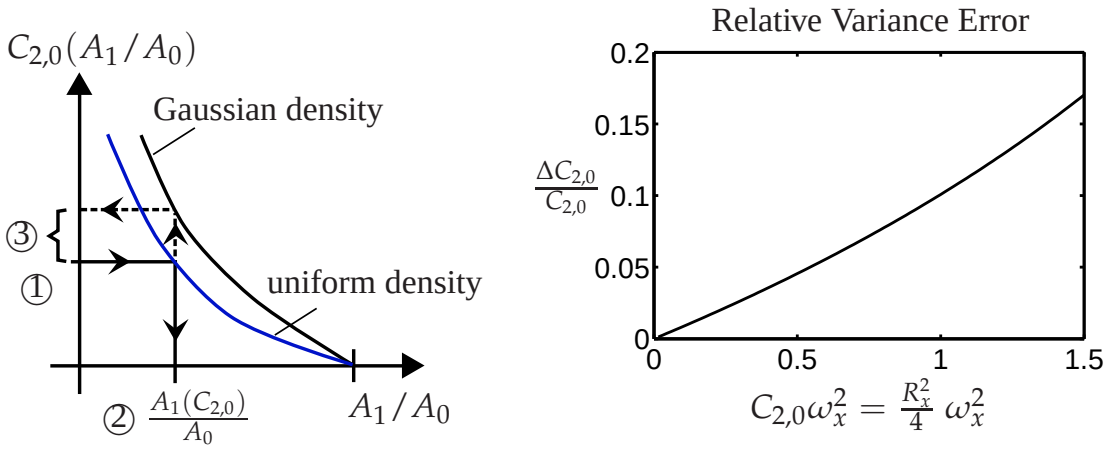

Figure 3.15: Estimation error for the bunch variance if the density is uniform and not Gaussian. **Left**: error calculation. **Right**: estimation error versus the bunch variance.

becomes apparent. The right image shows the results for a uniform density. The calculated and simulated values of A_1 agree for values up to $\sigma_\varphi \approx 3$. For very large bunches there is a small deviation, because the upper and lower boundary values (cf. (3.26)) are outside the bunch interval. The described two curves are also compared with (3.44b), this demonstrates that the spectrum is indeed similar for uniform and Gaussian densities.

Equation (3.41) can be used to calculate the bunch variance $C_{2,0}$ from spectrum measurements. If the bunch density is not Gaussian, there will be an estimation error. To express this error quantitatively, it is assumed that there is an ellipsoidal bunch with a uniform density in the ring with the variance $C_{2,0}$ (① in the left image of Figure 3.15). Equation (3.31) specifies the amplitude A_1 that will be measured ②:

$$\frac{A_1(C_{2,0})}{A_0} = 2\frac{J_1\left(\omega_x\sqrt{4C_{2,0}}\right)}{\omega_x\sqrt{4C_{2,0}}}.$$

If the estimation $\tilde{C}_{2,0}$ of the variance is however based on Equation (3.41) for Gaussian densities, this results in the relative estimation error ③

$$\frac{\Delta C_{2,0}}{C_{2,0}} = \frac{\frac{2}{\omega_x^2}\ln\left(\frac{A_0}{A_1(C_{2,0})}\right) - C_{2,0}}{C_{2,0}} = \frac{2}{C_{2,0}\omega_x^2}\ln\left(\frac{\sqrt{4C_{2,0}\omega_x^2}}{2J_1\left(\sqrt{4C_{2,0}\omega_x^2}\right)}\right) - 1,$$

where $\Delta C_{2,0} := \tilde{C}_{2,0} - C_{2,0}$. This relative error is shown in the right diagram of Figure 3.15. It is about 10% for a variance of $C_{2,0}\omega_x^2 = 1$ which corresponds to rather large bunches with $R_\varphi = 2$ or $\sigma_\varphi = 1$.

Estimation Errors Due to Landau Damping The previous figures show that the conversion formula (3.42a) performs well for bunches with Gaussian densities and even for bunches with uniform densities with $R_\varphi \leq 2$, if an estimation error of 10% is acceptable. However, so far no Landau damping has been included in the considerations. Due

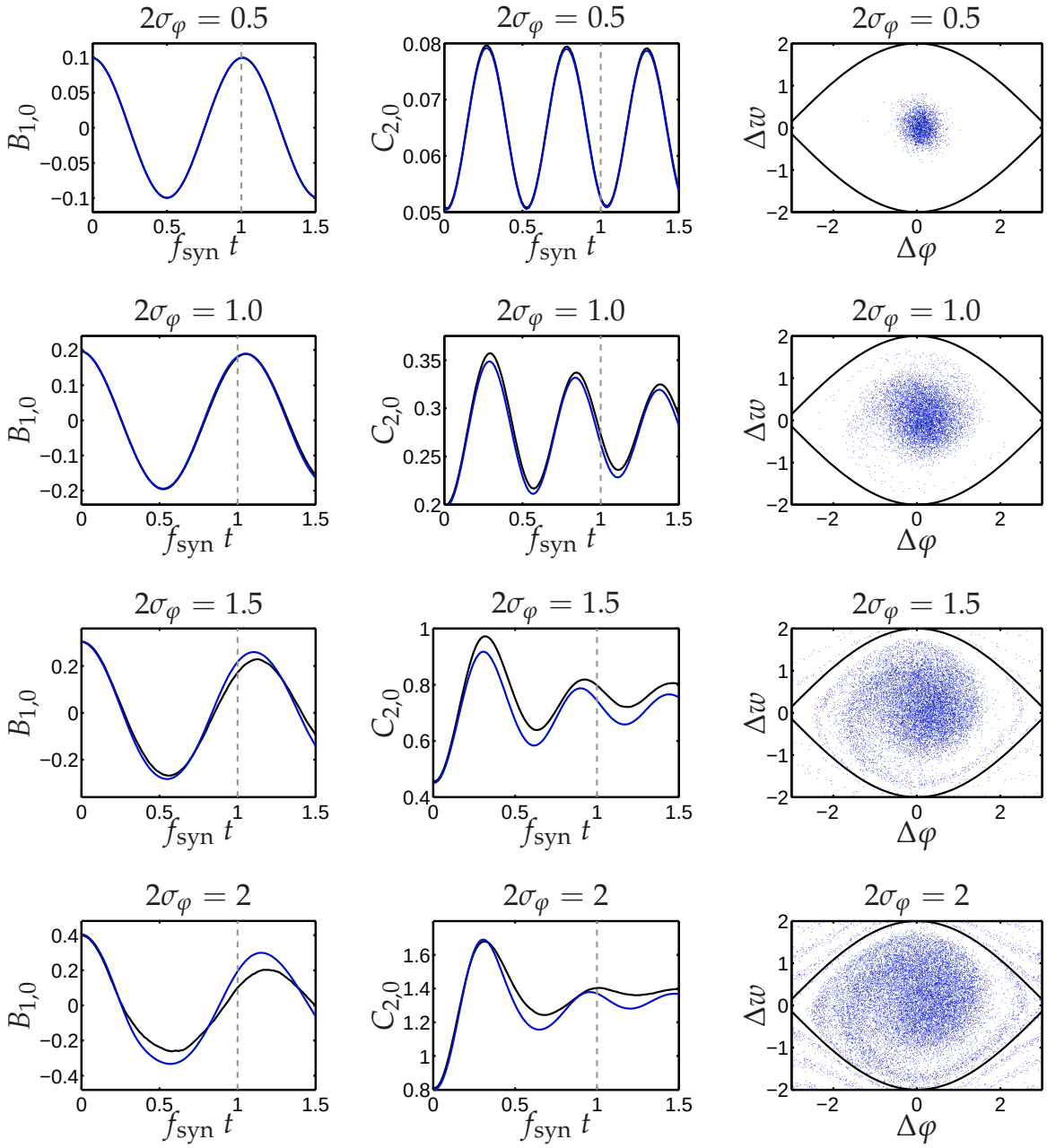

Figure 3.16: Particle tracking simulation with Gaussian densities comparing the real bunch moments (black) with the estimated moments by means of the beam spectrum (blue) for different bunch sizes σ_x. The phase plane plots on the right show the final configuration of the bunches (not every particle is plotted).

to Landau damping, the elliptic shape of the bunches will be altered and this will lead to estimation errors even for Gaussian densities. To evaluate these errors, nonlinear tracking simulations are performed for different bunch sizes. All simulations in this section have a stationary bucket, i. e. $\varphi_{\mathrm{R}} = 0$.

Figure 3.16 shows the results for Gaussian densities. The initial bunch configurations are distributed according to (3.33) with

$$2\sigma_\varphi = 2\sigma_x \in \{0.5\,,1\,,1.5\,,2\}\,, \quad \sigma_{1x} = 0.9\,\sigma_x,\ \sigma_{2x} = 1.1\,\sigma_x,\ x_0 = 0.4\,\sigma_x,\ \Phi = 0,$$

i. e. the bunches are ellipsoidal and have a mismatch in both position and length such that coherent modes $m = 1$ and $m = 2$ appear. The plots of the moments $B_{1,0}$ and $C_{2,0}$ compare the real bunch moments of (3.45) with the FFT-based calculations of (3.42a), assuming Gaussian densities. For large bunch sizes, the Landau damping of the bunch variance is considerable and the final bunch shape is clearly non-ellipsoidal. However, the estimation of the moments can still be acceptable for control purposes. The particle number is $N_{\text{macro}} = 4 \cdot 10^4$ and the number of bins is $N_{\text{bin}} \in [200\,;\,400]$.

The simulation results for uniform densities are shown in Figure 3.17. The estimation of the moments is again based on (3.42a) for Gaussian densities. As already noticeable in Figure 3.15, this formula overestimates the bunch variance for uniform densities. However, the estimation error is even smaller compared to the Gaussian case. This is due to the fact that the Landau damping for the uniform densities seems to be much smaller than the Landau damping of comparable bunches of Gaussian density. The initial bunch configurations are distributed according to (3.25) with

$$R_\varphi = R_x \in \{0.5\,,1\,,1.5\,,2\}\,,\ R_{1x} = 0.9\,\sigma_x, \quad R_{2x} = 1.1\,\sigma_x,\ x_0 = 0.2\,R_x, \quad \Phi = 0$$

and the particle and bin numbers are $N_{\text{macro}} = 10^4$ and $N_{\text{bin}} \in [200,\,400]$.

It has to be noted that for smaller mismatches of the bunch variance, a considerable offset of the estimated variance might become apparent. For example, for a bunch with $R_\varphi = 1$, the variance equals $C_{2,0} = 0.25$ and the relative estimation error is about 10%, cf. Figure 3.15. This leads to an absolute error of 0.025. In Figure 3.17, the oscillation amplitude of the variance is much larger and this offset is barely visible, but will become apparent for smaller oscillation amplitudes. As will be discussed in Chapter 5, common controller types for coherent modes have a differentiating structure or at least suppress the DC component of the measurements. In this case, the described offset is not relevant if it is approximately time-independent.

3.5.5 Effective Synchrotron Frequency

Besides Landau damping, Figures 3.16 and 3.17 shows another interesting property of coherent oscillations as a result of the nonlinear beam dynamics. For small bunch sizes, the frequency of the oscillation in $B_{1,0}$ is f_{syn} and 2 f_{syn} for oscillations in $C_{2,0}$. This corresponds to the frequency mf_{syn} of the coherent mode m. For larger bunch sizes, the simulations show that the oscillation period T_m of mode m increases, thus the frequency f_m decreases. This is consistent with the fact that large bunches have a large synchrotron frequency spread and a large number of particles with a frequency $f_{\text{syn,eff}}$ that is smaller than the linear synchrotron frequency f_{syn}, cf. Figure 2.14.

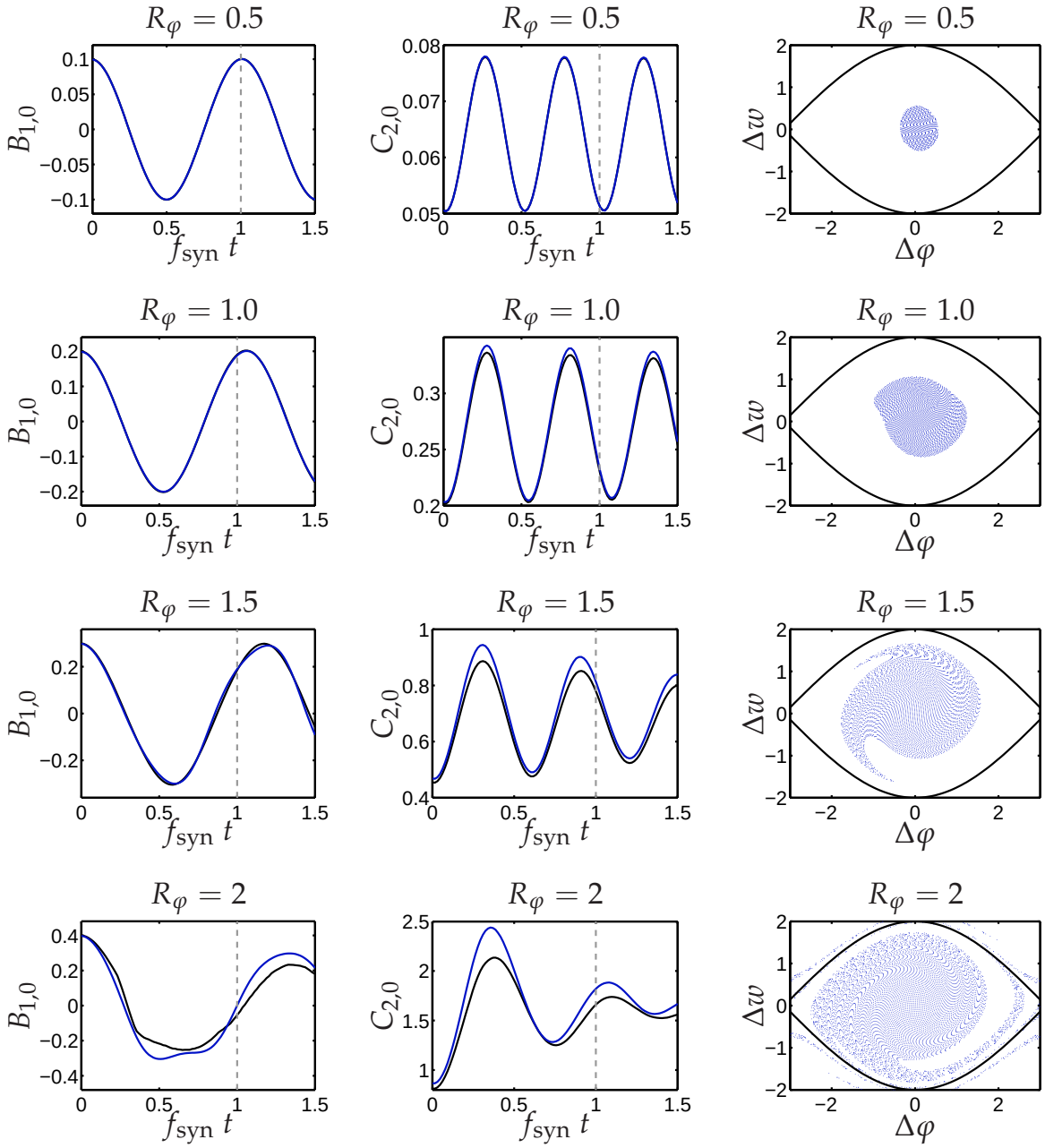

Figure 3.17: Particle tracking simulation with uniform densities comparing the real bunch moments (black) with the estimated moments by means of the beam spectrum (blue) for different bunch sizes R_x. The phase plane plots on the right show the final configuration of the bunches (not every particle is plotted).

The relative periods and frequencies obtained in the simulation of the modes $m = 1$ and $m = 2$ of Figures 3.16 and 3.17

$$\frac{f_m}{m\, f_{\mathrm{syn}}} = \frac{T_{\mathrm{syn}}}{m\, T_m}$$

are given in Table 3.7. For the smallest bunch size, the mode frequencies f_m are approximately f_{syn} and $2\, f_{\mathrm{syn}}$, as expected. For larger bunch sizes, the mode frequencies

Table 3.7: Frequencies of the oscillation modes in Figure 3.16.

	Gaussian					Uniform			
$2\sigma_\varphi$	$\frac{T_{m=1}}{T_{syn}}$	$\frac{2\,T_{m=2}}{T_{syn}}$	$\frac{f_{m=1}}{f_{syn}}$	$\frac{f_{m=2}}{2\,f_{syn}}$	R_φ	$\frac{T_{m=1}}{T_{syn}}$	$\frac{2\,T_{m=2}}{T_{syn}}$	$\frac{f_{m=1}}{f_{syn}}$	$\frac{f_{m=2}}{2\,f_{syn}}$
	$B_{1,0}$	$C_{2,0}$	$B_{1,0}$	$C_{2,0}$		$B_{1,0}$	$C_{2,0}$	$B_{1,0}$	$C_{2,0}$
0.5	1.02	1.02	0.98	0.98	0.5	1.02	1.02	0.98	0.98
1	1.06	1.09	0.94	0.92	1	1.07	1.07	0.93	0.93
1.5	1.13	1.28	0.89	0.78	1.5	1.2	1.2	0.83	0.83

decrease. In case of the Gaussian distribution, there is a noticeable difference between the two modes.

To analyze the general dependency of the oscillation frequency f_m on the bunch size, further simulation results with a larger variety of bunch sizes are considered in Figure 3.18. In these simulations, initial bunch distributions with variances $C_{2,0}$ and bunch sizes

$$2\sqrt{C_{2,0}} := \begin{cases} R_\varphi & \text{uniform density} \\ 2\sigma_\varphi & \text{Gaussian density} \end{cases}$$

are tracked numerically for the stationary case $\varphi_R = 0$ during a few synchrotron periods and the frequencies of the modes $m = 1$ and $m = 2$ are recorded. The results are only rough estimations, since the mode frequencies change in the course of the simulation due to Landau damping and an attempt was made to estimate the frequencies at the beginning of the simulation. The obtained frequencies are summarized in Appendix C.1 and shown in Figure 3.18. The left image of the figure shows that the mode frequencies can be approximately described by (solid line)

$$\frac{f_m\left(2\sqrt{C_{2,0}}\right)}{m\,f_{syn}} \approx \frac{f_{syn,eff}\left(r_\varphi = 2\sqrt{C_{2,0}}\right)}{f_{syn}}, \qquad m \in \{1, 2\}, \tag{3.46}$$

where $f_{syn,eff}$ is the nonlinear synchrotron frequency (2.63) for the stationary case with $\Delta\varphi_+ = r_\varphi$ and this leads to the hypothesis that the frequency of mode m is

$$\omega_{m,hy} = m\,\omega_{syn}\,\frac{\pi}{2K\left(\sin\left(\sqrt{C_{2,0}}\right)\right)} \tag{3.47}$$

For the uniform density, this implies that the frequencies of the modes $m = 1{,}2$ approximately depend on the synchrotron frequency that applies to the boundary R_φ of the bunch. In case of Gaussian densities, it is the synchrotron frequency at the radius $2\sigma_\varphi$ that is decisive. This is demonstrated in the right image of Figure 3.18: for each mode, the obtained frequency f_m is converted to the corresponding amplitude r_φ of a particle with the synchrotron frequency $f_{syn,eff} = f_m/m$ using (3.47). The accumulation of the measurements around $r_\varphi = 2\sqrt{C_{2,0}}$ is again an indication that the synchrotron frequency at $2\sqrt{C_{2,0}}$ determines the mode frequencies.

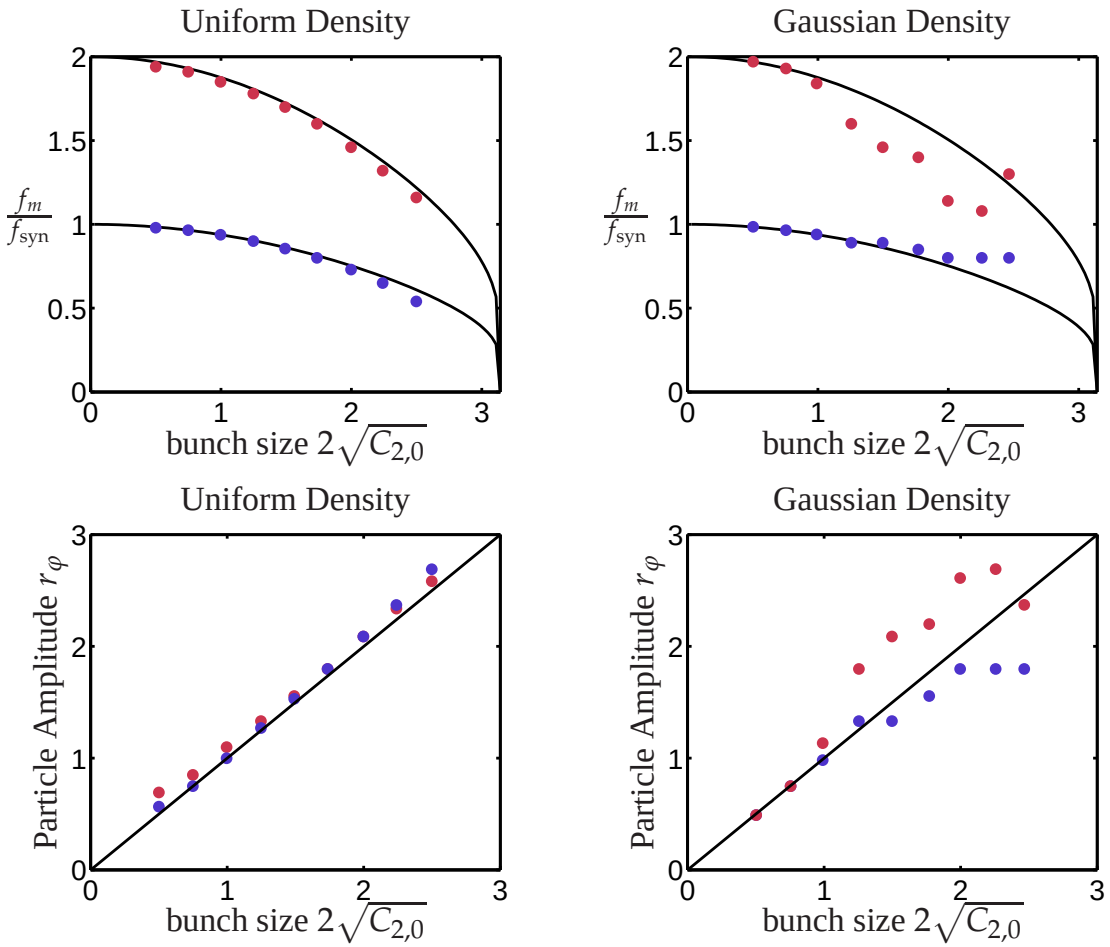

Figure 3.18: Top: Dipole and quadrupole mode frequencies f_1 (blue dots) and f_2 (red dots) versus the bunch size $C_{2,0}$ for uniform densities and Gaussian densities, comparison with relative nonlinear synchrotron frequency $f_{\mathrm{syn,eff}}/f_{\mathrm{syn}}$ (black, solid). **Bottom**: Amplitude r_φ of a single particle with a nonlinear synchrotron frequency $f_{\mathrm{syn,eff}}$ that is equal to the mode frequency f_m/m for $m = 1$ (blue dots) and $m = 2$ (red dots) of the corresponding bunch size for uniform Gaussian densities and $\Delta\varphi_+ = 2\sqrt{C_{2,0}}$ (black, solid).

3.6 Conclusion

Proceeding from single-particle dynamics to a particle ensemble introduces new dynamical phenomena; the shape of the particle bunch may perform coherent oscillations. To describe these oscillations, the particle distribution has been considered as a statistical realization of a probability density function. The evolution of this density function can be described by a partial differential equation. Next, different density functions have been examined as candidates to describe coherent oscillations. Ellipsoidal bunches can describe two basic coherent oscillations: bunch phase and bunch length oscillations. Analytical relations between the beam current spectrum of ellipsoidal bunches with uniform or Gaussian density functions and their center of gravity and variance have been derived.

This step is important for the modeling of the measurement in the RF feedback loop; the beam current spectrum is easily accessible for measurements, whereas the bunch shape in phase space is not. The derived formulas for Gaussian densities have been shown to be sufficiently accurate even in case of significant filamentation. In addition, they may be used for other distributions such as uniform densities, if the DC component of the measurement is suppressed by the feedback loop. Ellipsoidal bunches cannot be used to describe higher order coherent oscillations. For this purpose, different density functions are proposed to describe the within-bunch modes m. Simulation results demonstrate that in a single-harmonic nonlinear bucket, the oscillation frequency of a bunch mode m is not a multiple of the synchrotron frequency. Rather, the mode frequency depends on the bunch length and decreases for increasing bunch sizes.

The classical approach in the frequency domain with the long-term spectrum I_{beam} (cf. Section 3.5.1) needs a linearization of the synchrotron oscillation. The disadvantages are:

- Constant synchrotron frequency for all particles and a neglect of Landau damping
- Complicated calculation for higher order modes
- It is not evident how to calculate the dynamics, i. e. the influence of the feedback on the modes

Because of these difficulties in the frequency domain, a new modeling approach in the time domain based on moments is proposed in the next chapter. Since the moments such as the bunch variance are not directly measurable, the proposed calculations of the short-term spectrum in Section 3.5.2 will be important in the following. These calculations show that the bunch center of gravity and variance can be deduced from the Fourier coefficients of the short-term spectrum.

4 Models of Coherent Oscillations

Many models of coherent oscillations rely on the frequency domain. As shown in Section 3.5, a common method is to measure the beam current signal over one synchrotron period and to analyse its frequency spectrum. The advantage of this is that the control problem is easy to formulate. A train of h matched bunches is periodic with h times the revolution frequency f_R and should therefore have only frequency components at multiples of $h\omega_\mathrm{R}$. Coherent oscillations lead to sidebands around these fundamental harmonics with offsets proportional to multiples of the synchrotron frequency ω_syn. Thus, if sidebands occur in the spectrum, they should be detected and damped by a feedback system. However, as was pointed out in Section 3.5.1, there is no strict one-to-one correspondence of modes and specific sidebands, if the modes are defined as density modulations that repeat themselves after a fraction of the synchrotron period. In addition, the design of a feedback system relies on models that describe the input-output behavior, that is the response of the modes (outputs) with respect to modulations of the RF phase and amplitude (inputs). Thus, the question remains how to model the dependencies between the RF inputs of the gap voltage and the spectrum components. This is the subject of this chapter. The modeling is performed in the time domain. This has the advantage that nonlinear RF dynamics can be taken into account, whereas common modeling schemes in the frequency domain are based on a linearization of the RF dynamics.

The chapter is organized as follows: Section 4.1 introduces a short summary of existing RF feedback models for coherent modes and highlights a question concerning the controllability of higher order modes that arises from simulation results. Section 4.2 gives a definition of the control problem based on the particle density function. Section 4.3 reviews basic definitions and theorems concerning the controllability of linear and nonlinear systems. A new modeling scheme for coherent oscillations is developed in Section 4.4. The scheme is based on a moment method and a truncation method. The moment method by itself is well-known. Moment approaches as used in this chapter have been proposed before for the simulation of beam dynamics in linear accelerators [18]. Recent papers use moment methods to obtain fast and efficient beam dynamics for a variety of simulation applications [3, 4, 29]. However, the use for coherent oscillations in a nonlinear bucket and the subsequent control-theoretic analysis are the novel contribution of this chapter. The modeling scheme is used in Sections 4.5 and 4.6 to obtain and analyze models for the linear and nonlinear bucket, respectively. Finally, a conclusion is drawn in Section 4.7.

4.1 Introduction

Table 4.1 shows selected publications that present feedback models for longitudinal single-bunch oscillations in synchrotrons. These references will be compared with the

Table 4.1: Existing models for coherent oscillation modes.

Mode m	1	2	3	4	> 4
Linear Bucket	[13, 107]	[13, 40, 107]	?	?	?
Nonlinear Bucket	?	?	?	?	?

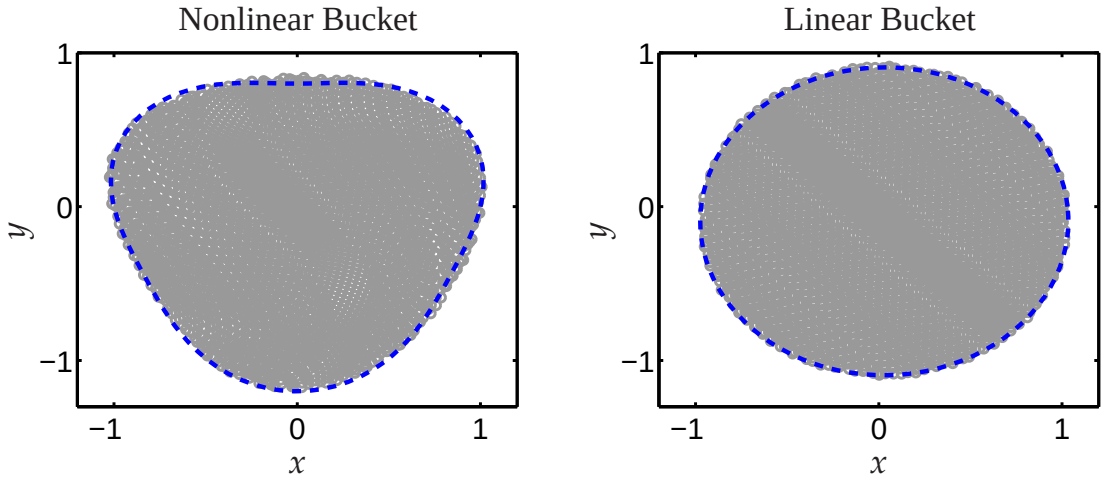

Figure 4.1: Tracking simulation with a phase modulation with $3\omega_{\mathrm{syn}}$. The dashed lines show the boundaries $r_{\mathrm{nl}}(\theta)$ and $r_{\mathrm{lin}}(\theta)$. **Left**: nonlinear bucket. **Right**: linear bucket.

results of this chapter in detail in Section 4.7.1. However, it is already apparent from Table 4.1 that the models are restricted to the modes $m = 1$ and $m = 2$ and to the linear bucket.

Simulations indicate however that higher order modes with $m > 2$ cannot be excited or damped in a linear bucket. This can be demonstrated by tracking simulations, as has been done for different distributions and bunch sizes in [94]. In this section, a similar simulation is performed for a uniform density to enable a straightforward interpretation of the bunch boundary.

The first simulation is performed in a stationary nonlinear bucket. The initial bunch shape is a circle with radius $r(\theta) = 1$. A phase modulation of

$$u_\varphi(t) = \frac{\pi}{18} \sin(3\omega_{\mathrm{syn}} t)$$

is used to excite a sextupole oscillation. The resulting bunch shape after $t/T_{\mathrm{syn}} = 1.12$ is shown in the left diagram of Figure 4.1. The bunch shape can be circumscribed by

$$r_{\mathrm{nl}}(\theta) = 1 + 0.1 \sin(\theta - \pi) + 0.1 \sin(3\theta)$$

which can be interpreted as a combination of a dipole and sextupole mode with $r_1 = r_3 = 0.1$.

The second simulation is performed in a stationary linear bucket. The initial bunch shape and the phase modulation are the same as before. The final bunch shape after

$t/T_{\text{syn}} = 1.12$ is shown in the right diagram of Figure 4.1. The bunch shape can be circumscribed by

$$r_{\text{lin}}(\theta) = 1 + 0.1\sin(\theta - 3.45).$$

Thus, only a dipole oscillation is excited.

Similar results can be obtained for other higher order modes with $m > 2$. This is a strong indication that higher order modes are not controllable in a linear bucket. This clearly shows that

> the nonlinearity of the RF potential plays an essential role in the control of the modes and should be considered in the modeling process.

4.2 Characterisation of the Dynamics

4.2.1 Beam Dynamics as Partial Differential Equation

As described in Section 3.2, the longitudinal beam dynamics can be formulated by the Liouville-Vlasov equation, a partial differential equation of the form

$$\frac{\partial f}{\partial t} + \frac{\partial f}{\partial x}\dot{x} + \frac{\partial f}{\partial y}\dot{y} = 0, \qquad \dot{x} = a_1(x, y), \quad \dot{y} = a_2(x, y). \tag{4.1}$$

The functions a_1 and a_2 describe the nonlinear beam dynamics in the longitudinal phase plane (x, y). The phase plane coordinates x and y should be canonically conjugate for a preservation of phase space in the correct coordinates. If the time segment of interest – for instance the damping behavior of a feedback system during a few synchrotron periods – is small compared to the complete acceleration cycle, other coordinates are however also possible. In the following, the coordinates of table 3.5 will be applied, since this scales the trajectories in a favorable way and eases the formulation of the control problem.

In contrast to ordinary differential equations (ODEs), partial differential equations (PDEs) contain derivatives with respect to more than one variable. In physical problems, the variables usually include the time and several spatial or other variables. The most general form of a PDE is given by the following

Definition 4.1 (General partial differential equation, [15, 23])**.** Given a region $\mathcal{D} = \mathcal{D}_t \times \mathcal{D}_x \subset \mathbb{R} \times \mathbb{R}^n$ and $\boldsymbol{x} = (x_1, \ldots, x_n)$, $(t, \boldsymbol{x}) \in \mathcal{D}$, a *partial differential equation of order k in $n+1$ independent variables* has the form

$$G\left(\boldsymbol{x}, f(t, \boldsymbol{x}), \frac{\partial f(t, \boldsymbol{x})}{\partial t}, \frac{\partial f(t, \boldsymbol{x})}{\partial x_1}, \ldots, \frac{\partial f(t, \boldsymbol{x})}{\partial x_n}, \ldots, \frac{\partial^k f(t, \boldsymbol{x})}{\partial^{k_0} t \partial^{k_1} x_1 \ldots \partial^{k_n} x_n}, \ldots\right) = 0$$

and the highest derivative is of order $k = k_0 + k_1 + \ldots + k_n$.

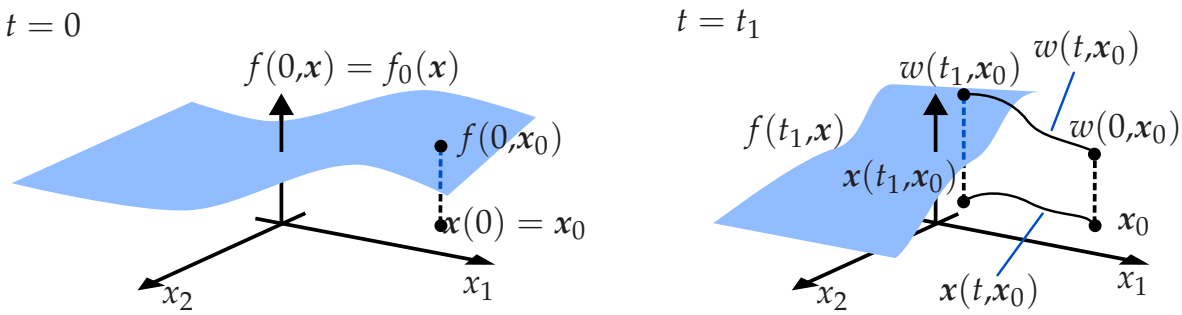

Figure 4.2: Characteristic and base characteristic for an initial value problem with $n = 2$. **Left**: initial value $f(t = 0,\boldsymbol{x})$ and an arbitrary point $\boldsymbol{x}_0$. **Right**: evolved solution at $t = t_1$ and characteristic $w(t,\boldsymbol{x}_0)$ and base characteristic $\boldsymbol{x}(t,\boldsymbol{x}_0)$.

For the special case $n = 0$, the PDE becomes an ODE. The solution of a PDE is a class of functions $f(t, \boldsymbol{x})$ that are defined on $\mathcal{D}$ and are called a *classical solution*, if the functions are smooth, i. e. belong to the set of functions that is at least k times continuously differentiable [83].

A PDE can be *linear* or *nonlinear*. Roughly speaking, a PDE is linear if the sum of two different solutions or a multiple of a solution does again satisfy the PDE. If the time t is not included as an independent variable, the PDE is a *steady-state* equation, else it is called an *evolution* equation.

The most general form of a linear partial differential evolution equation of first order is given by

$$\frac{\partial f(t, \boldsymbol{x})}{\partial t} + \sum_{j=1}^{n} a_j(t, \boldsymbol{x}) \frac{\partial f(t, \boldsymbol{x})}{\partial x_j} = b(t,\boldsymbol{x}) f(t, \boldsymbol{x})$$

with arbitrary functions a_j and b. If $b \equiv 0$, the PDE is *homogeneous*. Thus, Equation (4.1) is a linear homogeneous PDE of first order in three independent variables t, $x_1 = x$, and $x_2 = y$. More specifically, it belongs to the class of *transport* equations.

A unique solution of (4.1) can be obtained if the initial bunch density $f(t = 0, x, y)$ is given. This leads to the following *initial value problem*:

$$\begin{aligned} &f_t(t, \boldsymbol{x}) + \boldsymbol{a}(t, \boldsymbol{x})^{\mathrm{T}} f_{\boldsymbol{x}}(t, \boldsymbol{x}) = 0 \\ &f(t = 0, \boldsymbol{x}) = f_0(\boldsymbol{x}) \qquad \text{initial condition, } f_0(\boldsymbol{x}) \text{ is given.} \end{aligned} \tag{4.2}$$

In these equations, f_t is a short notation for the partial derivative of f with respect to t, $\boldsymbol{a}^{\mathrm{T}} = (a_1(t, \boldsymbol{x}), \ldots, a_n(t, \boldsymbol{x}))$ is a general nonlinear vector function and $f_{\boldsymbol{x}} = (f_{x_1}, \ldots, f_{x_n})^{\mathrm{T}}$ is the gradient of f with respect to $\boldsymbol{x}$.

For this special problem, there exists a constructive method to find the solution: the *method of characteristics*. First, the *characteristic*

$$w(t, \boldsymbol{x}_0) := f(t, \boldsymbol{x}(t, \boldsymbol{x}_0)) \tag{4.3}$$

is defined as the curve that is obtained if the initial value $\boldsymbol{x}(0) = \boldsymbol{x}_0$ is chosen and the values of f are recorded along the trajectory $\boldsymbol{x}(t)$ that starts from $\boldsymbol{x}_0$. The trajectory $\boldsymbol{x}$ is

referred to as the *base characteristic*. The definitions are illustrated in Figure 4.2. The rate of change of w is

$$\frac{\mathrm{d}w(t,\boldsymbol{x}_0)}{\mathrm{d}t} = f_t(t,\boldsymbol{x}(t,\boldsymbol{x}_0)) + \frac{\mathrm{d}\boldsymbol{x}}{\mathrm{d}t} f_{\boldsymbol{x}}(t,\boldsymbol{x}(t,\boldsymbol{x}_0)).$$

Comparing this with the initial value problem (4.2), the choice

$$\frac{\mathrm{d}\boldsymbol{x}}{\mathrm{d}t} = \boldsymbol{a}(t,\boldsymbol{x})^{\mathrm{T}} \tag{4.4}$$

leads directly to

$$\frac{\mathrm{d}w(t,\boldsymbol{x}_0)}{\mathrm{d}t} = 0, \quad \Rightarrow \quad w(t,\boldsymbol{x}_0) = \text{const.} = w(0,\boldsymbol{x}_0) = f(0,\boldsymbol{x}_0) = f_0(\boldsymbol{x}_0). \tag{4.5}$$

Equation (4.4) is a system of n ODEs that are called the *characteristic equations*. If it is possible to obtain a trajectory $\boldsymbol{x}(t,\boldsymbol{x}_0)$ of these ODEs depending on an initial value $\boldsymbol{x}(t=0) = \boldsymbol{x}_0$ and this trajectory can be finally solved for the initial value

$$\boldsymbol{x}_0 = \boldsymbol{x}_0(t,\boldsymbol{x}),$$

the solution of the initial value problem (4.2) can be written with (4.3) and (4.5) as

$$f(t,\boldsymbol{x}) = w(t,\boldsymbol{x}_0) = f_0(\boldsymbol{x}_0(t,\boldsymbol{x})). \tag{4.6}$$

For every smooth function f_0, this solution is unique. Equation (4.6) shows that the designation *transport equation* is indeed appropriate: the value of f_0 is conserved and transported along the base characteristic $\boldsymbol{x}$.

The method of characteristics will now be applied to the longitudinal beam dynamics. For a particle with a small oscillation amplitude, the longitudinal motion is given by (2.43) and the characteristic equations are thus

$$\frac{\mathrm{d}\boldsymbol{x}}{\mathrm{d}t} = \frac{\mathrm{d}}{\mathrm{d}t}\begin{bmatrix} x \\ y \end{bmatrix} = \begin{bmatrix} -\omega_{\mathrm{syn}} y \\ \omega_{\mathrm{syn}} x \end{bmatrix}, \qquad \boldsymbol{x}_0 = \begin{bmatrix} x_0 \\ y_0 \end{bmatrix}.$$

The solution of this initial value problem is

$$\boldsymbol{x}(t,\boldsymbol{x}_0) = \begin{bmatrix} x(t,\boldsymbol{x}_0) \\ y(t,\boldsymbol{x}_0) \end{bmatrix} = \begin{bmatrix} x_0 \cos(\omega_{\mathrm{syn}} t) - y_0 \sin(\omega_{\mathrm{syn}} t) \\ x_0 \sin(\omega_{\mathrm{syn}} t) + y_0 \cos(\omega_{\mathrm{syn}} t) \end{bmatrix}$$

and solving for $\boldsymbol{x}_0$ yields

$$\boldsymbol{x}_0(t,\boldsymbol{x}) = \begin{bmatrix} x\cos(\omega_{\mathrm{syn}} t) + y\sin(\omega_{\mathrm{syn}} t) \\ -x\sin(\omega_{\mathrm{syn}} t) + y\cos(\omega_{\mathrm{syn}} t) \end{bmatrix} \tag{4.7}$$

The final solution of the PDE is

$$f(t,x,y) = f_0\left(x\cos(\omega_{\mathrm{syn}} t) + y\sin(\omega_{\mathrm{syn}} t)\ ,\ -x\sin(\omega_{\mathrm{syn}} t) + y\cos(\omega_{\mathrm{syn}} t)\right).$$

It can be verified easily that this is indeed a solution of the initial value problem by employing f in the PDE (4.1).

Expectedly, the initial bunch distribution f_0 rotates in the phase plane with the frequency ω_{syn} and the bunch shape is conserved. Because the quantity $x_0^2 + y_0^2 = x^2 + y^2$ is constant, cf. (4.7), every smooth initial distribution that can be written as

$$f_0(x, y) = f_0(x^2 + y^2)$$

leads to a time-independent solution f, as is also discussed in Section 3.3.4.

In case of larger synchrotron amplitudes, the nonlinear ODEs (4.4) cannot be solved analytically and this applies in particular to the solution of the PDE. For conservative Hamiltonian dynamics however, it is known that the Hamiltonian $H(x, y)$ is a constant of motion along the trajectories $(x(t),y(t))$. Thus, it can be concluded that an initial distribution of the form

$$f_0(x, y) = f_0\left(H(x, y)\right)$$

also leads to a time-independent solution $f(t, x, y) = f_0(x_0,y_0) = f_0(H(x_0,y_0)) = f_0(H(x, y))$.

4.2.2 Definition of Input Variables

So far, no input variables have been discussed. The beam dynamics can be extended in such a way that an input vector $\boldsymbol{u} = [u_1, \ldots, u_m]^{\mathrm{T}}$ is included. This does only change the characteristic equations, but not the structure of the PDE. The dynamics with dependency on the input variables can be written as

$$\frac{\partial f}{\partial t} + \frac{\partial f}{\partial x}\dot{x} + \frac{\partial f}{\partial y}\dot{y} = 0, \qquad \dot{x} = a_1(x,y,\boldsymbol{u}), \quad \dot{y} = a_2(x,y,\boldsymbol{u}).$$

Two very common input variables of the longitudinal dynamics are phase and amplitude modulations of the RF gap voltage. They can be included in Equations (2.33a) and (2.33b). Choosing $k_{\text{RF}} = 1$, the amplitude modulation $\hat{U}_1(t) = \hat{U}_{1,\text{R}}[1 + u_\varepsilon(t)]$, the phase modulation $u_\varphi = -\varphi_{\text{f}}$ and the coordinate $x = \varphi_k - \varphi_{\text{R}} - \varphi_{\text{f}}$ yields with (2.34) the nonlinear dynamics

$$\ddot{x}(t) = \frac{Qh\eta_{\text{R}}\omega_{\text{R}}^2\hat{U}_{1,\text{R}}}{2\pi\beta_{\text{R}}W_{\text{R}}}\left[[1 + u_\varepsilon(t)]\sin(\varphi_{\text{R}} + x(t) - u_\varphi(t)) - \sin\varphi_{\text{R}}\right].$$

With the synchrotron frequency ω_{syn} from (2.38) and $y = -\dot{x}/\omega_{\text{syn}}$, the longitudinal dynamics finally can be written as

$$\dot{x}(t) = a_1(y) = -\omega_{\text{syn}}y(t), \tag{4.8a}$$

$$\dot{y}(t) = a_2(x,u_\varepsilon,u_\varphi) = \frac{\omega_{\text{syn}}}{\cos\varphi_{\text{R}}}\left[[1 + u_\varepsilon(t)]\sin(\varphi_{\text{R}} + x(t) - u_\varphi(t)) - \sin\varphi_{\text{R}}\right]. \tag{4.8b}$$

4.2.3 Definition of the Control Problem

In the framework of the Vlasov equation, it is simple to state the control objective. Mismatches of the bunch or coherent oscillations should be damped away for $t \to \infty$. Formally, this can be expressed as

$$\lim_{t\to\infty} f_t\left(t, x, y, u_\varepsilon(t), u_\varphi(t)\right) = 0.$$

In fact, this can already be achieved for $(u_\varepsilon, u_\varphi) \equiv \mathbf{0}$ by Landau damping. However, this will increase the longitudinal emittance. A criterion for the feedback performance should thus be taken into account and a possible choice is the area occupied by the bunch

$$J_{\text{control}}(t) = C_{2,0}(t)\, C_{0,2}(t) - C_{1,1}(t)^2,$$

where $C_{2,0}$ and $C_{0,2}$ denote the variances and $C_{1,1}$ is the covariance in the phase plane. The increase of J_c should be as small as possible.

Although the formulation of the control objective is straightforward, the analysis of the dynamics or the design of a feedback controller are much more demanding, since it is impossible to find an exact analytical solution to the nonlinear control problem. Existing methods rely on a linearization of the longitudinal beam dynamics so that every particle has the same synchrotron frequency, but this is a coarse approximation. In Section 4.4, a new modeling scheme based on moments will be proposed to incorporate model nonlinearities. Prior to that, controllability theorems for linear and nonlinear systems will be reviewed.

4.3 Controllability

In this section, theorems concerning the controllability of control systems are reviewed that will be used in the subsequent sections.

4.3.1 Linear Systems

A linear time-invariant system is given by

$$\Sigma_{\mathbf{A},\mathbf{B}}: \qquad \begin{aligned} \dot{\boldsymbol{x}}(t) &= \mathbf{A}\boldsymbol{x}(t) + \mathbf{B}\boldsymbol{u}(t), \qquad \boldsymbol{x}(t=0) = \boldsymbol{x}_0, \\ \boldsymbol{y}(t) &= \mathbf{C}\boldsymbol{x}(t), \end{aligned} \tag{4.9}$$

where $\boldsymbol{x} \in \mathbb{R}^n$ is the n-dimensional state vector, $\boldsymbol{u} \in \mathbb{R}^m$ is the input vector, and $\mathbf{A} \in \mathbb{R}^n \times \mathbb{R}^n$ and $\mathbf{B} \in \mathbb{R}^n \times \mathbb{R}^m$ are constant real matrices. The matrix $\mathbf{C} \in \mathbb{R}^r \times \mathbb{R}^n$ is the output matrix and $\boldsymbol{y}$ is the r-dimensional output vector with quantities that can be measured. The time is denoted by $t \in \mathbb{R}$ and $\boldsymbol{x}_0$ is the initial condition at $t = 0$.

The concept of *controllability* is concerned with the question whether the system can be influenced in such a way that an arbitrary initial state $\boldsymbol{x}_0$ is transferred to another state $\boldsymbol{x}_1$ in a final time t_1:

Definition 4.2 (Controllability, [79], p.88)**.** The linear system (4.9) is said to be completely (state) controllable if and only if for every $\boldsymbol{x}_0 \in \mathbb{R}^n$, $\boldsymbol{x}_1 \in \mathbb{R}^n$ a piecewise continuous function $\boldsymbol{u}^*(t)$, $t \in [0,t_1]$ and $0 < t_1 < \infty$ can be found such that for the initial condition $\boldsymbol{x}(0) = \boldsymbol{x}_0$ and the input $\boldsymbol{u} = \boldsymbol{u}^*(t)$, the solution $\boldsymbol{x}(t)$ of (4.9) satisfies $\boldsymbol{x}(t_1) = \boldsymbol{x}_1$.

The following theorems can be used to check for controllability.

Theorem 4.1 (Kalman, [79], p.88)**.** *A necessary and sufficient condition for system* (4.9) *to be completely controllable is that the rank of the Kalman controllability matrix*

$$\mathcal{C}(\mathbf{A},\mathbf{B}) = \begin{bmatrix}\mathbf{B} & \mathbf{AB} & \dots & \mathbf{A}^{n-1}\mathbf{B}\end{bmatrix} \in \mathbb{R}^n \times \mathbb{R}^{nm} \tag{4.10}$$

is equal to n.

Hautus' criterion is useful to check individual eigenvalues for their controllability and also in case the matrices $\mathbf{A}$ and $\mathbf{B}$ are parameter-dependent.

Theorem 4.2 (Hautus, [84], p.72)**.** *The linear system* (4.9) *is completely controllable if and only if the condition*

$$\operatorname{rank}\begin{bmatrix}\lambda_i\mathbf{I}-\mathbf{A} & \mathbf{B}\end{bmatrix} = n$$

is fulfilled for all eigenvalues λ_i *(*$i = 1,2,\dots,n$*) of* $\mathbf{A}$*, where* $\mathbf{I}$ *denotes the unity matrix with the appropriate dimension* $n \times n$.

If the system is not completely controllable, it is possible to consider a subspace ([84], p.81)

$$\mathcal{S} = \{\tilde{\boldsymbol{x}} \in \mathbb{R}^r \,:\, \tilde{\boldsymbol{x}} = \mathbf{H}\boldsymbol{x}, \quad \boldsymbol{x} \in \mathbb{R}^n\} \tag{4.11}$$

of the state space with a matrix $\mathbf{H}$ of size $r \times n$ and $r < n$. A necessary and sufficient condition for complete controllability in $\mathcal{S}$ is

$$\operatorname{rank}[\mathbf{H}\mathcal{C}] = \operatorname{rank}\begin{bmatrix}\mathbf{HB} & \mathbf{HAB} & \dots & \mathbf{HA}^{n-1}\mathbf{B}\end{bmatrix} = r.$$

4.3.2 Nonlinear Systems

A general class of nonlinear systems is given by

$$\begin{aligned}\dot{\boldsymbol{x}}(t) &= \boldsymbol{f}(\boldsymbol{x}(t),\boldsymbol{u}(t)), \qquad \boldsymbol{x}(t=0) = \boldsymbol{x}_0,\\ \boldsymbol{y}(t) &= \boldsymbol{h}(\boldsymbol{x}(t)),\end{aligned} \tag{4.12}$$

with the vector fields $\boldsymbol{f}$ and $\boldsymbol{h}$, the input $\boldsymbol{u} \in \mathbb{R}^m$, time $t \in \mathcal{T} \subset \mathbb{R}$ and the state vector $\boldsymbol{x} \in \mathcal{U} \subset \mathbb{R}^n$ which lies in an open subset of the state space. The initial condition at $t = 0$ is denoted by $\boldsymbol{x}_0$ and the output vector is $\boldsymbol{y} \in \mathbb{R}^r$.

In contrast to linear systems, properties of nonlinear systems such as stability and controllability are usually not global, but only local. It is thus useful to formulate the new

Definition 4.3 ([79], p.96)**.** System (4.12) is said to be *locally controllable* at the equilibrium point $(\boldsymbol{x}_\mathrm{e}, \boldsymbol{u}_\mathrm{e})$ if for all real $\varepsilon > 0$ there exists a real $\eta > 0$ such that for every pair of vectors $\boldsymbol{x}_0 \in \mathbb{R}^n$ and $\boldsymbol{x}_1 \in \mathbb{R}^n$ close enough to the equilibrium point, namely satisfying $||\boldsymbol{x}_0 - \boldsymbol{x}_\mathrm{e}|| < \eta$ and $||\boldsymbol{x}_1 - \boldsymbol{x}_\mathrm{e}|| < \eta$, there exists a piecewise continuous control $\boldsymbol{u}^*(t)$ on $t \in [0;\ \varepsilon]$ such that $||\boldsymbol{u}^*(t)|| < \varepsilon\ \forall t \in [0;\ \varepsilon]$ and the integral curve of (4.12) at time ε, generated by $\boldsymbol{u}^*$ from $\boldsymbol{x}_0$ at time 0, equals $\boldsymbol{x}_1$.

In general, the test for local controllability can be a complex task. Usually, it is useful to calculate the tangent linear system around the equilibrium $(\boldsymbol{x}_\mathrm{e}, \boldsymbol{u}_\mathrm{e})$

$$\dot{\boldsymbol{x}} = \mathbf{A}\boldsymbol{x} + \mathbf{B}\boldsymbol{u}, \quad \mathbf{A} = \frac{\partial \boldsymbol{f}}{\partial \boldsymbol{x}}(\boldsymbol{x}_\mathrm{e}, \boldsymbol{u}_\mathrm{e}), \quad \mathbf{B} = \frac{\partial \boldsymbol{f}}{\partial \boldsymbol{u}}(\boldsymbol{x}_\mathrm{e}, \boldsymbol{u}_\mathrm{e}) \tag{4.13}$$

and check for first-order controllability first:

Definition 4.4 ([79], p.96)**.** System (4.12) is said to be *first-order controllable* at the equilibrium point $(\boldsymbol{x}_\mathrm{e}, \boldsymbol{u}_\mathrm{e})$ if the rank of $\mathcal{C}$, defined by (4.10) for the tangent linear system (4.13), is equal to n.

If the tangent linear system is controllable, system (4.12) is first-order controllable and the following theorem holds.

Theorem 4.3 ([79], p.97)**.** *If system* (4.12) *is first-order controllable at the equilibrium point* $(\boldsymbol{x}_\mathrm{e}, \boldsymbol{u}_\mathrm{e})$*, it is locally controllable at* $(\boldsymbol{x}_\mathrm{e}, \boldsymbol{u}_\mathrm{e})$.

Remark 4.1. The inverse is not always true: a nonlinear system that is locally controllable at an equilibrium does not have to be first-order controllable.

4.4 Modeling Scheme for Single-Bunch Oscillations

This section introduces a new modeling scheme that takes into account the nonlinearity of the beam dynamics. The scheme is based on moments and leads to models that can be used for controller analysis or design. It requires that the beam dynamics are given as or can be approximated by a polynomial expression [76].

The modeling scheme is valid for a particle bunch with N particles at positions (x_k, y_k) in the phase plane, but also for a bunch density $f(x, y, t)$ with the properties

$$\int_{-\infty}^{\infty}\int_{-\infty}^{\infty} f(x, y, t)\ \mathrm{d}x\ \mathrm{d}y = 1, \qquad \frac{\mathrm{d}f}{\mathrm{d}t} = 0, \tag{4.14}$$

i. e. it is assumed that the density is normalized and the flow is Hamiltonian which means that the local phase space density is conserved.

4.4.1 Moments

A particle bunch can be regarded as a realization of a random process; assuming an initial probability density function $f(x, y, t = 0)$, the initial particle distribution at $t = 0$ is obtained by choosing randomly N positions (x_k,y_k) in phase space using the probability density f. If the number of particles N is large, the number of particles ΔN in a small area ΔA around a point (x_0,y_0) will be approximately $\Delta N \simeq f(x_0, y_0)\Delta A$, i. e. the measured particle density $\Delta N/\Delta A$ will tend to the probability density f. A thorough introduction to random processes and probabilities can be found for example in [106] and the subsequent line of argument partly follows this reference.

A density function can be characterized by its moments. The mean values of a two-dimensional probability density are given by

$$B_{1,0}(t) := \int_{-\infty}^{\infty}\int_{-\infty}^{\infty} x\, f(x, y, t)\, \mathrm{d}x\, \mathrm{d}y, \qquad B_{0,1}(t) := \int_{-\infty}^{\infty}\int_{-\infty}^{\infty} y\, f(x, y, t)\, \mathrm{d}x\, \mathrm{d}y. \tag{4.15}$$

and will be denoted as *basic moments* in the following. General higher order moments can be defined as

$$R_{n,m}(t) := \int_{-\infty}^{\infty}\int_{-\infty}^{\infty} x^n\, y^m\, f(x, y, t)\, \mathrm{d}x\, \mathrm{d}y \tag{4.16}$$

and will be denoted as *raw moments*. Special cases are

$$R_{0,0}(t) = 1, \quad R_{1,0}(t) = B_{1,0}(t), \quad R_{0,1}(t) = B_{0,1}(t).$$

It is sometimes favorable to consider instead the *central moments*

$$C_{n,m}(t) := \int_{-\infty}^{\infty}\int_{-\infty}^{\infty} [x - B_{1,0}(t)]^n\ [y - B_{0,1}(t)]^m\ f(x, y, t)\, \mathrm{d}x\, \mathrm{d}y. \tag{4.17}$$

In particular,

$$C_{0,0}(t) = 1, \quad C_{1,0}(t) = C_{0,1}(t) = 0$$

holds. Fortunately, it is possible to express every central moment as a combination of raw moments and vice versa. Using the general first binomial rule, a central moment can be rewritten as

$$\begin{aligned} C_{n,m} &:= \int_{-\infty}^{\infty}\int_{-\infty}^{\infty} \sum_{k}^{n}\sum_{l}^{m} \binom{n}{k}\binom{m}{l}\, x^k\, y^l\ [-B_{1,0}]^{n-k}\, [-B_{0,1}]^{m-l}\ f(x, y, t)\, \mathrm{d}x\, \mathrm{d}y \\ &= \sum_{k}^{n}\sum_{l}^{m} \binom{n}{k}\binom{m}{l}\, R_{k,l}\ [-B_{1,0}]^{n-k}\, [-B_{0,1}]^{m-l}\,. \end{aligned} \tag{4.18}$$

Also, rewriting (4.16) as

$$R_{n,m} = \int_{-\infty}^{\infty}\int_{-\infty}^{\infty} [[x - B_{1,0}] + B_{1,0}]^n \; [[y - B_{0,1}] + B_{0,1}]^m \; f(x, y, t)\, \mathrm{d}x\, \mathrm{d}y$$

provides a simple way to calculate in a very similar way

$$R_{n,m} = \sum_{k=0}^{n}\sum_{l=0}^{m} \binom{n}{k}\binom{m}{l} C_{k,l}\; B_{1,0}^{n-k}\; B_{0,1}^{m-l}. \tag{4.19}$$

For example, the raw moment $R_{3,0}$ can be written as

$$R_{3,0} = C_{0,0}B_{1,0}^3 + 3C_{1,0}B_{1,0}^2 + 3C_{2,0}B_{1,0} + C_{3,0} = C_{3,0} + 3B_{1,0}C_{2,0} + B_{1,0}^3.$$

For the Gaussian and uniform densities (3.25) and (3.33) of ellipsoidal bunches, the basic moments $B_{1,0}$ and $B_{0,1}$ and the central moments $C_{2,0}$, $C_{1,1}$, and $C_{0,2}$ are sufficient to calculate all higher order moments. This is also apparent from Table C.1 (p.174). Thus, if the class of densities (3.25) and (3.33) is considered, the moments are uniquely determined by the density $f(x, y)$ and the density is uniquely determined by the moments.

In general, the uniqueness between moments and the probability density function is only valid under certain assumptions. Uniqueness theorems for one- and two-dimensional densities are stated in [106] and [46]. The proof of the uniqueness theorem involves the use of the *joint characteristic function*

$$\Phi(\omega_1, \omega_2) = \int_{-\infty}^{\infty}\int_{-\infty}^{\infty} f(x, y)\, \mathrm{e}^{\mathrm{i}[\omega_1 x + \omega_2 y]}\, \mathrm{d}x\, \mathrm{d}y, \tag{4.20}$$

where $\omega_1, \omega_2 \in \mathbb{R}$. This function is a two-dimensional Fourier transform of f. If f depends on the time t, the characteristic function will also be time-dependent.

The exponential function can be expanded into a series at the origin $(\omega_1, \omega_2) = (0, 0)$ and this yields

$$\Phi(\omega_1, \omega_2) = \int_{-\infty}^{\infty}\int_{-\infty}^{\infty} \sum_{p=0}^{\infty} \frac{[\mathrm{i}\omega_1]^p}{p!}\, x^p \sum_{q=0}^{\infty} \frac{[\mathrm{i}\omega_2]^q}{q!}\, y^q\, f(x, y)\, \mathrm{d}x\, \mathrm{d}y.$$

Exchanging the summation and integration, this leads with (4.16) to

$$\Phi(\omega_1, \omega_2) = \sum_{p=0}^{\infty}\sum_{q=0}^{\infty} \frac{[\mathrm{i}\omega_1]^p}{p!}\; \frac{[\mathrm{i}\omega_2]^q}{q!} R_{n,m}. \tag{4.21}$$

The calculation is however only valid if all moments $R_{n,m}$ are finite and the series converges near the origin. Under these assumptions, the joint characteristic function is

uniquely determined by the moments. Using the two-dimensional inverse Fourier transform, (4.20) can be solved for the density

$$f(x,y) = \frac{1}{4\pi^2} \int_{-\infty}^{\infty} \int_{-\infty}^{\infty} \Phi(\omega_1,\omega_2)\, \mathrm{e}^{-\mathrm{i}[\omega_1 x + \omega_2 y]}\, \mathrm{d}\omega_1\, \mathrm{d}\omega_2.$$

Thus, under the stated conditions, the density f is uniquely determined by its characteristic function or by its moments.

Theorem 4.4 (Uniqueness theorem [46], [106])**.** *Assume the probability density function $f(x,y)$ is piecewise continuous and has nonzero values only in a finite part of the plane $(x,y) \in \mathbb{R}^2$. Then moments $R_{n,m}$ of all orders exist and are finite. If, in addition, the series* (4.21) *converges near the origin, the moment sequence $\{R_{n,m}\}$ is uniquely determined by $f(x,y)$ and f is uniquely determined by the moment sequence.*

Remark 4.2. Because of (4.19), this also holds for a moment sequence comprising the basic and the central moments.

In Section 4.2.3, the aim of the control problem was stated to be $\lim_{t\to\infty} \partial f/\partial t = 0$, i. e. a constant density $f(x,y,t) = f_0(x,y)$ should be obtained for $t \to \infty$. With Theorem 4.4, the control problem can be reformulated as

$$\lim_{t\to\infty} \frac{\mathrm{d}R_{n,m}(t)}{\mathrm{d}t} = 0, \qquad \forall n,m, \tag{4.22}$$

if it can be guaranteed that the necessary assumptions remain valid during the control and evolution of the bunch. Again, this is equivalent to demanding that the basic and central moments should be constant. This argument justifies the use of moments instead of f to obtain models for a controller synthesis.

Because in reality or in a macro-particle tracking simulation, the bunch consists of N particles with discrete positions $(x_k, y_k), k = 1,\ldots,N$, it is also useful to define a discrete version of the moments. For a large N, they are reasonable estimates of the continuous moments. The discrete moments read

$$\tilde{R}_{n,m} := \frac{1}{N}\sum_{k=1}^{N} x_k^n\, y_k^m, \qquad \tilde{B}_{1,0} := \frac{1}{N}\sum_{k=1}^{N} x_k, \qquad \tilde{B}_{0,1} := \frac{1}{N}\sum_{k=1}^{N} y_k$$

$$\tilde{C}_{n,m} := \frac{1}{N}\sum_{k=1}^{N} [x_k - B_{1,0}]^n [y_k - B_{0,1}]^m$$

and the conversions (4.18) and (4.19) remain valid.

4.4.2 Basic Modeling Principle

The modeling approach will be discussed exemplarily for the basic moment $B_{1,0}$ in the discrete definition. Nevertheless, a modeling with the continuous moment definitions

is also possible and can be expected to be similar to existing moment approaches [3–5, 29, 64, 103].

In general, the moment will be a function of time and its derivative is given by

$$\dot{B}_{1,0}(t) = \frac{1}{N} \sum_{k=1}^{N} \dot{x}_k(t). \tag{4.23}$$

If the particle dynamics $\dot{x}_k$ can be written as a polynomial function

$$\dot{x}_k = a_{10} x_k \; + \; a_{01} y_k \; + \; a_{11} x_k y_k \; + \; \ldots, \tag{4.24}$$

Equation (4.23) can be rewritten as

$$\dot{B}_{1,0} = a_{1,0} B_{1,0} \; + \; a_{0,1} B_{0,1} \; + \; a_{1,1} R_{1,1} \; + \; \ldots \tag{4.25}$$

In this equation, the raw moment $R_{1,1}$ appears. This is disadvantageous, since Section 3.5.2 shows that the quantities that can be measured are rather linked to *central moments* such as $C_{2,0}$. To avoid raw moments, they simply can be replaced by using (4.19) and (4.25) can finally be written as

$$\begin{aligned} \dot{B}_{1,0} &= a_{1,0} B_{1,0} + a_{0,1} B_{0,1} + a_{1,1} \left(C_{1,1} + B_{1,0} B_{0,1} \right) + \ldots \\ &= f \left(B_{1,0}, B_{0,1}, C_{2,0}, C_{1,1}, \ldots \right), \end{aligned}$$

which is a function of basic and central moments. In a similar manner, the derivatives of the central moments can be calculated. In most cases, the presented calculation of the moment dynamics is tedious and has to be done using a computer algebra system.

4.4.3 Moments and Densities

Before proceeding with the derivation of equations that describe the dynamics of the central moments of the beam, this section deals with the question how the defined moments are related to the single-bunch oscillation modes m of Chapter 3. To answer this question, four different density functions are analyzed and their moments are calculated. The results will be used in subsequent sections for a model truncation.

Ellipsoidal Bunches In Section 3.5.3, ellipsoidal bunches with uniform and Gaussian densities were defined. These bunch models are sufficient if only dipole and quadrupole modes ($m = 1, 2$) are studied. The plots (a) and (b) of Figure 4.3 show examples for the uniform density (3.25) and the Gaussian density (3.33). For these density functions, it is possible to calculate the basic and central moments as defined in (4.15) and (4.17). The results of the calculations for moments up to the order $n_x + n_y = 14$ were obtained with the assistance of MATHEMATICA and are summarized in Table C.1 of Appendix C.2.1. These results show that all moments C_{n_x,n_y} with odd order $n_x + n_y$ are zero. Furthermore, all even moments with $n_x + n_y \geq 4$ can be expressed as nonlinear functions of the variances $C_{2,0}$ and $C_{2,0}$ and the coveriance $C_{1,1}$. This is particularly interesting in the following, because it allows order reduction of the models which will be used to describe the

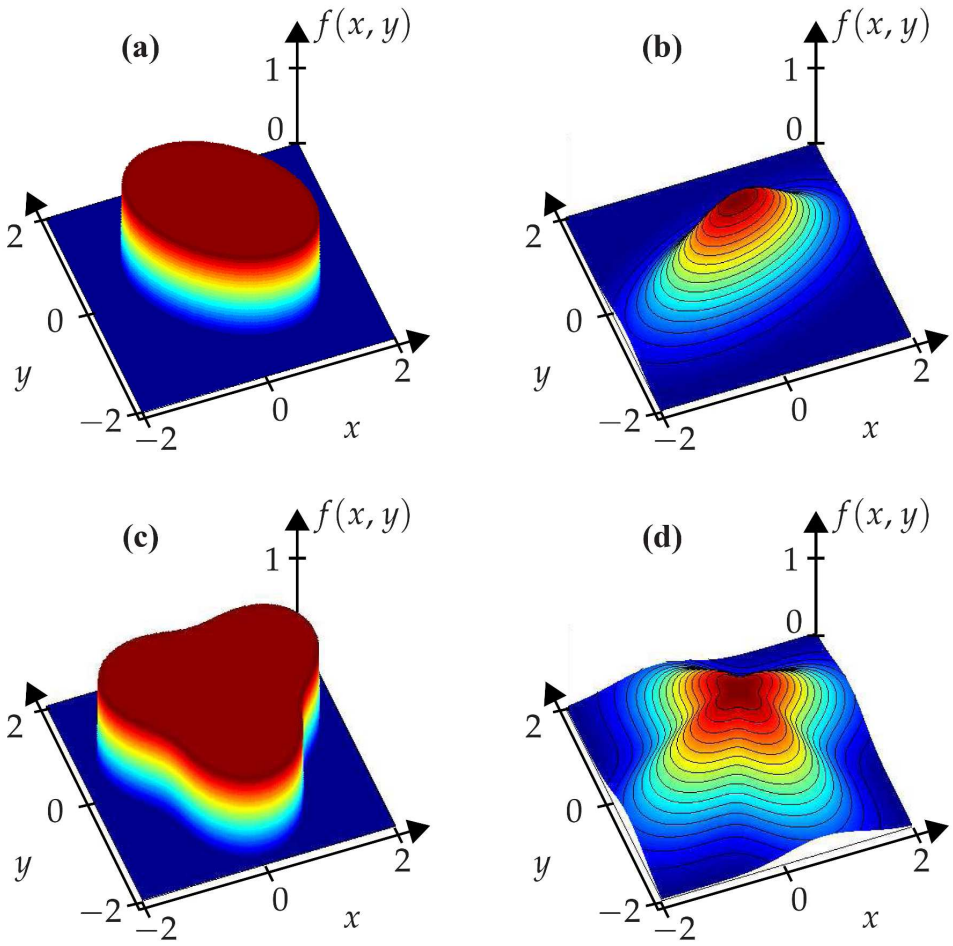

Figure 4.3: Density distribution functions with ellipsoidal (top) and mode (bottom) contour lines. **(a)**: uniform density (3.25) with $f_0 = 1$, $\Phi = -45°$, $R_{1x} = 1.5$, $R_{2x} = 1$, and $x_0 = y_0 = 0$. **(b)**: Gaussian density (3.33) with $f_0 = 1$, $\Phi = 50°$, $\sigma_{1x} = 1$, $\sigma_{2x} = .5$, and $x_0 = y_0 = 0$. **(c)**: uniform density (3.16) with $f_0 = 1$, $r_3 = .2$, $R_0 = 1.5$, and $\theta_{3,0} = 0$. **(d)**: Gaussian density (3.18) with $f_0 = 1$, $\sigma_0 = 1$, $r_4 = .2$, and $\theta_{4,0} = 0$.

dynamics of the moments. This order reduction goes without any approximation, because the higher order moments can be replaced by second order terms. However, this is only valid under the condition that the bunch is ellipsoidal. For large initial mismatches of the bunch, this condition may be violated due to filamentation.

Taking into account the basic moments $B_{1,0}$ and $B_{0,1}$, there are five degrees of freedom to uniquely determine the shape of the considered density functions. This corresponds to the parameters x_0, y_0, R_{1x}, R_{2x}, and Φ for the uniform density and to the parameters x_0, y_0, σ_{1x}, σ_{2x}, and Φ for the Gaussian density. A comparison of the columns of Table C.1 shows that equal variances are obtained for both density functions if $R_{1x} = 2\sigma_{1x}$ and $R_{2x} = 2\sigma_{2x}$ is chosen. In addition, the nonlinear functions for the higher moments are identical for both densities except for a constant factor. For equal central moments of

order $n_x + n_y = 2$, the moments relate as

$$\frac{C_{n_x,n_y,\text{gauss}}}{C_{n_x,n_y,\text{uniform}}} = \begin{cases} 1, & n_x + n_y = 2 \\ \frac{3}{2}, & n_x + n_y = 4 \\ 3, & n_x + n_y = 6 \\ \frac{15}{2}, & n_x + n_y = 8 \end{cases}$$

to each other. Note that for Gaussian densities, the higher order moments become relatively more important compared to uniform densities.

For very small bunch sizes, the considered densities are matched if $x_0 = y_0 = 0$, $C_{0,2} = C_{2,0}$, and $C_{1,1} = 0$. Thus, the bunch size $C_{2,0}$ remains as only degree of freedom and it determines small matched bunches with these densities. For large bunches, the considered density functions can only be approximations, because large matched bunches are not ellipsoidal. However, simulation results show that the following approximation seems to hold in the stationary bucket [56, 60]:

$$2\sqrt{C_{0,2}} \approx \Delta w_+ \left(\Delta\varphi_+ = 2\sqrt{C_{2,0}}\right) = \sqrt{2 - 2\cos\left(2\sqrt{C_{2,0}}\right)}, \tag{4.26}$$

where $\Delta w_+(\Delta\varphi_+)$ is function (2.54) that describes the height of a trajectory with maximum phase deviation $\Delta\varphi_+$ in the nonlinear stationary bucket, cf. also the right plot of Figure 2.12. Equation (4.26) is equivalent to the ratio

$$\frac{C_{0,2}}{C_{2,0}} \approx \frac{1 - \cos\left(2\sqrt{C_{2,0}}\right)}{2C_{2,0}}.$$

For small bunches, this implies $C_{0,2} \approx C_{2,0}$, whereas for larger bunches $C_{0,2} < C_{2,0}$. This leads to the following conclusion [56, 60]:

> The two-sigma length $2\sqrt{C_{2,0}}$ and height $2\sqrt{C_{0,2}}$ may be interpreted as the effective half axes of the bunch. The two-sigma length $2\sqrt{C_{2,0}}$ determines
>
> - the ratio between the bunch variances that is necessary for the density to be approximately matched and
> - the effective synchrotron frequency as described in Section 3.5.5.

For both densities, a constant of motion is given by

$$C_{2,0}C_{0,2} - C_{1,1}^2 = \begin{cases} \frac{R_{1x}^2 R_{2x}^2}{16} \\ \sigma_{1x}^2 \sigma_{2x}^2 \end{cases} \quad \sim \text{ bunch area and longitudinal emittance}$$

Bunches with Single-Bunch Modes The previous results are useful to construct models that describe dipole and quadrupole modes. For the analysis of higher order modes, the density functions (3.16) and (3.18) (p.58 and p.58) can be taken to represent higher mode numbers m. The plots (c) and (d) of Figure 4.3 show a sextupole mode ($m = 3$) and an octupole mode ($m = 4$) with a uniform and a Gaussian density, respectively. Both examples are pure modes, but a combination of different modes is also possible. The calculation of the moments (4.15) and (4.17) is computationally much more challenging in this case and it is advantageous to perform the integration in polar coordinates $x = r\cos\theta$ and $y = r\sin\theta$:

$$B_{1,0} = \int_0^{2\pi}\int_0^{\infty} r\cos\theta\; f(r,\theta,t)\; r\;\mathrm{d}r\;\mathrm{d}\theta, \quad B_{0,1} = \int_0^{2\pi}\int_0^{\infty} r\sin\theta\; f(r,\theta,t)\; r\;\mathrm{d}r\;\mathrm{d}\theta,$$

$$C_{n_x,n_y} = \int_0^{2\pi}\int_0^{\infty} \left[r\cos\theta - B_{1,0}\right]^{n_x}\; \left[r\sin\theta - B_{0,1}\right]^{n_y}\; f(r,\theta,t)\; r\;\mathrm{d}r\;\mathrm{d}\theta,$$

The basic and central moments are lengthy functions of the mode coefficients r_m, $m \in \{1, 2, 3, 4\}$ and only their first order approximations are given in Appendix C.2.2. Table C.2 (p.176) summarizes the moments for the uniform density and Table C.3 (p.177) shows the moments of the Gaussian density. Again, the functional relationship of the moments is the same for both densities except for a constant factor.

The interpretation of these tables shall be explained with the help of an example. Assume a Gaussian density with a mode $m = 2$. The moments for this configuration are summarized in the rows E_{n_x,n_y} and $\Delta C_{n_x,n_y}(r_2)$ of Table C.3. The row E_{n_x,n_y} presents the stationary or equilibrium part of the moments and $\Delta C_{n_x,n_y}(r_2)$ is the deviation due to the mode $m = 2$ with radius $r_2 > 0$ and orientation θ_0. The orientation can be used to introduce a time dependency, for example in a linear bucket $\theta_0 = \omega_{\mathrm{syn}} t$ can be chosen. It is important to note that the given $\Delta C_{n_x,n_y}$ are only first order approximations and thus valid for sufficiently small r_m only. For the moment $C_{2,0}$, the results reveal that

$$C_{2,0} \approx E_{2,0} - 2E_{2,0}\sin(2\theta_0)r_2 = E_{2,0}\left[1 - 2r_2\sin(2\omega_{\mathrm{syn}}t)\right].$$

This result is plausible, because it states that, in a linear bucket, the mode $m = 2$ will lead to an oscillation of the bunch variance with a frequency of $2\omega_{\mathrm{syn}}$ and a relative amplitude $2r_2$. For the moment $C_{3,0}$, the result is

$$C_{3,0} \approx \begin{cases} -\frac{9}{8}E_{2,0}^{3/2}\sqrt{\frac{\pi}{2}}r_1\sin(\theta_0) & \text{for mode } m = 1 \\ -\frac{15}{8}E_{2,0}^{3/2}\sqrt{\frac{\pi}{2}}r_3\sin(3\theta_0) & \text{for mode } m = 3 \end{cases}$$

and this shows that, besides the expected mode $m = 3$, $C_{3,0}$ also responds to the mode $m = 1$. Thus, mode $m = 1$ leads to oscillations not only in the basic moments, but also in the moments of order $n_x + n_y = 3$ (and $5, 7, \ldots$). A further example is available from

Table C.1, where the moments for an ellipsoidal bunch are presented. For a Gaussian density, some selected odd moments are

$$C_{4,0} = 3C_{2,0}^2, \quad C_{6,0} = 15C_{2,0}^3$$

and this shows that a bunch length oscillation $m = 2$ will be not only visible in moment $C_{2,0}$, but also in higher order even moments.

The following conclusions can be made:

In general, there is no one-to-one correspondence between moments and modes:

- the oscillation of a specific mode m is first visible in the moments of order $n_x + n_y = m$;
- the mode affects also higher order moments with odd (even) $n_x + n_y > m$, if m is odd (even). These higher order moments can be expressed as functions of the bunch size $E_{2,0}$ and the moments of order $n_x + n_y = m$.
- A moment of order $m = n_x + n_y$ shows oscillations if $r_m \neq 0$.
- A moment of order $m = n_x + n_y > 2$ with $r_m \neq 0$ shows oscillations for more than one mode.
- An exception is $m = 1$ for the uniform density; in first order approximation, this mode is only coupled with the basic moments.

For a given mode m with amplitude r_m

- the moments of order $n_x + n_y = m$ depend on $m\theta_0$ and
- the moments of order m and corresponding higher order moments oscillate with the frequency $m\omega_{\mathrm{syn}}$ in a linear bucket.

The conclusions show that the following statements are equivalent:

$$\text{stationary moments } \tfrac{\mathrm{d}}{\mathrm{d}t} B_{n_x,n_y} = 0 \text{ and } \tfrac{\mathrm{d}}{\mathrm{d}t} C_{n_x,n_y} = 0 \text{ for all } n_x, n_y > 0$$

$$\Updownarrow$$

$$\text{matched bunch with } r_m = 0$$

This is in agreement with (4.22), the reformulation of the control problem: if $r_m = 0$, all moments are stationary and the density has reached an equilibrium.

To study a specific mode, for example $m = 1$, any moment may be chosen that oscillates for this mode. However, it seems reasonable to choose the moment of lowest order:

$$\begin{array}{lll} m = 1 & \Rightarrow & B_{1,0} \text{ and } B_{0,1} \\ m = 2 & \Rightarrow & C_{2,0} \text{ and } C_{1,1} \text{ and } C_{0,2} \\ & \dots & \\ m & \Rightarrow & C_{m,0} \ \dots \ C_{0,m} \end{array}$$

Remark 4.3. The results in Tables C.2 and C.3 were derived for circular bunch shapes with $E_{2,0} = E_{0,2}$, but are expressed in such a way that they are also valid if the y-axis is multiplied by a constant and $E_{2,0} \neq E_{0,2}$. This is useful for larger bunches where $E_{0,2}$ may differ substantially from $E_{2,0}$ and an ellipsoidal bunch is a better approximation for the equilibrium than a circular bunch. It is thus possible to use $E_{0,2}$ of (4.50) to further improve the results. The following derivations will return to this point later on.

As already stated, the modes may also be combined, but care has to be taken, because in general there is no one-to-one correspondence. Section 4.6.2 will return to this problem.

Filamentation The density functions considered in this section have some degrees of freedom, but will not be able to reproduce filamentation of the bunch and will thus lead to a neglect of Landau damping of the coherent bunch oscillations. However, for realistic small bunch shape mismatches, there is reason to believe that the bunch shape will remain similar to a matched shape and the presented results are useful approximations.

4.5 Linear Bucket: the Small Bunch Assumption

In this section, a model is derived for the dynamics of bunches in a linear bucket or for very small bunches in a nonlinear bucket near their equilibrium [74]. It has to be noted that such small bunches are not realistic in real experiments. However, there are reasons why the analysis is nevertheless useful:

- Comparison with existing models that rely on a linearization of the nonlinear single-particle dynamics.
- Check of consistency of the nonlinear calculations of Section 4.6. These should simplify to the results of this section for small bunch sizes.
- Easier stability analysis.

4.5.1 Beam and Moment Dynamics

For small bunches, the particles are always in the vicinity of the equilibrium of the bucket and Equation (4.8b) of the longitudinal dynamics can be linearized. A simple linear approximation will cancel the amplitude modulation u_ε if $\varphi_\mathrm{R} = 0$, thus at least a bilinear

approximation is necessary. A general Taylor series expansion of this equation around the equilibrium point $(x, u_\varphi, u_\varepsilon) = (0, 0, 0) = \mathbf{0}$ is

$$\dot{y} = \underbrace{\dot{y}(\mathbf{0})}_{=0} + \left[x\frac{\partial \dot{y}}{\partial x}(\mathbf{0}) + u_\varepsilon \frac{\partial \dot{y}}{\partial u_\varepsilon}(\mathbf{0}) + u_\varphi \frac{\partial \dot{y}}{\partial u_\varphi}(\mathbf{0}) \right] + \frac{1}{2}\Big[x^2 \frac{\partial^2 \dot{y}}{\partial x^2}(\mathbf{0}) + u_\varepsilon^2 \frac{\partial^2 \dot{y}}{\partial u_\varepsilon^2}(\mathbf{0}) +$$
$$+ u_\varphi^2 \frac{\partial^2 \dot{y}}{\partial u_\varphi}(\mathbf{0}) + 2xu_\varepsilon \frac{\partial^2 \dot{y}}{\partial x \partial u_\varepsilon}(\mathbf{0}) + 2xu_\varphi \frac{\partial^2 \dot{y}}{\partial x \partial u_\varphi}(\mathbf{0}) + 2u_\varepsilon u_\varphi \frac{\partial^2 \dot{y}}{\partial u_\varepsilon \partial u_\varphi}(\mathbf{0}) \Big] + \dots$$

Taking into account only linear and bilinear terms, the approximation of the longitudinal dynamics is

$$\dot{x} = -\omega_{\text{syn}} y, \tag{4.27a}$$
$$\dot{y} \approx \omega_{\text{syn}}[1 + u_1]x \; + \; \omega_{\text{syn}} u_2 \tag{4.27b}$$

with the inputs

$$u_1 = u_\varepsilon + \tan\varphi_{\text{R}} u_\varphi, \qquad u_2 = \tan\varphi_{\text{R}} u_\varepsilon - u_\varphi - u_\varepsilon u_\varphi. \tag{4.27c}$$

The approximation sign will be omitted in the following, but it goes without saying that the obtained models will only be approximative and are valid for small bunch sizes only. With the dynamics (4.27), the time derivative of the basic moments is

$$\dot{B}_{1,0}(t) = -\omega_{\text{syn}} B_{0,1}(t), \tag{4.28a}$$
$$\dot{B}_{0,1}(t) = \omega_{\text{syn}}[1 + u_1]B_{1,0}(t) + \; \omega_{\text{syn}}\, u_2. \tag{4.28b}$$

Equation (4.28a) is equivalent to Equation (4.25) with $a_{01} = -\omega_{\text{syn}}$ and all other coefficients $a_{x,y} = 0$. For the central moments of order $n = n_x + n_y$

$$\dot{C}_{n,0} = -n\; \omega_{\text{syn}}\; C_{n-1,1} \tag{4.28c}$$
$$\dot{C}_{n-k,k}(t) = -[n-k]\; \omega_{\text{syn}}\; C_{n-k-1,k+1} \; + \; k\; \omega_{\text{syn}}\; [1+u_1]\; C_{n-k+1,k-1} \tag{4.28d}$$
$$\dot{C}_{0,n}(t) = n\; \omega_{\text{syn}}\; [1+u_1]\; C_{1,n-1} \tag{4.28e}$$

holds with integers $n \in [2, \infty[$, $k \in [1, n-1]$. This reveals three important facts:

- The rate of change of a moment of order $n = n_x + n_y$ only depends on moments of the same order, i. e. there is no dynamical coupling between different moment orders except for the input variable u_1.
- The inputs u_ε and u_φ act on both the basic and the central moments. Only for the stationary case $\varphi_{\text{R}} = 0$, the influence of u_φ on the central moments vanishes.
- It is interesting to note that the model (4.28) can be derived without any assumption about the particle density of the bunch.

Without feedback, the moment dynamics are decoupled. Also, the moments of order n can be taken as a measure for the mode $m = n$ as indicated by the results of Appendix C.2. Thus, the open loop dynamics of the modes are also decoupled. This is an intuitive result, because – due to the bilinearization – the dynamics (4.27) are linear in x in the open-loop case and there will be no synchrotron frequency spread and no Landau damping.

With feedback, the dynamics are coupled by the inputs. If a specific mode m has to be damped, it seems reasonable to consider only the moments of order $n = m$ to analyze the stability of the feedback with respect to this mode. However, this does not guarantee the stability or damping of the moments of different m. In the following, a model for moments up to order $n = 4$ will be analyzed. This will show that the moments with $n = 3$ and $n = 4$ are not first-order controllable. As these moments are correlated to the sextupole and octupole modes $m = 3$ and $m = 4$, this indicates that these modes are not controllable with respect to the inputs u_1 and u_2. The same seems to apply for $n > 4$ and this is supported by particle tracking simulations.

> In a linear bucket or in case of small bunches, it is therefore reasonable to limit the system (4.28) to the moments of order $n = 1$ and $n = 2$ and thus to the dipole and quadrupole modes $m = 1$ and $m = 2$.

4.5.2 Model Properties

The equilibrium of system (4.28) is obtained for $u_1 = u_2 = 0$ and $\dot{B}_{n_x,n_y} = \dot{C}_{n_x,n_y} = 0$ and reads

$$B_{1,0} = B_{0,1} = 0$$

and

$$\begin{bmatrix} C_{n,0} \\ \vdots \\ C_{(n-k),k} \\ \vdots \\ C_{0,n} \end{bmatrix} =: \begin{bmatrix} E_{n,0} \\ \vdots \\ E_{(n-k),k} \\ \vdots \\ E_{0,n} \end{bmatrix} = \begin{bmatrix} E_n \\ \vdots \\ \begin{cases} 0 & \text{for odd } k \\ \frac{1 \cdot 3 \cdot \ldots \cdot (k-1)}{(n-1) \cdot (n-3) \cdot \ldots \cdot (n-k+1)} E_n & \text{for even } k \end{cases} \\ \vdots \\ E_n \end{bmatrix}.$$

with positive real numbers

$$E_n \begin{cases} = 0 & \text{for odd } n, \\ > 0 & \text{for even } n. \end{cases}$$

This is in agreement with the values E_{n_x,n_y} of Tables C.2 and C.3. The equilibrium is not unique, since for each moment order there is a degree of freedom E_n. By choosing a

specific density function, all E_n with $n > 2$ can be expressed as functions of the bunch size E_2, which is then the only degree of freedom

In particular, the equilibrium of the first four central moments are

$$\begin{bmatrix} E_{2,0} \\ E_{1,1} \\ E_{0,2} \end{bmatrix} = \begin{bmatrix} E_2 \\ 0 \\ E_2 \end{bmatrix}, \qquad \begin{bmatrix} E_{3,0} \\ E_{2,1} \\ E_{1,2} \\ E_{0,3} \end{bmatrix} = \begin{bmatrix} 0 \\ 0 \\ 0 \\ 0 \end{bmatrix}, \qquad \begin{bmatrix} E_{4,0} \\ E_{3,1} \\ E_{2,2} \\ E_{1,3} \\ E_{0,4} \end{bmatrix} = \begin{bmatrix} E_4 \\ 0 \\ \frac{1}{3}E_4 \\ 0 \\ E_4 \end{bmatrix}. \tag{4.29}$$

System (4.28) can formulate as the nonlinear state-space model[1)]

$$\Sigma_{\mathrm{LB}}: \qquad \dot{\boldsymbol{x}} = \mathbf{A}_{\mathrm{LB}}\boldsymbol{x} + \mathbf{B}_{\mathrm{LB}}(\boldsymbol{x})\boldsymbol{u} = \mathbf{A}_{\mathrm{LB}}\boldsymbol{x} + \left[\mathbf{N_1}\boldsymbol{x} + \boldsymbol{B}_1\right] u_1 + \boldsymbol{B}_2 u_2. \tag{4.30}$$

The matrix $\mathbf{N}_1$ results from the fact that the input u_1 is multiplied with states such as $B_{1,0}$ or $C_{1,n-1}$ in Equations (4.28). System (4.30) is a nonlinear control-affine system. In addition, some authors assign this type of system to the subclass of bilinear systems [99, 120, 124], whereas other authors are more restrictive in their definition of bilinear systems. Bilinear systems are a first step in a generalization of linear systems towards nonlinear systems and are often good approximations for problems in engineering and physics. Significant theoretical progress has been made recently in the analysis and design of such systems. Introductions to the theory of bilinear and affine control systems can be found in the above mentioned references. Of course, also general methods for nonlinear systems are useful in the following. Mathematically oriented introductions to nonlinear systems can be found in [49, 55, 101, 119, 124]. Comprehensive discussions of analysis and design methods for nonlinear systems with a view to engineering applications are given in [6, 55, 123]. In [66], a computational approach is chosen with MATHEMATICA-based software algorithms. Newer methods such as flatness-based control are described in [79].

The state vector $\boldsymbol{x}$ is defined as

$$\begin{aligned} \boldsymbol{x} &= \begin{bmatrix} x_1 & x_2 & x_3 & x_4 & x_5 & \dots & x_k & \dots & x_L \end{bmatrix}^{\mathrm{T}} \\ &:= \begin{bmatrix} B_{1,0} & B_{0,1} & C_{2,0} & C_{1,1} & C_{0,2} & \dots & C_{n_x,n_y} & \dots & C_{0,n_{\mathrm{model}}} \end{bmatrix}^{\mathrm{T}}, \end{aligned} \tag{4.31}$$

where

$$C_{n_x,n_y} = x_k, \qquad k = \frac{n_x + n_y}{2}\left[1 + n_x + n_y\right] + n_y.$$

The equilibrium values are denoted by E_{n_x,n_y}, cf. (4.29), and the deviations from this equilibrium are

$$\Delta\boldsymbol{x} = \boldsymbol{x} - \boldsymbol{x}_{\mathrm{e}} = \begin{bmatrix} \dots & C_{n_x,n_y} - E_{n_x,n_y} & \dots \end{bmatrix}^{\mathrm{T}}.$$

The state vector $\boldsymbol{x}$ is defined to include the basic moments and the central moments up to a predefined finite order $n_{\mathrm{model}} < \infty$. Higher order moments are discarded to obtain a

[1)] The index LB refers to *linear bucket* model.

finite dimensional system and vector space $\boldsymbol{x} \in \mathbb{R}^L$. This is a truncation of the infinite dimensional system (4.28). However, this is no further approximation of the moment dynamics, since there is no coupling between the moment dynamics.

The dimension L of the system is

$$L = \sum_{n=1}^{n_{\text{model}}} [n+1] = \frac{n_{\text{model}}[3+n_{\text{model}}]}{2}.$$

In the following, system Σ_{LB} of (4.30) with $n_{\text{model}} = 4$ is analyzed. The dimension of this system is $L = 14$, it reads

$$\dot{\boldsymbol{x}} = \mathbf{A}_{\text{LB}}\boldsymbol{x} + \mathbf{B}_{\text{LB}}(\boldsymbol{x})\boldsymbol{u} = \begin{bmatrix} \mathbf{A}_1 & \mathbf{0} & \mathbf{0} & \mathbf{0} \\ \mathbf{0} & \mathbf{A}_2 & \mathbf{0} & \mathbf{0} \\ \mathbf{0} & \mathbf{0} & \mathbf{A}_3 & \mathbf{0} \\ \mathbf{0} & \mathbf{0} & \mathbf{0} & \mathbf{A}_4 \end{bmatrix} \boldsymbol{x} + \begin{bmatrix} \mathbf{b}_{1,1} & \mathbf{b}_{1,2} \\ \mathbf{b}_2 & \mathbf{0} \\ \mathbf{b}_3 & \mathbf{0} \\ \mathbf{b}_4 & \mathbf{0} \end{bmatrix} \begin{bmatrix} u_1 \\ u_2 \end{bmatrix} \tag{4.32}$$

and the matrices $\mathbf{A}_{\text{LB}}$ and $\mathbf{B}_{\text{LB}}$ are presented in detail in Appendix C.3. The null vectors and matrices $\mathbf{0}$ in (4.32) and in the following are assumed to have the appropriate dimensions to complete their matrices and vectors.

Since the system matrix $\mathbf{A}_{\text{LB}}$ has a block-diagonal shape, its eigenvalues are the eigenvalues λ of the matrices $\mathbf{A}_k$:

$$\lambda_{1,2}\{\mathbf{A}_1\} = \{\pm \mathrm{i}\omega_{\text{syn}}\}, \quad \lambda_{3,4,5}\{\mathbf{A}_2\} = \{0\,;\, \pm \mathrm{i}2\omega_{\text{syn}}\},$$
$$\lambda_{6-9}\{\mathbf{A}_3\} = \{\pm \mathrm{i}\omega_{\text{syn}}\,;\, \pm \mathrm{i}3\omega_{\text{syn}}\}, \quad \lambda_{10-14}\{\mathbf{A}_4\} = \{0\,;\, \pm \mathrm{i}2\omega_{\text{syn}}\,;\, \pm \mathrm{i}4\omega_{\text{syn}}\}$$

The eigenvalues $\pm \mathrm{i}m\omega_{\text{syn}}$ correspond to the frequencies of the coherent mode m. Again, there is no one-to-one correspondence between moments and modes, the eigenvalues are repeated in higher order moments. For instance, the eigenvalues $\pm \mathrm{i}\omega_{\text{syn}}$ appear in the matrix $\mathbf{A}_1$ of the basic moments and the matrix $\mathbf{A}_3$ of the central moments of order $n = 3$. Without feedback, the dynamics defined by the four matrices $\mathbf{A}_k$, $k = 1,\ldots,4$ are fully decoupled.

The equilibrium of system (4.32) for $u_1 = u_2 = 0$ is

$$\boldsymbol{x}_{\text{e}} = \begin{bmatrix} \boldsymbol{x}_{\text{e},1} \\ \boldsymbol{x}_{\text{e},2} \\ \boldsymbol{x}_{\text{e},3} \\ \boldsymbol{x}_{\text{e},4} \end{bmatrix}, \quad \boldsymbol{x}_{\text{e},1} = \begin{bmatrix} 0 \\ 0 \end{bmatrix}, \boldsymbol{x}_{\text{e},2} = \begin{bmatrix} E_2 \\ 0 \\ E_2 \end{bmatrix}, \boldsymbol{x}_{\text{e},3} = \begin{bmatrix} 0 \\ 0 \\ 0 \\ 0 \end{bmatrix}, \boldsymbol{x}_{\text{e},4} = \begin{bmatrix} E_4 \\ 0 \\ \frac{1}{3}E_4 \\ 0 \\ E_4 \end{bmatrix}. \tag{4.33}$$

These moments describe a matched bunch for a linear bucket. The basic moments are zero, i. e. the bunch is centered, and the variances $C_{2,0} = C_{0,2} = E_2$ are identical and the covariance is $E_{1,1} = 0$. Possible distributions that satisfy these conditions are a centered circle with a uniform density or a Gaussian distribution with circles as contour lines. If a specific density distribution is chosen, E_4 can be expressed as a function of E_2. This is shown in detail in Appendix C.2.1. For example, a Gaussian density yields $E_4 = 3E_2^2$ and the parameter E_2 fully determines the size and the equilibrium of the bunch.

The linearization of system (4.32) at the point $\boldsymbol{x} = \boldsymbol{x}_\mathrm{e}$ with $\Delta\boldsymbol{x} = \boldsymbol{x} - \boldsymbol{x}_\mathrm{e}$ simply reads

$$\Sigma_{\Delta\mathrm{LB}}: \qquad \Delta\dot{\boldsymbol{x}} = \mathbf{A}_\mathrm{LB}\Delta\boldsymbol{x} + \underbrace{\mathbf{B}(\boldsymbol{x}_\mathrm{e})}_{\mathbf{B}_\mathrm{e}}\boldsymbol{u}.$$

However, this linear model with dimension $L = 14$ will not be used further, since the dimension can be reduced due to two invariants of motion that are present in the nonlinear system (4.32):

$$I_2(t) = C_{2,0}C_{0,2} - C_{1,1}^2 = \text{const.} \tag{4.34a}$$

$$I_4(t) = C_{4,0}C_{0,4} - 4C_{3,1}C_{1,3} + 3C_{2,2}^2 = \text{const.} \tag{4.34b}$$

The two eigenvalues in the origin of the complex plane $\lambda_3 = \lambda_{10} = 0$ of matrices $\mathbf{A}_2$ and $\mathbf{A}_4$ are due to the invariants I_2 and I_4. The derivation of I_2 and I_4 with respect to the time and the insertion of the moment dynamics of system (4.32) verifies that these are constants. For example,

$$\begin{aligned}\dot{I}_2(t) &= \dot{C}_{2,0}C_{0,2} + C_{2,0}\dot{C}_{0,2} - 2C_{1,1}\dot{C}_{1,1}\\ &= (-2C_{1,1})\,C_{0,2} + C_{2,0}\,(2C_{1,1} + 2C_{1,1}u_2) - 2C_{1,1}\,(C_{2,0} - C_{0,2} + C_{2,0}u_1)\\ &= 0.\end{aligned}$$

The invariants define sub-manifolds of the state space. For example, for a given value I_2, the dynamics of $\boldsymbol{x}_\mathrm{LB}(t)$ are bounded to the sub-manifold

$$C_{2,0}C_{0,2} - C_{1,1}^2 = x_3(t)x_5(t) - x_4^2(t) = I_2.$$

For given values of I_2 and I_4, only those equilibrium points of the set $\boldsymbol{x}_\mathrm{e}$ can be reached that belong to the sub-manifold. At the equilibrium point $\boldsymbol{x}_\mathrm{LB} = \boldsymbol{x}_\mathrm{e}$, cf. (4.33),

$$I_2 = E_2^2 = \text{const.}, \qquad I_4 = \frac{4}{3}E_4^2 = \text{const.}$$

holds. Since only $E_2 > 0$ and $E_4 > 0$ represent physical meaningful bunches, this can be rewritten as

$$E_2 = \sqrt{I_2}, \qquad E_4 = \sqrt{\frac{3}{4}I_4},$$

and this defines a unique equilibrium.

Each subsystem with moments of an even order n has an invariant, for example

$$I_6 = C_{6,0}C_{0,6} - 6C_{5,1}C_{1,5} + 15C_{4,2}C_{2,4} - 10C_{3,3}^2 \tag{4.35}$$

is the invariant for the order $n = 6$.

There are several possibilities to use the invariants for a reduction of the dimension L, one choice is to rewrite (4.34) as

$$C_{0,2} = \frac{I_2 + C_{1,1}^2}{C_{2,0}}, \qquad C_{0,4} = \frac{I_4 + 4C_{3,1}C_{1,3} - 3C_{2,2}^2}{C_{4,0}}. \tag{4.36}$$

This is always possible, since the moments $C_{2,0}$ and $C_{4,0}$ are strictly positive for positive and nonzero real distributions $f(x, y)$. A linearization of (4.36) around the equilibrium (4.33) leads to $\Delta C_{0,2} \approx -\Delta C_{2,0}$ and $\Delta C_{0,4} \approx -\Delta C_{4,0} - 2\Delta C_{2,2}$.

With the relations (4.36), the nonlinear system (4.32) can be reduced to $\tilde{L} = 12$ state variables. The new state vector will be denoted by $\boldsymbol{x}_{\mathrm{LBR}}$, this vector results from $\boldsymbol{x}$ by discarding the states $x_5 = C_{0,2}$ and $x_{14} = C_{0,4}$ and the reduced nonlinear system is

$$\Sigma_{\mathrm{LBR}}: \qquad \dot{\boldsymbol{x}}_{\mathrm{LBR}} = \mathbf{A}_{\mathrm{LBR}}\boldsymbol{x}_{\mathrm{LBR}} + \mathbf{B}_{\mathrm{LBR}}(\boldsymbol{x}_{\mathrm{LBR}})\boldsymbol{u}.$$

If only the basic and second central moments are considered, the reduced nonlinear system reads

$$\begin{bmatrix} \dot{B}_{1,0} \\ \dot{B}_{0,1} \\ \dot{C}_{2,0} \\ \dot{C}_{1,1} \end{bmatrix} = \omega_{\mathrm{syn}} \begin{bmatrix} -B_{0,1} \\ B_{1,0} + B_{1,0}u_1 + u_2 \\ -2C_{1,1} \\ C_{2,0} - \frac{I_2 + C_{1,1}^2}{C_{2,0}} + C_{2,0}u_1 \end{bmatrix}. \tag{4.37}$$

A linearization of the complete reduced system of $\boldsymbol{x}_{\mathrm{LBR}}$ yields the linear system

$$\Sigma_{\Delta\mathrm{LBR}}: \qquad \Delta\dot{\boldsymbol{x}}_{\mathrm{LBR}} = \mathbf{A}_{\mathrm{LBR}}\Delta\boldsymbol{x}_{\mathrm{LBR}} + \mathbf{B}_{\mathrm{LBR}}(E_2, E_4)\boldsymbol{u}. \tag{4.38}$$

The matrices $\mathbf{A}_{\mathrm{LBR}}$ and $\mathbf{B}_{\mathrm{LBR}}$ are given in Appendix C.3.

The controllability of the multi-input multi-output (MIMO) system $\Sigma_{\Delta\mathrm{LBR}}$ is determined by its controllability matrix $\mathcal{C}(\mathbf{A}_{\mathrm{LBR}}, \mathbf{B}_{\mathrm{LBR}})$ as defined by (4.10); for $E_2 > 0$, its rank equals 4 and is thus smaller than the system dimension $\tilde{L} = 12$. However, a controllable subspace $\mathcal{S}$ as given in (4.11) can be found:

$$\mathbf{H} = \begin{bmatrix} \mathbf{I} & \mathbf{0} \end{bmatrix} \quad \Rightarrow \quad \operatorname{rank} \mathbf{H}\mathcal{C} = 4,$$

where $\mathbf{H}$ is a 4×12 matrix, $\mathbf{I}$ the 4×4 unity matrix and $\mathbf{0}$ the 4×8 zero matrix. This shows that the subspace consisting of the first four states is fully controllable. According to Theorem 4.3, this leads to the conclusion that the nonlinear system (4.37) is locally controllable at the equilibrium.

The set of states $\mathcal{R}$ that can be reached from the origin $\Delta\boldsymbol{x}_{\mathrm{LBR}}$ (equivalent to the equilibrium $\boldsymbol{x}_{\mathrm{e}}$) can be obtained by calculating the column space of $\mathcal{C}$. Basis vectors $\boldsymbol{m}_k$, $k = 1, \ldots, 4$, that span this column space are summarized in Appendix C.3. Each reachable state is then given by a linear combination of these vectors:

$$\mathcal{R} = \left\{ \Delta\boldsymbol{x}_{\mathrm{LBR}} \in \mathbb{R}^{12} \;:\; \Delta\boldsymbol{x}_{\mathrm{LBR}} = c_1\boldsymbol{m}_1 + c_2\boldsymbol{m}_2 + c_3\boldsymbol{m}_3 + c_4\boldsymbol{m}_4 \;:\; c_1, c_2, c_3, c_4 \in \mathbb{R} \right\}.$$

The analysis of this set shows that – for the linearized system – arbitrary values $\Delta B_{1,0}$, $\Delta B_{0,1}$, $\Delta C_{2,0}$, and $\Delta C_{1,1}$ can be reached if the bunch size E_2 is nonzero:

$$\Delta B_{1,0} = c_1, \quad \Delta B_{0,1} = c_2, \quad \Delta C_{2,0} = c_3 E_2, \quad \Delta C_{1,1} = c_4 E_2,$$

whereas the remaining states are zero or depend on the first four states:

$$\Delta C_{3,0} = \Delta C_{2,1} = \Delta C_{1,2} = \Delta C_{0,3} = 0,$$
$$\Delta C_{4,0} = 2\frac{E_4}{E_2}\Delta C_{2,0}, \quad \Delta C_{3,1} = \frac{E_4}{E_2}\Delta C_{1,1}, \quad \Delta C_{2,2} = 0, \quad \Delta C_{1,3} = \Delta C_{3,1}. \tag{4.39}$$

On the other hand, this implies that, for a linear bucket, any initial bunch distribution with deviations in the bunch center or variance may be stabilized to the equilibrium shape. The controllability of the linearized system implies local controllability near the equilibrium of the nonlinear system Σ_{LBR} in the subspace with the states $B_{1,0}$, $B_{0,1}$, $C_{2,0}$, and $C_{1,1}$, i. e. System (4.37) is locally controllable near $\begin{bmatrix}0 & 0 & E_2 & 0\end{bmatrix}^{\mathrm{T}}$. This means that for sufficiently small deviations in the states $B_{1,0}$, $B_{0,1}$, $C_{2,0}$, and $C_{1,1}$, the beam can be stabilized and damped to the equilibrium. In practice, constraints such as input saturations may limit the set of stabilizability. For the higher order moments, a general statement about the local controllability cannot be made at this point based on the linearization.

The result (4.39) is consistent with the calculations of the moments of an ellipsoidal bunch in Appendix C.2.1. For example, the moment $C_{4,0}$ can be written as $C_{4,0} = 3\, C_{2,0}^2$ for a Gaussian densities (cf. Table C.1). A linearization around the equilibrium $C_{2,0} = E_2$, $C_{4,0} = E_4$ yields

$$E_4 = 3\, E_2^2 \quad \Rightarrow \quad E_2 = \frac{E_4}{3E_2}$$
$$\Delta C_{4,0} \approx 6\, E_2\, \Delta C_{2,0} = 2\, \frac{E_4}{E_2}\, \Delta C_{2,0},$$

which is in agreement with (4.39).

For control purposes, it is favorable to calculate the transfer functions of the linear system (4.38). It is assumed that the moments $\Delta B_{1,0}$, $\Delta C_{2,0}$, $\Delta C_{3,0}$, and $\Delta C_{4,0}$ can be measured. The resulting transfer functions are

$$\begin{bmatrix} \frac{\Delta B_{1,0}}{u_1} & \frac{\Delta C_{2,0}}{u_1} & \frac{\Delta C_{3,0}}{u_1} & \frac{\Delta C_{4,0}}{u_1} \\ \frac{\Delta B_{1,0}}{u_2} & \frac{\Delta C_{2,0}}{u_2} & \frac{\Delta C_{3,0}}{u_2} & \frac{\Delta C_{4,0}}{u_2} \end{bmatrix} = \begin{bmatrix} 0 & \frac{-2E_2\omega_{\mathrm{syn}}^2}{s^2+4\omega_{\mathrm{syn}}^2} & 0 & \frac{-4E_4\omega_{\mathrm{syn}}^2\left(s^2+16\omega_{\mathrm{syn}}^2\right)}{\left(s^2+4\omega_{\mathrm{syn}}^2\right)\left(s^2+16\omega_{\mathrm{syn}}^2\right)} \\ \frac{\omega_{\mathrm{syn}}^2}{s^2+\omega_{\mathrm{syn}}^2} & 0 & 0 & 0 \end{bmatrix} \tag{4.40}$$

The Laplace variable is denoted by s. Again, the frequency domain shows that the eigenvalues $\pm\mathrm{i}3\omega_{\mathrm{syn}}$ and $\pm\mathrm{i}4\omega_{\mathrm{syn}}$ are not controllable. First, the gain for $\Delta C_{3,0}$ is zero. Second, the eigenvalues $\pm\mathrm{i}4\omega_{\mathrm{syn}}$ are cancelled in the transfer function of $\Delta C_{4,0}/u_1$ and third, the remaining part of this transfer function is proportional to $\Delta C_{2,0}/u_1$.

Finally, the following important conclusions can be made concerning the damping of longitudinal bunch oscillations *for very small bunches* or bunches in a *linear bucket*:

- Only in the stationary case, the phase modulation acts solely on the center of gravity (mode $m = 1$) and the amplitude modulation acts solely on the bunch length (mode $m = 2$). In the acceleration case, the input variables are mixed. In general, the dynamics of the moments are nonlinear with respect to the feedback u_1.

- For the subspace consisting of the moments $B_{1,0}$, $B_{0,1}$, $C_{2,0}$, and $C_{0,2}$, the equilibrium is locally controllable and sufficiently small deviations in these quantities can be damped by a feedback system.

- Higher order moment dynamics are not first-order controllable with respect to phase and amplitude modulations. Local controllability may still be possible, cf. Remark 4.1, but the decision of this question requires full nonlinear controllability analysis. The simulation results of Section 4.1 indicate that the higher order dynamics are indeed not locally controllable. This implies that oscillations of higher order modes such as $\pm\mathrm{i}3\omega_{\mathrm{syn}}$ and $\pm\mathrm{i}4\omega_{\mathrm{syn}}$ cannot be damped if u_ε and u_φ are used as control inputs.

A full nonlinear controllability analysis will not be deployed, because the next section will deal with the nonlinear bucket and show that first-order controllability and thus local controllability is also given for higher order moment dynamics, if the nonlinearity is taken into account.

4.6 Nonlinear Bucket

For larger bunches in a nonlinear bucket[2)], the bilinearized dynamics (4.27) are no longer suitable and higher order terms have to be taken into account. In principle, the calculation of the moment dynamics is still straightforward, if higher order terms are included. However, higher order terms introduce coupling between the moment dynamics of different order n. This requires a new strategy for the truncation and order reduction.

Anticipating some results of this section regarding the controllability, it is interesting to note that the approximation of (4.8b) determines the controllability properties of the moments:

- A linearization of (4.8b) cancels the input u_1 and leads to a local controllability subspace containing only the basic moments;

- bilinearization leads to the results of the last section, i. e. to a system where both basic moments and moments of order two can be stabilized;

- taking into account further terms of (4.8b) extends the controllable subspace to higher order central moments.

[2)] This means that the nonlinear single-particle dynamics are used and not the linearization of these dynamics.

4.6.1 Model Derivation

Beam and Moment Dynamics

Equation (4.8b) can be rewritten with the use of the addition theorems [37]

$$\sin(a \pm b) = \sin a \cos b \pm \cos a \sin b, \qquad \cos(a \pm b) = \cos a \cos b \mp \sin a \sin b$$

as

$$\begin{aligned}\dot{y} = {} & \omega_{\mathrm{syn}}[1+u_\varepsilon]\left[\sin x \cos u_\varphi - \cos x \sin u_\varphi\right] + \\ & + \omega_{\mathrm{syn}}[1+u_\varepsilon]\tan\varphi_{\mathrm{R}}\left[\cos x \cos u_\varphi + \sin x \sin u_\varphi\right] - \omega_{\mathrm{syn}}\tan\varphi_{\mathrm{R}}\end{aligned} \tag{4.41}$$

The trigonometric functions in (4.41) can be expanded as Taylor series

$$\sin x = \sum_{k=0}^{\infty}[-1]^k\frac{x^{2k+1}}{[2k+1]!} = x - \frac{x^3}{3!} + \frac{x^5}{5!} - \ldots + \frac{[-1]^k x^{2k+1}}{[2k+1]!} + \ldots \tag{4.42a}$$

$$\cos x = \sum_{k=0}^{\infty}[-1]^k\frac{x^{2k}}{[2k]!} = 1 - \frac{x^2}{2!} + \frac{x^4}{4!} - \ldots + \frac{[-1]^k x^{2k}}{[2k]!} + \ldots \tag{4.42b}$$

and the truncation of these series at $k = \hat{k}$ leads to an approximation of the longitudinal beam dynamics which is polynomial in x and y:

$$\begin{aligned}\dot{x} &= -\omega_{\mathrm{syn}}\, y \\ \dot{y} &\approx \omega_{\mathrm{syn}}[1+u_\varepsilon]\left[a_1(x)\cos u_\varphi - a_2(x)\sin u_\varphi\right] + \\ &\quad + \omega_{\mathrm{syn}}[1+u_\varepsilon]\tan\varphi_{\mathrm{R}}\left[a_2(x)\cos u_\varphi + a_1(x)\sin u_\varphi\right] - \omega_{\mathrm{syn}}\tan\varphi_{\mathrm{R}},\end{aligned}$$

with polynomials

$$a_1(x) = x + \ldots + \frac{[-1]^{\hat{k}}x^{2\hat{k}+1}}{[2\hat{k}+1]!}, \qquad a_2(x) = 1 + \ldots + \frac{[-1]^{\hat{k}}x^{2\hat{k}}}{[2\hat{k}]!}.$$

In the following, the moment dynamics are calculated for the stationary case $\varphi_{\mathrm{R}} = 0$ with $\hat{k} \leq 3$ for a model with moments up to the order $n_{\mathrm{model}} = 6$ with the assistance of MATHEMATICA [138]. In principle, the calculation for the more general case $\varphi_{\mathrm{R}} \neq 0$ and for higher $\hat{k}$ can be performed in the very same manner, but with an increase in calculation effort. The calculation yields the moment dynamics in the nonlinear, stationary bucket

$$\Sigma_{\mathrm{NB}}: \qquad \dot{\boldsymbol{x}}(t) = \boldsymbol{f}_{\mathrm{NB}}\left(\boldsymbol{x}(t), \boldsymbol{x}_*(t), u_\varepsilon(t), u_\varphi(t), \varphi_{\mathrm{R}}\right), \tag{4.43}$$

where the state vector $\boldsymbol{x}$ again contains the moments

$$\boldsymbol{x} = \begin{bmatrix} B_{1,0} & B_{0,1} & C_{2,0} & C_{1,1} & C_{0,2} & \ldots & C_{n_x,n_y} & \ldots & C_{0,n_{\mathrm{model}}}\end{bmatrix}^{\mathrm{T}}.$$

The function $\boldsymbol{f}_{\mathrm{NB}}$ depends on the Taylor series truncation order $\hat{k}$. In contrast to the calculation for the linear bucket, $\boldsymbol{f}_{\mathrm{NB}}$ also depends on the additional state vector

$$\boldsymbol{x}_* = \begin{bmatrix} C_{n_{\mathrm{model}}+1,0} & \ldots & C_{0,n_{\max}}\end{bmatrix}^{\mathrm{T}}$$

that contains moments up to an order of

$$n_{\max} = n_{\text{model}} + 2\hat{k}, \tag{4.44}$$

if the dynamics of moments of order up to $n_x + n_y = n_{\text{model}}$ are considered. A linear bucket implies $\hat{k} = 0$ and thus $n_{\max} = n_{\text{model}}$. As soon as a nonlinear bucket with higher order terms in x is considered, coupling is introduced between the orders and moments appear of order $n_x + n_y > n_{\text{model}}$.

The question is how the nonlinear equations of motion change compared to the case of a linear bucket. For the stationary case $\varphi_{\text{R}} = 0$ and $\hat{k} = 2$, the calculation yields

$$\frac{\dot{B}_{1,0}}{\omega_{\text{syn}}} = -B_{0,1} \tag{4.45a}$$

$$\begin{aligned}\frac{\dot{B}_{0,1}}{\omega_{\text{syn}}} = {} & [1+u_\varepsilon]\cos u_\varphi \left[B_{1,0} + \frac{1}{6}\left[-B_{1,0}^3 - 3B_{1,0}C_{2,0} - C_{3,0}\right] + \frac{1}{120}\left[B_{1,0}^5 + \right.\right. \\ & \left.\left. + 10B_{1,0}^3 C_{2,0} + 10B_{1,0}^2 C_{3,0} + 5B_{1,0}C_{4,0} + C_{5,0}\right]\right] - [1+u_\varepsilon]\sin u_\varphi \left[1 + \right. \\ & \left. + \frac{1}{2}\left[-B_{1,0}^2 - C_{2,0}\right] + \frac{1}{24}\left[B_{1,0}^4 + 6B_{1,0}^2 C_{2,0} + 4B_{1,0}C_{3,0} + C_{4,0}\right]\right].\end{aligned} \tag{4.45b}$$

Compared to the case of a linear bucket, there are two main differences:

- the dynamics are highly nonlinear
- there is a strong coupling with higher order central moments up to order $n_{\max} = 1 + 2 \cdot 2 = 5$

This is also true for the dynamics of the central moments. In the following, the calculations will focus on the stationary case $\varphi_{\text{R}} = 0$.

The performance of a truncation of the Taylor series (4.42) at $\hat{k} = 3$ is shown in Figure 4.4. The relative approximation error grows for increasing x, but is below 5% for most of the interval $[-\pi;\ \pi]$, this is indicated by the dashed lines.[3)] However, conclusions about the overall model accuracy in terms of the solution $\boldsymbol{x}(t)$ of the moment dynamics is not readily deducible from these plots; rather, simulations are necessary to evaluate the model accuracy.

An alternative to the Taylor series expansion would be to fit a polynomial of a given degree to the nonlinear function of the RF voltage. The coefficients of the polynomial can for example be obtained by a least squares method. For more complex nonlinearities, this will be usually superior in terms of accuracy compared to the Taylor series for a given polynomial degree. Nevertheless, the Taylor series will be used in the following, because this leads to models that are equivalent to the case of a linear bucket for very small bunch sizes. Thus, it will be easier to check the results for plausibility. In addition, the accuracy of the series is satisfactory for the given nonlinearities of sine and cosine for the single harmonic RF case.

[3)] The relative error at and near the zero crossings of $\cos(x)$ is not taken into account in this consideration.

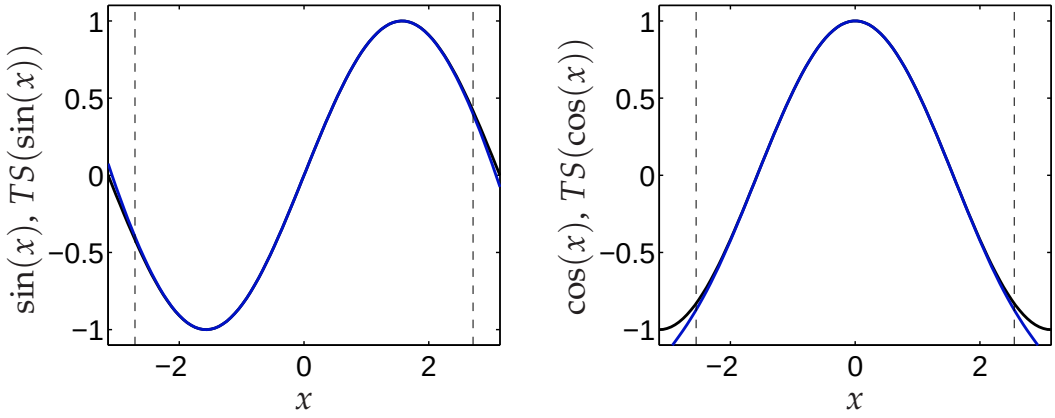

Figure 4.4: Taylor series approximations (TS, blue) of sine and cosine (black) for $k \leq \hat{k} = 3$ and boundary of the domain with a relative error below 5% (dashed lines).

Equilibrium and Linearization for a Stationary Beam

The equilibrium of the nonlinear dynamics (4.43) can be calculated with $\dot{\boldsymbol{x}} = 0$ and $u_\varepsilon = u_\varphi = 0$. This results in a set of n_{model} nonlinear equations that contains moments up to an order of $n_{\max}$ as given by (4.44). For the stationary case, the assumption that all moments of odd order

$$B_{1,0} = B_{0,1} = C_{3,0} = C_{2,1} = C_{1,2} = C_{0,3} = C_{5,0} = \ldots = 0 \tag{4.46}$$

are equal to zero greatly simplifies the equations to calculate the equilibrium. This assumption is reasonable, because the stationary bucket has trajectories that are symmetric with respect to the y-axis of the phase space. A particle density that represents a matched bunch will have to be axially symmetric as well, this implies that the moments of odd order must be zero. With assumption (4.46), $\varphi_{\text{R}} = 0$, and $\hat{k} = 3$, the equilibrium reads

$$\boldsymbol{x}_{\text{e}} = \begin{bmatrix} 0 & 0 & E_{2,0} & 0 & E_{0,2} & \ldots & E_{0,6} \end{bmatrix}^{\text{T}} \tag{4.47}$$

with

$$E_{0,2} = E_{2,0} - \frac{1}{6} E_{4,0} + \frac{1}{120} E_{6,0} - \frac{1}{5040} E_{8,0}.$$

The complete equilibrium for $n_x + n_y \leq 6$ can be found in Appendix C.4.1 for $\hat{k} = 3$. As before, the variable E_{n_x,n_y} is used to denote the equilibrium of the central moment C_{n_x,n_y}. In the following, it will be assumed that the equilibrium values for the higher order moments with $n_x + n_y > n_{\text{model}} = 6$ have the same pattern as (4.47), i. e. $E_{n_x,n_y} = 0$ for odd $n_x + n_y$ and odd pairs (n_x,n_y).

The equilibrium is similar to the case of a linear bucket. A linear bucket is obtained for $\hat{k} = 1$ or for very small bunch sizes $E_{2,0}$. For very small bunch sizes, the higher order moments can be neglected with respect to the moments of order 2 and 4 and (4.47)

simplifies to (4.29). It is important to note that – as in the case of the linear bucket – the equilibrium still has some degree of freedom. The moments $E_{2,0}, E_{4,0}, \ldots$ are again determined by the bunch size and the particular density distribution that is chosen. For example, a bunch with a given variance $E_{2,0}$ and a uniform density will have different higher order moments $E_{4,0}$,$E_{6,0}, \ldots$ as a bunch with the same variance but a Gaussian density.

The nonlinear model can be linearized around the equilibrium $\boldsymbol{x}_\mathrm{e}$. The resulting linear model

$$\Sigma_{\Delta\mathrm{NB}}: \qquad \Delta\dot{\boldsymbol{x}}(t) = \mathbf{A}_\mathrm{NB} \begin{bmatrix} \Delta\boldsymbol{x} \\ \Delta\boldsymbol{x}_* \end{bmatrix} + \mathbf{B}_\mathrm{NB} \begin{bmatrix} u_\varepsilon \\ u_\varphi \end{bmatrix} \tag{4.48}$$

describes small deviations $\Delta\boldsymbol{x} = \boldsymbol{x} - \boldsymbol{x}_\mathrm{e}$ of the bunch shape with respect to its matched shape. The linear equations for $n_\mathrm{model} = 4$ and $\hat{k} = 3$ are given in Appendix C.4.2. The result shows that the maximum moment order agrees with (4.44) and is $n_\mathrm{max} = 4 + 2 \cdot 3 = 10$.

Before proceeding, the result can be checked for plausibility with a simple calculation. Assume an ellipsoidal bunch with a uniform density (3.25). The moments of this bunch have been summarized in Appendix C.2.1. Further, assume the orientation $\Phi = 0$. In many cases, this might be an appropriate approximation for a matched bunch in a stationary bucket. The only degrees of freedom are the half-axes $R_x := R_{1x}$ and $R_y := R_{2x}$. The following moments can be taken from Table C.1, p.174:

$$C_{2,0} = \frac{R_x^2}{4}, \quad C_{0,2} = \frac{R_y^2}{4}, \quad C_{4,0} = 2C_{2,0}^2, \quad C_{6,0} = 5C_{2,0}^3, \quad C_{8,0} = 14C_{2,0}^4. \tag{4.49}$$

In the following, the bunch is considered a model for a matched bunch, i. e. the moments are denoted by E_{n_x,n_y}, for instance $C_{2,0} = E_{2,0}$. The above calculated equilibrium for $C_{0,2}$ is given by

$$E_{0,2} = E_{2,0} - \frac{1}{6}E_{4,0} + \frac{1}{120}E_{6,0} - \frac{1}{5040}E_{8,0}. \tag{4.50}$$

Inserting the moments (4.49) yields the condition

$$R_y^2 = R_x^2 - \frac{1}{12}R_x^4 + \frac{1}{384}R_x^6 - \frac{1}{23040}R_x^8 \tag{4.51}$$

for the semi-axes of the matched bunch. This can be compared to the trajectory property (2.54), p.32. The exact shape of the matched bunch must be equal to the trajectory, thus the intersections will give a good estimation of the semi-axes of the bunch. Renaming $\Delta w_+ = R_y$ and $\Delta\varphi_+ = R_x$, Equation (2.54) can be rewritten as

$$R_y = \sqrt{2\left[1 - \cos(R_x)\right]} = \sqrt{R_x^2 - \frac{1}{12}R_x^4 + \frac{1}{360}R_x^6 - \frac{1}{20160}R_x^8 + \mathcal{O}(R_x^9)}$$

This equation can be regarded as the exact condition between R_x and R_y for matched bunches with a uniform density. The comparison with (4.51) shows a good agreement in spite of the approximations that were made.

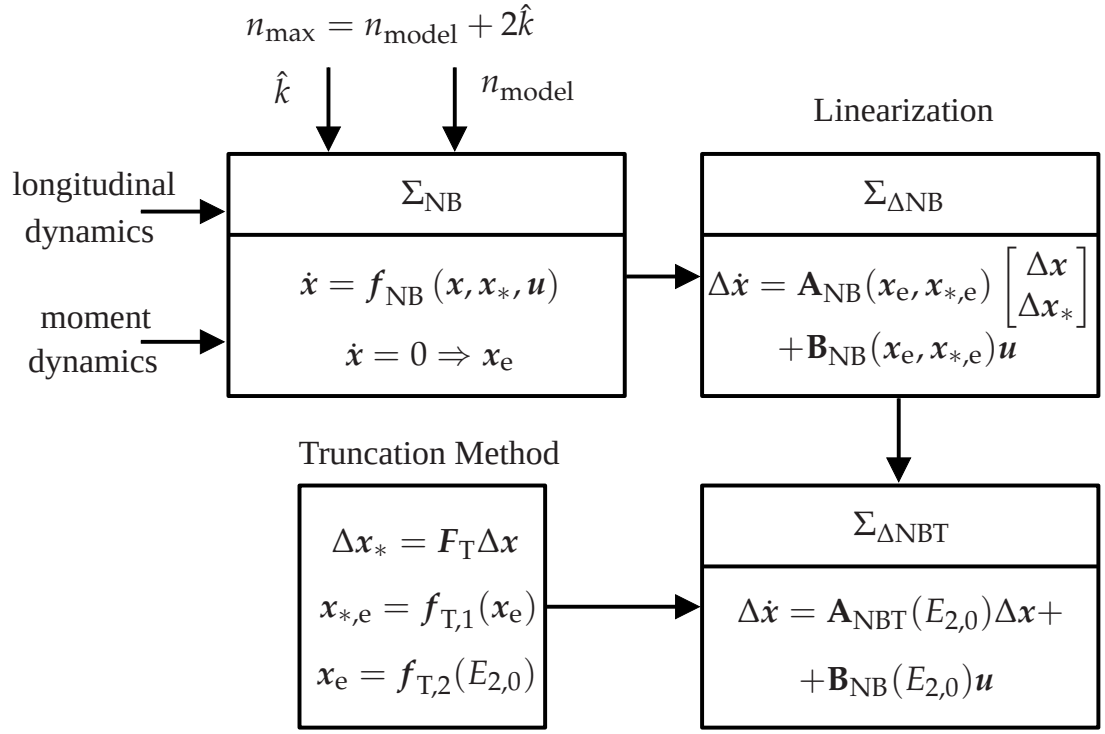

Figure 4.5: Linearization and truncation of the nonlinear system Σ_{NB}. The state vectors $\boldsymbol{x}_*$ and $\Delta\boldsymbol{x}_*$ contain moments C_{n_x,n_y} that are beyond the scope of the model, i. e. with $n_x + n_y > n_{\text{model}}$. The truncation method expresses these moments as a function of the moments with $n_x + n_y \leq n_{\text{model}}$. The result is the linear, truncated system $\Sigma_{\Delta\text{NBT}}$.

Truncation

As stated above, the equations for a nonlinear bucket still contain moments with $n_x + n_y > n_{\text{model}}$, this is due to (4.44). Without any further simplifications, it would be necessary to calculate the dynamics of every central moment C_{n_x,n_y} and to investigate an infinite dimensional system. To obtain simpler finite dimensional models for a controller design, a truncation of the state vector is necessary. In the following, different models are derived, but the truncation procedure is always similar. A first approach is shown in Figure 4.5. After calculation of the nonlinear system with parameters $\hat{k}$ and n_{model}, a linearization around the equilibrium $(\boldsymbol{x}, \boldsymbol{x}_*, \boldsymbol{u}) = (\boldsymbol{x}_{\text{e}}, \boldsymbol{x}_{*,\text{e}}, \mathbf{0})$. The resulting system $\Sigma_{\Delta\text{NB}}$ still contains the state $\Delta\boldsymbol{x}_*$ that establishes the coupling with higher order moments. This coupling is resolved through the truncation

$$\Delta\boldsymbol{x}_* = \boldsymbol{F}_{\text{T}}\Delta\boldsymbol{x}, \quad \boldsymbol{x}_{*,\text{e}} = \boldsymbol{f}_{\text{T,e}}(\boldsymbol{x}_{\text{e}}), \quad \boldsymbol{x}_{\text{e}} = \boldsymbol{f}_{\text{T},2}(E_{2,0})$$

where $\boldsymbol{F}_{\text{T}}$ is a matrix with the dimension $2\hat{k} \times n_{\text{model}}$ and $\boldsymbol{f}_{\text{T},1} : \mathbb{R}^{n_{\text{model}}} \mapsto \mathbb{R}^{2\hat{k}}$, $\boldsymbol{f}_{\text{T},2} : \mathbb{R} \mapsto \mathbb{R}^{n_{\text{model}}}$ are real functions. The matrix and functions depend on the truncation method and the assumed density distribution. The result is a truncated linear state-space system $\Sigma_{\Delta\text{NBT}}$ that depends only on the bunch size $E_{2,0}$.

An alternative approach is given in Figure 4.6: The truncation is directly chosen as a function of the state vector $\boldsymbol{x}$ and applied to the nonlinear system, before the linearization.

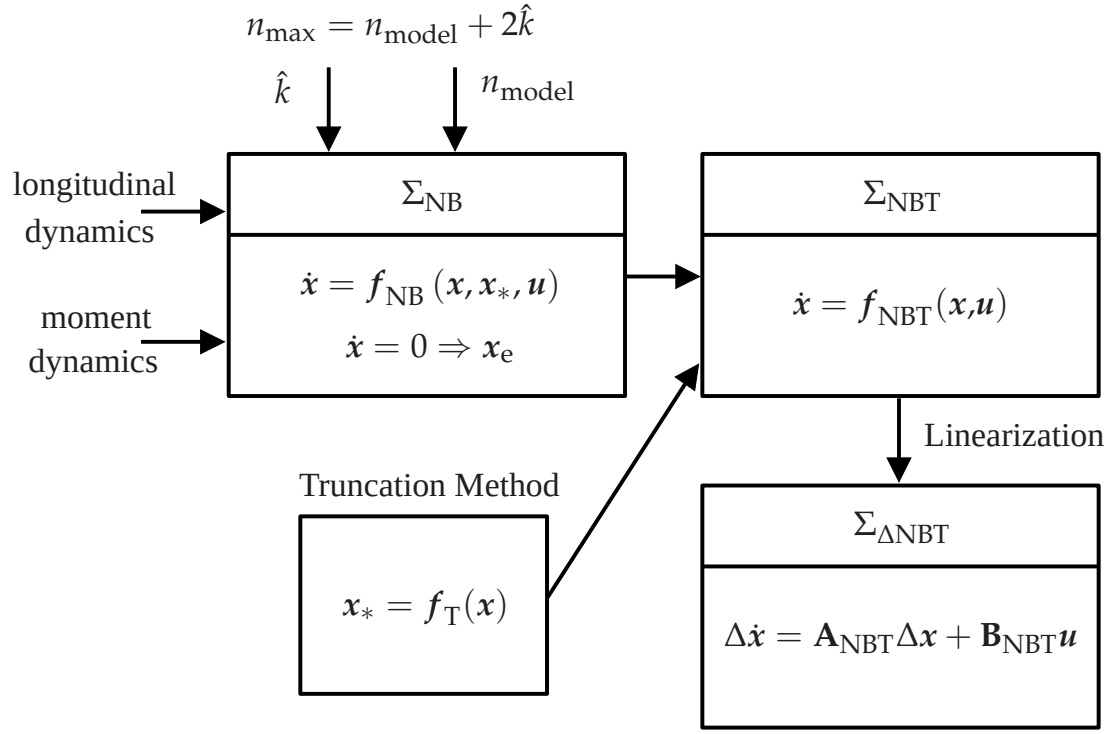

Figure 4.6: Alternative to Figure 4.5. The truncation is applied before the linearization.

The shown procedures are quite general and also include the case of a linear bucket with $\hat{k} = 1$. However, in that case the truncation functions are obsolete, because the state vector $\boldsymbol{x}_*$ is empty.

There are several possibilities for a truncation and elimination of the higher order moments:

T1 The simplest solution is to neglect higher order moments with $n_x + n_y > n_{\text{model}}$ and to set their equilibrium and deviations equal to zero: $\boldsymbol{x}_* = \Delta\boldsymbol{x}_* = \mathbf{0}$. There is however no reason to believe that this will lead to accurate results [18].

T2 The moments with $n_x + n_y > n_{\text{model}}$ can be assumed to be approximately constant: $\boldsymbol{x}_* = \boldsymbol{x}_{*,\text{e}}$ or $\Delta\boldsymbol{x}_* = \mathbf{0}$. If the particle density is approximately Gaussian or uniform and the bunch shape is ellipsoidal, the moments of Table C.3 can be used. For example, the density is Gaussian and $E_{8,0} = 105E_{2,0}^4$ and $\Delta C_{8,0} = 0$. This may be more exact, but does not represent the dependencies between $\boldsymbol{x}_*$ and $\boldsymbol{x}$ and does not lead to the correct bunch shape oscillation frequencies.

T3 In Appendix C.2, the moments of mode-shaped bunches are summarized. These relations are approximations of first order and can be used to implement the truncation of Figure 4.5. This will be described in more detail in Section 4.6.2.

T4 In Appendix C.1, the moments of ellipsoidal bunches are presented. These relations enable the use of the procedure of Figure 4.6 and this will be subject of Section 4.6.3.

At first sight, it seems that truncation method T1 needs no additional assumptions about the density. However, the equilibrium (C.4.1) does not specify $E_{2,0}$, $E_{4,0}$ and other higher order moments. These values must be specified by defining a bunch size $E_{2,0}$ and further assumptions about the density function must be made. For example, a Gaussian density implies that $E_{4,0}$ is approximately equal to $3E_{2,0}^2$. Because the values $E_{2,0}$, $E_{4,0}$, and $E_{6,0}$ are unknown and depend on the bunch size and density, these quantities have to be measured or estimated.

> Although the derivation of the moment dynamics is only based on the longitudinal dynamics of the beam and does not depend on the density distribution function, the final feedback models will depend on the bunch size and density function. This is also true for the case $\hat{k} = 1$ of a linear bucket, since there are additional parameters (such as E_4) that depend on the bunch size and the density function.

4.6.2 Models for Coherent Modes

The results of Tables C.2 and C.3 and of Section 4.4.3 enable the procedure of Figure 4.5. This will be demonstrated first for the dipole mode.

Dipole Mode Assume the linearized dynamics (C.1) for the basic moments, cf. p.180. This is system $\Sigma_{\Delta\mathrm{NB}}$ of Figure 4.5 for $\hat{k} = 3$ and $n_{\mathrm{model}} = 1$. The highest moment order is $n_{\max} = 7$. Assuming the uniform density and using row $\Delta C_{n_x,n_y}(r_1)$ of Table C.2, the truncation functions may be chosen as

$$\Delta C_{3,0} = \Delta C_{5,0} = \Delta C_{7,0} = 0 \cdot \Delta B_{1,0} \quad \Rightarrow \quad \Delta \boldsymbol{x}_* = \mathbf{0}$$

and the equilibrium $E_{4,0} = 2E_{2,0}^2$ and $E_{6,0} = 5E_{2,0}^3$. This leads to the linear system $\Sigma_{\Delta\mathrm{NBT}}$, written as a transfer function:

$$G_{1,u}(s) = \frac{\Delta B_{1,0}(s)}{u_\varphi(s)} = \frac{\omega_{\mathrm{syn}}^2 \left[1 - \frac{E_{2,0}}{2} + \frac{E_{2,0}^2}{12} - \frac{E_{2,0}^3}{144}\right]}{s^2 + \omega_{\mathrm{syn}}^2 \left[1 - \frac{E_{2,0}}{2} + \frac{E_{2,0}^2}{12} - \frac{E_{2,0}^3}{144}\right]}.$$

This is the transfer function of a harmonic oscillator that depends on the bunch size. For very small bunches, the frequency is ω_{syn}. For larger bunches, the dipole mode frequency for uniform densities is

$$\omega_{1,\mathrm{u}}\left(E_{2,0}\right) = \omega_{\mathrm{syn}} \sqrt{1 - \frac{1}{2}E_{2,0} + \frac{1}{12}E_{2,0}^2 - \frac{1}{144}E_{2,0}^3}. \tag{4.52}$$

This can be compared with the tracking simulations in Section 3.5.5. These simulations lead to the hypothesis (3.47) that estimates the frequency of mode m with

$$\omega_{m,\mathrm{hy}} = m\, \omega_{\mathrm{syn}}\, \frac{\pi}{2K\left(\sin\left(\sqrt{C_{2,0} = E_{2,0}}\right)\right)}. \tag{4.53}$$

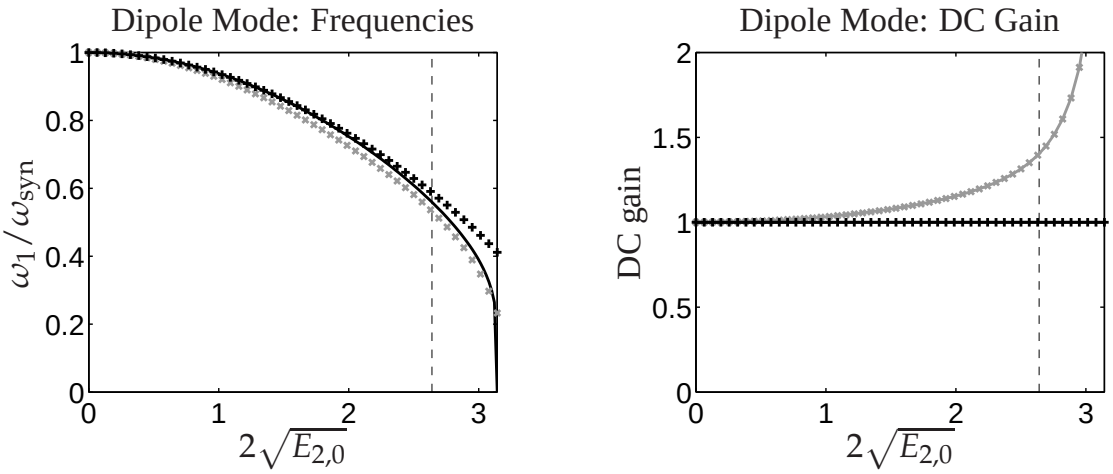

Figure 4.7: Properties of the dipole mode $m = 1$ transfer function for a uniform (black, $+$) and Gaussian (gray, $\times$) density. **Left**: frequency $\omega_1/\omega_{\text{syn}}$ versus the bunch size $E_{2,0}$ and $\omega_{1,\text{hy}}$ (solid line). **Right**: DC gain of the transfer function. The dashed line marks the bunch size where $[\omega_{1,\text{u}} - \omega_{1,\text{hy}}]/\omega_{1,\text{hy}}$ grows larger than 5%.

The expansion of function (4.53) in a Taylor series yields

$$\left[\frac{\pi}{2K\left(\sin\left(\sqrt{E_{2,0}}\right)\right)}\right]^2 = 1 - \frac{1}{2}E_{2,0} + \frac{7}{96}E_{2,0}^2 - \frac{19}{2880}E_{2,0}^3 + \ldots.$$

This is very similar to the result (4.52) of the uniform density.

For a Gaussian density, the procedure is analog. Table C.3 yields

$$\boldsymbol{x}_* = \begin{bmatrix}\Delta C_{3,0} & \Delta C_{5,0} & \Delta C_{7,0}\end{bmatrix}^{\text{T}} = \begin{bmatrix}\frac{3}{4}E_{2,0} & \frac{55}{8}E_{2,0}^2 & \frac{4305}{64}E_{2,0}^3\end{bmatrix}^{\text{T}} \Delta B_{1,0}$$

and the equilibrium $E_{4,0} = 3E_{2,0}^2$ and $E_{6,0} = 15E_{2,0}^3$, leading to

$$G_{1,g}(s) = \frac{\Delta B_{1,0}(s)}{u_\varphi(s)} = \frac{\omega_{\text{syn}}^2\left[1 - \frac{E_{2,0}}{2} + \frac{E_{2,0}^2}{8} - \frac{E_{2,0}^3}{48}\right]}{s^2 + \omega_{\text{syn}}^2\left[1 - \frac{5E_{2,0}}{8} + \frac{35E_{2,0}^2}{192} - \frac{35E_{2,0}^3}{1024}\right]}.$$

with the frequency

$$\omega_{1,\text{g}}\left(E_{2,0}\right) = \omega_{\text{syn}}\sqrt{1 - \frac{5}{8}E_{2,0} + \frac{35}{192}E_{2,0}^2 - \frac{35}{1024}E_{2,0}^3}.$$

The left image of Figure 4.7 compares the frequencies $\omega_{1,\text{u}}$ and $\omega_{1,\text{g}}$ with the frequency $\omega_{1,\text{hy}}$. This shows that $\omega_{1,\text{hy}}$ is indeed a very good estimate for the dipole mode frequency. There is reason to assume that $\omega_{1,\text{hy}}$ may be very close or even equal to the exact solution for a uniform density:

- Observation: For small and medium bunch sizes, $\omega_{1,\mathrm{u}}$ is very close to $\omega_{1,\mathrm{hy}}$. This holds not only for the dipole mode, but also for higher m, as the subsequent figures will show.

- Physical interpretation: For a matched bunch with a uniform density, the bunch size $2\sqrt{E_{2,0}}$ is equal to the radius of the bunch. Very small deviations due to a mode will change the boundary of the bunch slightly, but inside the bunch will remain unchanged. The frequency of the modes thus mainly depends on the frequency of the particles on the boundary of the bunch, i. e. the synchrotron frequency at $x = 2\sqrt{E_{2,0}}$. This frequency is given by $\omega_{1,\mathrm{hy}}$.

The differences between $\omega_{1,\mathrm{u}}$ and $\omega_{1,\mathrm{hy}}$ are due to the following reasons:

- The Taylor series truncation of the nonlinear RF potential introduces an error, but this has been shown to be rather small. The error grows for an increasing bunch size.

- The moments for a specific mode from Tables C.2 and C.3 are approximations. They are exact for ellipsoidal bunch shapes only. These approximations will introduce an error that increases with the bunch size.

- The linearization and truncation of the model.

Both error sources lead to an error that increases with $E_{2,0}$. This is in agreement with the observations of Figure 4.7 (left image). Therefore, the quantity $e_\mathrm{f} = [\omega_{1,\mathrm{u}} - \omega_{1,\mathrm{hy}}]/\omega_{1,\mathrm{hy}}$ will be used in the following as a measure for the accuracy of the transfer functions. In the figures, the dashed lines indicate the bunch size $\hat{E}_{2,0}$ for which e_f becomes 5%. For $E_{2,0} < \hat{E}_{2,0}$ the accuracy of the transfer functions is assumed to be acceptable. It has to be noted that – as the exact analytical solution is not known – this is only a reasonable estimate.

Quadrupole Mode If the model size is extended to $n_\mathrm{model} = 2$, transfer functions for the quadrupole mode are readily obtained. This is due to the fact that the dynamics of the basic moments (C.1) and moments of order $n_x + n_y = 2$ (C.2) are completely independent from each other, at least in the considered stationary case with $\varphi_\mathrm{R} = 0$.

The transfer function of the quadrupole mode $m = 2$ has the shape

$$G_2(s) = \frac{s}{s} \cdot \frac{-2b_2(E_{2,0})\omega_\mathrm{syn}^2}{s^2 + a_2(E_{2,0})\omega_\mathrm{syn}^2},$$

where b_2 and a_2 are functions of $E_{2,0}$. A summary of these functions for Gaussian and uniform densities is given in Appendix C.4.3. Transfer function $G_2(s)$ has a zero and pole at $s = 0$ that cancel each other, this means that the pole at $s = 0$ is neither controllable nor observable. The pole $s = 0$ is due to the invariant of motion I_2 that was already discussed in (4.34a) for the linear bucket. The physical interpretation is as follows: due to the linearization, only infinitesimal deviations ΔC from the matched shape are considered.

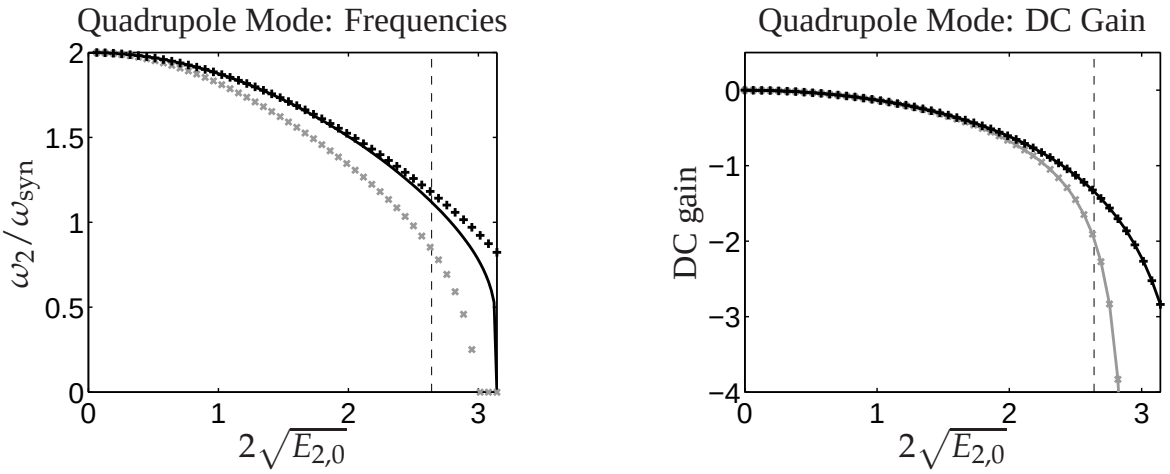

Figure 4.8: Frequencies and DC gains of the transfer functions of the quadrupole mode $m = 2$ for uniform (+, black) and Gaussian densities (x, gray) compared to the frequencies $\omega_{2,\mathrm{hy}}$ of (4.53) (solid, black). The dashed lines mark a relative error between the uniform density and $\omega_{2,\mathrm{hy}}$ of 5%.

From the fact that the eigenvalues of the transfer functions are still purely imaginary, it can be concluded that Landau damping or filamentation does not occur, even for large bunches, and the bunch area I_2 is a constant of motion. For small bunch sizes, $a_2 = 4$, and a quadrupole frequency of $2\omega_{\mathrm{syn}}$ is obtained. This is consistent with the results for a linear bucket.

Modes $m \in \{1,2,3,4\}$ The same procedure will now be used to construct a model that describes the dynamics of the first four modes. The modeling parameters are $\hat{k} = 3$ and $n_{\mathrm{model}} = 4$. It will be assumed that the bunch shape is a combination of all four modes, its boundary is defined by (cf. (3.17))

$$\hat{r}(\theta) = 1 + \sum_{m=1}^{4} r_m \sin\left(m[\theta - \theta_{m,0}]\right).$$

There is one complication that has to be taken into account due to the fact that one mode may excite several moments. For example, Table C.2 reveals that for a uniform density

$$\Delta C_{6,0} \approx \begin{cases} 45E_{2,0}^2 \Delta C_{2,0} & \text{for } m = 2 \\ 12E_{2,0}\Delta C_{4,0} & \text{for } m = 4 \end{cases} \tag{4.54}$$

holds. In case of a combination of the modes $m = 2$ and $m = 4$, the moment $\Delta C_{6,0}$ should not be replaced by the sum of these two components, but by

$$\Delta C_{6,0} = 15E_{2,0}^2[\Delta C_{2,0} - \underbrace{0}_{\Delta C_{2,0}(m=4)}] + 6E_{2,0}[\Delta C_{4,0} - \underbrace{4E_{2,0}\Delta C_{2,0}}_{\Delta C_{4,0}(m=2)}]. \tag{4.55}$$

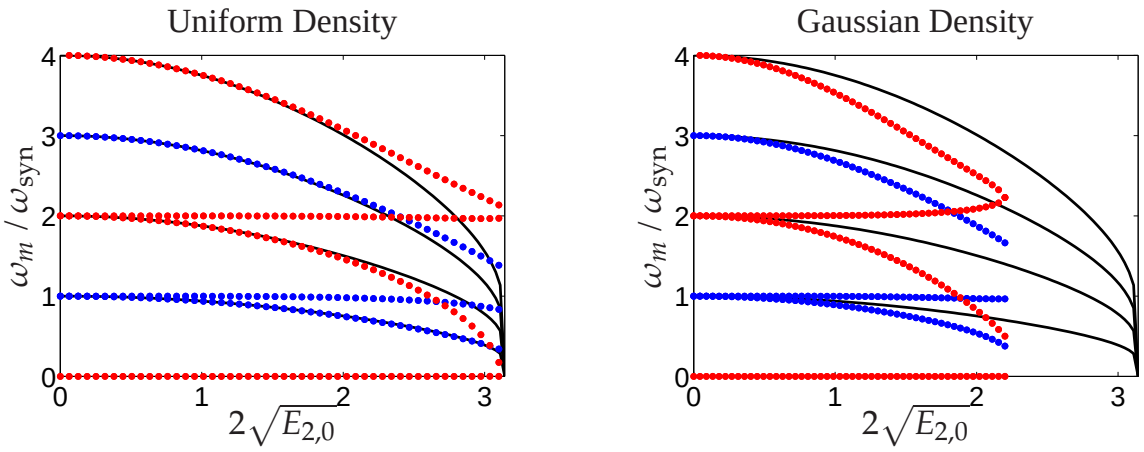

Figure 4.9: Eigenvalues of systems (4.56). The 14 eigenvalues are purely imaginary and each dotted line represents a complex conjugated pair of the odd (dotted, blue) or even (dotted, red) model. The solid lines are the nonlinear synchrotron frequencies $\omega_{m,\mathrm{hy}}$. **Right**: Truncation for a uniform density. **Left**: Truncation for a Gaussian density.

This can be explained as follows: For the mode $m = 2$, $\Delta C_{4,0}$ is not zero. To obtain the correct result (4.54), a correction term $\Delta C_{4,0}(m = 2)$ has to be included in (4.55). The same applies for $\Delta C_{2,0}$. This guarantees that (4.55) is in agreement with (4.54) for $m = 2$ and $m = 4$. Analog correction terms will be used for all other odd and even moments of Tables C.2 and C.3 to obtain the truncation matrix $\mathbf{F}_\mathrm{T}$ of Figure 4.5; an example for a Gaussian density is

$$\Delta C_{5,0} = \frac{55}{8} E_{2,0}^2 [B_{1,0} - \underbrace{0}_{\Delta B_{1,0}(m=3)}] + \frac{35}{4} E_{2,0} [\Delta C_{3,0} - \underbrace{\frac{3}{4} E_{2,0} B_{1,0}}_{\Delta C_{3,0}(m=1)}].$$

To obtain the functions $\boldsymbol{f}_{\mathrm{T},1}$ and $\boldsymbol{f}_{\mathrm{T},2}$, the equilibrium of Appendix C.4.1 is used. In addition, $E_{4,0}$ and higher order E_{n_x,n_y} with $n_x + n_y > 4$ are taken from Tables C.2 and C.3. This results in functions $\boldsymbol{f}_{\mathrm{T},1}$ and $\boldsymbol{f}_{\mathrm{T},2}$ that only depend on $E_{2,0}$. In principle, it would also be possible to take all E_{n_x,n_y} as functions directly from Tables C.2 and C.3. But, as stated in Remark 4.3, the use of the equilibrium of Appendix C.4.1 improves the result.

The final result is the state-space model $\Sigma_{\Delta\mathrm{NBT}}$ with dimension 14 and this model depends on the single parameter $E_{2,0}$. The odd and even moments in this model are completely decoupled and can be written as two independent SISO systems:

$$\begin{aligned} \Delta\dot{\boldsymbol{x}}_\mathrm{even} &= \mathbf{A}_\mathrm{even}(E_{2,0})\Delta\boldsymbol{x}_\mathrm{even} + \boldsymbol{b}_\mathrm{even}(E_{2,0})u_1 \\ \Delta\dot{\boldsymbol{x}}_\mathrm{odd} &= \mathbf{A}_\mathrm{odd}(E_{2,0})\Delta\boldsymbol{x}_\mathrm{odd} + \boldsymbol{b}_\mathrm{odd}(E_{2,0})u_2 \end{aligned} \tag{4.56}$$

The system matrices and input vectors are summarized in Appendix C.4.3 for uniform and Gaussian densities. For $E_{2,0} \ll 1$, the dynamics are approximately equal to the linear bucket case.

The matrices A_odd and A_even of systems (4.56) have in total 7 pairs of purely imaginary, complex conjugated eigenvalues $\pm\mathrm{i}\omega_k$, $k = 1,\ldots,7$. The frequencies ω_k are plotted

versus the bunch size $E_{2,0}$ in Figure 4.9 and compared with the frequencies $\omega_{m,\mathrm{hy}}$. For uniform densities, the agreement between the eigenvalue and hypothesis frequencies is excellent if $E_{2,0} \leq 1$. This result is also in agreement with the tracking simulations of Figure 3.18 for $m = 1$ and $m = 2$. Besides the obvious 8 eigenvalues due to the modes $m \in \{1,2,3,4\}$, there are additional eigenvalues

$$\pm \mathrm{i}0 \cdot \omega_{\mathrm{syn}}, \quad \pm \mathrm{i}1 \cdot \omega_{\mathrm{syn}}, \quad \pm \mathrm{i}2 \cdot \omega_{\mathrm{syn}}.$$

For the Gaussian density, the eigenvalues tend to be slightly smaller and are only shown up to $E_{2,0} = 1.21$, because they then become real. This indicates that the calculation for a Gaussian density is less accurate and a higher $\hat{k}$ would be preferrable to increase the model accuracy. The results of Figures 4.7 and 4.8 for $n_{\mathrm{model}} \in \{1,2\}$ seem more accurate and a possible reason may be that for higher n_{model}, $\hat{k}$ should also be increased to obtain a similar accuracy. However, the calculations of Table C.3 are computationally demanding; higher $\hat{k}$ will therefore be chosen in Section 4.6.3 for an alternative truncation method that is computationally easier to handle.

Hautus' criterion shows that all eigenvalues of the models (4.56) are controllable, except for the eigenvalues $\lambda_{1,2} = \pm \mathrm{i}0$. As for the linear bucket, the uncontrollable eigenvalues $\lambda_{1,2}$ are due to invariants such as (4.32), as the models do not include Landau damping and the emittance is a constant of motion. The fact that all other eigenvalues of the linear models are controllable strongly indicates that first-order controllability and thus local controllability is given for system Σ_{NB}. However, an exact proof is challenging and Theorem 4.3 is not sufficient, since system (4.43) is infinite-dimensional and models (4.56) can only be obtained after a linearization and truncation.

Despite the open theoretical questions that were addressed, there are strong indications to make the following conclusions. These conclusions are supported by the simulation results of Section 4.1

In a stationary nonlinear bucket:

- the odd moments and modes $m = 1$, $m = 3$ are dynamically coupled and can be damped by phase modulations $u_2 = u_\varphi$
- the even moments and modes $m = 2$, $m = 4$ are dynamically coupled and can be damped by amplitude modulations $u_1 = u_\varepsilon$
- the purely imaginary eigenvalues demonstrate that Landau damping is not included in the model; this may be due to the linearization or the truncation
- the frequency of mode m obeys $\omega_m = \omega_{m,\mathrm{hy}}$ with $\omega_{m,\mathrm{hy}}$ of hypothesis (3.47) for uniform densities

For a controller design, odd and even moments may be treated independently. However, a seperate feedback design for every single mode seems not feasible, because mode $m = 3$ is coupled with $m = 1$ and mode $m = 4$ with $m = 2$.

4.6.3 Models for Ellipsoidal Bunches

If only the center of gravity and the variance of the bunch are of interest and an ellipsoidal bunch shape is a sufficient model, the alternative truncation of Figure 4.6 can be used to create a model of the bunch shape dynamics. In this case, the relations of Table C.1 can be used. As the results of Table C.1 are exact for ellipsoidal bunches, its relations can be used in the nonlinear dynamics to obtain a nonlinear model. However, this will again lead to a neglect of filamentation and Landau damping, because of the assumption that the bunch shape will remain ellipsoidal even in presence of disturbances; this does not allow any filamentation of the bunch. For small deviations of the ellipsoidal shape, the filamentation is usually small and the model provides an appropriate description of the bunch dynamics. Since feedback systems for small deviations are of interest, a linearization of the resulting equations is reasonable.

The relations of Table C.1 show that for ellipsoidal bunches, moments with order $n_x + n_y > 2$ can be expressed as functions of the moments of order $n_x + n_y = 2$. It is thus possible to reduce the state vector to

$$\boldsymbol{x} = \begin{bmatrix} B_{1,0} & B_{0,1} & C_{2,0} & C_{1,1} & C_{0,2} \end{bmatrix}^{\mathrm{T}}.$$

After inserting the relations (function $\boldsymbol{f}_{\mathrm{T}}(\boldsymbol{x}$ of the truncation block in Figure 4.6), the resulting nonlinear model is

$$\Sigma_{\mathrm{NBT}}: \qquad \dot{\boldsymbol{x}}(t) = \boldsymbol{f}_{\mathrm{NBT}}\left(\boldsymbol{x}(t), u_\varepsilon(t), u_\varphi(t)\right) \tag{4.57}$$

and depends on the set of density functions $\mathcal{D}$ that is assumed, i. e. Gaussian or uniform density functions. Calculations for both density functions show that the invariant I_2 of (4.34a) is also an invariant of motion for this system (4.57). This clearly demonstrates that this model neglects filamentation.

A linearization around the reference $\boldsymbol{x}_{\mathrm{e}} = \begin{bmatrix} 0 & 0 & E_{2,0} & 0 & E_{0,2} \end{bmatrix}^{\mathrm{T}}$ yields system $\Sigma_{\Delta\mathrm{NBT}}$:

$$\frac{\Delta\dot{\boldsymbol{x}}}{\omega_{\mathrm{syn}}} = \begin{bmatrix} -\Delta B_{0,1} \\ a_1\left(E_{2,0}, \hat{k}, \mathcal{D}\right)\Delta B_{1,0} \\ -2\Delta C_{1,1} \\ a_2\left(E_{2,0}, \hat{k}, \mathcal{D}\right)\Delta C_{2,0} - \Delta C_{0,2} \\ a_3\left(E_{2,0}, \hat{k}, \mathcal{D}\right)\Delta C_{1,1} \end{bmatrix} + \begin{bmatrix} 0 \\ -a_1\left(E_{2,0}, \hat{k}, \mathcal{D}\right)u_\varphi \\ 0 \\ b_1\left(E_{2,0}, \hat{k}, \mathcal{D}\right)u_\varepsilon \\ 0 \end{bmatrix}, \tag{4.58}$$

with

$$\Delta\boldsymbol{x} = \boldsymbol{x} - \boldsymbol{x}_{\mathrm{e}} =: \begin{bmatrix} \Delta B_{1,0} & \Delta B_{0,1} & \Delta C_{2,0} & \Delta C_{1,1} & \Delta C_{0,2} \end{bmatrix}^{\mathrm{T}}.$$

The coefficients a_1, a_2, a_3, and b_1 are functions of the bunch size $E_{2,0}$, the parameter $\hat{k}$ of the Taylor series truncation, and the type of density function $\mathcal{D}$. The functions a_1, a_2, a_3,

and b_1 are presented in Appendix C.4.4 for uniform and Gaussian densities and $\hat{k} = 6$. The following transfer functions can be derived from the state space model $\Sigma_{\Delta\text{NBT}}$:

$$\frac{\Delta B_{1,0}(s)}{u_\varphi(s)} = \frac{\omega_{\text{syn}}^2 a_1}{s^2 + \omega_{\text{syn}}^2 a_1}, \qquad \frac{\Delta C_{2,0}(s)}{u_\varepsilon(s)} = \frac{s}{s} \cdot \frac{-2\omega_{\text{syn}}^2 b_1}{s^2 + \omega_{\text{syn}}^2 [2a_2 + a_3]}. \tag{4.59}$$

These transfer functions are very similar to the transfer functions of (4.40) for a linear bucket. In fact, for very small bunches with $E_{2,0} \ll 1$ the approximations

$$a_1 \approx 1, \qquad b_1 \approx E_{2,0}, \qquad a_2 \approx 1, \qquad a_3 \approx 2$$

hold for both the uniform and the Gaussian density, leading to exactly the same transfer functions as for the linear bucket. Thus, the calculation for the nonlinear bucket is as expected a generalization of the linear bucket case.

Regardless of the bunch size, the transfer function of $\Delta C_{2,0}$ reveals an uncontrollable pole at $s = 0$, as it is canceled by a zero at $s = 0$. As before, this is due to the invariance I_2 of the bunch area and confirms the statement that filamentation is not included in model. This can also be explained as follows: The invariant I_2 of (4.34a) can be written in differential form by assuming the case of a stationary bucket with

$$C_{2,0} = E_{2,0} + \Delta C_{2,0}, \quad C_{1,1} = \Delta C_{1,1}, \quad C_{0,2} = E_{0,2} + \Delta C_{0,2}.$$

Introducing these relations in (4.34a) and neglecting higher order terms (i. e. $\Delta C_{1,1}^2$) leads to

$$\Delta I_2 = 0 = E_{0,2}\Delta C_{2,0} + E_{2,0}\Delta C_{0,2},$$

where $I_2 = \text{const.} \Rightarrow \Delta I_2 = 0$ was used. This can be written as

$$\Delta C_{0,2} = -\frac{E_{0,2}}{E_{2,0}}\Delta C_{2,0} = -\left[1 - \frac{E_{4,0}}{6} + \frac{E_{6,0}}{120} - \frac{E_{8,0}}{5040} + \dots\right]\Delta C_{2,0}, \tag{4.60}$$

where the equilibrium for the stationary bucket of Appendix C.4.1 was used. For a uniform density (cf. Table C.2), this equals

$$\Delta C_{0,2} = -\left[1 - \frac{E_{2,0}}{3} + \frac{E_{2,0}^2}{24} - \frac{E_{2,0}^3}{360} + \dots\right]\Delta C_{2,0}, \tag{4.61}$$

Thus, there exists an algebraic relation between the states $C_{0,2}$ and $C_{2,0}$ and they cannot be changed independently from each other. The same information is included in model $\Sigma_{\Delta\text{NBT}}$ of (4.58). Comparing the third and fifth row of the state space model yields

$$\begin{aligned}\Delta\dot{C}_{0,2} &= -\frac{a_3}{2}\Delta\dot{C}_{2,0} \\ \Rightarrow \Delta C_{0,2}(t) - \Delta C_{0,2}(t_0) &= -\frac{a_3}{2}\left[\Delta C_{2,0}(t) - \Delta C_{2,0}(t_0)\right]\end{aligned}$$

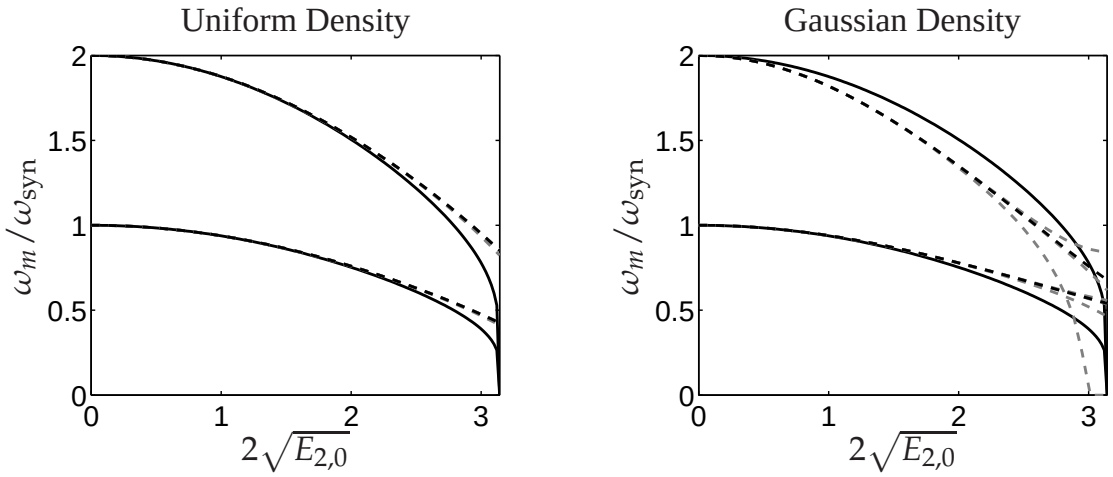

Figure 4.10: Frequencies ω_1, ω_2 of the linearized model for ellipsoidal bunches $\Sigma_{\Delta\mathrm{NBT}}$. The solid lines are the nonlinear synchrotron frequencies $\omega_{m,\mathrm{hy}}$ of (3.47) (p. 79), the dashed lines are the eigenvalues of model (4.58) for different $\hat{k}$ and are gray for $\hat{k} \in \{3,4,5\}$ and black for $\hat{k} = 6$. **Left**: uniform density. **Right**: Gaussian density.

with the initial values $\Delta C_{2,0}(t_0)$ and $\Delta C_{0,2}(t_0)$. At the equilibrium $\Delta C_{2,0}(t) = \Delta C_{0,2}(t) = 0$ must hold, thus the equilibrium can only be reached for $\Delta C_{2,0}(t_0) = -a_3 \Delta C_{0,2}(t_0)/2$ and this leads to

$$\Delta C_{0,2} = -\frac{a_3}{2}\Delta C_{2,0} = -\left[1 - \frac{E_{2,0}}{3} + \frac{E_{2,0}^2}{24} - \frac{E_{2,0}^3}{360} + \ldots\right]\Delta C_{2,0}, \tag{4.62}$$

where a_3 was replaced with the function for uniform densities. This is in agreement with (4.61). An analog result is obtained for the Gaussian density and the relation

$$a_3 = 2\frac{E_{0,2}}{E_{2,0}}$$

that follows from (4.60) and (4.62) seems to hold in general.

The remaining poles of the transfer functions are purely imaginary for the considered domain of $E_{2,0}$ and can be written as

$$s_{1,2} = \pm \mathrm{i}\omega_1 = \pm \mathrm{i}\omega_{\mathrm{syn}}\sqrt{a_1}, \qquad s_{3,4} = \pm \mathrm{i}\omega_2 = \pm \mathrm{i}2\omega_{\mathrm{syn}}\sqrt{\frac{2a_2 + a_3}{4}}.$$

Figure 4.10 displays the frequencies ω_1 and ω_2 as a function of the bunch size for different $\hat{k}$. The dashed gray lines are the frequencies of the model for $\hat{k} \in \{3,4,5\}$ and the dashed lines in black belong to $\hat{k} = 6$. The curves for different $\hat{k}$ allow an estimation of the convergence of the solutions to the exact solution for $\hat{k} \to \infty$. Also, the frequencies are compared to $\omega_{m,\mathrm{hy}}$ of (4.53). The results show that:

- For a uniform density, the curve for $\hat{k} = 3$ is already very close to the real solution, whereas the convergence in case of the Gaussian density is slower and $\hat{k} = 6$ is necessary for a satisfactory solution.

- For the uniform density, the hypothesis (4.53) is excellent. For larger bunch sizes, the assumption of ellipsoidal bunches is only a rough model for matched bunches and the differences for $E_{2,0} > 1$ may be mainly due to this reason. Compared to the uniform density, the Gaussian density leads to a frequency of $B_{1,0}$ that is slightly larger, whereas the frequency of $C_{2,0}$ is distinctly smaller. This is in agreement with the tracking simulation results of Figure 3.18.

- It is interesting to note that for a uniform distribution $2a_2 + a_3 = 4a_1$ holds. This implies that independently of the bunch size, the moment $C_{2,0}$ oscillates with exactly two times the frequency of $B_{1,0}$, just as one expects from simplified physical considerations.

- In addition, the DC gain of the transfer function of $B_{1,0}(s)$ is exactly 1 for both the uniform and Gaussian density. This result deviates from the right image of Figure 4.7. For the interpretation of this difference, it has to be kept in mind that there is no exact one-to-one correspondence between the dipole mode $m = 1$ and the basic moment $B_{1,0}$.

4.6.4 Models of Filamentation

The models of the previous sections use truncation methods **T3** and **T4**. This leads to a good estimate of the mode frequencies, but neglects filamentation and Landau damping, because **T3** and **T4** assume bunch shapes that cannot filament.

To study filamentation, the nonlinear equations (4.43) can be combined with truncation method **T2**, where the moment vector $\boldsymbol{x}_*$ is assumed to be constant. This yields the dynamics

$$\dot{\boldsymbol{x}}(t) = \boldsymbol{f}_{\mathrm{NBT2}}\left(\boldsymbol{x}(t), u_\varepsilon(t), u_\varphi(t)\right). \tag{4.63}$$

The calculation of the invariant $I_2 = C_{2,0}C_{0,2} - C_{1,1}^2$ yields

$$\dot{I}_2(t) = f_{\mathrm{I}_2}(u_\varepsilon, u_\varphi, B_{1,0}, C_{2,0}, C_{1,1}, \ldots) \neq 0.$$

Consequently, the model may represent some effects of the filamentation. Inserting the equilibrium moments $\boldsymbol{x} = \boldsymbol{x}_\mathrm{e}$ for a matched bunch leads to $\dot{I}_2 = 0$. This does make sense, since a matched bunch will neither oscillate nor experience filamentation.

A linearization of the dynamics $\dot{I}_2$ around the equilibrium of a matched bunch for small deviations reads

$$\begin{aligned}\dot{I}_2(t) &\approx \frac{\partial \dot{I}_2}{\partial \boldsymbol{x}}\Delta\boldsymbol{x} + \frac{\partial \dot{I}_2}{\partial \left[u_\varepsilon, u_\varphi\right]}\begin{bmatrix} u_\varepsilon \\ u_\varphi \end{bmatrix} \\ &= \left[\frac{E_{4,0}}{3} - \frac{E_{6,0}}{60} + \ldots\right]\Delta C_{1,1} - \frac{E_{2,0}}{3}\Delta C_{3,1} + \frac{E_{2,0}}{60}\Delta C_{5,1} \neq 0.\end{aligned}$$

For a small bunch ($E_{2,0} \ll 1$) with a uniform density, the following approximations are valid:

$$I_2 \approx E_{2,0}^2, \quad E_{4,0} \approx 2E_{2,0}^2, \quad E_{6,0} \approx 5E_{2,0}^3$$

and this leads to

$$\frac{\dot{I}_2}{I_2} \approx \left[\frac{2}{3} - \frac{E_{2,0}}{12} + \ldots\right] \Delta C_{1,1} - \frac{\Delta C_{3,1}}{3E_{2,0}} + \frac{\Delta C_{5,1}}{60E_{2,0}}.$$

Further, it is reasonable to assume that

$$\Delta C_{1,1} \sim \mathcal{O}\left(E_{2,0}\right), \quad \Delta C_{3,1} \sim \mathcal{O}\left(E_{2,0}^2\right), \quad \Delta C_{5,1} \sim \mathcal{O}\left(E_{2,0}^3\right),$$

i. e. the moment $\Delta C_{1,1}$ depends on $E_{2,0}$ and for a decreasing $E_{2,0}$, it will decrease by the same order of magnitude, and so forth. Thus, for $E_{2,0} \to 0$, we also have $\dot{I}_2 / I_2 \to 0$, i. e. the relative change of the emittance becomes negligible. This is in agreement with the observation that very small bunches in a nonlinear bucket behave similar to bunches in a linear bucket and show few filamentation.

This leads to the following conclusions with respect to the invariants and filamentation:

- In a linear bucket, there are invariants of motion I_2, I_4, and I_6 that are due to the invariant bunch area. Filamentation or Landau damping does not occur. It is reasonable to expect that there is an infinite number of invariants, one for each even moment order m, i. e. I_8, I_{10}, etc.
- For very small bunches in a nonlinear bucket, the situation is approximately the same as for the linear bucket case.
- For large matched bunches in a nonlinear bucket, the bunch area is still invariant and there is no filamentation.
- Large bunches with mismatches in nonlinear buckets lose the invariants of motion due to filamentation.

4.7 Conclusion

4.7.1 Comparison of RF Feedback Models

Transfer functions for bunch phase and length oscillations are presented for example in [107] and in [13]. These transfer functions are equivalent to (4.40) if $\varphi_R = 0$ is assumed. In addition, the models use the synchrotron frequency ω_{syn} so that the models are valid for linear buckets or very small bunches only.

Table 4.2: Developed models for coherent oscillation modes, stationary bucket.

Mode m	1	2	3	4	> 4
Linear Bucket	✓	✓	✓	✓	?
Nonlinear Bucket	✓	✓	✓	✓	?

An early model for the control of bunch-shape oscillations $m = 2$ was given by Hereward [40]. Hereward defined quantities that are similar to the variance $C_{2,0}$ and the covariance $C_{1,1}$. As a main quantity, he considered the difference of the variances $\overline{q_2} = C_{2,0} - C_{0,2}$. Appropriate damping leads to a matched bunch with $\overline{q_2} = 0$. However, it is obvious that this calculation is valid for a linear bucket or small bunches only, since only then the trajectories can be normalized as circles and $C_{2,0} = C_{0,2}$ for matched bunches. In [40], the nonlinearity of the RF dynamics is approximated by a function in $x = \Delta\varphi$ and x^2. After the linearization, the model for the bunch length oscillations is a harmonic oscillator with the frequency $2\omega_{\mathrm{syn}}$. This is consistent with the transfer function $\Delta C_{2,0}/u_1$ of (4.40). Hereward proposed the phase input u_φ to damp the bunch length oscillations. Equation (4.27c) shows that this is possible only for $\varphi_{\mathrm{R}} \neq 0$, because only then the input u_1 is coupled with u_φ. This is in agreement with [40], since Hereward's model depends on φ_{R}.

The model was further developed in [113]. The model derivation is equivalent to [40]. To damp quadrupole modes, both amplitude and phase modulations are proposed as feedback. In case of amplitude modulations, the damping rate is given as

$$\alpha_{\mathrm{d}} \approx \frac{K}{\hat{U}_1}\,\omega_{\mathrm{syn}}^{3/2},$$

where K is a feedback gain, and in case of phase modulations as

$$\alpha_\varphi \approx \tan(\varphi_{\mathrm{R}})\,\frac{K}{4}\,\omega_{\mathrm{syn}}^{3/2}.$$

> This is consistent with the results of this chapter, because it was shown that in a stationary bucket, i. e. $\varphi_{\mathrm{R}} = 0$, the phase has no influence on the moments of second order and thus on the quadrupole mode and the damping rate must be $\alpha_\varphi = 0$.

The mentioned references show that the typical models used to analyze bunch oscillations are based on a linearization of the single-particle dynamics. One drawback of these models is that they cannot be used to analyze the damping of higher order modes. Another disadvantage is that the frequency of the modes is not represented correctly.

Table 4.2 summarizes the contribution of this chapter. New models have been obtained and analyzed for modes $m \leq 4$ for the linear and nonlinear bucket. In addition, System (4.56) models not only the dynamics, but also the coupling between the modes.

So far, all models are valid for the stationary case. However, the modeling scheme may be applied to the general case $\varphi_R \neq 0$. Also, higher order modes $m > 4$ can be analyzed in principle. So far, the only limiting factor for the modeling scheme is given by the calculations of Section 4.4.3; to obtain the moments of a given density function, this function has to integrated analytically and the effort increases with the moment order.

4.7.2 Summary of the Results

The statistical description of the particle ensemble leads to a simple formulation of the control problem: A particle bunch has reached its equilibrium if the density function is time-invariant. The advantage of this formulation is that it is also valid for nonlinear RF potentials. Still, the controller analysis and design for this system is a complex task, as its dynamics are governed by a PDE. To obtain simplified models, a modeling approach has been suggested based on moments. Moment methods have already been in use for time-efficient simulations of beam dynamics and some moment-based models exist for the coherent mode $m = 2$. These models are however valid for linear buckets only. What is novel in this chapter is the use of a moment method to obtain models for bunch shape oscillations in the nonlinear bucket and the subsequent analysis using methods from control theory.

The modeling scheme is based on raw and central moments in the longitudinal phase space. It has been shown that the control problem can be reformulated in terms of moments under mild assumptions. Time-invariant moments are then equivalent to a time-invariant density function and thus to a matched bunch. It has been demonstrated that although there is no one-to-one correlation between the within-bunch modes m and the moments, the central moments of order m are useful as a measure for the within-bunch mode m. The calculation of the moment dynamics leads to a set of nonlinear equations that describe the coherent oscillations. In case of a linear bucket, these dynamics are only coupled with respect to the input variables. A linearization leads to transfer functions for the bunch center and variance that are in agreement with known models. An analysis of the higher order moments indicates that they are not controllable and thus cannot be damped in a linear bucket by phase or amplitude modulations. In case of a nonlinear bucket, the nonlinear RF potential has to be approximated by a finite polynomial series so that the rate of change of the moments can be expressed as a function of the moments. Due to the nonlinearity, the obtained model is not closed and a truncation is necessary. Different truncation methods have been proposed. One truncation method uses the relations between moments and within-bunch modes m to derive a state-space model for the modes. The eigenvalues of this model depend on the bunch size quantity $2\sqrt{E_{2,0}}$ and the frequencies fall for increasing bunch sizes, which is in agreement with the simulation results. A second truncation method is applicable for ellipsoidal bunches and leads to models for the bunch phase and length. Both truncation methods and the linearization lead to models that neglect Landau damping. It has to be noted that Landau damping is a highly complex and nonlinear process. It can only be described accurately by the Vlasov equation, i. e. an infinite dimensional model, or a particle ensemble, i. e. a high-dimensional model.

5 Damping of Single-Bunch Oscillations

In this chapter, the models (4.58) and (4.59) that were derived in the last chapter are used in Section 5.1 to analyze a bunch length feedback system of the heavy-ion synchrotron SIS18 at GSI. The stability of the feedback is analyzed and the performance evaluated by means of tracking simulations. In Section 5.2, measurements of a beam experiment are used to verify the analytical and simulation results. Finally, some possible applications of nonlinear methods for stability analysis and controller design are discussed in Section 5.3.

5.1 Analysis of RF Feedback Systems of the SIS18 at GSI

In this section, mathematical models are developed for two RF feedback loops at GSI. These models are simplified, leading to linear transfer functions that approximate the closed-loop behavior. Next, the stability of the linear model is analyzed and finally, simulations are used to evaluate the performance of the feedback.

5.1.1 Structure of RF Feedback Loops

A simplified diagram of the feedback structure at GSI for the bunch position and length is shown in Figure 5.1. The individual blocks are described in the following.

Cavity The cavity produces the sinusoidal RF voltage

$$U_{\mathrm{gap}}(t) = \hat{U}_{1,\mathrm{R}}[1 + u_{\varepsilon}(t)] \sin\left(\varphi(t) - u_{\varphi}(t)\right), \tag{5.1}$$

where the phase φ is the integral over time of the RF frequency ω_{RF}. Strictly speaking, the cavity itself is a subsystem with dynamics and even feedback loops of its own. Often, the cavity is modeled as a parallel resonant circuit. The cavity is driven by an amplifier and a DDS (Direct Digital Synthesis) unit. The DDS receives the frequency ω_{RF} and produces a sinusoidal signal with this frequency using a look-up table. The amplitude modulator AM receives the reference amplitude $\hat{U}_{1,\mathrm{R}}$. The output of the modulator is then amplified and fed to the cavity, where it drives the resonator to induce the voltage U_{gap}. Feedback loops are used to stabilize the amplitude and phase of U_{gap} at their reference values. In case of a high-current beam, the beam current i_{beam} acts back on the cavity, because a voltage is induced in the cavity by the beam. This changes the gap voltage and is referred to as *beam loading*. Beam loading or other collective effects will not be considered directly as mentioned above.

These remarks about the RF cavity already show that it is a complex subsystem and there are still important open research questions concerning its behavior and control.

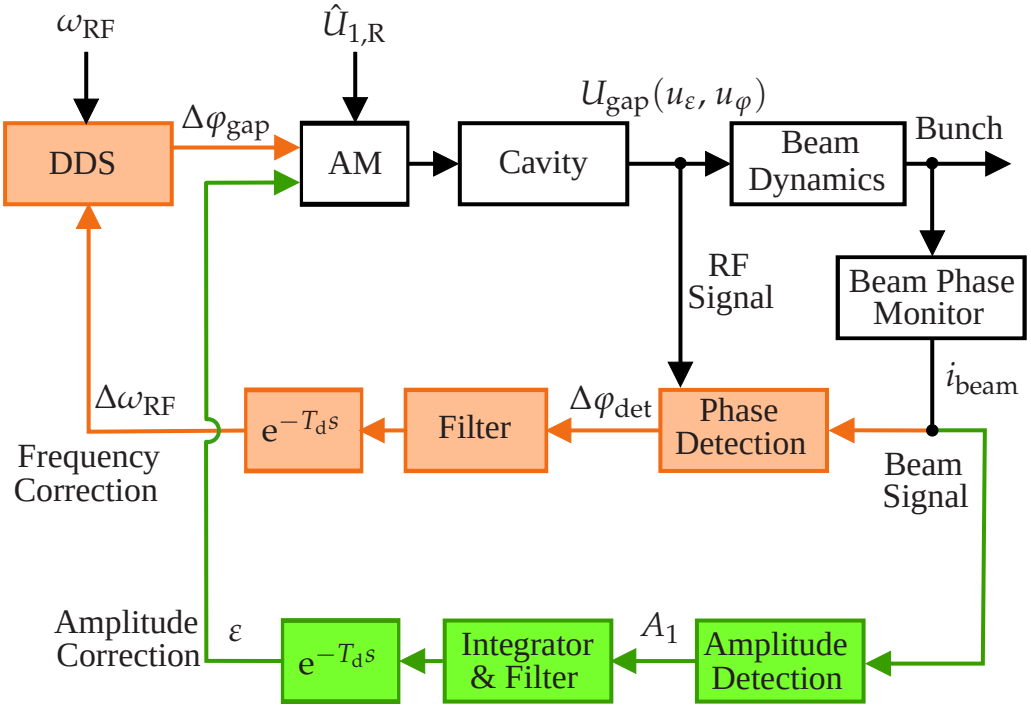

Figure 5.1: Simplified feedback structure of bunch phase and variance at GSI, AM: amplitude modulator. Courtesy H. Klingbeil (GSI), [60].

However, in many cases it is sufficient to model the cavity in a simpler way. Important conditions are:

- moderate rate of change of the modulations u_ε and u_φ
- well adjusted control loops for phase and amplitude of U_{gap}

However, it has to be noted that is difficult to choose specific boundaries for the above mentioned conditions. It will be assumed that these conditions are fulfilled, but the model restrictions have to be kept in mind.

The DDS unit sums up the frequency correction values $\Delta\omega_{RF}$ and can be modeled as an integrator [59]

$$\Delta\varphi_{gap} = -\int \Delta\omega_{RF}\,\mathrm{d}t \quad \Rightarrow \quad G_{DDS}(s) = \frac{\Delta\varphi_{gap}(s)}{\Delta\omega_{RF}(s)} = -\frac{1}{s}.$$

Due to the cavity dynamics, i. e. its finite bandwith, the phase modulation u_φ from the gap voltage (5.1) is not exactly equal to $\Delta\varphi_{gap}$. Assuming a controlled cavity, the phase modulation u_φ will follow changes in $\Delta\varphi_{gap}$ with a certain time constant $T_{cav,\varphi}$ and this may be described by the first order system

$$u_\varphi(t) + T_{cav,\varphi}\dot{u}_\varphi(t) = \Delta\varphi_{gap}(t) \quad \Rightarrow \quad G_{cav,\varphi}(s) = \frac{u_\varphi(s)}{\Delta\varphi_{gap}(s)} = \frac{1}{T_{cav,\varphi}s + 1}. \tag{5.2}$$

Similarly, the amplitude correction is modeled by the first order system

$$u_\varepsilon(t) + T_{\text{cav},\varepsilon}\dot{u}_\varepsilon(t) = \varepsilon(t) \quad \Rightarrow \quad G_{\text{cav},\varepsilon}(s) = \frac{u_\varepsilon(s)}{\varepsilon(s)} = \frac{1}{T_{\text{cav},\varepsilon}s + 1}. \tag{5.3}$$

Typically, the time constants of the cavity feedback loops are considerably smaller than the time constants of the closed bunch position and bunch length feedback loops. For this reason, the time constants $T_{\text{cav},\varepsilon}$ and $T_{\text{cav},\varphi}$ will be neglected in Section 5.1.3 and subsequent sections.

Bunch Phase A detailed description of the phase loop is presented in [59]. The main parts are shortly summarized for the sake of completeness.[1)]

For an ellipsoidal bunch with only small variations from the equilibrium, the moments $B_{1,0}$ and $C_{2,0}$ are sufficient to describe the dynamics of the beam with respect to the modulations and transfer functions (4.59) can be used. The transfer function for the bunch position is

$$G_{\text{bp}}(s) = \frac{\Delta B_{1,0}(s)}{u_\varphi(s)} = \frac{\omega_{\text{syn}}^2 a_1}{s^2 + \omega_{\text{syn}}^2 a_1}.$$

The bunch position is not measured directly. Rather, a beam phase monitor (BPM) measures the beam current i_{beam} and the phase detection subsystem compares the gap voltage and the first harmonic of the beam current. The density distribution of a bunch is often approximately Gaussian and in this case Equations (3.44) hold. Due to (3.44b), the phase of the first harmonic of i_{beam} is $\varphi_1 = -\Delta B_{1,0}$. The phases φ_k are defined in such a way that $\varphi_k > 0$ implies an advanced wave, cf. definition (A.5). Because the phases of the beam and the gap voltage are defined in the opposite way, the beam phase

$$\Delta\varphi_{\text{beam}} = -\varphi_1 = \Delta B_{1,0}$$

will be used instead. The comparison in the *phase detection* subsystem yields the detected phase

$$\Delta\varphi_{\text{det}} = \Delta\varphi_{\text{beam}} - u_\varphi = \Delta B_{1,0} - u_\varphi, \quad \Rightarrow \quad \frac{\Delta\varphi_{\text{det}}(s)}{u_\varphi(s)} = G_{\text{bp}}(s) - 1.$$

The detected phase $\Delta\varphi_{\text{det}}$ is used as input of a finite impulse response (FIR) filter. The basic idea of the FIR filter is to have a band-pass filter that lets pass frequency components near the frequency of the mode that should be detected and damped [59]. The center frequency of the passband will be denoted by f_{pass}. If for example the dipole mode is considered, it is reasonable to choose f_{pass} close to the synchrotron frequency f_{syn} to detect bunch phase oscillations.

[1)] An important difference of this summary compared to [59] is the refined beam model that depends on the bunch size. The theoretical analysis of [59] is however still valid, because the shape of the transfer functions remains the same. The only difference is the change from the synchrotron frequency ω_{syn} to the effective frequency $\sqrt{a_1}\omega_{\text{syn}}$ with a_1 from Appendix C.4.4.

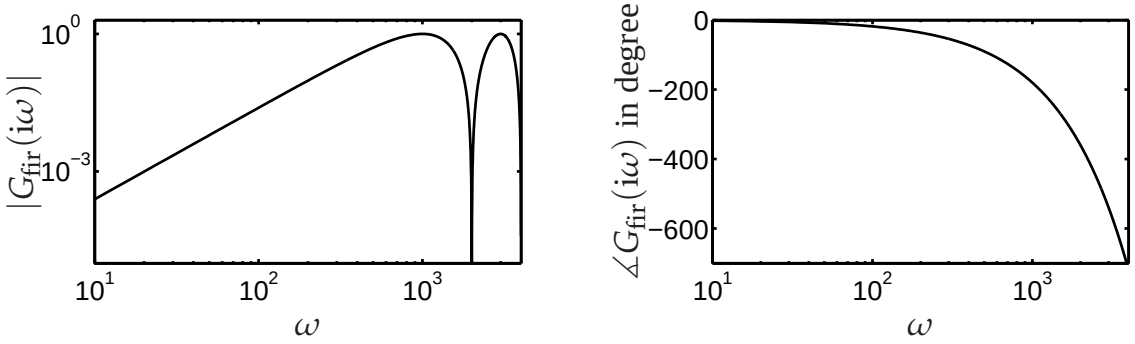

Figure 5.2: Magnitude and phase of $G_{\mathrm{fir}}(\mathrm{i}\omega)$ for $\omega_{\mathrm{pass}} = 1\,\mathrm{kHz}$ (logarithmic and semi-logarithmic scale).

Additional desired filter properties are a rejection of the DC component and a phase lag of -180° at f_{pass}. The rejection of the DC component is important, because in general measured quantities of the bunch such as $B_{1,0}$ and $C_{2,0}$ may contain DC offsets. In addition, the exact equilibrium of the variance $C_{2,0}$ is not known and a DC rejection is useful to obtain relative quantities such as $\Delta B_{1,0}$ and $\Delta C_{2,0}$. The phase shift of -180° is important for the stability, a detailed analysis can be found in [59].

The FIR filter has the discrete form [59]

$$y_{\mathrm{fir}}(n) = -\frac{1}{4}x_{\mathrm{fir}}(n) + \frac{1}{2}x_{\mathrm{fir}}\left(n - \frac{f_{\mathrm{samp}}}{2f_{\mathrm{pass}}}\right) - \frac{1}{4}x_{\mathrm{fir}}\left(n - \frac{f_{\mathrm{samp}}}{f_{\mathrm{pass}}}\right), \tag{5.4}$$

where x_{fir} are the input, y_{fir} the output, and $f_{\mathrm{samp}} = \omega_{\mathrm{samp}}/2\pi$ the sampling rate of the filter, respectively. The discrete time steps are $t(n) = n/f_{\mathrm{samp}}$. Writing the discrete filter as a transfer function yields

$$G_{\mathrm{fir}}(s = \mathrm{i}\omega) = \frac{1}{2}\mathrm{e}^{-\frac{s}{2f_{\mathrm{pass}}}}\left[1 - \frac{\mathrm{e}^{\frac{s}{2f_{\mathrm{pass}}}} + \mathrm{e}^{-\frac{s}{2f_{\mathrm{pass}}}}}{2}\right].$$

The frequency response is thus given by

$$G_{\mathrm{fir}}(s = \mathrm{i}\omega) = \frac{1}{2}\mathrm{e}^{-\mathrm{i}\pi\frac{\omega}{\omega_{\mathrm{pass}}}}\left[1 - \cos\left(\pi\frac{\omega}{\omega_{\mathrm{pass}}}\right)\right].$$

The magnitude $|G_{\mathrm{fir}}(\mathrm{i}\omega)|$ and phase $\measuredangle G_{\mathrm{fir}}(\mathrm{i}\omega)|$ are shown in Figure 5.2 for $\omega_{\mathrm{pass}} = 1\,\mathrm{kHz}$. The filter indeed has a bandpass characteristic at $\omega = [2k+1]\omega_{\mathrm{pass}}$ ($k = 0, 1, \ldots$).

Finally, the filter is followed by a gain K_1 and a time delay T_{d}. The time delay covers the time that the digital and analog hardware needs to process the information. The resulting frequency correction is

$$\Delta\omega_{\mathrm{RF}}(s) = \mathrm{e}^{-T_{\mathrm{d}}s}\, K_1\, G_{\mathrm{fir}}(s)\, \Delta\varphi_{\mathrm{det}}(s).$$

Bunch Length The transfer function of the bunch length is given by (cf. (4.59))

$$G_{\mathrm{bl}}(s) = \frac{\Delta C_{2,0}(s)}{u_\varepsilon(s)} = \frac{-2\omega_{\mathrm{syn}}^2 b_1}{s^2 + \omega_{\mathrm{syn}}^2[2a_2 + a_3]}. \tag{5.5}$$

After measuring the beam current, the amplitude A_1 of the first harmonic is determined. Assuming a Gaussian density, (3.44b) yields

$$A_1(t) = 2\bar{i}_{\mathrm{beam}} \mathrm{e}^{-\frac{1}{2}C_{2,0}}.$$

Linearizing around $C_{2,0} = E_{2,0}$ yields

$$\begin{aligned} A_1 \approx A_{1,\mathrm{e}} + \Delta A_1 &= 2\bar{i}_{\mathrm{beam}} \mathrm{e}^{-\frac{1}{2}E_{2,0}} - \bar{i}_{\mathrm{beam}} \mathrm{e}^{-\frac{1}{2}E_{2,0}} \Delta C_{2,0} \\ \Rightarrow \quad G_{\mathrm{A}} = \frac{\Delta A_1}{\Delta C_{2,0}} &= -\bar{i}_{\mathrm{beam}} \mathrm{e}^{-\frac{1}{2}E_{2,0}}. \end{aligned} \tag{5.6}$$

If a similar FIR filter as (5.4) is chosen, the DC component $A_{1,\mathrm{e}}$ is rejected and only ΔA_1 is relevant. In [93, 95], an FIR filter is proposed that has exactly the same structure as (5.4). The only differences are the choice of f_{pass}, which will be close to the frequency of transfer function (5.5), and an additional discrete integrator

$$y_{\mathrm{I}}(n) = y_{\mathrm{I}}(n-1) + K_{\mathrm{I,d}} x_{\mathrm{I}}(n) \quad \Rightarrow \quad G_{\mathrm{I}}(z) = \frac{y_{\mathrm{I}}(z)}{x_{\mathrm{I}}(z)} = K_{\mathrm{I,d}} \frac{z}{z-1}.$$

Its continuous transfer function is approximately [9]

$$G_{\mathrm{I}}(s) = \frac{K_{\mathrm{I,d}}}{T_{\mathrm{samp}}} \frac{1}{s},$$

where $T_{\mathrm{samp}} = 1/f_{\mathrm{samp}}$ is again the sampling time of the feedback loop. With the time delay T_{d}, the amplitude correction reads

$$\varepsilon(s) = \mathrm{e}^{-T_{\mathrm{d}}s} \frac{K_{\mathrm{I,d}}}{T_{\mathrm{samp}}} \frac{1}{s} G_{\mathrm{fir}}(s)\, G_{\mathrm{A}}\, \Delta C_{2,0}(s)$$

and the modeling of the control loops is complete.

Remark 5.1. The transfer function (5.6) introduces a dependency on the mean beam current. If $\bar{i}_{\mathrm{beam}}$ can be measured as well, this can be avoided if $A_1/A_0 = A_1/(2\bar{i}_{\mathrm{beam}})$ is used as input to the filter. This has the advantage that the same controller gains could be used for experiments with different beam current levels.

Remark 5.2. There is an alternative to the described measurement of the bunch length. In [13], the measurement of the peak line density of the bunches is said to be a usual procedure and the transfer function

$$\frac{\Delta l/l}{\varepsilon(s)} = \frac{[2\omega_{\mathrm{syn}}]^2 \alpha}{s^2 + [2\omega_{\mathrm{syn}}]^2}, \tag{5.7}$$

is given, where it is stated that $\alpha = 1/4$ for small bunches. The bunch height l corresponds to the peak line density or peak beam current $\hat{i}_{\mathrm{beam}}$. Assuming an ellipsoidal bunch with a Gaussian density, (3.44a) yields a peak beam current of

$$\hat{i}_{\mathrm{beam}} = i_{\mathrm{beam}}(x=0) = \bar{i}_{\mathrm{beam}} \sqrt{\frac{2\pi}{C_{2,0}}}.$$

The equilibrium can be defined as $\hat{i}_{\mathrm{beam,e}} = \bar{i}_{\mathrm{beam}} \sqrt{2\pi / E_{2,0}}$ and the relative change in this peak current is then

$$\frac{\hat{i}_{\mathrm{beam}} - \hat{i}_{\mathrm{beam,e}}}{\hat{i}_{\mathrm{beam,e}}} = \frac{\Delta l}{l} = \sqrt{\frac{E_{2,0}}{C_{2,0}}} - 1 \approx -\frac{\Delta C_{2,0}}{2E_{2,0}},$$

and the approximation is valid for small deviations $\Delta C_{2,0} = C_{2,0} - E_{2,0}$. This leads with (5.5) to the transfer function

$$\frac{\Delta l / l(s)}{\varepsilon(s)} = \frac{\Delta l / l(s)}{\Delta C_{2,0}(s)} \, \frac{\Delta C_{2,0}(s)}{\varepsilon(s)} = \frac{\frac{b_1}{E_{2,0}} \omega_{\mathrm{syn}}^2}{s^2 + \omega_{\mathrm{syn}}^2 [2a_2 + a_3]}. \tag{5.8}$$

Indeed, for small bunches, $b_1 / E_{2,0} \approx 1$ and $2a_2 + a_3 \approx 4$ holds and (5.7) is obtained with $\alpha = 1/4$. It has to be noted that (5.7) is given without derivation and only α is said to depend on on the bunch size. As the last considerations show, a more precise transfer function is given by (5.8) in case of larger bunches.

An advantage of this transfer function is that is does not depend on the mean beam current. However, the measurement of the peak beam current may be prone to noise, whereas the calculation of the first harmonic amplitude A_1 is equivalent to a low-pass filtering of the beam current signal.

Open Loop Transfer Functions The pass filter frequency of the bunch phase loop will be denoted by $f_{\mathrm{pass},1}$, whereas for the bunch length loop the frequency $f_{\mathrm{pass},2}$ will be used. The complete open loop transfer function of the bunch phase can be written as

$$\begin{aligned} G_1(s) &= -\left[G_{\mathrm{bp}}(s) - 1\right] \; G_{\mathrm{fir}}(s) \; G_{\mathrm{DDS}}(s) \; G_{\mathrm{cav},\varphi}(s) \; K_1 \; \mathrm{e}^{-T_{\mathrm{d}} s} \\ &= -K_1 \frac{s}{\left[s^2 + \omega_1^2\right] \left[T_{\mathrm{cav},\varphi} s + 1\right]} \; \frac{\mathrm{e}^{-\frac{s}{2f_{\mathrm{pass},1}}}}{2} \left[1 - \frac{\mathrm{e}^{\frac{s}{2f_{\mathrm{pass},1}}} + \mathrm{e}^{-\frac{s}{2f_{\mathrm{pass},1}}}}{2}\right] \; \mathrm{e}^{-T_{\mathrm{d}} s}, \end{aligned} \tag{5.9}$$

where $\omega_1 = \omega_{\mathrm{syn}} \sqrt{a_1}$ is the effective synchrotron frequency of the phase.

The open loop of the amplitude is described by

$$\begin{aligned} G_2(s) &= -G_{\mathrm{bl}}(s) \; G_{\mathrm{A}} \; G_{\mathrm{fir}}(s) \; G_{\mathrm{I}}(s) \; G_{\mathrm{cav},\varepsilon}(s) \; \mathrm{e}^{-T_{\mathrm{d}} s} \\ &= K_2 \frac{\omega_2^2}{s^2 + \omega_2^2} \; \frac{1}{s} \; \frac{1}{T_{\mathrm{cav},\varepsilon} s + 1} \; \frac{\mathrm{e}^{-\frac{s}{2f_{\mathrm{pass},2}}}}{2} \left[1 - \frac{\mathrm{e}^{\frac{s}{2f_{\mathrm{pass},2}}} + \mathrm{e}^{-\frac{s}{2f_{\mathrm{pass},2}}}}{2}\right] \; \mathrm{e}^{-T_{\mathrm{d}} s}, \end{aligned} \tag{5.10}$$

with the effective frequency $\omega_2 = 2\pi f_2$ and the gain K_2

$$\omega_2 := \omega_{\text{syn}}\sqrt{2a_2 + a_3}, \qquad K_2 := -2\bar{i}_{\text{beam}}\mathrm{e}^{-\frac{1}{2}E_{2,0}}\frac{K_{\text{I,d}}}{T_{\text{samp}}}\frac{b_1}{2a_2 + a_3}.$$

The purpose of the feedback design is to choose the feedback parameters K_1, $K_{\text{I,d}}$, $f_{\text{pass,1}}$, and $f_{\text{pass,2}}$ such that the loops are stable and well damped. The other parameters depend on the synchrotron design and the beam properties. For the stationary case that is considered here, all parameters are constant for a given beam size.

5.1.2 Stability of Linear Time Delay Systems

Both the bunch phase and bunch length feedback loop have the form of the general feedback loop with multiple delays shown in Figure 5.3. The loop consists of a transfer function $G_0(s)$ and a sum of delays with real $\tau_l \geq 0$, $l = 1, \ldots, L$, and real coefficients k_l. For example, for the transfer function $G_2(s)$ in (5.10), a possible choice of $G_0(s)$ is given by

$$G_0(s) = K_2\frac{\omega_2^2}{s^2 + \omega_2^2}\,\frac{1}{s}\,\frac{1}{T_{\text{cav},\varepsilon}\,s + 1}.$$

In the following it is assumed that $G_0(s)$ is a rational function with real coefficients and its numerator and denominator do not have a common root and G_0 is strictly proper, i. e. $G_0(\infty) = 0$. The closed-loop transfer function between w and y is given by

$$\frac{Y(s)}{W(s)} = G(s) = \frac{G_0(s)}{1 + G_0(s)\sum_{l=1}^{L} k_l\,\mathrm{e}^{-\tau_l s}}.$$

This system can also be expressed in the time domain, if $G_0(s)$ is written in state space representation

$$\frac{\mathrm{d}\boldsymbol{x}(t)}{\mathrm{d}t} = \boldsymbol{A}_0\boldsymbol{x}(t) + \boldsymbol{b}_0 u(t), \qquad y(t) = \boldsymbol{c}_0^{\mathrm{T}}\boldsymbol{x}(t),$$

with $u = -\tilde{y}$ and leads to the linear time-invariant delay differential equation (LTDDE)

$$\frac{\mathrm{d}\boldsymbol{x}(t)}{\mathrm{d}t} = \boldsymbol{A}_0\boldsymbol{x}(t) + \sum_{l=1}^{L}\boldsymbol{A}_l\boldsymbol{x}(t - \tau_l), \tag{5.11}$$

where $\boldsymbol{x}$ is the n-dimensional state vector and $\boldsymbol{A}_0$, $\boldsymbol{A}_l = -\boldsymbol{b}_0 k_l \boldsymbol{c}_0^{\mathrm{T}}$ are constant real $n \times n$ matrices.

In case of a single delay, i. e. $L = 1$, and provided that $G_0(0) > 0$, the poles of $G(s)$ are the zeros of the characteristic equation

$$1 + G_0(s)k_1\mathrm{e}^{-\tau_1 s} = 0 \tag{5.12}$$

and the closed loop is stable if and only if all roots of this *characteristic equation* lie in the open left complex plane $\mathbb{C}_-$ [26]. These roots are also called *characteristic roots*.

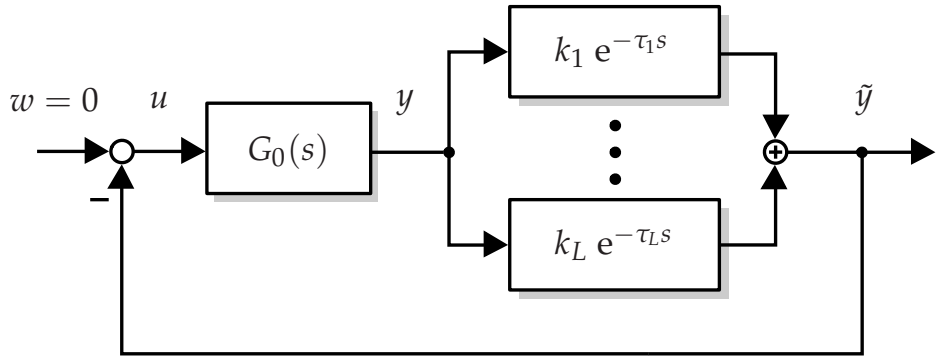

Figure 5.3: Linear feedback system with multiple delays.

Since Equation (5.12) is a quasi-polynomial for nonzero delays and thus a transcendental equation, the number of roots in the complex plane $\mathbb{C}$ is infinite and their analysis not straightforward [122]. However, it can be shown that the general Nyquist criterion (cf. [8, 27]) can be applied [26]. This leads to the analysis of the root locus $G_0(s = \mathrm{i}\omega)$ and its encirclements of the critical point -1 in the complex plane.

In the general case of multiple delays, the Laplace transform of (5.11) leads to the characteristic equation

$$1 + G_0(s) \sum_{l=1}^{L} k_l \mathrm{e}^{-\tau_l s} = 0. \tag{5.13}$$

Again, (5.11) is stable if and only if all the characteristic roots of (5.13) lie in $\mathbb{C}_-$ [10]. Thus, it is necessary and sufficient that the root with the largest real part lies in $\mathbb{C}_-$. To analyze the roots, use is made of the fact that their movement with respect to changing parameters in $\mathbb{C}$ is continuous. For zero delays $\tau_l = 0$, $l = 1,\ldots,L$, the stability is determined by the finite number of roots of G_0. As soon as the delays increase and become nonzero, an infinite number of new roots appear. For sufficiently small delays, all of these roots lie in $\mathbb{C}_-$ and their absolute values tend to infinity for $\tau_l \to 0^+$, i. e. they proceed in $\mathbb{C}_-$ from the left with increasing delays [133]. With increasing delays, the roots due to the delays and the eigenvalues of $\boldsymbol{A}_0$ will move and may cross the imaginary axis. Due to the continuity of the movement, a necessary condition for a transition of stability to instability or vice versa is the crossing of the imaginary axis. Many stability conditions thus rely on the calculation of the characteristic roots for $s = \mathrm{i}\omega$, which is similar to the Nyquist criterion. For commensurate delays, i. e. for delays $\tau_l = l\tau$ that are multiples of a basic delay τ, it can be shown that the crossings of the imaginary axis are finite in number and stability tests exist [133]. Unfortunately, the delays of (5.9) and (5.10) are not commensurate in general.

In general delays are not desirable because they reduce the phase margin of the open loop system. However, it is also possible to give examples where feedback containing time delays may stabilize an otherwise unstable system for certain values of the delay [122]. One possible example are unstable systems that can be stabilized using a derivative con-

troller. The continuous derivative may be approximated by the finite difference

$$\dot{y} \approx \frac{y(t) - y(t - T_0)}{T_0}$$

with the sample time T_0. The right hand side contains a time delay T_0. For sufficiently small T_0, the approximation error is small and the closed loop will be stable. For larger T_0, this is no longer valid and the closed loop may become unstable. In general, the stability will depend on the specific value of the time delay and there may be several intervals on the T_0-axis with closed-loop stability.

For $T_{\mathrm{cav},\varepsilon} \approx 0$ and without the delays, the bunch length feedback loop has the form

$$\frac{K_2\omega_2^2}{s[s^2 + \omega_2^2]}.$$

This linear system can be stabilized by the (non-proper) transfer function s^2 of a second derivative. In the following, filter (5.4) is shown to be similar to a second derivative. This indicates that the given FIR filter is indeed useful for the stabilization of the open loop.

Writing the derivative $y(t) = \ddot{x}(t)$ as a difference quotient

$$\begin{aligned} y(t) = \ddot{x}(t) &\approx \frac{1}{T_0}\left[\frac{x(t) - x(t - T_0)}{T_0} - \frac{x(t - T_0) - x(t - 2T_0)}{T_0}\right] \\ &= -\frac{4}{T_0^2}\left[-\frac{1}{4}x(t) + \frac{1}{2}x(t - T_0) - \frac{1}{4}x(t - 2T_0)\right] \end{aligned} \tag{5.14}$$

with sample time T_0 leads to the same structure as (5.4) if $T_0 = 1/2f_{\mathrm{pass}}$ and an additional gain $-4/T_0^{-2}$ are applied to the FIR filter. However, approximation (5.14) is valid only if T_0 is sufficiently small. This is apparent from the transfer function of (5.14)

$$G(s) = \frac{1}{T_0^2}\left[1 - 2\mathrm{e}^{-T_0 s} + \mathrm{e}^{-2T_0 s}\right].$$

Using a series representation for the exponential functions, G may be rewritten as

$$\begin{aligned} G(s) &= \frac{1}{T_0^2}\left[1 - 2\left[1 - T_0 s + \frac{T_0^2 s^2}{2} - \ldots\right] + \left[1 - 2T_0 s + \frac{4T_0^2 s^2}{2} - \ldots\right]\right], \\ &= s^2 + \frac{1}{T_0^2}\mathcal{O}\left([T_0 s]^3\right). \end{aligned}$$

Thus, for $T_0 \to 0$ the transfer function of a second derivative is obtained.

More precisely, T_0 should be considerably smaller than the time constant of the dynamics of $x(t)$. For the bunch length feedback, the time constant of the dynamics is $1/f_2$ and the condition $T_0 \ll 1/f_2$ is then equivalent to $f_{\mathrm{pass}} \gg f_2$. Together with the integral controller, the second derivative leads to the necessary phase shift of 90° for damping. In case the time delay T_{d} and measurement noise are neglible, the feedback with $f_{\mathrm{pass}} \gg f_2$ is stable for $K_2 > 0$.

For the considered feedback loops, there are several reasons why the simple previous stability analysis for $f_{\text{pass}} \gg f_2$ does not automatically apply.[2)] First, a typical choice is $f_{\text{pass}} \approx f_2$, because bunch length oscillations should pass the filter. Second, a pure derivative will increase the effect of noise and this imposes an upper bound on f_{pass}. Third, a bound is given by the digital hardware and the fact that Equation (5.4) is only feasible for $f_{\text{pass}} \leq f_{\text{samp}}/2$. The conclusion is that a general stability analysis for arbitrary values of f_{pass} is needed.

In the next section, the stability analysis of (5.10) will rely on the calculation of the zero crossings of the imaginary axis. From (5.13) it follows that this is equivalent to calculating the crossing of the critical point -1 by the root locus $G_2(\mathrm{i}\omega) = G_0(\mathrm{i}\omega)\sum_{l=1}^{L} k_l \mathrm{e}^{-\tau_l \mathrm{i}\omega}$. Nyquist plots will be used in addition to check the direction of traverse of the root locus.

5.1.3 Stability Analysis of Bunch Length Feedback

In this section, the stability of the bunch length feedback is analyzed depending on the feedback parameters K_2 and f_{pass} for the stationary case. All other parameters of the system are fixed and can be calculated from known parameters of the synchrotron and RF setup and from the beam properties. An important beam property is the bunch size, because the mode frequencies ω_1 and ω_2 depend on it.

The stability of the phase loop has been considered in detail in [59] and its analysis is also valid for large bunches, if the synchrotron frequency is adjusted appropriately from the linear frequency ω_{syn} to the effective frequency

$$\omega_1 = \omega_{\text{syn}} \sqrt{a_1\,(E_{2,0})},$$

with a_1 from Section 4.6.3 depending on the bunch size $E_{2,0}$. For this reason, the stability analysis will focus on the feedback loop for the bunch length. The line of argument is based on the Nyquist criterion and is similar to [59].

The frequency response of the open loop is obtained by replacing $s = \mathrm{i}\omega$ in (5.10) and reads

$$G_2(\mathrm{i}\omega) = \frac{K_2}{2} \frac{1}{1 - \frac{\omega^2}{\omega_2^2}} \frac{\mathrm{e}^{-\mathrm{i}\omega\left[\frac{\pi}{\chi_2\omega_2} + T_{\mathrm{d}}\right]}}{\omega\left[\mathrm{i} - T_{\text{cav},\varepsilon}\omega\right]} \left[1 - \cos\left(\frac{\pi\omega}{\chi_2\omega_2}\right)\right],$$

where the definition

$$\boxed{\chi_2 := \tfrac{f_{\text{pass},2}}{f_2}, \qquad f_2 = \tfrac{\omega_2}{2\pi} = 2\omega_{\text{syn}}\sqrt{\tfrac{2a_2 + a_3}{4}}}$$

was used. Due to the symmetry of the frequency response with regard to ω, only positive frequencies $\omega > 0$ will be regarded in the following. The filter frequency $f_{\text{pass},2}$ will

[2)] In spite of the following considerations, it is interesting to note what the properties of the control loop are for the limit case $f_{\text{pass}} \gg f_2$.

be chosen close to the mode frequency f_2, i. e. $\chi_2 \approx 1$. The frequency response has a singularity at $\omega = \omega_2$, its magnitude is

$$|G_2(\mathrm{i}\omega)| = \frac{|K_2| \left[1 - \cos\left(\frac{\pi\omega}{\chi_2\omega_2}\right)\right]}{2|\omega| \left|1 - \frac{\omega^2}{\omega_2^2}\right| \sqrt{1 + T_{\mathrm{cav},\varepsilon}^2\omega^2}}$$

and its phase is

$$\measuredangle G_2(\mathrm{i}\omega) = \begin{cases} -\omega\left[\frac{\pi}{\chi_2\omega_2} + T_\mathrm{d}\right] - \left[\frac{\pi}{2} + \arctan\left(T_{\mathrm{cav},\varepsilon}\omega\right)\right] & \text{for } K_2,\ \omega \in \mathcal{A}_1, \\ \pi - \omega\left[\frac{\pi}{\chi_2\omega_2} + T_\mathrm{d}\right] - \left[\frac{\pi}{2} + \arctan\left(T_{\mathrm{cav},\varepsilon}\omega\right)\right] & \text{for } K_2,\ \omega \in \mathcal{A}_2, \end{cases}$$

where

$$\mathcal{A}_1 = \{K_2, \omega \in \mathbb{R} \ :\ [K_2 > 0 \text{ and } 0 < \omega < \omega_2] \text{ or } [K_2 < 0 \text{ and } \omega > \omega_2]\},$$
$$\mathcal{A}_2 = \{K_2, \omega \in \mathbb{R} \ :\ [K_2 > 0 \text{ and } \omega > \omega_2] \text{ or } [K_2 < 0 \text{ and } 0 < \omega < \omega_2]\}.$$

The Nyquist plots of G_2 in Figure 5.4 show that for $\chi_2 = 1$, a necessary condition for stability is $K_2 > 0$, as the locus $G_2(\mathrm{i}\omega)$ is traversed in clockwise direction for $K_2 < 0$. On the other hand, a necessary condition for a transition from stability to instability is that $G_2(\mathrm{i}\omega)$ crosses the critical point -1. The frequency at which the crossing

$$|G_2(\mathrm{i}\omega_\mathrm{crit})| = 1 \tag{5.15a}$$
$$\measuredangle G_2(\mathrm{i}\omega_\mathrm{crit}) = -p\pi, \qquad p \in \{1;3;5;\ldots\} \tag{5.15b}$$

occurs will be denoted by $\omega_{2,\mathrm{crit}}$ and the gain by $K_{2,\mathrm{crit}}$. Under the assumption that the cavity feedback loops have a fast response, more precisely $|T_{\mathrm{cav},\varepsilon}\,\omega| \ll 1$, the time constant $T_{\mathrm{cav},\varepsilon}$ can be neglected[3)] and (5.15b) can be solved analytically for $\omega = \omega_{2,\mathrm{crit}}$:[4)]

$$\xi(p) := \frac{\omega_{2,\mathrm{crit}}(p)}{\omega_2} = \begin{cases} \frac{p-\frac{1}{2}}{\frac{1}{\chi_2}+2T_\mathrm{d}f_2} & \text{for } \xi < 1 \text{ and } K_2 > 0, \\ \frac{p+\frac{1}{2}}{\frac{1}{\chi_2}+2T_\mathrm{d}f_2} & \text{for } \xi > 1 \text{ and } K_2 > 0. \end{cases} \tag{5.16}$$

Solving (5.15a) for $K_2(p)$ yields

$$\frac{|K_2(p)|}{\omega_2} = 2\frac{\left|\xi(p)\left[1 - \xi^2(p)\right]\right|}{1 - \cos\left(\frac{\pi\xi(p)}{\chi_2}\right)}. \tag{5.17}$$

For a given χ_2 the critical gain $K_{2,\mathrm{crit}}$ is the lowest $K_2(p)$:

$$|K_{2,\mathrm{crit}}| = \min_p |K_2(p)|, \quad p \in \{1;3;5;\ldots\}.$$

[3)] For a small but nonzero $T_{\mathrm{cav},\varepsilon}$, this assumption can only be satisfied in a limited frequency range $|\omega| < \omega_\mathrm{max}$.

[4)] The ratio ξ appears on both the left hand and right hand side, because the phase of G_2 is discontinuous at $\omega = \omega_2$, cf. the definition of $\mathcal{A}_1$ and $\mathcal{A}_2$. The calculation of ξ is performed separately for $\xi > 1$ and $\xi < 1$.

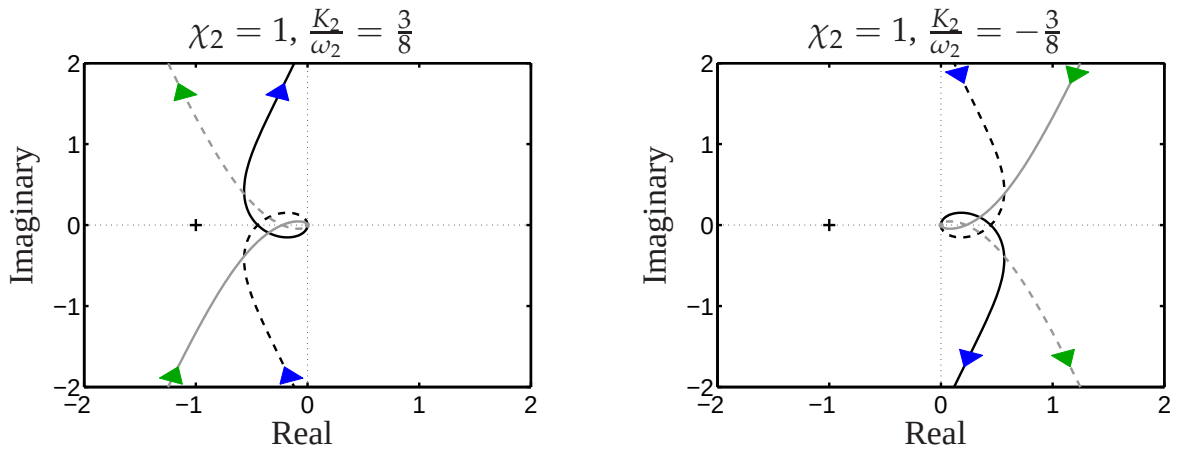

Figure 5.4: Nyquist plots of $G_2(\mathrm{i}\omega)$ for $\omega_2 = 31.32\,\mathrm{kHz}$, $T_\mathrm{d} = 10^{-5}\,\mathrm{s}$, and $T_{\mathrm{cav},\varepsilon} = 0$. The locus consists of the following sections: $-\infty < \omega < -\omega_2$ (gray, dashed), $-\omega_2 < \omega < 0$ (black, dashed), $0 < \omega < \omega_2$ (black, solid), $\omega_2 < \omega < \infty$ (gray, solid).

Table 5.1: Calculation of the critical gain for $\chi_2 = 1$, $T_\mathrm{d} = 10^{-5}\,\mathrm{s}$, and $f_2 = 4985\,\mathrm{Hz}$.

	$p=1$		$p=3$		$p=5$		...
	ξ_2	$\frac{K_2}{\omega_2}$	ξ_2	$\frac{K_2}{\omega_2}$	ξ_2	$\frac{K_2}{\omega_2}$	...
$\xi < 1$:	0.455	0.841	-		-		...
$\xi > 1$:	1.36	1.66	3.18	31.6	5	120	...

The decision about the sign of $K_{2,\mathrm{crit}}$ for a certain χ_2 can be made by analyzing the direction of traverse of the Nyquist plot as already described. Table 5.1 shows an example of the calculation. The minimal gain is obtained for $p = 1$ and the critical gain is $K_{2,\mathrm{crit}} = 0.841$. With this procedure, a stability diagram can be obtained that shows the critical gain as a function of the filter frequency. Figure 5.5 shows the stability diagrams for the bunch phase and length for typical values of ω_1, ω_2, and T_d. The diagram of the bunch phase is based on the calculation of [59]. The shape of the bunch length diagram does only depend on the product $T_\mathrm{d} f_2 \approx 0.05$. This follows directly from (5.16) and (5.17).

5.1.4 Tracking, Linear Model, and Feedback Performance

The derived diagram describes the stability of the feedback, but does not reveal anything about the feedback performance. To evaluate this performance, parameter scans are presented in this section for both bunch phase and bunch length oscillations in the linear and nonlinear bucket. The parameters of the tracking simulations are summarized in Table 5.2.

The stability analysis of the FIR feedback relies on the linear transfer functions $G_1(s)$ and $G_2(s)$, cf. Equations (5.9) and (5.10). It is thus reasonable to start with an evaluation of these continuous models. All elements in the feedback loop – transfer functions, time

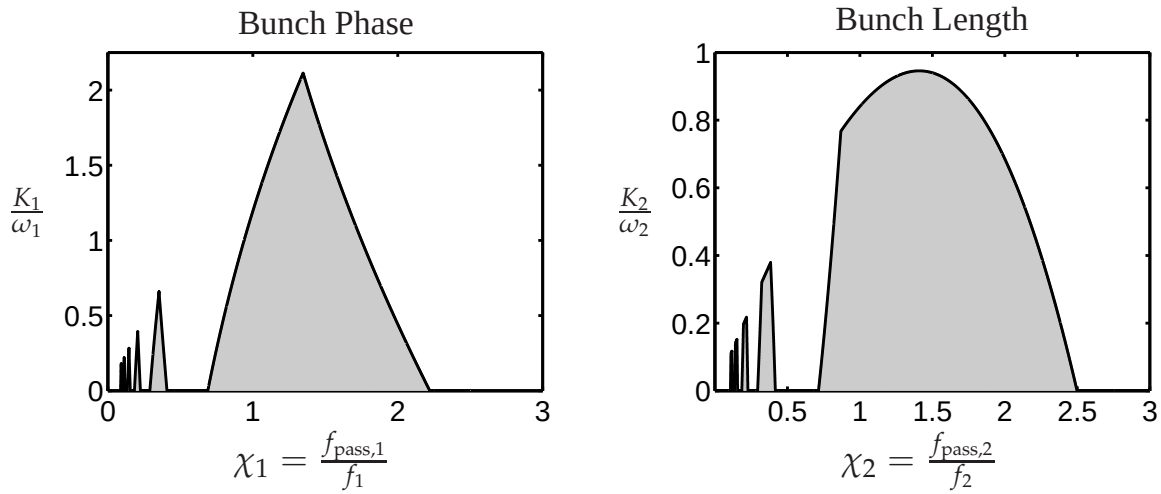

Figure 5.5: Stability diagrams for the bunch phase (dipole mode, [59]) and the bunch length (quadrupole mode) for $\omega_1 = 15.66\,\text{kHz}$, $\omega_2 = 31.32\,\text{kHz}$, and $T_\text{d} = 10^{-5}\,\text{s}$. The gray areas are combinations of gain and filter frequency that yield a stable closed loop.

Table 5.2: Parameters for simulation and experiment.

Ion species	$^{40}\text{Argon}^{18+}$	Kinetic energy	$11.4\,\frac{\text{MeV}}{\text{u}}$
γ_R	1.0122	β_R	0.15503
T_R	$4.663 \cdot 10^{-6}\,\text{s}$	γ_T	5.45
h	8	f_RF	1.715 MHz
$\hat{U}_{1,\text{R}}$	$5\,\text{kV} \rightarrow 10\,\text{kV}$	f_syn at 10 kV	3312 Hz
T_d	$10^{-5}\,\text{s}$	Orbit length L_R	216.72 m
$\bar{i}_\text{beam}$	2 mA	$f_\text{samp} = T_\text{samp}^{-1}$	375.44 kHz

delays, FIR filter, and feedback – are discretized with a basic sample time T_0. With regard to the simulation accuracy, the sample time T_0 should be chosen as small as possible, but of course this is limited by the available computing power. As a compromise, $T_0 = T_\text{R}/7$ is chosen for the simulation of the bunch length feedback and $T_0 = 2T_\text{R}/7$ for the bunch phase feedback. For the latter simulation, the sample time can be chosen twice as high, because the bunch phase oscillation frequency ω_1 is lower by a factor of about two compared to the bunch lenght oscillation frequency ω_2. Based on the discretized models, parameter scans with different χ_i and K_i, $i = 1,2$, are then performed. It is assumed that the bunch density is Gaussian, the parameters of the scans are summarized in Table 5.3.

To evaluate the performance, the following quality measure

$$J_{\text{lin},1}(\chi_1,K_1) := \frac{\text{absolute area of } \Delta B_{1,0} \text{ with feedback}}{\text{absolute area without feedback}} = \frac{\int_0^{T_\text{end}} |\Delta B_{1,0}(\chi_1,K_1,t)|\,\text{d}t}{\int_0^{T_\text{end}} |\Delta B_{1,0}(0,0,t)|\,\text{d}t}$$

is defined for the beam phase and

$$J_{\mathrm{lin},2}(\chi_2,K_2) := \frac{\int_0^{T_{\mathrm{end}}} |\Delta C_{2,0}(\chi_2,K_2,t)|\,\mathrm{d}t}{\int_0^{T_{\mathrm{end}}} |\Delta C_{2,0}(0,0,t)|\,\mathrm{d}t}$$

for the beam length. If the feedback is effective and increases the damping of the bunch phase and length oscillations, the absolute area under the functions $\Delta B_{1,0}(t)$ and $\Delta C_{2,0}(t)$ will be smaller compared to the uncontrolled case and $J_{\mathrm{lin},1}, J_{\mathrm{lin},2} \in]0;1[$. Perfect control in the sense of immediate damping implies $J_{\mathrm{lin}} = 0$. In the following, runs that are unstable or lead to $J_{\mathrm{lin}} > 1$ will be assigned the value $J_{\mathrm{lin}} = 1$. Since the following simulations are discrete, the integrals of $J_{\mathrm{lin},1}$ and $J_{\mathrm{lin},2}$ are approximated by sums.

Figure 5.6 shows the results of the scan. For this scan, only simulations of the closed loop systems using the transfer functions G_1 and G_2 are used. The performance matches well with the theoretical stability limits. The best result for the bunch phase is obtained for $\chi_1 = 0.97$ and $K_1/\omega_1 = 0.32$, the performance is $J_{\mathrm{lin},1} = 0.034$. The best result for the bunch length is $J_{\mathrm{lin},2} = 0.041$ and is obtained for $\chi_2 = 1.15$ and $K_2/\omega_2 = 0.34$. The first contour line around the optimum in both diagrams is $J_{\mathrm{lin}} = 0.1$. Thus it can be concluded that there is a rather large parameter area with a good performance.

Linear Bucket The transfer functions G_1 and G_2 are already approximations for a linear bucket, because they rely on linearized dynamics. In addition, there might be an influence because of the different sampling times of beam (T_{R}) and feedback (T_{samp}). Figure 5.7 compares three different cases:

- simulation of the transfer functions G_1 and G_2 with the basic sample time T_0,
- tracking simulation for a linear bucket (cf. Section 4.5) with the basic sample time T_0,
- tracking simulation for a linear bucket with realistic sample times T_{R} (beam) and T_{samp} (feedback).

For the tracking simulations, an ellipsoidal bunch with a Gaussian density is initialized with a random distribution of $N_{\mathrm{macro}} \approx 6 \cdot 10^4$ macro particles in the phase space. The bunch parameters are $x_0 = 0.1$, $y_0 = 0$, $\sigma_x = 1.01$, $\sigma_y = 0.927$, and $E_{2,0} = 0.92$. The histogram of the beam current has $N_{\mathrm{bin}} = 50$ bins.

It can be observed from Figure 5.7 that the difference due to linearization[5)] is small, whereas the sample times have a larger impact. However, all models show a similar behavior.

Nonlinear Bucket and Large Mismatch The simulations are repeated for a nonlinear bucket. This time, nonlinear particle tracking simulations are used to evaluate the feedback performance. The longitudinal mapping equations of the beam are already discrete

[5)] The dynamics for a linear bucket are nonlinear in the inputs. The transfer functions are based on a linearization of these nonlinear dynamics, whereas the tracking simulations are exact.

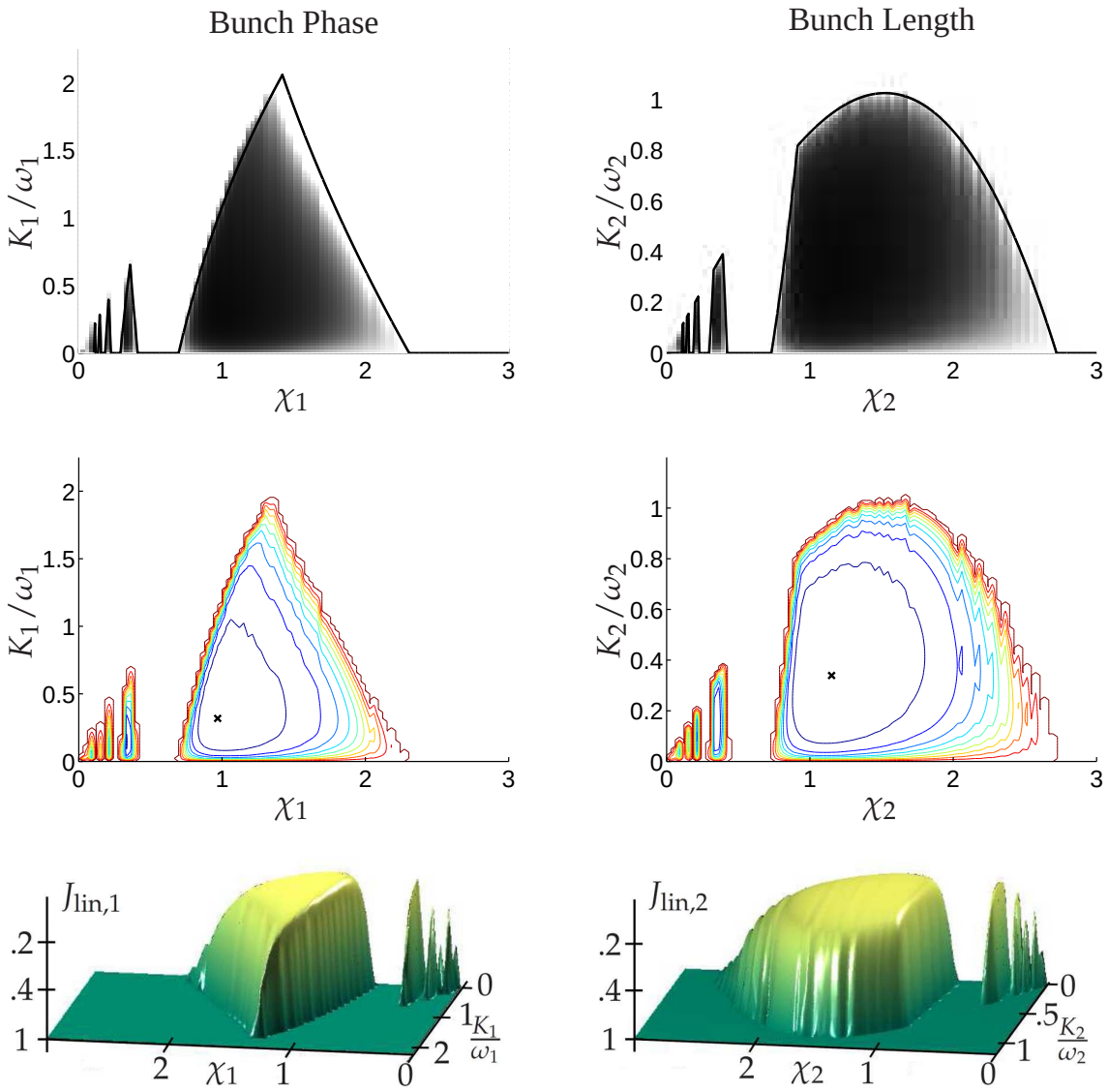

Figure 5.6: Parameter scan for the ideal linear bucket. The contour lines of the center diagrams are $J = [0.1, 0.2, \ldots, 1]$.

with the sample time $T_\mathrm{R} = 4.663\ \mu$s. On the other hand, the feedback loop has its own frequency f_samp and sample time $T_\mathrm{samp} = 2.664\ \mu$s as given in Table 5.2. To obtain a realistic result, the basic sample time T_0 should be chosen such that T_R and T_samp are approximately multiples of T_0. The choice $T_0 = T_\mathrm{R}/7$ leads to $4T_0 = 2.665\ \mu$s and this is very close to T_samp. The simulation is thus performed with the basic sample time T_0; the mapping equations are evaluated only every seventh time step and the feedback loop only every fourth time step.

For the scans of the bunch phase feedback, the initial bunch distribution is matched for 10 kV with a bunch size of $E_{2,0} = 0.928.$ and the bunch is shifted by 0.1 rad in phase. In case of the bunch length feedback, the initial bunch distribution is matched for 5 kV and the voltage is raised stepwise at $t = 0$ to 10 kV, leading to a large mismatch of the bunch length. The bunch size after the voltage step is $\tilde{E}_{2,0} = 0.928.$ The parameters of

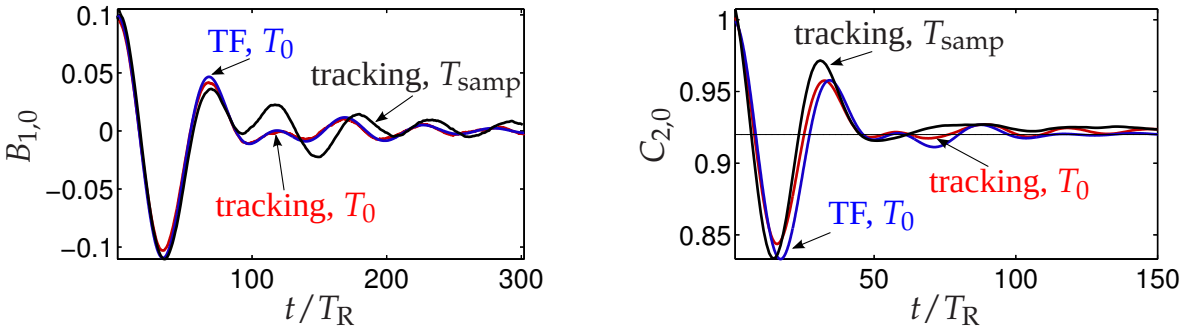

Figure 5.7: Linear bucket, closed-loop damping of the bunch phase and bunch length oscillations. Optimal parameters $(\chi_1; K_1/\omega_1) = (0.97; 0.32)$ and $(\chi_2; K_2/\omega_2) = (1.15; 0.34)$. Simulation of transfer functions $G_1(s)$ and $G_2(s)$ with sample time T_0 (blue). Tracking simulation with T_0 (red). Tracking simulation with realistic sample times for beam and feedback (black).

the tracking simulations are given in Table 5.2 and the additional parameters of the scan can be found in Table 5.3.

In case of the nonlinear bucket, the modeling differences between the tracking simulations and the transfer functions G_1, G_2 are not only due to linearization and the sampling times, but also due to the fact that G_1 and G_2 do not include Landau damping. To evaluate the feedback performance, a new quantity is chosen that directly reflects the increase in bunch area and is thus directly related to the beam quality. For both the bunch phase and length, it is chosen as

$$J_{\text{nl}} = \frac{I_2(\chi_i, K_i, T_{\text{end}}) - I_2(0,0,0)}{I_2(0,0,T_{\text{end}}) - I_2(0,0,0)},$$

where $I_2(\chi_i, K_i, t) = C_{2,0}(t)C_{0,2}(t) - C_{1,1}^2(t)$ is the square of the bunch area in case of feedback with the parameters χ_i and K_i, $i = 1, 2$. Again, without any feedback, J_{nl} equals 1 and with perfect control, $J_{\text{nl}} = 0$.

The results of the scan for the nonlinear bucket are shown in Figure 5.8 for both J_{lin} and J_{nl} and the performances are given in Table 5.3. The following observations can be made:

- The performance J_{lin} for the nonlinear bucket is inferior compared to the linear bucket. This could be expected, because in a nonlinear bucket, the controller has to outperform the fast Landau damping. Simulation results show that Landau and controller damping times cannot be added together in a linear way.

- The bunch phase control is very effective in terms of J_{nl}. For the optimum, the increase in I_2 for the closed loop is only 6% compared to the increase for the open loop. Both optima have similar parameters $(\chi_1, K_1/\omega_1)$.

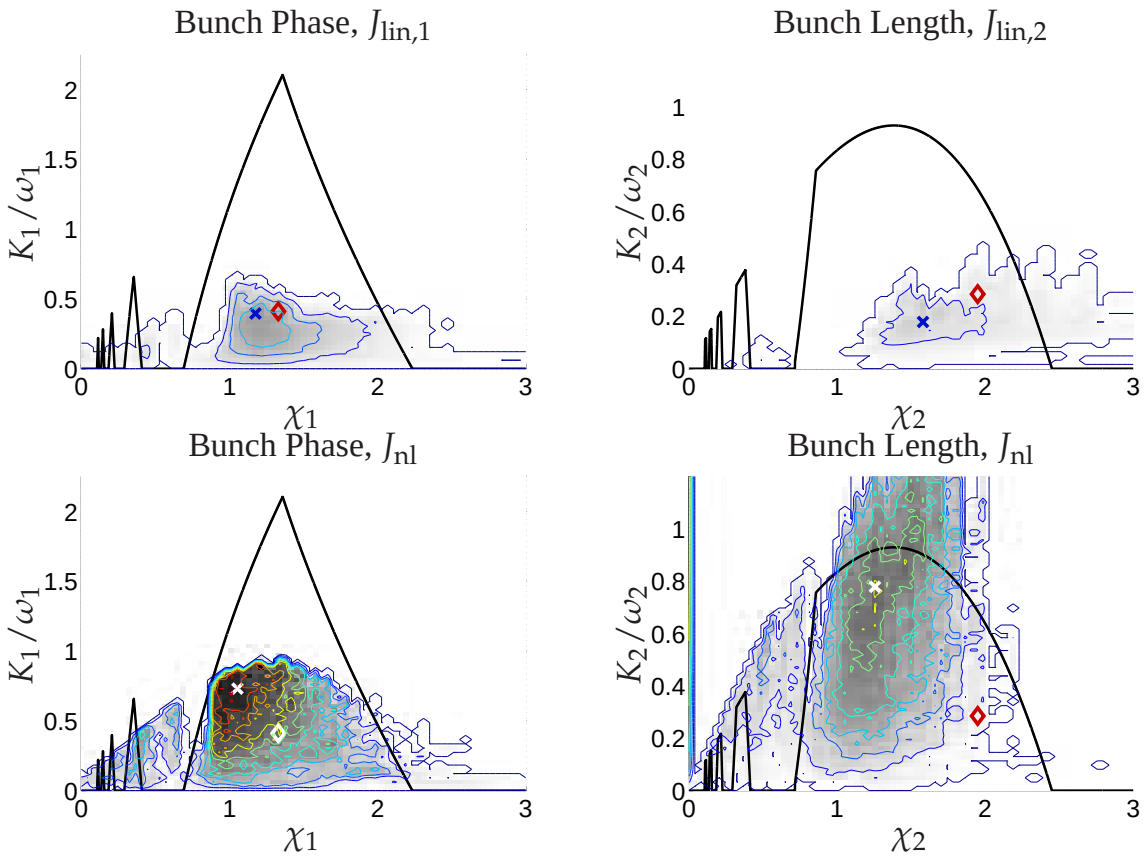

Figure 5.8: Parameter scan for the nonlinear bucket. Again, the contour lines mark differences $\Delta J_{\mathrm{nl}} = 0.1$ in the performance J_{nl}. ($\times$): Optima of the scans. ($\diamond$): Settings of the experiment.

- The bunch length control shows a good efficiency $J_{\mathrm{nl}} = 38\%$, but a poor damping performance in terms of J_{lin}. In addition, both optima occur at considerably different gains K_2.

It has to be noted that the stability regions in the parameter space (χ, K) of the bunch position and bunch length feedback for the nonlinear bucket are not readily apparent from the scans of Figure 5.8. These scans show the feedback performance relative to the open loop simulation, i. e. relative to Landau damping. The white areas are parameter settings for which the integral of the absolute error or the emittance increase is larger than in case of the open loop system. This does not automatically imply instability.

Figure 5.9 compares the results of the feedback in the nonlinear bucket for the transfer functions and the tracking simulation. The choice of the parameters is not the optimum obtained in Figure 5.8, but is rather chosen with regard to the analysis of a beam experiment in Section 5.2. In contrast to the earlier Figure 5.7, the models do vary significantly, because the transfer functions do not reproduce the Landau damping, which is larger than the damping due to feedback in this particular simulation. The initial frequencies of the nonlinear oscillations are however reproduced very well by the transfer functions. As can be expected, simulations show that the smaller the bunch size in a nonlinear bucket, the

Table 5.3: Performance scans.

	Bunch phase	Bunch length
	Linear Bucket	
Bunch size	$\tilde{E}_{2,0} = 0.92$	$\tilde{E}_{2,0} = 0.92$
Transfer fct.	$a_1 = 1$	$b_1 = \tilde{E}_{2,0}$, $2a_2 + a_3 = 4$
Frequencies	$f_1 = f_{\mathrm{syn}}$	$f_2 = 2f_{\mathrm{syn}}$
Sample time	$T_0 = \frac{2}{7}T_{\mathrm{R}}$	$T_0 = \frac{1}{7}T_{\mathrm{R}}$
Sim. length	$3000T_{\mathrm{R}}$	$1500T_{\mathrm{R}}$
Initial values	$B_{1,0} = 0.1$, $B_{0,1} = 0$	$C_{2,0} = 1$, $C_{1,1} = 0$, $C_{0,2} = 0.84$
Optimum J_{lin}	$\left(\chi_1;\ \frac{K_1}{\omega_1};\ J_{\mathrm{lin},1}\right) =$ $(0.97;\ 0.32;\ 0.034)$	$\left(\chi_2;\ \frac{K_2}{\omega_2};\ J_{\mathrm{lin},2}\right) =$ $(1.15;\ 0.34;\ 0.041)$
	Nonlinear Bucket	
Bunch size	$\tilde{E}_{2,0} = 0.928$	$\tilde{E}_{2,0} = 0.928$
Transfer fct.	$a_1 = 0.62876$	$2a_2 + a_3 = 1.9316$, $b_1 = 0.58349$
Frequencies	$f_1 = 0.793 f_{\mathrm{syn}}$	$f_2 = 0.69491 \cdot 2f_{\mathrm{syn}}$
Sample time	$T_0 = \frac{1}{7}T_{\mathrm{R}}$ (basic), T_{R} (beam), and T_{samp} (feedback)	
Sim. length J_{lin}	$1000T_{\mathrm{R}}$	$400T_{\mathrm{R}}$
Sim. length J_{nl}	$3000T_{\mathrm{R}}$	$1500T_{\mathrm{R}}$
Initial distribution	matched at 10 kV, phase shift of 0.1 rad	matched at 5 kV, voltage step to 10 kV
Optimum J_{lin}	$\left(\chi_1;\ \frac{K_1}{\omega_1};\ J_{\mathrm{lin},1}\right) =$ $(1.18;\ 0.395;\ 0.62)$	$\left(\chi_2;\ \frac{K_2}{\omega_2};\ J_{\mathrm{lin},2}\right) =$ $(1.58;\ 0.178;\ 0.80)$
Optimum J_{nl}	$\left(\chi_1;\ \frac{K_1}{\omega_1};\ J_{\mathrm{nl}}\right) =$ $(1.05;\ 0.73;\ 0.06)$	$\left(\chi_2;\ \frac{K_2}{\omega_2};\ J_{\mathrm{nl}}\right) =$ $(1.26;\ 0.78;\ 0.38)$

more the behavior becomes similar to the linear bucket case. This is demonstrated in Figure 5.10 which shows a similar simulation for a smaller bunch size $\tilde{E}_{2,0} = 0.55$. The damping of the tracking solution is slightly larger due to additional Landau damping, but the results do agree well.

The results of this section lead to the following conclusions:

- The transfer functions G_1 and G_2 describe the feedback dynamics very well for the linear bucket. They can be used for the stability analysis and a controller design. In addition, the simulation of the transfer functions is considerably faster than the corresponding tracking simulations.

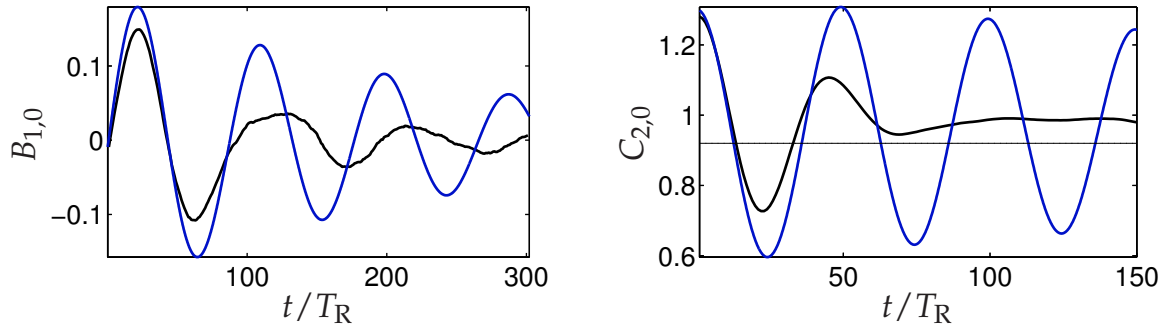

Figure 5.9: Nonlinear bucket, closed-loop damping of the bunch phase and bunch length oscillations with parameters $(\chi_1; K_1/\omega_1) = (1.33; 0.41)$ and $(\chi_2; K_2/\omega_2) = (1.95; 0.285)$. (solid, blue): transfer functions $G_1(s)$ and $G_2(s)$ with the basic sample time $T_0 = \frac{1}{7}T_R$, (solid, black): tracking simulation with realistic sample times.

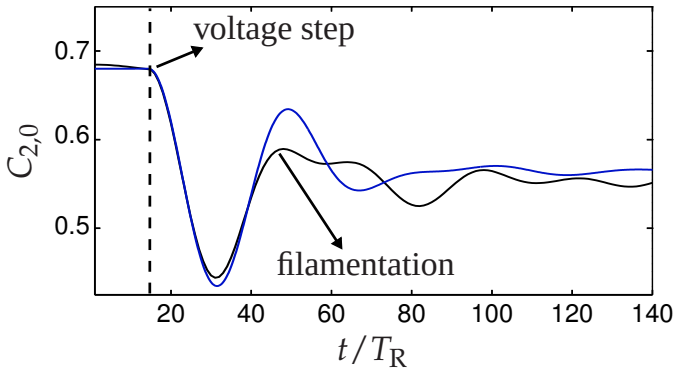

Figure 5.10: Comparison of transfer functions (blue) and tracking (black) for a smaller bunch with feedback on. Same simulation parameters as Fig 5.9 except for the the bunch size $\tilde{E}_{2,0} = 0.55$ and a voltage step from 10 kV to 15 kV.

- In case of the nonlinear bucket, the transfer functions can be used if the damping of the feedback is large compared to Landau damping. This is usually the case, because this is the objective of the controller design. A possible improvement could be to introduce additional damping terms in the transfer functions to approximate Landau damping.

5.2 Analysis of a Beam Experiment

The results of a beam experiment are used in this section to verify the developed theory and the simulation results.[6)] A more detailed description of the experimental setup can be found in [60] and [95].

[6)] The beam experiment was realized at the SIS18 at GSI by Dr. Harald Klingbeil, Monika Mehler, Dr. Bernhard Zipfel, Dr. Ulrich Laier, and Dr. Klaus-Peter Ningel. The measurement data in this section is courtesy of Dr. Harald Klingbeil, GSI.

5.2.1 Introduction

The simulation parameters of Section 5.1.4 were chosen such that they match with the beam experiment. The parameters of Table 5.2 are thus also valid in this section.

The initial RF amplitude is again 5 kV and is raised stepwise to 10 kV to induce large amplitudes of bunch length oscillations. The evolution of the bunch shape is shown in Figure 5.11 in a simplified way. The figures show a uniform distribution, but the reasoning is equally valid for other distributions.

First, the bunch is matched before the voltage step. The bunch has a size of $2\sigma_\varphi = \hat{\varphi}$ and a variance $E_{2,0}$. The bunch shape matches with a trajectory in the phase space $(\Delta\varphi, \Delta\dot{\varphi})$. In a linear approximation the solution (2.37)

$$\Delta\varphi(t) = \hat{\varphi}\cos(\omega_{\mathrm{syn}}t)$$

holds and the intersections of the trajectory are $\Delta\varphi = \hat{\varphi}$ and $\Delta\dot{\varphi} = \hat{\varphi}\omega_{\mathrm{syn}}$. The constant $\Phi_{k,0}$ is not important here and will be omitted.

Second, the voltage is doubled and this changes the synchrotron frequency by a factor of $\sqrt{2}$, as follows from (2.38). This leads to

$$\Delta\varphi(t) = \hat{\varphi}\cos(\sqrt{2}\omega_{\mathrm{syn}}t)$$

and the trajectories are stretched by a factor of $\sqrt{2}$ in direction of $\Delta\dot{\varphi}$ (Figure 5.11, center). The bunch shape is not altered by the voltage step but is now mismatched, i. e. $\tilde{C}_{2,0} = E_{2,0}$. The particles of the bunch will then follow the new trajectories, resulting in bunch length oscillations.

Third, the bunch will settle at a new equilibrium due to filamentation or feedback. If the feedback is fast enough and filamentation is negligible, the bunch area will remain constant. The new equilibrium is then given by $\tilde{E}_{2,0} = E_{2,0}/\sqrt{2}$ (Figure 5.11, right).

The relative mismatch of the bunch due to the voltage step can thus be expressed as

$$\frac{\tilde{C}_{2,0} - \tilde{E}_{2,0}}{\tilde{E}_{2,0}} = \sqrt{2} - 1 \approx 41\%.$$

In normalized coordinates $(x = \Delta\varphi, y = \Delta w)$, the increase of the RF amplitude does not change the trajectories, but corresponds to a compression of the bunch in direction of y by a factor of $\sqrt{2}$. The final bunch area is thus smaller by a factor of $\sqrt{2}$ compared to the area before the voltage step.

It has to be emphasized that this experiment is an extreme situation that usually should not occur during normal operation. The large oscillation amplitudes are intended to test the theory and the validity of the feedback setup [60].

The experiment comprised three runs:

L The feedback loops were switched off and the oscillations were only damped by Landau damping.

Q The quadrupole (i. e. bunch length) feedback loop was switched on.

DQ Both the dipole (i. e. bunch phase) and quadrupole (i. e. bunch length) feedback loops were switched on.

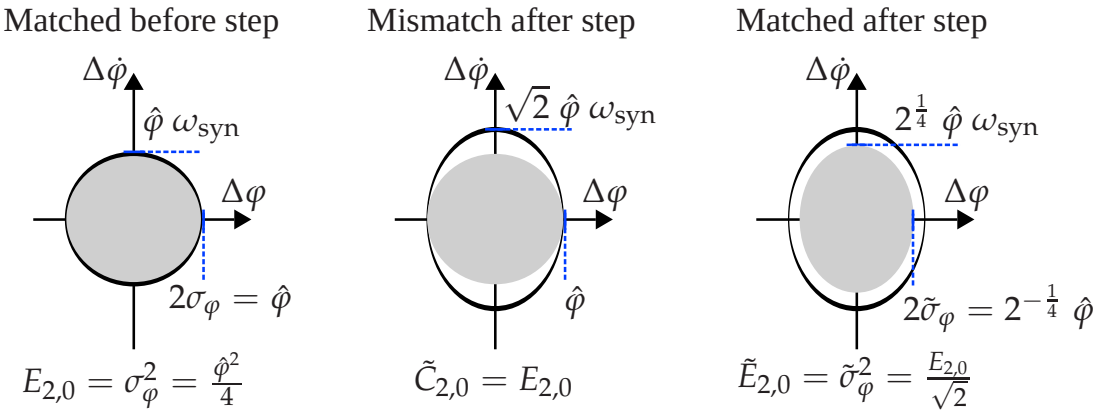

Figure 5.11: Simplified evolution of the bunch shape during the experiment.

5.2.2 Beam Profile

To be able to simulate the experimental setup, the following missing parameters have to be defined: the bunch density function and the parameters of the feedback loop.

It is assumed that the bunch approximately has the Gaussian density (3.33). For a matched bunch, the translation $\boldsymbol{r}$ and the orientation Φ can be set to zero and the remaining degrees of freedom are the standard deviations $\sigma_x := \sigma_{1x}$ and $\sigma_y := \sigma_{2x}$. In addition, the choice of one standard deviation will determine the other standard deviation. For example, for small bunches it will be reasonable to choose $\sigma_x = \sigma_y$. For large bunches, the density (3.33) will not lead to exactly matched shapes, but it is possible to make a good approximation. As it has become clear in Chapter 4, the variable $2\sigma_x$ is an important quantity that determines the bunch dynamics. A possible conclusion that is confirmed by simulations is to interpret $2\sigma_x$ and $2\sigma_y$ as effective half-axes of the bunch [56, 60]. It seems thus reasonable to match the bunch at the contour line of $\hat{x} = 2\sigma_x$. This is done as follows. In a nonlinear stationary bucket the intersections of the trajectories are given by (cf. (2.54))

$$\hat{y} = \sqrt{2\,[1 - \cos\hat{x}]},$$

where again $x := \Delta\varphi$ and $y := \Delta w$ was used. Choosing $\hat{y} = 2\sigma_y$ and $\hat{x} = 2\sigma_x$ finally leads to

$$\sigma_y = \sqrt{\frac{1 - \cos(2\sigma_x)}{2}}. \tag{5.18}$$

This gives an extra condition for the matched shape and only σ_x remains as the last degree of freedom.

Equation (5.18) is only used to have a good starting point for σ_y. A subsequent fine-tuning in the simulation is done for σ_x and σ_y to minimize any bunch oscillations before the voltage step. As the measurements are given in arbitrary units, the fitting procedure also includes finding appropriate scaling factors. It is assumed that the measurements y_{beam} of the beam current i_{beam} are scaled with the gain S_1 and the offset S_0 as

$$y_{\text{beam}}(t) = S_1 \cdot i_{\text{beam}}(t) - S_0. \tag{5.19}$$

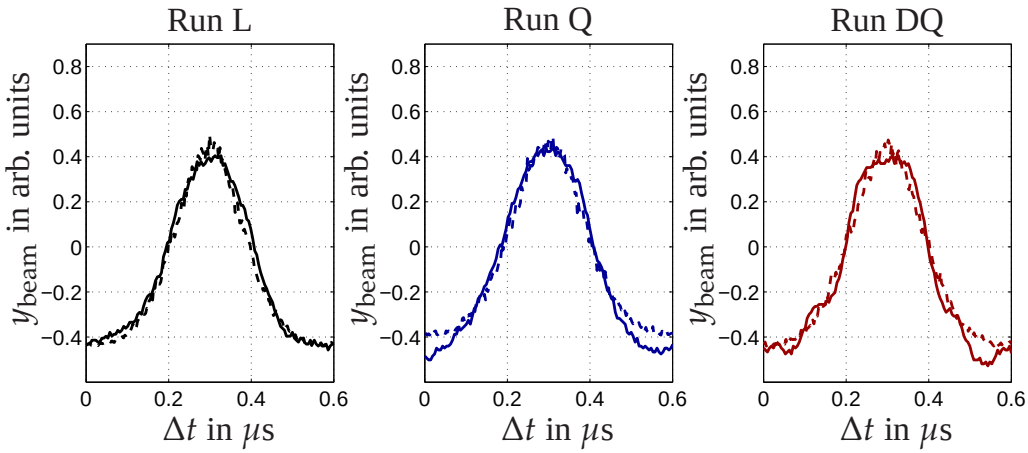

Figure 5.12: Beam current measurements y_{beam} before the voltage step for the three runs L (only Landau damping), Q (bunch length feedback), and DQ (bunch phase and length feedback): measurement (solid) and nonlinear tracking simulation (dotted).

Table 5.4: Initial shape and scaling parameters of the bunches before the voltage step.

	σ_x	σ_y	(5.18)	$E_{2,0} = \sigma_x^2$	$E_{0,2} = \sigma_y^2$	S_1	S_0
unit	rad	rad	rad	rad^2	rad^2	A^{-1}	1
Run L	1.0654	0.8313	0.87497	1.135	0.691	180	0.475
Run Q	1.1476	0.8894	0.91178	1.317	0.791	195	0.45
Run DQ	1.1459	0.8881	0.91107	1.313	0.789	200	0.5

It is also assumed that S_1 and S_0 do not change during a given experiment, but may vary between different experiments.

With the two standard deviations and the scaling parameters, there are four degrees of freedom for the fitting. Three features of the beam current are chosen: the maximum, the minimum, and the width of the beam current $y_{\mathrm{beam}}(t)$. The parameters σ_x, σ_y, S_1, and S_0 were chosen such that the features of the simulation match the measurement and such that the bunch oscillations before the voltage step are minimal (matched bunch).

The result of the fitting is shown in Figure 5.12 for the three different runs and Table 5.4 summarizes the standard deviations and compares these with (5.18). The difference between the fine-tuned σ_y and (5.18) is only a few percent. The scaling parameters are also given in Table 5.4.

Now that the bunch size $E_{2,0}$ before the voltage step has been determined, the equilibrium $\tilde{E}_{2,0}$ after the voltage step can be calculated according to the considerations of

Table 5.5: Effective frequencies and gains.

	$E_{2,0}$	$\tilde{E}_{2,0} = \frac{E_{2,0}}{\sqrt{2}}$	$\frac{\omega_1}{\omega_{\text{syn}}}\left(\tilde{E}_{2,0}\right)$	$\frac{\omega_2}{2\omega_{\text{syn}}}\left(\tilde{E}_{2,0}\right)$	$\frac{b_1}{2a_2+a_3}\left(\tilde{E}_{2,0}\right)$
Run L	1.135	0.803	0.818	0.731	0.251
Run Q	1.317	0.931	0.792	0.694	0.303
Run DQ	1.313	0.928	0.793	0.695	0.302

Figure 5.11. With $\tilde{E}_{2,0} = E_{2,0}/\sqrt{2}$, the effective frequencies

$$\frac{\omega_1}{\omega_{\text{syn}}}\left(\tilde{E}_{2,0}\right) = \sqrt{a_1\left(\tilde{E}_{2,0}\right)}, \quad \frac{\omega_2}{2\omega_{\text{syn}}}\left(\tilde{E}_{2,0}\right) = \sqrt{\frac{2a_2\left(\tilde{E}_{2,0}\right) + a_3\left(\tilde{E}_{2,0}\right)}{4}}$$

can be calculated using the coefficients a_1, a_2, a_3, and b_1 of Appendix C.4.4 for Gaussian densities. The results are presented in Table 5.5.

5.2.3 Tracking Simulations

The experimental results are now compared with the nonlinear tracking simulations. The simulation program uses the nonlinear discrete mapping equations in $\Delta\varphi$ and $\Delta W/\omega_{RF}$ for the longitudinal dynamics. The particle positions in phase space are converted to the (x, y) plane with the variables $x = \Delta\varphi$ and $y = \Delta w = -\Delta\dot{\varphi}/\omega_{\text{syn}}$. The beam current signal is calculated as a histogram using bins on the $\Delta\varphi$-axis. The beam signal amplitude and phase are obtained by a FFT of the beam current signal. Since coherent modes were excited in the experiment, only one bunch is simulated and compared with one bunch of the $h = 8$ measured bunch signals. At the voltage step at 10 kV, the cavity dynamics are taken into account by the time constants $T_{\text{cav},\varepsilon} = 20\ \mu$s and $T_{\text{cav},\varphi} = 0\ \mu$s, cf. Equations (5.2) and (5.3). This improves the agreement between the simulation and experimental results. In addition, a small dipole oscillation is excited by shifting the bunch in the phase space. These additional assumptions increase the agreement between the simulation and the measured data. The reason for the excitation of a small dipole oscillation seems to be that the cavity was detuned at the moment the voltage was increased.

The parameters of the feedback loops are given in Table 5.6. Because the two runs Q and DQ are very similar in terms of the bunch size, only the bunch size of the run DQ is considered. The filter frequencies f_{pass} are exactly known from the experiment. The resulting relative filter frequencies χ_1 and χ_2 can be calculated, because the effective frequencies f_1 and f_2 were already determined in Table 5.5.

In contrast to the frequencies f_{pass}, the gains K_1 and $K_{\text{I,d}}$ of the feedback loops are not exactly known. For this reason, they are adjusted in the simulation as well to optimize the agreement between simulation and experiment of the amplitude A_1 and the phase $\Delta\varphi_{\text{det}}$. These results are shown in Figure 5.13. They agree well with the measurements that are presented in [60]. Particularly, the oscillation of run L in Figure 5.13 shows a

Table 5.6: Feedback parameters.

Bunch phase		Bunch length	
f_1	$0.793 \cdot f_{\mathrm{syn}}$	f_2	$0.695 \cdot f_{\mathrm{syn}}$
$f_{\mathrm{pass},1}$	3500 Hz	$f_{\mathrm{pass},2}$	9000 Hz
K_1	6711	$K_{\mathrm{I,d}}$	-28.9
$\frac{K_1}{\omega_1}$	0.41	$\frac{K_2}{\omega_2}$	0.285
$\chi_1 = \frac{f_{\mathrm{pass},1}}{f_1}$	1.33	$\chi_2 = \frac{f_{\mathrm{pass},2}}{f_2}$	1.95
$J_{\mathrm{lin},1}$	0.72	$J_{\mathrm{lin},2}$	0.94
J_{nl}	0.38	J_{nl}	0.96

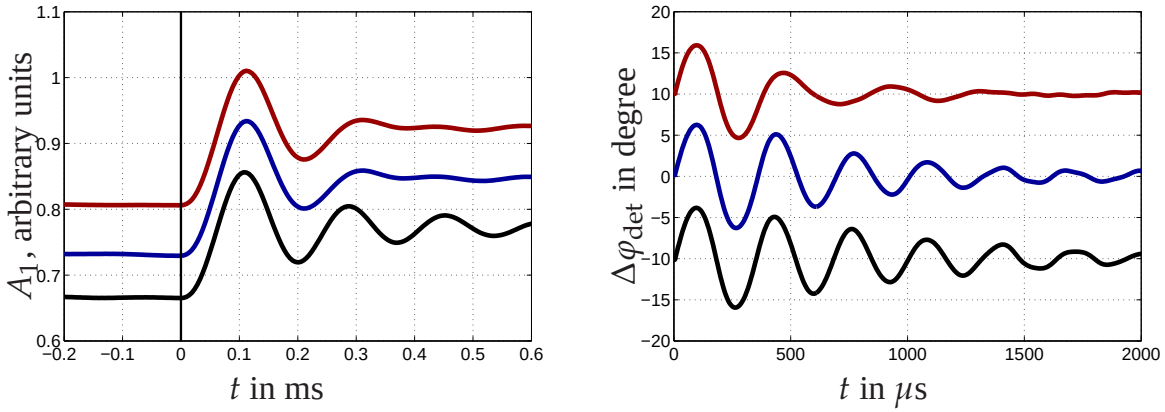

Figure 5.13: Nonlinear tracking simulations: amplitude A_1 and phase $\Delta\varphi_{\mathrm{det}}$. Run L (lower curves), run Q (middle curves), and run DQ (upper curves). The scaling and offset parameters are given in Table 5.7.

period of about 200 μs. The period of a quadrupole oscillation in a linear bucket would be $(2f_{\mathrm{syn}})^{-1} = 150$ μs, this corresponds to a ratio of 0.75 which is very close to the calculated ratio $\omega_2/2\omega_{\mathrm{syn}} = 0.731$ of Table 5.5. Again, A_1 is measured in arbitrary units and a scaling as in (5.19) is assumed. The corresponding scaling factors are given in Table 5.7.

It is important to note that all scaling parameters except for the feedback gains K_1 and $K_{\mathrm{I,d}}$ are fitted only for the beginning of the simulation, i. e. for $t = 0$ to have the same initial configuration for simulation and experiment.

The upper diagram of Figure 5.14 compares the measured and simulated beam current at the first maximum of A_1 after the voltage jump. There are some deviations, but the general agreement between experiment and simulation is fine. The same is valid for the comparison at the end of the simulation, shown in the lower diagram of Figure 5.14.

Figure 5.15 shows the variances obtained by the tracking simulations. The initial variances before the voltage step at $t = 0$ are the variances $E_{2,0}$ of Table 5.5. The calculation

Table 5.7: Scaling parameters of Figure 5.13.

	$S_1(A_1)$	$S_0(A_1)$	$S_1(\Delta\varphi_{\text{det}})$	$S_0(\Delta\varphi_{\text{det}})$
Run L	$289\,\frac{1}{\text{A}}$	0	1	$-10°$
Run Q	$289\,\frac{1}{\text{A}}$	0.125	1	$0°$
Run DQ	$289\,\frac{1}{\text{A}}$	0.2	1	$10°$

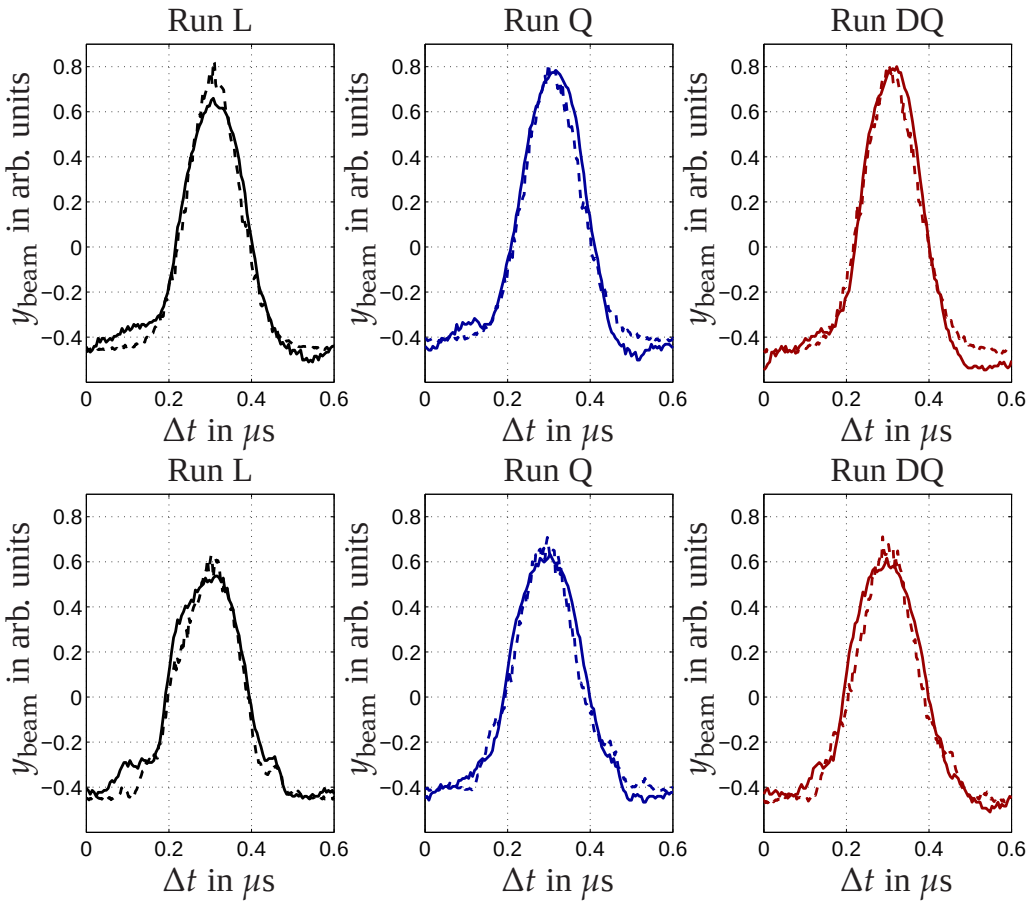

Figure 5.14: Top: Beam current measurements y_{beam} at the first maximum of A_1 after the voltage step ($t = 0.11\,\text{ms}$) for the three runs L, Q, and DQ: measurement (solid) and simulation (dotted). **Bottom**: Beam current measurements y_{beam} at the end of the simulation for the three runs L ($t = 1\,\text{ms}$), Q ($t = 0.6\,\text{ms}$), and DQ ($t = 0.6\,\text{ms}$): measurement (solid) and simulation (dotted).

of the equilibria $\tilde{E}_{2,0}$ given in the same table and defined in Figure 5.11 is based on the assumption that there is no filamentation. Consequently, the variances $C_{2,0}$ at the end of the nonlinear tracking simulations are slightly larger, as can be observed from Figure 5.15. A comparison yields an increase in variance between 5% and 10%.

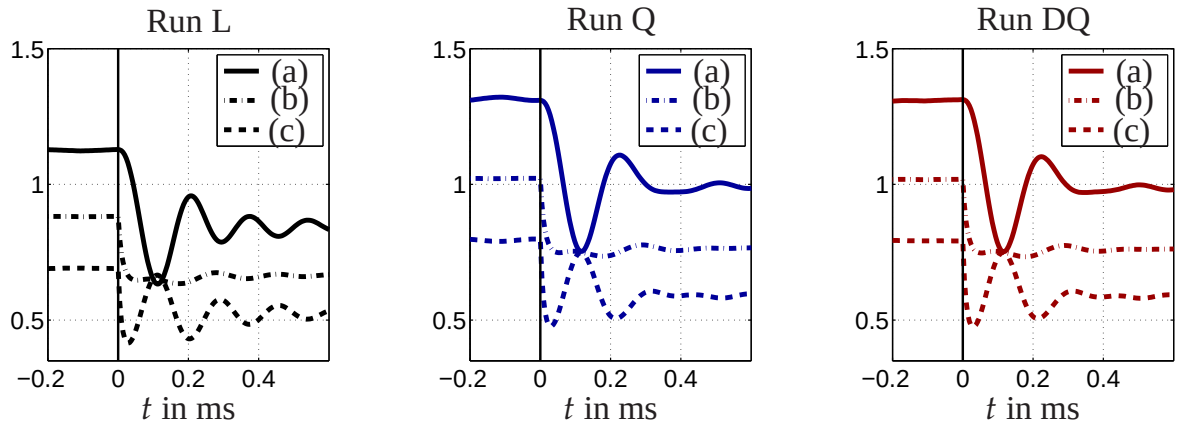

Figure 5.15: Tracking simulations: variances $C_{2,0}$ and $E_{2,0}$ for coordinates x and y. (a): $C_{2,0}$, (b): $\sqrt{C_{2,0}C_{0,2} - C_{1,1}^2}$, (c): $C_{0,2}$.

The results show that the most important dynamics of the beam and the feedback loops have been taken into account in the nonlinear macro particle simulation and the results obtained in Section 5.1 can be applied. In particular, Figure 5.8 shows that the feedback parameters in the experiment were chosen close to the optima with respect to J_{lin}.

5.3 Exemplary Nonlinear Controller Design

The previous stability results rely on linearized models. In this section, two nonlinear approaches for the stability analysis and controller design are proposed for Model (4.37). The intention is to show how nonlinear methods could be used to enhance the feedback analysis and performance. An important topic will be the definition of and the explicit consideration of input constraints for u_1. Due to limited RF power and high-voltage constraints, the amplitude of the gap voltage is limited. Therefore, it will be assumed in the following that the amplitude modulation $u_\varepsilon = u_1$ is limited to 10% of the nominal gap voltage amplitude, i. e. $u_{1,\max} = 0.1$. This value is reasonable for the present RF setup of the synchrotron SIS18. The section presents preliminary results that should be extended before they can be used in real experiments. Nevertheless, the examples show what is possible in principle.

The methods in this section rely on the stability theory of Lyapunov, more specifically on the direct method [123]. The validity of the results is restricted to very small bunches or bunches in a linear bucket. In addition, no time delays are taken into account. In principle, methods based on convex optimization exist that are able to include time delays. At present, the manageable model complexity is however limited to systems with a few states due to computational reasons. New developments or solvers might overcome this limitation.

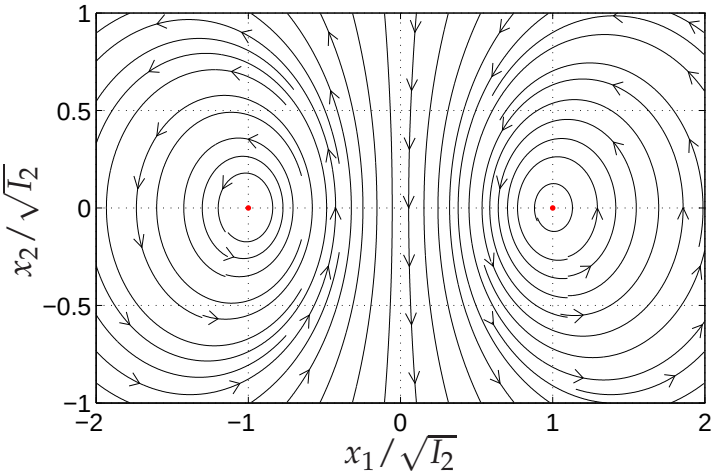

Figure 5.16: Trajectories of system (5.20) with $u_1 = 0$. The coordinates are normalized with $E_2 = \sqrt{I_2}$. I_2 is constant, since the dynamics are valid for a linear bucket without filamentation.

5.3.1 Stability of the Quadrupole Mode

System (4.37) has one coupling term $B_{1,0}u_1$ that couples the basic moments with the second order moments. Damping oscillations of the variance may thus induce oscillations of the bunch center. The coupling is weak, since both $B_{1,0}$ and u_1 are usually small, and can be cancelled by choosing the control law

$$u_2 = u_2^* - B_{1,0}u_1.$$

The actuator variables u_1 and u_2 are given in (4.27c) and are a combination of the phase modulation u_φ and the amplitude modulation u_ε.

Considering only the second order moments, system (4.37) can be rewritten as

$$\dot{\boldsymbol{x}}(t) = \omega_{\text{syn}} \begin{bmatrix} -2x_2(t) \\ x_1(t) - \frac{I_2 + x_2^2(t)}{x_1(t)} \end{bmatrix} + \omega_{\text{syn}} \begin{bmatrix} 0 \\ x_1(t) \end{bmatrix} u_1(t) = \boldsymbol{a}(\boldsymbol{x}) + \boldsymbol{b}(\boldsymbol{x})u_1 \qquad (5.20)$$

with the states $x_1 = C_{2,0}$ and $x_2 = C_{1,1}$. A linearization of this system, as has been considered in (4.38) may be a valid approximation in the vicinity of the equilibrium, but in general it will be more accurate to analyze the nonlinear dynamics. Figure (5.16) shows the trajectories of the uncontrolled nonlinear system in the state space $(x_1,x_2) \in \mathbb{R}^2$. Only the open right half-plane $x_1 = C_{2,0} > 0$ is of physical interest, since a positive density function leads to a positive variance. As can be expected, the trajectories do not cross the axis $x_1 = 0$. Near the equilibrium $\boldsymbol{x}_{\text{eq}} = (x_1,x_2) = (\sqrt{I_2},0)$, the trajectories become similar to the linearization (4.38), i. e. to the trajectories of a harmonic oscillator. For larger amplitudes, the trajectories are deformed but remain closed.

The majority of methods for nonlinear control systems rely on the Lyapunov theory. If it is possible to find a Lyapunov or a so-called *Control-Lyapunov function* candidate, further methods can be applied [6, 124]. Roughly speaking, a Lyapunov function $V(\boldsymbol{x})$ represents a generalized energy function of the nonlinear system. If it can be shown that the energy or value of V decreases along the trajectories of the system, it can be concluded that the system is asymptotically stable, without the necessity to explicitly calculate the trajectories $\boldsymbol{x}(t)$ of the system.

The method of Krasovskii is a constructive method to generate a Lyapunov function candidate [123]. The basic idea is to simply check whether the choice

$$V(\boldsymbol{x}) = \boldsymbol{a}(\boldsymbol{x})^{\mathrm{T}}\boldsymbol{a}(\boldsymbol{x}) = \left[-2I_2 + x_1^2 + 2x_2^2 + \left[\frac{I_2 + x_2^2}{x_1}\right]^2\right]\omega_{\mathrm{syn}}^2 \tag{5.21}$$

is a Lyapunov function of the autonomous system (5.20), i. e. for $u_1 = 0$. For the uncontrolled system, the derivative of V with respect to time is

$$\dot{V} = \left[2x_1\dot{x}_1 + 4x_2\dot{x}_2 + 2\left[\frac{I_2 + x_2^2}{x_1}\right]\frac{2x_2\dot{x}_2x_1 - [I_2 + x_2^2]\dot{x}_1}{x_1^2}\right]\omega_{\mathrm{syn}}^2 \overset{(5.20)}{=} 0.$$

In addition $V(\boldsymbol{x}) \geq V(\boldsymbol{x}_{\mathrm{eq}}) = 0$. Thus, V is a constant of motion for the uncontrolled system and is a possible Lyapunov function.

For the controlled system with a feedback $u_1 = u_1(\boldsymbol{x})$

$$\dot{\boldsymbol{x}} = \boldsymbol{a}(\boldsymbol{x}) + \boldsymbol{b}(\boldsymbol{x})u_1(\boldsymbol{x}) := \boldsymbol{g}(\boldsymbol{x}), \tag{5.22}$$

the derivative of V is

$$\dot{V} = \boldsymbol{a}(\boldsymbol{x})^{\mathrm{T}}V_{\boldsymbol{x}}(\boldsymbol{x}) + \left[\boldsymbol{b}^{\mathrm{T}}(\boldsymbol{x})V_{\boldsymbol{x}}(\boldsymbol{x})\right]u_1(\boldsymbol{x}) = 4\omega_{\mathrm{syn}}^2x_1x_2\left[1 + \frac{I_2 + x_2^2}{x_1^2}\right]u_1(\boldsymbol{x}),$$

where $V_{\boldsymbol{x}}$ denotes the gradient of V, and the controller $u_1 = u_1(\boldsymbol{x})$ can be chosen such that $\dot{V} < 0$ on the open right half-plane except for the set

$$\boldsymbol{b}(\boldsymbol{x})^{\mathrm{T}}V_{\boldsymbol{x}}(\boldsymbol{x}) = 0 \quad \Rightarrow \quad \mathcal{M}_0 := \left\{\boldsymbol{x} \in \mathbb{R}^2 \,:\, x_1 > 0 \text{ and } x_2 = 0\right\}. \tag{5.23}$$

For example, a possible choice would be $u_1(\boldsymbol{x}) = -x_1x_2$. In the set $\mathcal{M}_0$ the input u_1 has no influence on the system and $\dot{V} = 0$.

This shows that V is not a Control-Lyapunov function [6, 124], because there are regions in the open right half-plane where $\dot{V}$ equals zero.

The following definition of invariant sets is now useful.

Definition 5.1 ([123], p.68)**.** A set $\mathcal{M}_{\mathrm{I}}$ is an *invariant set* for a dynamic system if every system trajectory which starts from a point in $\mathcal{M}_{\mathrm{I}}$ remains in $\mathcal{M}_{\mathrm{I}}$ for all future time.

In the set $\mathcal{M}_0$ of (5.23), only the equilibrium is an invariant set; since for every element of $\mathcal{M}_0$ with $x_1 > 0$

$$\dot{x}_2 \overset{(5.20)}{=} \left[x_1 - \frac{I_2}{x_1}\right]\omega_{\mathrm{syn}}\begin{cases} = 0 & \text{for } x_1 = \sqrt{I_2} \\ \neq 0 & \text{else} \end{cases}$$

holds, every trajectory that enters the set $\mathcal{M}_0$ will immediately leave it, except for the equilibrium

$$\mathcal{M}_{\mathrm{I}} = \left\{\boldsymbol{x} \,:\, x_1 = \sqrt{I_2},\, x_2 = 0\right\}. \tag{5.24}$$

Next, to guarantee asymptotic stability, the invariance principle of Barbashin, Krasovskii, and LaSalle can be applied.

Theorem 5.1 (Local Invariant Set Theorem, [123], p.69)**.** *Consider the nonlinear, autonomous system* (5.22) *with a continuous vector field* $g : \mathcal{X} \to \mathbb{R}^n$ *defined on the open subset* $\mathcal{X}$ *of* $\mathbb{R}^n$*. Let* $V(\boldsymbol{x})$ *be a scalar function with continuous first partial derivatives. Assume further that*

- *for some* $l > 0$*, the region* $\mathcal{V}_l$ *defined by* $V(\boldsymbol{x}) < l$ *is bounded and*
- $\dot{V}(\boldsymbol{x}) \leq 0$ *for all* $\boldsymbol{x} \in \mathcal{V}_l$*.*

Let $\mathcal{M}_0$ *be the set of all points within* $\mathcal{V}_l$ *where* $\dot{V}(\boldsymbol{x})$ *equals zero, and* $\mathcal{M}_\mathrm{I}$ *be the largest invariant set in* $\mathcal{M}_0$*. Then, every solution* $\boldsymbol{x}(t)$ *originating in* $\mathcal{V}_l$ *tends to* $\mathcal{M}_\mathrm{I}$ *as* $t \to \infty$*.*

For $V \leq 0$, the Lyapunov function (5.21) is equivalent to the equation

$$\frac{V}{4\omega_\mathrm{syn}^2} = \left[x_1 - \sqrt{I_2 + \frac{V}{4\omega_\mathrm{syn}^2}} \right]^2 + x_2^2.$$

This equation describes circles in the open right half-plane $x_1 > 0$ with the radius $r = \sqrt{V}/2\omega_\mathrm{syn}$ and the center $(\sqrt{I_2 + r^2},0)$ and it can thus be concluded that the set

$$\mathcal{V}_l = \left\{ \boldsymbol{x} \;\middle|\; V(\boldsymbol{x}) < l,\ 0 \leq l < \infty \right\} \tag{5.25}$$

with $V(\boldsymbol{x})$ from (5.21) is bounded.

If, in addition, the controller $u_1(\boldsymbol{x})$ is chosen such that

$$\dot{V} = 4\omega_\mathrm{syn}^2 x_1 x_2 \left[1 + \frac{I_2 + x_2^2}{x_1^2} \right] u_1(\boldsymbol{x}) < 0 \ \text{ for } \ \boldsymbol{x} \in \left\{ \boldsymbol{x} \in \mathbb{R}^2 \;\middle|\; x_1 > 0 \text{ and } x_2 \neq 0 \right\}, \tag{5.26}$$

the second condition $\dot{V} \leq 0$ of Theorem 5.1 is also satisfied in $\mathcal{V}_l$ and the system tends to the invariant set $\mathcal{M}_\mathrm{I}$ that contains only equilibrium (5.24). This equilibrium is asymptotically stable and domains of attraction are given by (5.25) for any finite l.

The following important statement can be made:

> In a linear bucket, assuming dynamics (5.20), any controller $u_1(\boldsymbol{x})$ that satisfies (5.26) will lead to asymptotic stability of the bunch length $C_{2,0}$ for arbitrary initial values.

Remark 5.3. This statement is also valid for saturating controllers, i. e. controllers that have a saturation of their amplitude $|u_1| < u_{1,\max}$, with a given $u_{1,\max}$. This can be shown as follows: For every given $\mathcal{V}_l$, a nonsaturating controller can be found: $u_1 = h(\boldsymbol{x}) = -kx_2$ with $k > 0$ satisfies (5.26) and k can be chosen small enough such that $|h(\boldsymbol{x})| < u_{1,\max}$ in $\mathcal{V}_l$. According to the stability theorems for saturating controllers, cf. [47, 77] and [78, Theorem 2], it is then sufficient to find a second control law $u_1 =$

$k(\boldsymbol{x})$ that also satisfies (5.26), but is allowed to have amplitudes larger than $u_{1,\max}$. The controller

$$u_1 = \mathrm{sat}\left(k(\boldsymbol{x})\right) := \begin{cases} -u_{1,\max} & \text{for } k(\boldsymbol{x}) < -u_{1,\max} \\ k(\boldsymbol{x}) & \text{for } |k(\boldsymbol{x})| < u_{1,\max} \\ u_{1,\max} & \text{for } k(\boldsymbol{x}) > u_{1,\max} \end{cases}$$

will then lead to an asymptotic stable equilibrium (5.24).

Strictly speaking, the mentioned theorems from [47, 77, 78] require $\dot{V} < 0$ on the complete set $\mathcal{V}_l \setminus \mathcal{M}$ and this is not the case for the system under consideration. However, the theorems can be adjusted using Theorem 5.1.

5.3.2 Optimization Based Controller Design

Sum of Squares The last section has shown the stability analysis based on a Lyapunov function for a given controller $k(\boldsymbol{x})$. The set of possible control laws is large and, usually, stability is not the only important criterion. Further requirements can be the damping rate or the size of the region of attraction. If the controller is chosen rather randomly, an iterative trial-and-error search will be necessary during which several controllers are chosen and their performance is evaluated by means of simulations. Usually, optimization based approaches can improve the controller design. In many cases, performance criteria can be included in the optimization process.

Especially for nonlinear systems with actuator saturation, sum of squares techniques are an active research topic. The sum of squares decomposition relies on the fact that a sufficient condition for a given polynomial to be nonnegative can be expressed as a validation problem with linear matrix inequalities (LMIs) [33].[7)] The underlying idea is that if the polynomial can be written as a sum of squared polynomials, i. e. if it belongs to the class of SOS polynomials, it surely is nonnegative. The approach is somewhat conservative, because there exist nonnegative polynomials that cannot be written as an SOS polynomial. However, the approach is advantageous, because efficient computer algorithms exist for LMI problems. In control applications, polynomials are used as Lyapunov functions and conditions for stability and other performance criteria can be written as a set of LMI conditions, which are then solved numerically.

A short overview of SOS is presented in [128]. Survey papers are [104] and [21]. A detailed description of the underlying optimization methods of the following results can be found in [33, 34, 36]. The following design can be found in [75], preliminary results are given in [111].

Design Assumptions With the new normalized coordinates

$$\tau = \omega_{\mathrm{syn}} t, \quad \tilde{x}_1 = \frac{C_{2,0} - E_2}{E_2} = \frac{x_1}{\sqrt{I_2}} - 1, \quad \tilde{x}_2 = \frac{C_{1,1}}{E_2} = \frac{x_2}{\sqrt{I_2}},$$

[7)] The optimization results with SOS in this section are courtesy of Thomas Gußner.

System (5.20) can be rewritten as

$$\dot{\tilde{\boldsymbol{x}}} = \begin{bmatrix} -2\tilde{x}_2 \\ \tilde{x}_1 + \frac{1+\tilde{x}_2^2}{1+\tilde{x}_1} \end{bmatrix} + \begin{bmatrix} 0 \\ 1+\tilde{x}_1 \end{bmatrix} u_1(\tilde{\boldsymbol{x}}). \tag{5.27}$$

It is assumed that the initial state $\tilde{\boldsymbol{x}}(t=0)$ is contained in the set

$$\mathcal{X}_0 = \left\{ \boldsymbol{x} \in \mathbb{R}^2 \;\middle|\; \sqrt{\tilde{x}_1^2 + 4\tilde{x}_2^2} \leq 0.2 \right\}. \tag{5.28}$$

Design Method and Results In [36], a design method is proposed for polynomial systems which can also be applied to rational systems. The method is based on sum of squares decomposition and convex optimization. The results of this design are a polynomial or rational control law $k(\boldsymbol{z})$ and an estimate of the region of attraction[8)]. The control law

$$u_1 = \mathrm{sat}(k(\tilde{\boldsymbol{x}}))$$

is allowed to saturate, i. e. $|k(\tilde{\boldsymbol{x}})| > u_{1,\max} = 0.1$ might occur during stabilization. The stability analysis is based on an extension of a theorem in [47]. In the following, two different scenarios and design objectives are discussed that may be of interest during the operation in a synchrotron:

- Maximize the region of attraction: This is useful if large deviations or disturbances are to be expected, e. g. at injection of the beam in the ring.
- Maximize the decay rate for the given set of initial values (5.28): a fast damping time can maintain the beam quality, e. g. during acceleration of the beam.

For the first scenario, a polynomial controller of degree 3 and a polynomial Lyapunov function of degree 4 are optimized with respect to the region of attraction. The resulting controller has only significant coefficients in the linear terms $\tilde{x}_1$ and $\tilde{x}_2$:

$$u_{1,\mathrm{roa}}(\tilde{\boldsymbol{x}}) = \mathrm{sat}(0.014\tilde{x}_1 - 0.252\tilde{x}_2). \tag{5.29}$$

Since control algorithms in modern RF feedback systems are typically implemented using technologies like field programmable gate arrays (FPGAs), cf. [7, 59], this simple linear controller is appealing from a practical point of view.

For the second scenario, a rational control law of degree 3 and a polynomial Lyapunov function of degree 4 are optimized with respect to the decay rate, which yields

$$u_{1,\mathrm{dr}}(\tilde{\boldsymbol{x}}) = \mathrm{sat}\left(\frac{\boldsymbol{a} \cdot \begin{bmatrix} \tilde{x}_1 & \tilde{x}_2 & \tilde{x}_1^3 & \tilde{x}_1^2\tilde{x}_2 & \tilde{x}_1\tilde{x}_2^2 & \tilde{x}_2^3 \end{bmatrix}^{\mathrm{T}}}{\boldsymbol{b} \cdot \begin{bmatrix} 1 & \tilde{x}_1 & \tilde{x}_2 & \tilde{x}_1^2 & \tilde{x}_2^2 & \tilde{x}_1\tilde{x}_2 \end{bmatrix}^{\mathrm{T}}} \right), \tag{5.30}$$

$$\boldsymbol{a} = \begin{bmatrix} 0.38 & -2.54 & 0.032 & -0.076 & 0.012 & -0.12 \end{bmatrix},$$

$$\boldsymbol{b} = \begin{bmatrix} 0.57 & 0.45 & 0.24 & 0.38 & 0.92 & 0.11 \end{bmatrix}.$$

Table 5.8: Tracking simulation parameters.

Ion species	protons	ω_S	3625.7 Hz
Macro-particles	647	φ_R	0
Initial $m_{2\varphi}$	0.25	Bunch length	$2\,\text{rad} \approx 115\,^\circ$

Simulation Results Two different methods were used to compare the performance of the control strategies:

- Simulation of the closed loop system (5.27). This can be performed independently of the synchrotron parameters and the size of the bunch.
- The numerical results of a nonlinear macro particle tracking simulation. An ellipsoidal particle bunch with a homogeneous distribution was used. The simulation parameters are shown in Table 5.8.

The performance of the controllers and their region of attraction are shown in Figure 5.17 for both simulation methods. Comparing these results, the following observations can be made:

- For the chosen bunch size, the model (5.27) agrees very well with the nonlinear particle tracking and the control performance is very similar for both simulations. This indicates that model (5.27) can be used for a controller design for small and medium-sized bunches in a nonlinear bucket.
- Controller (5.29) with a large region of attraction allows deviations of the second moments of more than 50%.

In both cases, the Lyapunov function was part of the optimization process and is assumed to be a polynomial of a given order with unknown coefficients. The use of the Lyapunov function (5.21) could be used to further improve the results.

Limitations Before the designed controllers may be implemented, some important issues have to be considered. Both controllers use the complete state vector and the normalized deviation of the variance $\tilde{x}_1 = \Delta C_{2,0} / E_{2,0}$. Since the equilibrium $E_{2,0}$ is usually not directly accessible to measurements, $E_{2,0}$ has to be estimated. The same applies to the covariance $C_{1,1}$. Possible solutions are the design of a nonlinear observer or a dynamic output-feedback control. The conventional FIR filters that were presented in previous sections of this chapter have a slower damping, but are of the output-feedback type and do not require the estimation of $E_{2,0}$ due to their DC rejection.

The presented design with SOS is valid for linear buckets and is dependent on the measurement or an estimation of both variances $C_{2,0}$ and $C_{0,2}$ and the equilibrium E_2. Thus, for realistic bunch sizes, the existing FIR feedback considered in Section 5.1 has

[8] The results are obtained using the Matlab toolboxes of [82] and [127].

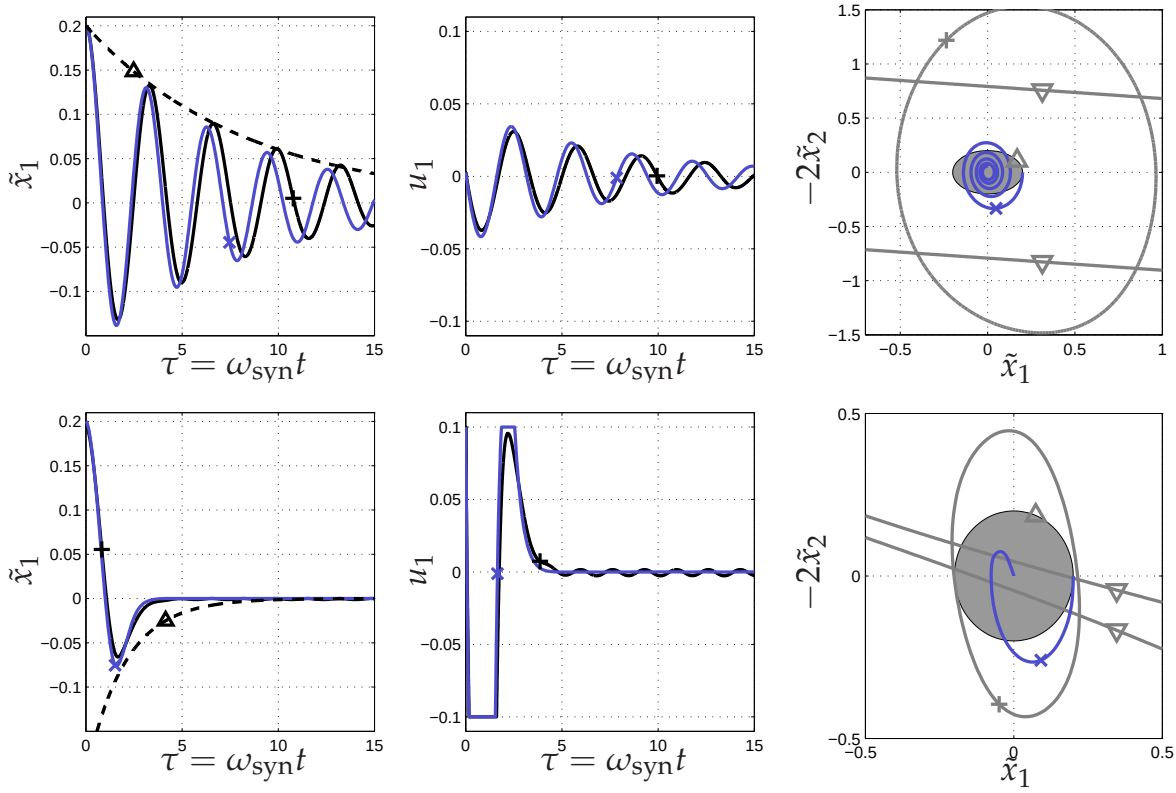

Figure 5.17: Upper diagrams: control (5.29) with optimized region of attraction. **Lower diagrams**: control (5.30) with optimized decay rate. **Left and center**: state $\tilde{x}_1$ and input u_1 versus normalized time τ ($+$: tracking simulation, $\times$: simulation of system (5.27), $\triangle$: top $f(\tau) = 0.2\ \mathrm{e}^{-0.25\tau}$, bottom $f(\tau) = 0.2\ \mathrm{e}^{-0.5\tau}$). **Right**: stability analysis ($\times$: trajectory of system (5.27), $\triangle$: set $\mathcal{X}_0$, $+$: domain of attraction, ∇: limits of actuator saturation).

several advantages. Nevertheless, further work may use some of the nonlinear methods discussed in this section to improve the feedback performance.

5.4 Conclusion

The derived models have been used to analyze RF feedback loops at GSI. The closed-loop dynamics have been described by a linear time-invariant delay-difference equation. A stability analysis has been performed analytically and leads to stability regions in the control parameter space. Tracking simulations have then been used to evaluate the performance of the feedback and of the additional Landau damping for a nonlinear bucket. A comparison with measurements from a beam experiment shows that there is a good agreement between measurements, simulations, and models. In particular, the measured frequency of the quadrupole mode agrees well with the frequency predicted by the model for the specific bunch size. Nevertheless, the results show some limitation of the proposed models. If Landau damping is considerably larger than the damping introduced by the feedback

loop, the validity of the linear models is limited. However, this limitation is usually not serious, because a desired result of the feedback design is typically a damping rate that is considerably larger compared to Landau damping.

6 Conclusion

The transport of bunched beams in a synchrotron is determined by the initial particle distribution and the electromagnetic fields in the ring. Even for the ideal case where interactions between the particles and self-fields of the bunch can be neglected, this is a high-dimensional, nonlinear problem and analytical solutions exist only for drastic simplifications. Therefore, numerical particle tracking simulations are typically used to evaluate the beam dynamics. RF feedback loops are active measures to stabilize the bunched beam in the longitudinal phase plane. Numerical simulations lead to valuable conclusions, but these are restricted to specific beam and synchrotron parameters. It is therefore desirable to have simplified, approximate models that describe the closed-loop dynamics in an analytical way. Existing models of RF feedback loops are based on a linearization of the single-particle dynamics. This limits their applicability to small bunches in the linear regime of the bucket with bunch shape oscillations of order $m = 1$ and $m = 2$.

The main topic in this thesis is the question how longitudinal single-bunch oscillations can be damped. The steps that were taken in this thesis to tackle the problem are the following. First, new models of the bunch shape oscillations were developed. These are state-space models that describe the dynamics of the moments of the bunch with RF phase and amplitude modulations as inputs. The models were obtained using a newly developed modeling procedure that comprises a moment approach and a truncation method. Second, methods from control theory were used to analyse the properties such as the controllability and stability of the models. Third, the complete RF feedback loops for bunch position and bunch length feedback were modeled. An important new contribution for this part was the modeling of the short-term spectrum of the beam current signal and the derivation of simplified relations between the Fourier coefficients of the beam current signal and the bunch shape, i. e. the bunch position and bunch length.

New insights and results of this thesis are summarized in the following. It has been shown that, in general, the dynamics of the moments are coupled and nonlinear and a model truncation is necessary to obtain a low-dimensional model. For the stationary case, the coupling is only between the odd moments on the one hand and the even moments on the other hand. The moments of order m are correlated with mode m, but in general there is no one-to-one correspondence. In the special case of the linear bucket, the moment dynamics are decoupled for different moment orders. In general, the inputs, i. e. the phase and amplitude modulations, act on all moments. A special case is the stationary case, where the phase modulation acts only on the basic moments, i. e. the center of gravity of the bunch, and the amplitude modulation acts only on the central moments.

Concerning the controllability in the nonlinear bucket, a nonlinear truncated model with moments and modes up to order four was analyzed. This model is an approximation to the real high-dimensional dynamics, because of the truncation and the Taylor series approxi-

mation of the beam dynamics. The model was shown to be first-order controllable and it can be concluded that the moments up to order four are locally controllable with the considered inputs, i. e. RF phase and amplitude modulations. However, it has to be noted that, as the model is an approximation due to the reasons stated above, a final rigorous proof for the original high or infinite-dimensional system remains an open topic. Nevertheless, the controllability analysis provides a very strong argument that the first four bunch modes can be damped by the two inputs phase and amplitude. For the linear bucket, a similar model was analyzed which was shown to be not first-order controllable. A more advanced nonlinear controllability analysis would be necessary to decide if the model is indeed not locally controllable. However, simulation results support the indication that only dipole and quadrupole oscillations can be damped in a linear bucket. An important result of the thesis is the calculation of the mode frequencies, i. e. the oscillation frequencies of the bunch shape. It has been demonstrated that the mode frequencies depend on the bunch size and the type of density function. An important parameter for this is the two-sigma length of the bunch, which can be interpreted as the effective half axis of the bunch shape.

The preceding theory has been used to analyze the stability of a bunch length feedback loop. A stability diagram for this feedback loop has been calculated and compared with tracking simulations. In these simulations, two different definitions of the damping performance have been compared: a fast damping rate versus a small increase of the longitudinal emittance. For the bunch length feedback, these definitions lead to different feedback parameters for an optimal performance. The comparison of a beam experiment with the tracking simulations and the analytical stability analysis shows a good agreement between the real beam behavior, the tracking simulations, and the developed models. The only major difference between the models and the simulations is the fact that the models do not reproduce Landau damping or filamentation. In many cases, the feedback is introduced to increase the damping if Landau damping is not sufficient. In these cases, the damping of the feedback should be considerably larger than Landau damping and the developed models are perfectly suitable for a feedback design. An essential overall result of this thesis is the conclusion that nonlinearities in the beam dynamics should be taken into account in the modeling procedure, because they have a strong impact on the properties of the RF feedback loops; important effects are the dependency of the mode frequencies on the bunch size and the controllability of higher order modes.

Further work could focus on the refinement of the derived models and the effects of Landau damping. Also, the existing control algorithm for the bunch length may be further optimized to achieve a larger damping. Because the mode frequencies depend on the bunch length, it would be desirable to adapt the feedback parameters to the bunch length. For higher order oscillation modes, the derived models of this thesis may be used for further analysis and controller design. The controllability of higher modes in a linear bucket could be further elaborated using methods to analyze nonlinear controllability. Also, the models developed in this thesis are valid for stationary linear and nonlinear buckets. It would be desirable and is in principle possible to apply the developed modeling approach for accelerating buckets as well. As the moment approach is versatile, the investigation of more complex RF potentials should be viable as well. Finally, more effects of longitudinal beam dynamics could be included to examine RF feedback in case of large beam currents.

A Mathematical Formulae

A.1 Elliptic Integrals

The (incomplete) elliptic integral of the first kind is

$$F(\varphi,k) = \int_0^{\varphi} \frac{\mathrm{d}\theta}{\sqrt{1-k^2\sin^2\theta}}. \tag{A.1}$$

For $k > 1$, the following transformation is given in Abramowitz/Stegun [2]:

$$F(\varphi,k) = \frac{1}{k} F\left(\arcsin(k\sin\varphi), \frac{1}{k}\right).$$

For the special case $k = \csc\varphi = \sin^{-1}\varphi$, this leads to

$$F(\varphi, \csc\varphi) = \sin\varphi\, K(\sin\varphi), \tag{A.2}$$

where $K(k)$ is the complete elliptic integral of the first kind

$$K(k) = F\left(\frac{\pi}{2},k\right).$$

Special values are

$$K(0) = \frac{\pi}{2}, \quad K(1) = \infty.$$

The (incomplete) elliptic integral of the second kind is

$$E(\varphi,k) = \int_0^{\varphi} \sqrt{1-k^2\sin^2\theta}\, d\theta.$$

The complete elliptic integral of the second kind reads

$$E(k) = E\left(\frac{\pi}{2},k\right).$$

Special values are

$$E(0) = \frac{\pi}{2}, \quad E(1) = 1.$$

In the special case $E(\varphi,\csc\varphi)$, the incomplete elliptic integral of the second kind can be written as a combination of the complete integrals of the first and second kind [135]:

$$E(\varphi,\csc\varphi) = \csc\varphi\, E(\sin\varphi) - \cos\varphi\cot\varphi\, K(\sin\varphi), \qquad -\frac{\pi}{2} < \varphi < \frac{\pi}{2}. \tag{A.3}$$

Table A.1: Properties of Bessel functions

$J_p(-x) = (-1)^p J_p(x) = J_{-p}(x)$
$J_p'(x) = \frac{1}{2}\left[J_{p-1}(x) - J_{p+1}(x)\right]$
$J_p(0) = \begin{cases} 1 & p = 0 \\ 0 & \text{else} \end{cases}$

A.2 Special Functions

A large variety of properties and formulas for special functions can be found in [2] and a summary of properties of the Bessel functions is given in [19].

The Bessel function of the first kind $J_p(x)$ of order p can be defined as the series

$$J_p(x) = \sum_{k=0}^{\infty} \frac{[-1]^k}{k!\,\Gamma(p+k+1)} \left[\frac{x}{2}\right]^{2k+p}$$

with the Gamma function $\Gamma(n)$. For positive integers n, the Gamma function reduces to the factorial function

$$\Gamma(n) = [n-1]! = [n-1]\cdot[n-2]\cdot\ \ldots\ \cdot 2\cdot 1$$

and the Bessel function of the first kind of order p is

$$J_p(x) = \sum_{k=0}^{\infty} \frac{[-1]^k}{k!\,[1+p+k]!} \left[\frac{x}{2}\right]^{2k+p} = \frac{1}{p!}\left[\frac{x}{2}\right]^p - \frac{1}{2![p+1]!}\left[\frac{x}{2}\right]^{p+2} + \ldots.$$

Further properties of J_p are summarized in Table A.1. The Bessel function of the first kind of order 1 is

$$J_1(x) = \sum_{k=0}^{\infty} \frac{[-1]^k}{k!\,[1+k]!} \left[\frac{x}{2}\right]^{2k+1} = \frac{x}{2} - \frac{x^3}{16} + \frac{x^5}{384} - \frac{x^7}{18432} + \ldots.$$

For small $x \ll 1$, the following approximation holds:

$$\frac{J_1(x)}{x} \approx \frac{1}{2} - \frac{x^2}{16}. \tag{A.4}$$

The function J_1 is also a solution of the integral

$$\int_{-1}^{1} \sqrt{1-x^2}\,\mathrm{e}^{-\mathrm{i}ax}\,\mathrm{d}x = \begin{cases} \frac{\pi}{2} & a = 0, \\ \frac{\pi J_1(a)}{a} & a \neq 0. \end{cases}$$

A.3 Spectrum of Phase Modulated Signals

To calculate the spectrum of frequency modulated signals, the expressions in this section are useful. An overview of the theory of signal processing can for example be found in [53] and modulation processes are described in more detail in [50].

A.3.1 General Notation

A periodic function $f(t)$ with period T_0 and the frequency $\omega_0 = 2\pi/T_0$

$$f(t+T_0) = f(t) \quad \forall t \in \mathbb{R}$$

can be written as a Fourier series

$$f(t) = \frac{A_0}{2} + \sum_{k=1}^{\infty} A_k \cos(k\omega_0 t + \varphi_k) = \sum_{k=-\infty}^{\infty} c_k \mathrm{e}^{\mathrm{i}k\omega_0 t}. \tag{A.5}$$

The complex Fourier coefficients can be calculated as

$$c_k = \frac{1}{T_0} \int_{t_0}^{t_0+T_0} f(t)\, \mathrm{e}^{-\mathrm{i}k\omega_0 t}\, \mathrm{d}t$$

with an arbitrary real constant t_0. If $f(t)$ is a real function for all t,

$$c_{-k} = \bar{c}_k$$

holds, where $\bar{c}$ denotes the conjugate-complex value of c. The amplitudes A_k and the phases φ_k are given by

$$A_k = 2\,|c_k|\,, \qquad \varphi_k = \measuredangle c_k = \arctan \frac{\operatorname{Im} c_k}{\operatorname{Re} c_k}.$$

If $f(t)$ is a time-limited, aperiodic signal, the limit $T_0 \to \infty$ can be considered and the Fourier series becomes a Fourier transform

$$F(\omega) = \int_{-\infty}^{\infty} f(t)\, \mathrm{e}^{-\mathrm{i}\omega t}\, \mathrm{d}t \tag{A.6}$$

and $F(\omega)$ is the spectral density of $f(t)$. The inverse transformation is

$$f(t) = \frac{1}{2\pi} \int_{-\infty}^{\infty} F(\omega)\, \mathrm{e}^{\mathrm{i}\omega t}\, \mathrm{d}\omega.$$

With these transformations, the following symmetry property holds (cf. [28], pp.192):

$$f(t) \circ\!\!-\!\!\bullet\, F(\omega) \quad \Leftrightarrow \quad F(t) \circ\!\!-\!\!\bullet\, 2\pi f(-\omega).$$

In particular, this leads to the correspondence for the Dirac function

$$\delta(t+\alpha) \circ\!\!-\!\!\bullet\, \mathrm{e}^{\mathrm{i}\omega\alpha}, \quad \mathrm{e}^{\mathrm{i}\omega_0 t} \circ\!\!-\!\!\bullet\, 2\pi\delta(\omega-\omega_0). \tag{A.7}$$

A more formal and general theorem is the Poisson Sum Rule [121]. If $F(\omega)$ is the Fourier transform of $f(t)$, then

$$\sum_{n=-\infty}^{\infty} f(t=\alpha n) = \frac{1}{\alpha}\sum_{n=-\infty}^{\infty} F\left(\omega=\frac{2\pi n}{\alpha}\right) \tag{A.8}$$

holds.

A.3.2 Dirac Series and Phase Modulation

An infinite comb of Dirac delta functions

$$f(t) = \sum_{n=-\infty}^{\infty} \delta(t-nT_0)$$

can be written as a Fourier series. The coefficients are $c_k = 1/T_0$ and

$$f(t) = \sum_{n=-\infty}^{\infty} \delta(t-nT_0) = \frac{1}{T_0}\sum_{k=-\infty}^{\infty} \mathrm{e}^{\mathrm{i}k\omega_0 t}. \tag{A.9}$$

This series can be Fourier transformed element by element and this leads to the correspondence

$$\frac{1}{T_0}\sum_{k=-\infty}^{\infty} \mathrm{e}^{\mathrm{i}k\omega_0 t} \quad \overset{(A.7)}{\circ\!\!-\!\!\bullet} \quad \frac{2\pi}{T_0}\sum_{k=-\infty}^{\infty} \delta(\omega-k\omega_0) \tag{A.10a}$$

$$\overset{(A.9)}{=} \sum_{n=-\infty}^{\infty} \delta(t-nT_0) \qquad \overset{(A.9)}{=} \sum_{n=-\infty}^{\infty} \mathrm{e}^{\mathrm{i}nT_0\omega} \tag{A.10b}$$

A.3.3 Aperiodic and Periodic Signals

If the aperiodic signal $f_{\mathrm{ap}}(t)$ with length T_0 is continued such that it becomes a periodic function

$$f_{\mathrm{p}} = \sum_{n=-\infty}^{\infty} f_{\mathrm{ap}}(t-nT_0)$$

with period T_0 and frequency $\omega_0 = 2\pi/T_0$, a Fourier series calculation yields

$$c_k = \frac{1}{T_0}\int_{-\infty}^{\infty} f_{\mathrm{ap}}(t)\,\mathrm{e}^{-\mathrm{i}k\omega_0 t}\,\mathrm{d}t = \frac{1}{T_0}F_{\mathrm{ap}}(k\omega_0), \tag{A.11}$$

where $F_{\mathrm{ap}}(\omega)$ is the spectral density of the aperiodic signal $f_{\mathrm{ap}}(t)$ and the fact that $f_{\mathrm{ap}}(t)$ is zero outside the interval $t \in [t_0\,;\, t_0+T_0]$ was used. In addition, T_0 has to be chosen such that there is no overlapping. This calculation demonstrates that the Fourier series coefficients c_k can be interpreted as sampling values of $F_{\mathrm{ap}}(\omega)$ with the sampling frequency ω_0. The periodic signal can be written as the Fourier series

$$f_{\mathrm{p}}(t) = \sum_{k=-\infty}^{\infty} c_k \, \mathrm{e}^{\mathrm{i}k\omega_0 t}.$$

Its spectral density follows using (A.10) and is

$$F_{\mathrm{p}}(\omega) = 2\pi \sum_{k=-\infty}^{\infty} c_k \, \delta(\omega - k\omega_0) = \omega_0 \sum_{k=-\infty}^{\infty} F_{\mathrm{ap}}(k\omega_0) \, \delta(\omega - k\omega_0).$$

B Accelerator Physics

B.1 Relativistic Relations

The aim of this section is to summarize some relativistic relations that are needed in the calculations of the main part of the thesis. A more complete selection of relativistic formulas can be found in [14, 58].

Definitions To deduce the following relations, we have to define the relativistic normalized velocity β, the relativistic normalized energy γ, the total energy W, the kinetic energy W_{kin}, the momentum p, and the relativistic mass m:

$$\beta = \frac{v}{c} \qquad \gamma = \frac{1}{\sqrt{1-\left[\frac{v}{c}\right]^2}} \qquad m = \gamma m_0$$

$$W = \gamma m_0 c^2 \qquad W_{\text{kin}} = W - m_0 c^2 = [\gamma - 1] m_0 c^2 \qquad p = mv = \gamma m_0 \beta c$$

Relations The following relations are derived by using only the above definitions. It is possible to express each variable as a function of just one other variable:

$$\gamma = \frac{1}{\sqrt{1-\beta^2}} = \frac{W}{m_0 c^2} = \frac{W_{\text{kin}}}{m_0 c^2} + 1 = \sqrt{1 + \left[\frac{p}{m_0 c}\right]^2} \tag{B.1}$$

$$\begin{aligned} \beta &= \sqrt{1-\gamma^{-2}} = \sqrt{1 - \left[\frac{m_0 c^2}{W}\right]^2} = \sqrt{1 - \left[\frac{m_0 c^2}{W_{\text{kin}} + m_0 c^2}\right]^2} \\ &= \frac{p}{\sqrt{m_0^2 c^2 + p^2}} \end{aligned} \tag{B.2}$$

$$W = \gamma m_0 c^2 = \frac{m_0 c^2}{\sqrt{1-\beta^2}} = W_{\text{kin}} + m_0 c^2 = \sqrt{c^2 p^2 + m_0^2 c^4} \tag{B.3}$$

$$W_{\text{kin}} = [\gamma - 1] m_0 c^2 = \left[\frac{1}{\sqrt{1-\beta^2}} - 1\right] m_0 c^2 = \sqrt{c^2 p^2 + m_0^2 c^4} - m_0 c^2$$

$$p = \sqrt{\gamma^2 - 1} m_0 c = \frac{\beta m_0 c}{\sqrt{1-\beta^2}} = \frac{1}{c}\sqrt{W^2 - m_0^2 c^4}$$
$$= \frac{1}{c}\sqrt{W_{\text{kin}}[W_{\text{kin}} + 2m_0 c^2]}$$

Relative Deviations The derivation of W with respect to p leads to

$$\frac{\mathrm{d}W}{\mathrm{d}p} = \frac{2c^2 p}{2\sqrt{c^2 p^2 + m_0^2 c^4}} = \frac{c^2 p}{W}. \tag{B.4}$$

Equation (B.4) can also be written as

$$\mathrm{d}W = \frac{c^2 p}{W}\mathrm{d}p = \frac{c^2 \gamma m_0 \beta c}{\gamma m_0 c^2}\mathrm{d}p = \beta c \, \mathrm{d}p. \tag{B.5}$$

Equation (B.4) leads to

$$\frac{\mathrm{d}W}{W} = \frac{c^2 p^2}{W^2}\frac{\mathrm{d}p}{p} \overset{\text{(B.3)}}{=} \frac{c^2 p^2}{c^2 p^2 + m_0^2 c^4}\frac{\mathrm{d}p}{p} \overset{\text{(B.2)}}{=} \frac{p^2}{p^2 + m_0^2 c^2}\frac{\mathrm{d}p}{p} = \beta^2 \frac{\mathrm{d}p}{p}.$$

Derivating

$$p = \frac{\beta m_0 c}{\sqrt{1-\beta^2}} = \frac{v m_0}{\sqrt{1 - \dfrac{v^2}{c^2}}}$$

with respect to v yields

$$\frac{\mathrm{d}p}{\mathrm{d}v} = m_0 \frac{1}{\left[1 - \dfrac{v^2}{c^2}\right]^{3/2}} = m_0 \gamma^3.$$

Thus, we have

$$\frac{\mathrm{d}p}{p} = \frac{m_0 \gamma^3 v}{p}\frac{\mathrm{d}v}{v} = \gamma^2 \frac{\mathrm{d}v}{v}.$$

Similar derivations lead to

$$\frac{\mathrm{d}v}{v} = \frac{d\beta}{\beta} = \frac{1}{\gamma^2 - 1}\frac{\mathrm{d}\gamma}{\gamma} = \frac{1}{\gamma^2 \beta^2}\frac{\mathrm{d}\gamma}{\gamma} = \frac{1}{\gamma^2 \beta^2}\frac{\mathrm{d}W}{W}.$$

For small deviations the obtained results can be summarized in the following approximation:

$$\frac{\Delta p}{p} \approx \beta^{-2}\frac{\Delta W}{W} \approx \beta^{-2}\frac{\Delta \gamma}{\gamma} \approx \gamma^2 \frac{\Delta v}{v} \approx \gamma^2 \frac{\Delta \beta}{\beta}. \tag{B.6}$$

As $\beta \in [0;1]$ and $\gamma \in [1;\infty[$, Equation (B.6) has the consequence

$$\frac{\Delta p}{p} \geq \frac{\Delta W}{W} = \frac{\Delta \gamma}{\gamma}, \quad \frac{\Delta p}{p} \geq \frac{\Delta v}{v} = \frac{\Delta \beta}{\beta}, \tag{B.7}$$

i. e. the relative momentum deviation is an upper limit for the relative deviations in energy and velocity.

B.2 Simulation Parameters

Basic Constants and Parameters of the Heavy-Ion Synchrotron SIS18

Parameter	Symbol	Value
Circumference	L_R	216.72 m
Transition energy	γ_tr	5.45
Momentum compaction	$\alpha_\mathrm{P} = \gamma_\mathrm{tr}^{-2}$	0.03367
Curvature radius	r	10 m
Speed of light	c	$2.99792458 \cdot 10^8$ m/s
Atomic mass	m_amu	$1.660538782 \cdot 10^{-27}$ kg
Rest energy of 1 amu	W_amu	$931.494028 \cdot 10^6$ eV
Elementary charge	e	$1.602176487(40) \cdot 10^{-19}$ C

Parameters of Several Beam Experiments

Parameter	Unit	Protons	$^{40}\mathrm{Argon}^{18+}$	$^{238}\mathrm{Uran}^{73+}$
h		4	4	4
φ_R		0	0	0
m_0	amu	1.0079	39.948	238.03
Q	e	+1	+18	+73
W_kin/m_0	$\frac{\mathrm{eV}}{\mathrm{amu}}$	$2 \cdot 10^9$	$80 \cdot 10^6$	$11.4 \cdot 10^6$
W_R	J	$4.7339 \cdot 10^{-10}$	$6.4739 \cdot 10^{-9}$	$3.5959 \cdot 10^{-8}$
γ_R		3.1471	1.0859	1.0122
β_R		0.94817	0.38978	0.15503
$\hat{U}_1$	V	16000	12000	8000
T_R	s	$7.6241 \cdot 10^{-7}$	$1.8546 \cdot 10^{-6}$	$4.6629 \cdot 10^{-6}$
f_syn	Hz	666.3	2302.9	1728.3
$T_\mathrm{syn}/T_\mathrm{R}$	Hz	1968.5	234.13	124.09
B_R	T	0.93452	0.29186	0.15899

B.3 Longitudinal Tracking Algorithm

In this section the equations are summarized that are necessary for a longitudinal tracking algorithm. With the main focus on the implementation, discrete equations are considered. The notation will be as follows: $f(n)$ refers to the discrete value f at turn n.

Step 1 At the beginning of the acceleration cycle, it is necessary to determine the following machine and beam constants: the charge Q and rest mass m_0 per particle, the bending radius r of the dipole magnets, the harmonic number h, the length L_R of the reference orbit, and the momentum compaction α_p. The acceleration cycle itself is determined by the choice of the magnetic field $B_\mathrm{R}(n)$. The initial magnetic field can be calculated from the injection energy.

Step 2 If the initial kinetic energy $W_{\mathrm{R,kin}}(0)$ or the initial total energy

$$W_\mathrm{R}(0) = W_{\mathrm{R,kin}} + m_0 c^2$$

per particle is given, the momentum

$$p_\mathrm{R}(0) = \frac{1}{c}\sqrt{W_\mathrm{R}^2(0) - m_0^2 c^4},$$

the magnetic field

$$B_\mathrm{R}(0) = \frac{p_\mathrm{R}(0)}{Qr} = \frac{1}{cQr}\sqrt{W_\mathrm{R}^2(0) - m_0^2 c^4},$$

and the following parameters can be calculated:

$$\gamma_\mathrm{R}(0) = \frac{W_\mathrm{R}(0)}{m_0 c^2}, \qquad \beta_\mathrm{R}(0) = \sqrt{1 - \gamma_\mathrm{R}^{-2}(0)}, \qquad T_\mathrm{R}(0) = \frac{L_\mathrm{R}}{v_\mathrm{R}(0)} = \frac{L_\mathrm{R}}{\beta_\mathrm{R}(0)c}$$

$$f_\mathrm{R}(0) = \frac{\beta_\mathrm{R}(0)c}{L_\mathrm{R}}, \quad \omega_\mathrm{RF}(0) = h\omega_\mathrm{R}(0) = h2\pi f_\mathrm{R}(0)$$

Step 3 The initial distribution of a particle bunch with N particles has to be chosen:

$$\Delta\boldsymbol{W}(0) = \left[\Delta W_1(0) \ldots \Delta W_k(0) \ldots \Delta W_N(0)\right]^\mathrm{T}$$
$$\boldsymbol{\varphi}(0) = \left[\varphi_1(0) \ldots \varphi_k(0) \ldots \varphi_N(0)\right]^\mathrm{T}$$

with as phase space coordinates the RF phase φ and the energy deviation ΔW. The remaining degree of freedom is the choice of the series $B_\mathrm{R}(n)$, $n = 0,1,\ldots,n_\mathrm{end}$, that describe the rate of change of the magnetic field

$$\dot{B}_\mathrm{R}(t) \approx \frac{B_\mathrm{R}(n+1) - B_\mathrm{R}(n)}{T_\mathrm{R}(n)}.$$

The magnetic field should be chosen such that the necessary reference voltage

$$U_\mathrm{R} \approx L_\mathrm{R} r \dot{B}_\mathrm{R},$$

is lower than the maximum voltage of the cavity. Furthermore, the maximum and minimum values of B are limited by the magnet design. Thus, B_R has an upper limit that has to be taken into account.

Step 4 The simulation from turn n to $n+1$ is achieved by the following three steps:

4.I Mapping of the reference energy: The reference voltage can be calculated as

$$U_{\mathrm{R}}(n+1) = m_0c^2\sqrt{1+\left[\frac{QrB_{\mathrm{R}}(n+1)}{m_0c}\right]^2} - m_0c^2\sqrt{1+\left[\frac{QrB_{\mathrm{R}}(n)}{m_0c}\right]^2},$$

which leads to the new reference energy

$$W_{\mathrm{R}}(n+1) = W_{\mathrm{R}}(n) + QU_{\mathrm{R}}(n+1).$$

If the reference phase is needed, it can be calculated as

$$\varphi_{\mathrm{R}} = U_{\mathrm{gap}}^{-1}(U_{\mathrm{R}}(n)),$$

where U_{gap}^{-1} denotes the inverse function of the RF voltage. For a single-harmonic cavity, this equals

$$\varphi_{\mathrm{R}} = \arcsin\left(\frac{U_{\mathrm{R}}}{\hat{U}_1}\right).$$

The last equation shows that $\hat{U}_1$ should be chosen larger than U_{R}.

4.II Calculation of the other time varying parameters:

$$p_{\mathrm{R}}(n+1) = \frac{1}{c}\sqrt{W_{\mathrm{R}}^2(n+1) - m_0^2c^4} \qquad \gamma_{\mathrm{R}}(n+1) = \frac{W_{\mathrm{R}}(n+1)}{m_0c^2}$$

$$\beta_{\mathrm{R}}(n+1) = \sqrt{1-\gamma_{\mathrm{R}}^{-2}(n+1)} \qquad \omega_{\mathrm{R}}(n+1) = 2\pi\frac{\beta_{\mathrm{R}}(n+1)c}{L_{\mathrm{R}}}$$

$$\eta_{\mathrm{R}}(n+1) = \alpha_{\mathrm{p}} - \gamma_{\mathrm{R}}^{-2}(n+1)$$

4.III Mapping of the particles:

$$\Delta W_k(n+1) = \Delta W_k(n) \;+\; Q\left[U_{\mathrm{gap}}(\varphi_k(n)) - U_{\mathrm{R}}(n+1)\right]$$

$$\varphi_k(n+1) = \frac{\beta_{\mathrm{R}}(n+1)}{\beta_{\mathrm{R}}(n)}\left[\varphi_k(n) - \varphi_{\mathrm{f}}(n) - k_{\mathrm{RF}}\varphi_{\mathrm{R}}(n)\right] + \\ + \frac{2\pi h\eta_{\mathrm{R}}}{\beta_{\mathrm{R}}^2 W_{\mathrm{R}}}(n+1)\Delta W_k(n+1) + \varphi_{\mathrm{f}}(n+1) + k_{\mathrm{RF}}\varphi_{\mathrm{R}}(n+1).$$

The constant k_{RF} is 0 or 1, depending on which cavity RF program has been chosen, cf. (2.25). In this thesis, $k_{\mathrm{RF}} = 1$. In principle also other phase space coordinates may be used for the mapping, as long as the discrete equations are chosen such that their Jacobian is correct. The RF voltage $U_{\mathrm{gap}}(\varphi)$ can be chosen as a single-harmonic function, but also as a higher harmonic or a general periodic function with fast varying amplitude and phase.

C Modeling Results

C.1 Coherent Oscillation Frequencies

The following table summarizes the frequencies of the coherent dipole and quadrupole mode of oscillation of Figure 3.18. The relative frequency f_{rel} is defined as

$$f_{\text{rel}} = \frac{f_m}{m\, f_{\text{syn}}},$$

where $m = 1{,}2$ is the mode number, f_m the coherent oscillation frequency of mode m obtained from tracking simulations and f_{syn} is the linear synchrotron frequency.

Uniform				Gaussian			
Dipole ($m = 1$)		Quadrupole ($m = 2$)		Dipole ($m = 1$)		Quadrupole ($m = 2$)	
$C_{2,0}$	f_{rel}	$C_{2,0}$	f_{rel}	$C_{2,0}$	f_{rel}	$C_{2,0}$	f_{rel}
0.0624	0.98	0.0624	0.97	0.0631	0.985	0.0631	0.985
0.14	0.965	0.14	0.955	0.1423	0.965	0.1423	0.965
0.248	0.938	0.248	0.925	0.245	0.94	0.245	0.92
0.389	0.9	0.389	0.89	0.394	0.89	0.394	0.80
0.556	0.855	0.556	0.85	0.56	0.89	0.56	0.73
0.753	0.8	0.753	0.8	0.783	0.85	0.783	0.7
0.997	0.73	0.997	0.73	0.996	0.8	0.996	0.57
1.254	0.65	1.254	0.66	1.273	0.8	1.273	0.54
1.56	0.54	1.56	0.58	1.52	0.8	1.52	0.65

C.2 Moments and Modes

C.2.1 Ellipsoidal Bunches

The bunch is assumed to be ellipsoidal with the uniform density function $f(x,y,x_0,y_0,\Phi)$ of (3.25) or the Gaussian density function of (3.33). The parameters x_0, y_0, and Φ may be functions of time or depend on $\omega_{\text{syn}}t$ to obtain a rotating bunch in the phase plane as shown in (3.24). The basic and central moments B_{n_x,n_y} and C_{n_x,n_y} are given in Table C.1. Because of the symmetry between the moments $C_{i,j}$ and $C_{j,i}$, only half of the results are summarized for higher order modes.

Table C.1: Moments of ellipsoidal bunches.

	Uniform Density	**Gaussian Density**
$B_{1,0}$	x_0	x_0
$B_{0,1}$	y_0	y_0
$C_{2,0}$	$\frac{1}{4}\left[R_{1x}^2\cos^2\Phi + R_{2x}^2\sin^2\Phi\right]$	$\sigma_{1x}^2\cos^2\Phi + \sigma_{2x}^2\sin^2\Phi$
$C_{1,1}$	$\frac{1}{8}\left[R_{1x}^2 - R_{2x}^2\right]\sin(2\Phi)$	$\frac{1}{2}\left[\sigma_{1x}^2 - \sigma_{2x}^2\right]\sin(2\Phi)$
$C_{0,2}$	$\frac{1}{4}\left[R_{1x}^2\sin^2\Phi + R_{2x}^2\cos^2\Phi\right]$	$\sigma_{1x}^2\sin^2\Phi + \sigma_{2x}^2\cos^2\Phi$
$C_{n_x+n_y=3}$	0	0
$C_{4,0}$	$2C_{2,0}^2$	$3C_{2,0}^2$
$C_{3,1}$	$2C_{2,0}C_{1,1}$	$3C_{2,0}C_{1,1}$
$C_{2,2}$	$\frac{4}{3}C_{1,1}^2 + \frac{2}{3}C_{2,0}C_{0,2}$	$2C_{1,1}^2 + C_{2,0}C_{0,2}$
$C_{1,3}$	$2C_{0,2}C_{1,1}$	$3C_{0,2}C_{1,1}$
$C_{0,4}$	$2C_{0,2}^2$	$3C_{0,2}^2$
$C_{n_x+n_y=5}$	0	0
$C_{6,0}$	$5C_{2,0}^3$	$15C_{2,0}^3$
$C_{5,1}$	$5C_{2,0}^2C_{1,1}$	$15C_{2,0}^2C_{1,1}$
$C_{4,2}$	$C_{2,0}\left[4C_{1,1}^2 + C_{2,0}C_{0,2}\right]$	$3C_{2,0}\left[4C_{1,1}^2 + C_{2,0}C_{0,2}\right]$
$C_{3,3}$	$C_{1,1}\left[2C_{1,1}^2 + 3C_{2,0}C_{0,2}\right]$	$3C_{1,1}\left[2C_{1,1}^2 + 3C_{2,0}C_{0,2}\right]$
$C_{n_x+n_y=7}$	0	0
$C_{8,0}$	$14C_{2,0}^4$	$105C_{2,0}^4$
$C_{7,1}$	$14C_{2,0}^3C_{1,1}$	$105C_{2,0}^3C_{1,1}$
$C_{6,2}$	$2C_{2,0}^2\left[6C_{1,1}^2 + C_{2,0}C_{0,2}\right]$	$15C_{2,0}^2\left[6C_{1,1}^2 + C_{2,0}C_{0,2}\right]$
$C_{5,3}$	$2C_{2,0}C_{1,1}\left[4C_{1,1}^2 + 3C_{2,0}C_{0,2}\right]$	$15C_{2,0}C_{1,1}\left[4C_{1,1}^2 + 3C_{2,0}C_{0,2}\right]$
$C_{4,4}$	$\frac{6}{5}C_{2,0}^2C_{0,2}^2 + \frac{48}{5}C_{2,0}C_{0,2}C_{1,1}^2 + \frac{16}{5}C_{1,1}^4$	$9C_{2,0}^2C_{0,2}^2 + 72C_{2,0}C_{0,2}C_{1,1}^2 + 24C_{1,1}^4$
$C_{n_x+n_y=9}$	0	0
$C_{10,0}$	$42C_{2,0}^5$	$945C_{2,0}^5$
$C_{9,1}$	$42C_{2,0}^4C_{1,1}$	$945C_{2,0}^4C_{1,1}$
$C_{8,2}$	$\frac{14}{3}C_{2,0}^3\left[8C_{1,1}^2 + C_{2,0}C_{0,2}\right]$	$105C_{2,0}^3\left[8C_{1,1}^2 + C_{2,0}C_{0,2}\right]$
$C_{7,3}$	$14C_{2,0}^2C_{1,1}\left[2C_{1,1}^2 + C_{2,0}C_{0,2}\right]$	$315C_{2,0}^2C_{1,1}\left[2C_{1,1}^2 + C_{2,0}C_{0,2}\right]$
$C_{6,4}$	$2C_{2,0}\left[8C_{1,1}^4 + 12C_{1,1}^2C_{2,0}C_{0,2} + C_{2,0}^2C_{0,2}^2\right]$	$45C_{2,0}\left[8C_{1,1}^4 + 12C_{1,1}^2C_{2,0}C_{0,2} + C_{2,0}^2C_{0,2}^2\right]$
$C_{5,5}$	$\frac{2}{3}C_{1,1}\left[8C_{1,1}^4 + 40C_{1,1}^2C_{2,0}C_{0,2} + 15C_{2,0}^2C_{0,2}^2\right]$	$15C_{1,1}\left[8C_{1,1}^4 + 40C_{1,1}^2C_{2,0}C_{0,2} + 15C_{2,0}^2C_{0,2}^2\right]$
$C_{n_x+n_y=11}$	0	0
$C_{12,0}$	$132C_{2,0}^6$	$10395C_{2,0}^6$
$C_{11,1}$	$132C_{2,0}^5C_{1,1}$	$10395C_{2,0}^5C_{1,1}$

Continued on next page

Table C.1 – continued from previous page

	Uniform Density	**Gaussian Density**
$C_{10,2}$	$12C_{2,0}^4\left[10C_{1,1}^2+C_{2,0}C_{0,2}\right]$	$945C_{2,0}^4\left[10C_{1,1}^2+C_{2,0}C_{0,2}\right]$
$C_{9,3}$	$12C_{2,0}^3C_{1,1}\left[8C_{1,1}^2+3C_{2,0}C_{0,2}\right]$	$945C_{2,0}^3C_{1,1}\left[8C_{1,1}^2+3C_{2,0}C_{0,2}\right]$
$C_{8,4}$	$4C_{2,0}^2\Big[16C_{1,1}^4+16C_{1,1}^2C_{2,0}C_{0,2}+$ $+C_{2,0}^2C_{0,2}^2\Big]$	$315C_{2,0}^2\Big[16C_{1,1}^4+16C_{1,1}^2C_{2,0}C_{0,2}+$ $+C_{2,0}^2C_{0,2}^2\Big]$
$C_{7,5}$	$\Big[8C_{1,1}^4+20C_{1,1}^2C_{2,0}C_{0,2}+$ $+5C_{2,0}^2C_{0,2}^2\Big]4C_{1,1}C_{2,0}$	$\Big[8C_{1,1}^4+20C_{1,1}^2C_{2,0}C_{0,2}+$ $+5C_{2,0}^2C_{0,2}^2\Big]315C_{1,1}C_{2,0}$
$C_{6,6}$	$\frac{4}{7}\Big[16C_{1,1}^6+120C_{1,1}^4C_{2,0}C_{0,2}+$ $+90C_{1,1}^2C_{2,0}^2C_{0,2}^2+5C_{2,0}^3C_{0,2}^3\Big]$	$45\Big[16C_{1,1}^6+120C_{1,1}^4C_{2,0}C_{0,2}+$ $+90C_{1,1}^2C_{2,0}^2C_{0,2}^2+5C_{2,0}^3C_{0,2}^3\Big]$
$C_{n_x+n_y=13}$	0	0
$C_{14,0}$	$429C_{2,0}^7$	$135135C_{2,0}^7$
$C_{13,1}$	$429C_{2,0}^6C_{1,1}$	$135135C_{2,0}^6C_{1,1}$
$C_{12,2}$	$33C_{2,0}^5\left[12C_{1,1}^2+C_{2,0}C_{0,2}\right]$	$10395C_{2,0}^5\left[12C_{1,1}^2+C_{2,0}C_{0,2}\right]$
$C_{11,3}$	$33C_{2,0}^4C_{1,1}\left[10C_{1,1}^2+3C_{2,0}C_{0,2}\right]$	$10395C_{2,0}^4C_{1,1}\left[10C_{1,1}^2+3C_{2,0}C_{0,2}\right]$
$C_{10,4}$	$3C_{2,0}^3\Big[8C_{1,1}^4+60C_{1,1}^2C_{2,0}C_{0,2}+$ $+3C_{2,0}^2C_{0,2}^2\Big]$	$945C_{2,0}^3\Big[8C_{1,1}^4+60C_{1,1}^2C_{2,0}C_{0,2}+$ $+3C_{2,0}^2C_{0,2}^2\Big]$
$C_{9,5}$	$\Big[48C_{1,1}^4+80C_{1,1}^2C_{2,0}C_{0,2}+$ $+15C_{2,0}^2C_{0,2}^2\Big]3C_{1,1}C_{2,0}^2$	$\Big[48C_{1,1}^4+80C_{1,1}^2C_{2,0}C_{0,2}+$ $+15C_{2,0}^2C_{0,2}^2\Big]945C_{1,1}C_{2,0}^2$
$C_{8,6}$	$C_{2,0}\Big[64C_{1,1}^6+240C_{1,1}^4C_{2,0}C_{0,2}+$ $+120C_{1,1}^2C_{2,0}^2C_{0,2}^2+5C_{2,0}^3C_{0,2}^3\Big]$	$315C_{2,0}\Big[64C_{1,1}^6+240C_{1,1}^4C_{2,0}C_{0,2}+$ $+120C_{1,1}^2C_{2,0}^2C_{0,2}^2+5C_{2,0}^3C_{0,2}^3\Big]$
$C_{7,7}$	$C_{1,1}\Big[16C_{1,1}^6+168C_{1,1}^4C_{2,0}C_{0,2}+$ $+210C_{1,1}^2C_{2,0}^2C_{0,2}^2+35C_{2,0}^3C_{0,2}^3\Big]$	$315C_{1,1}\Big[16C_{1,1}^6+168C_{1,1}^4C_{2,0}C_{0,2}+$ $+210C_{1,1}^2C_{2,0}^2C_{0,2}^2+35C_{2,0}^3C_{0,2}^3\Big]$

C.2.2 Bunches with Single-Bunch Modes

In this section, the density functions (3.16) and (3.18) are considered. Only the first four modes will be analyzed, i. e. the coefficients r_m are set to zero for $m > 4$. Only the first order approximations will be given in the following. The basic moments are denoted by $B_{1,0}$ and $B_{0,1}$. The central moments C_{n_x,n_y} have equilibrium values that will be denoted by E_{n_x,n_y}. For odd orders $n_x + n_y$ or odd n_y $E_{n_x,n_y} = 0$ holds, cf. (4.33). Choosing a mode $r_m \neq 0$ leads to deviations

$$\Delta C_{n_x,n_y} = C_{n_x,n_y} - E_{n_x,n_y}.$$

of the equilibrium E_{n_x,n_y}.

Uniform Density The bunch is assumed to have a uniform density and a bunch shape according to the mode definition (3.16) and f_0 is chosen such that the integral of f over the phase plane equals unity. The moments for $n_x + n_y \leq 10$ are given in Table C.2. These are first order approximations. Also, the bunch radius r_0 is replaced by $r_0 = 2\sigma_0$, this makes it easier to compare these results with the results for Gaussian densities of Table C.3. Because of the symmetry between $C_{i,j}$ and $C_{j,i}$, only half of the results are summarized for higher order modes.

Table C.2: Moments of coherent bunch oscillations for uniform densities (first order approximations).

Uniform Density, $r_0 = 2\sigma_0$					
C_{n_x,n_y}	E_{n_x,n_y}	$\Delta C_{n_x,n_y}(r_1)$	$\Delta C_{n_x,n_y}(r_2)$	$\Delta C_{n_x,n_y}(r_3)$	$\Delta C_{n_x,n_y}(r_4)$
$B_{1,0}$	0	$-2\sigma_0 \sin(\theta_0) r_1$	0	0	0
$B_{0,1}$	0	$2\sigma_0 \cos(\theta_0) r_1$	0	0	0
$C_{2,0}$	$E_{2,0} = \sigma_0^2$	0	$-2\sigma_0^2 \sin(2\theta_0) r_2$	0	0
$C_{1,1}$	0	0	$2\sigma_0^2 \cos(2\theta_0) r_2$	0	0
$C_{0,2}$	$E_{0,2} = \sigma_0^2$	0	$2\sigma_0^2 \sin(2\theta_0) r_2$	0	0
$C_{3,0}$	0	0	0	$-2\sigma_0^3 \sin(3\theta_0) r_3$	0
$C_{2,1}$	0	0	0	$2\sigma_0^3 \cos(3\theta_0) r_3$	0
$C_{1,2}$	0	0	0	$2\sigma_0^3 \sin(3\theta_0) r_3$	0
$C_{0,3}$	0	0	0	$-2\sigma_0^3 \cos(3\theta_0) r_3$	0
$C_{4,0}$	$2E_{2,0}^2$	0	$4E_{2,0}\Delta C_{2,0}$	0	$-2\sigma_0^4 \sin(4\theta_0) r_4$
$C_{3,1}$	0	0	$2E_{2,0}\Delta C_{1,1}$	0	$2\sigma_0^4 \cos(4\theta_0) r_4$
$C_{2,2}$	$\frac{2}{3} E_{2,0} E_{0,2}$	0	0	0	$2\sigma_0^4 \sin(4\theta_0) r_4$
$C_{1,3}$	0	0	$2E_{0,2}\Delta C_{1,1}$	0	$-2\sigma_0^4 \cos(4\theta_0) r_4$
$C_{0,4}$	$2E_{0,2}^2$	0	$4E_{0,2}\Delta C_{0,2}$	0	$-2\sigma_0^4 \sin(4\theta_0) r_4$
$C_{5,0}$	0	0	0	$5E_{2,0}\Delta C_{3,0}$	0
$C_{4,1}$	0	0	0	$3E_{2,0}\Delta C_{2,1}$	0
$C_{3,2}$	0	0	0	$E_{2,0}\Delta C_{1,2}$	0
$C_{6,0}$	$5E_{2,0}^3$	0	$15E_{2,0}^2\Delta C_{2,0}$	0	$6E_{2,0}\Delta C_{4,0}$
$C_{5,1}$	0	0	$5E_{2,0}^2\Delta C_{1,1}$	0	$4E_{2,0}\Delta C_{3,1}$
$C_{4,2}$	$E_{2,0}^2 E_{0,2}$	0	$E_{2,0}E_{0,2}\Delta C_{2,0}$	0	$2E_{2,0}\Delta C_{2,2}$
$C_{3,3}$	0	0	$3E_{2,0}E_{0,2}\Delta C_{1,1}$	0	0
$C_{7,0}$	0	0	0	$21E_{2,0}^2\Delta C_{3,0}$	0
$C_{6,1}$	0	0	0	$9E_{2,0}^2\Delta C_{2,1}$	0
$C_{5,2}$	0	0	0	$E_{2,0}^2\Delta C_{1,2}$	0
$C_{4,3}$	0	0	0	$3E_{2,0}E_{0,2}\Delta C_{2,1}$	0
$C_{8,0}$	$14E_{2,0}^4$	0	$56E_{2,0}^3\Delta C_{2,0}$	0	$28E_{2,0}^2\Delta C_{4,0}$
$C_{7,1}$	0	0	$14E_{2,0}^3\Delta C_{1,1}$	0	$14E_{2,0}^2\Delta C_{3,1}$
$C_{6,2}$	$2E_{2,0}^3 E_{0,2}$	0	$4E_{2,0}^2E_{0,2}\Delta C_{2,0}$	0	$4E_{2,0}^2\Delta C_{2,2}$
$C_{5,3}$	0	0	$6E_{2,0}^2E_{0,2}\Delta C_{1,1}$	0	$2E_{2,0}E_{0,2}\Delta C_{3,1}$
$C_{4,4}$	$\frac{6}{5} E_{2,0}^2 E_{0,2}^2$	0	0	0	$4E_{2,0}E_{0,2}\Delta C_{2,2}$
$C_{9,0}$	0	0	0	$84E_{2,0}^3\Delta C_{3,0}$	0
$C_{8,1}$	0	0	0	$28E_{2,0}^3\Delta C_{2,1}$	0

Continued on next page

Table C.2 – continued from previous page

Uniform Density, $r_0 = 2\sigma_0$					
C_{n_x,n_y}	E_{n_x,n_y}	$\Delta C_{n_x,n_y}(r_1)$	$\Delta C_{n_x,n_y}(r_2)$	$\Delta C_{n_x,n_y}(r_3)$	$\Delta C_{n_x,n_y}(r_4)$
$C_{7,2}$	0	0	0	0	0
$C_{6,3}$	0	0	0	$8E_{2,0}^2E_{0,2}\Delta C_{2,1}$	0
$C_{5,4}$	0	0	0	$4E_{2,0}^2E_{0,2}\Delta C_{1,2}$	0
$C_{10,0}$	$42E_{2,0}^5$	0	$210E_{2,0}^4\Delta C_{2,0}$	0	$120E_{2,0}^3\Delta C_{4,0}$
$C_{9,1}$	0	0	$42E_{2,0}^4\Delta C_{1,1}$	0	$48E_{2,0}^3\Delta C_{3,1}$
$C_{8,2}$	$\frac{14}{3}E_{2,0}^4E_{0,2}$	0	$14E_{2,0}^3E_{0,2}\Delta C_{2,0}$	0	$8E_{2,0}^3\Delta C_{2,2}$
$C_{7,3}$	0	0	$14E_{2,0}^3E_{0,2}\Delta C_{1,1}$	0	$8E_{2,0}^2E_{0,2}\Delta C_{3,1}$
$C_{6,4}$	$2E_{2,0}^3E_{0,2}^2$	0	$2E_{2,0}^2E_{0,2}^2\Delta C_{2,0}$	0	$8E_{2,0}^2E_{0,2}\Delta C_{2,2}$
$C_{5,5}$	0	0	$10E_{2,0}^2E_{0,2}^2\Delta C_{1,1}$	0	0

Gaussian Density The bunch is now assumed to have a Gaussian density and a bunch shape according to the mode definition (3.18) and f_0 is chosen such that the integral of f over the phase plane equals unity. The moments for $n_x + n_y \leq 10$ are given in Table C.3. Again, these are first order approximations and because of the symmetry between $C_{i,j}$ and $C_{j,i}$, only half of the results are summarized for higher order modes.

Table C.3: Moments of coherent bunch oscillations for Gaussian densities (first order approximations).

Gaussian Density					
	E_{n_x,n_y}	$\Delta C_{n_x,n_y}(r_1)$	$\Delta C_{n_x,n_y}(r_2)$	$\Delta C_{n_x,n_y}(r_3)$	$\Delta C_{n_x,n_y}(r_4)$
$B_{1,0}$	0	$-\frac{3}{2}\sqrt{\frac{\pi}{2}}\sigma_0\sin(\theta_0)r_1$	0	0	0
$B_{0,1}$	0	$\frac{3}{2}\sqrt{\frac{\pi}{2}}\sigma_0\cos(\theta_0)r_1$	0	0	0
$C_{2,0}$	$E_{2,0} = \sigma_0^2$	0	$-2\sigma_0^2\sin(2\theta_0)r_2$	0	0
$C_{1,1}$	0	0	$2\sigma_0^2\cos(2\theta_0)r_2$	0	0
$C_{0,2}$	$E_{0,2} = \sigma_0^2$	0	$2\sigma_0^2\sin(2\theta_0)r_2$	0	0
$C_{3,0}$	0	$\frac{3}{4}E_{2,0}B_{1,0}$	0	$-\frac{15}{8}\sqrt{\frac{\pi}{2}}\sigma_0^3\sin(3\theta_0)r_3$	0
$C_{2,1}$	0	$\frac{1}{4}E_{2,0}B_{0,1}$	0	$\frac{15}{8}\sqrt{\frac{\pi}{2}}\sigma_0^3\cos(3\theta_0)r_3$	0
$C_{1,2}$	0	$\frac{1}{4}E_{0,2}B_{1,0}$	0	$\frac{15}{8}\sqrt{\frac{\pi}{2}}\sigma_0^3\sin(3\theta_0)r_3$	0
$C_{0,3}$	0	$\frac{3}{4}E_{0,2}B_{0,1}$	0	$-\frac{15}{8}\sqrt{\frac{\pi}{2}}\sigma_0^3\cos(3\theta_0)r_3$	0
$C_{4,0}$	$3E_{2,0}^2$	0	$6E_{2,0}\Delta C_{2,0}$	0	$-3\sigma_0^4\sin(4\theta_0)r_4$
$C_{3,1}$	0	0	$3E_{2,0}\Delta C_{1,1}$	0	$3\sigma_0^4\cos(4\theta_0)r_4$
$C_{2,2}$	$E_{2,0}E_{0,2}$	0	0	0	$3\sigma_0^4\sin(4\theta_0)r_4$
$C_{1,3}$	0	0	$3E_{0,2}\Delta C_{1,1}$	0	$-3\sigma_0^4\cos(4\theta_0)r_4$
$C_{0,4}$	$3E_{0,2}^2$	0	$6E_{0,2}\Delta C_{0,2}$	0	$-3\sigma_0^4\sin(4\theta_0)r_4$
$C_{5,0}$	0	$\frac{55}{8}E_{2,0}^2B_{1,0}$	0	$\frac{35}{4}E_{2,0}\Delta C_{3,0}$	0
$C_{4,1}$	0	$\frac{11}{8}E_{2,0}^2B_{0,1}$	0	$\frac{21}{4}E_{2,0}\Delta C_{2,1}$	0
$C_{3,2}$	0	$\frac{11}{8}E_{2,0}E_{0,2}B_{1,0}$	0	$\frac{7}{4}E_{2,0}\Delta C_{1,2}$	0
$C_{6,0}$	$15E_{2,0}^3$	0	$45E_{2,0}^2\Delta C_{2,0}$	0	$12E_{2,0}\Delta C_{4,0}$
$C_{5,1}$	0	0	$15E_{2,0}^2\Delta C_{1,1}$	0	$8E_{2,0}\Delta C_{3,1}$

Continued on next page

Table C.4: State vector $\boldsymbol{x} = [x_1\ x_2\ \ldots]^{\mathrm{T}}$.

$x_1 = B_{1,0}$	$x_3 = C_{2,0}$	$x_6 = C_{3,0}$	$x_{10} = C_{4,0}$
$x_2 = B_{0,1}$	$x_4 = C_{1,1}$	$x_7 = C_{2,1}$	$x_{11} = C_{3,1}$
	$x_5 = C_{0,2}$	$x_8 = C_{1,2}$	$x_{12} = C_{2,2}$
		$x_9 = C_{0,3}$	$x_{13} = C_{1,3}$
			$x_{14} = C_{0,4}$

Table C.3 – continued from previous page

Gaussian Density					
	E_{n_x,n_y}	$\Delta C_{n_x,n_y}(r_1)$	$\Delta C_{n_x,n_y}(r_2)$	$\Delta C_{n_x,n_y}(r_3)$	$\Delta C_{n_x,n_y}(r_4)$
$C_{4,2}$	$3E_{2,0}^2 E_{0,2}$	0	$3E_{2,0}E_{0,2}\Delta C_{2,0}$	0	$4E_{2,0}\Delta C_{2,2}$
$C_{3,3}$	0	0	$9E_{2,0}E_{0,2}\Delta C_{1,1}$	0	0
$C_{7,0}$	0	$\frac{4305}{64} E_{2,0}^3 B_{1,0}$	0	$\frac{1323}{16} E_{2,0}^2 \Delta C_{3,0}$	0
$C_{6,1}$	0	$\frac{615}{64} E_{2,0}^3 B_{0,1}$	0	$\frac{567}{16} E_{2,0}^2 \Delta C_{2,1}$	0
$C_{5,2}$	0	$\frac{615}{64} E_{2,0}^2 E_{0,2} B_{1,0}$	0	$\frac{63}{16} E_{2,0}^2 \Delta C_{1,2}$	0
$C_{4,3}$	0	$\frac{369}{64} E_{2,0}^2 E_{0,2} B_{0,1}$	0	$\frac{189}{16} E_{2,0}E_{0,2}\Delta C_{2,1}$	0
$C_{8,0}$	$105E_{2,0}^4$	0	$420E_{2,0}^3\Delta C_{2,0}$	0	$140E_{2,0}^2\Delta C_{4,0}$
$C_{7,1}$	0	0	$105E_{2,0}^3\Delta C_{1,1}$	0	$70E_{2,0}^2\Delta C_{3,1}$
$C_{6,2}$	$15E_{2,0}^3 E_{0,2}$	0	$30E_{2,0}^2 E_{0,2}\Delta C_{2,0}$	0	$20E_{2,0}^2\Delta C_{2,2}$
$C_{5,3}$	0	0	$45E_{2,0}^2 E_{0,2}\Delta C_{1,1}$	0	$10E_{2,0}E_{0,2}\Delta C_{3,1}$
$C_{4,4}$	$9E_{2,0}^2 E_{0,2}^2$	0	0	0	$20E_{2,0}E_{0,2}\Delta C_{2,2}$
$C_{9,0}$	0	$\frac{97335}{128} E_{2,0}^4 B_{1,0}$	0	$\frac{14553}{16} E_{2,0}^3 \Delta C_{3,0}$	0
$C_{8,1}$	0	$\frac{10815}{128} E_{2,0}^4 B_{0,1}$	0	$\frac{4851}{16} E_{2,0}^3 \Delta C_{2,1}$	0
$C_{7,2}$	0	$\frac{10815}{128} E_{2,0}^3 E_{0,2} B_{1,0}$	0	0	0
$C_{6,3}$	0	$\frac{4635}{128} E_{2,0}^3 E_{0,2} B_{0,1}$	0	$\frac{693}{8} E_{2,0}^2 E_{0,2}\Delta C_{2,1}$	0
$C_{5,4}$	0	$\frac{4635}{128} E_{2,0}^2 E_{0,2} B_{1,0}$	0	$\frac{693}{16} E_{2,0}^2 E_{0,2}\Delta C_{1,2}$	0
$C_{10,0}$	$945E_{2,0}^5$	0	$4725E_{2,0}^4\Delta C_{2,0}$	0	$1800E_{2,0}^3\Delta C_{4,0}$
$C_{9,1}$	0	0	$945E_{2,0}^4\Delta C_{1,1}$	0	$720E_{2,0}^3\Delta C_{3,1}$
$C_{8,2}$	$105E_{2,0}^4 E_{0,2}$	0	$315E_{2,0}^3 E_{0,2}\Delta C_{2,0}$	0	$120E_{2,0}^3\Delta C_{2,2}$
$C_{7,3}$	0	0	$315E_{2,0}^3 E_{0,2}\Delta C_{1,1}$	0	$120E_{2,0}^2 E_{0,2}\Delta C_{3,1}$
$C_{6,4}$	$45E_{2,0}^3 E_{0,2}^2$	0	$45E_{2,0}^2 E_{0,2}^2\Delta C_{2,0}$	0	$120E_{2,0}^2 E_{0,2}\Delta C_{2,2}$
$C_{5,5}$	0	0	$225E_{2,0}^2 E_{0,2}^2\Delta C_{1,1}$	0	0

C.3 Moment Dynamics in a Linear Stationary Bucket

For $n_{\text{model}} = 4$, system Σ_{LB} of (4.30) has the state vector $\boldsymbol{x}$ as defined by (4.31) with dimension $L = 14$. The states are shown in Table C.4. The dynamics are

$$\dot{\boldsymbol{x}} = \mathbf{A}_{\text{LB}}\boldsymbol{x} + \mathbf{B}_{\text{LB}}(\boldsymbol{x})\boldsymbol{u} = \begin{bmatrix} \mathbf{A}_1 & \mathbf{0} & \mathbf{0} & \mathbf{0} \\ \mathbf{0} & \mathbf{A}_2 & \mathbf{0} & \mathbf{0} \\ \mathbf{0} & \mathbf{0} & \mathbf{A}_3 & \mathbf{0} \\ \mathbf{0} & \mathbf{0} & \mathbf{0} & \mathbf{A}_4 \end{bmatrix} \boldsymbol{x} + \begin{bmatrix} \mathbf{b}_{1,1} & \mathbf{b}_{1,2} \\ \mathbf{b}_2 & \mathbf{0} \\ \mathbf{b}_3 & \mathbf{0} \\ \mathbf{b}_4 & \mathbf{0} \end{bmatrix} \begin{bmatrix} u_1 \\ u_2 \end{bmatrix}$$

with

$$\mathbf{A}_1 = \omega_{\text{syn}} \begin{bmatrix} 0 & -1 \\ 1 & 0 \end{bmatrix}, \quad \mathbf{A}_2 = \omega_{\text{syn}} \begin{bmatrix} 0 & -2 & 0 \\ 1 & 0 & -1 \\ 0 & 2 & 0 \end{bmatrix},$$

$$\mathbf{A}_3 = \omega_{\text{syn}} \begin{bmatrix} 0 & -3 & 0 & 0 \\ 1 & 0 & -2 & 0 \\ 0 & 2 & 0 & -1 \\ 0 & 0 & 3 & 0 \end{bmatrix}, \quad \mathbf{A}_4 = \omega_{\text{syn}} \begin{bmatrix} 0 & -4 & 0 & 0 & 0 \\ 1 & 0 & -3 & 0 & 0 \\ 0 & 2 & 0 & -2 & 0 \\ 0 & 0 & 3 & 0 & -1 \\ 0 & 0 & 0 & 4 & 0 \end{bmatrix},$$

and

$$\frac{\mathbf{b}_{1,1}}{\omega_{\text{syn}}} = \begin{bmatrix} 0 & B_{1,0} \end{bmatrix}^{\mathrm{T}}, \frac{\mathbf{b}_{1,2}}{\omega_{\text{syn}}} = \begin{bmatrix} 0 & 1 \end{bmatrix}^{\mathrm{T}}, \frac{\mathbf{b}_2}{\omega_{\text{syn}}} = \begin{bmatrix} 0 & C_{2,0} & 2C_{1,1} \end{bmatrix}^{\mathrm{T}},$$

$$\frac{\mathbf{b}_3}{\omega_{\text{syn}}} = \begin{bmatrix} 0 & C_{3,0} & 2C_{2,1} & 3C_{1,2} \end{bmatrix}^{\mathrm{T}}, \frac{\mathbf{b}_4}{\omega_{\text{syn}}} = \begin{bmatrix} 0 & C_{4,0} & 2C_{3,1} & 3C_{2,2} & 4C_{1,3} \end{bmatrix}^{\mathrm{T}}.$$

The null vectors and matrices $\mathbf{0}$ are assumed to have the appropriate dimensions to complete their matrices and vectors.

The reduced and linearized system $\Sigma_{\Delta\text{LBR}}$ has the state vector $\Delta\boldsymbol{x}_{\text{LBR}}$ that is obtained from the difference vector $\boldsymbol{x} - \boldsymbol{x}_{\text{e}}$, if the states corresponding to $C_{0,2}$ and $C_{0,4}$ are removed, i. e. the states x_5 and x_{14} (cf. Table C.4). The equilibrium $\boldsymbol{x}_{\text{e}}$ is given in (4.33). System LBR reads

$$\Delta\boldsymbol{x}_{\text{LBR}} = \mathbf{A}_{\text{LBR}}\Delta\boldsymbol{x}_{\text{LBR}} + \mathbf{B}_{\text{LBR}}\boldsymbol{u} = \begin{bmatrix} \tilde{\mathbf{A}}_1 & \mathbf{0} & \mathbf{0} & \mathbf{0} \\ \mathbf{0} & \tilde{\mathbf{A}}_2 & \mathbf{0} & \mathbf{0} \\ \mathbf{0} & \mathbf{0} & \tilde{\mathbf{A}}_3 & \mathbf{0} \\ \mathbf{0} & \mathbf{0} & \mathbf{0} & \tilde{\mathbf{A}}_4 \end{bmatrix} \boldsymbol{x} + \begin{bmatrix} \tilde{\mathbf{b}}_{1,1} & \tilde{\mathbf{b}}_{1,2} \\ \tilde{\mathbf{b}}_2 & \mathbf{0} \\ \tilde{\mathbf{b}}_3 & \mathbf{0} \\ \tilde{\mathbf{b}}_4 & \mathbf{0} \end{bmatrix} \begin{bmatrix} u_1 \\ u_2 \end{bmatrix}$$

with dimension $\tilde{L} = 12$, where

$$\tilde{\mathbf{A}}_1 = \mathbf{A}_1, \quad \tilde{\mathbf{A}}_2 = \omega_{\text{syn}} \begin{bmatrix} 0 & -2 \\ 2 & 0 \end{bmatrix}, \quad \tilde{\mathbf{A}}_3 = \mathbf{A}_3, \quad \tilde{\mathbf{A}}_4 = \omega_{\text{syn}} \begin{bmatrix} 0 & -4 & 0 & 0 \\ 1 & 0 & -3 & 0 \\ 0 & 2 & 0 & -2 \\ 1 & 0 & 5 & 0 \end{bmatrix},$$

and

$$\frac{\tilde{\mathbf{b}}_{1,1}}{\omega_{\text{syn}}} = \begin{bmatrix} 0 \\ 0 \end{bmatrix}, \frac{\tilde{\mathbf{b}}_{1,2}}{\omega_{\text{syn}}} = \begin{bmatrix} 0 \\ 1 \end{bmatrix}, \frac{\tilde{\mathbf{b}}_2}{\omega_{\text{syn}}} = \begin{bmatrix} 0 \\ E_2 \end{bmatrix}, \frac{\tilde{\mathbf{b}}_3}{\omega_{\text{syn}}} = \begin{bmatrix} 0 \\ 0 \\ 0 \\ 0 \end{bmatrix}, \frac{\tilde{\mathbf{b}}_4}{\omega_{\text{syn}}} = \begin{bmatrix} 0 \\ E_4 \\ 0 \\ E_4 \end{bmatrix}.$$

The controllability matrix $\mathcal{C}(\mathbf{A}_{\mathrm{LBR}},\mathbf{B}_{\mathrm{LBR}})$ has dimension 12×24. Its column space is spanned by the vectors

$$\begin{aligned}
\boldsymbol{m}_1 &= \begin{bmatrix}1 & 0 & 0 & 0 & 0 & 0 & 0 & 0 & 0 & 0 & 0 & 0\end{bmatrix}^{\mathrm{T}} \\
\boldsymbol{m}_2 &= \begin{bmatrix}0 & 1 & 0 & 0 & 0 & 0 & 0 & 0 & 0 & 0 & 0 & 0\end{bmatrix}^{\mathrm{T}} \\
\boldsymbol{m}_3 &= \begin{bmatrix}0 & 0 & E_2 & 0 & 0 & 0 & 0 & 0 & 2E_4 & 0 & 0 & 0\end{bmatrix}^{\mathrm{T}} \\
\boldsymbol{m}_4 &= \begin{bmatrix}0 & 0 & 0 & E_2 & 0 & 0 & 0 & 0 & 0 & E_4 & 0 & E_4\end{bmatrix}^{\mathrm{T}}
\end{aligned}$$

C.4 Moment Dynamics in a Nonlinear Stationary Bucket

C.4.1 Equilibrium of the Stationary and Nonlinear Bucket

The Taylor series (4.42) are truncated with $k \leq \hat{k} = 3$. With assumption (4.46), $\varphi_{\mathrm{R}} = 0$, the equilibrium for the moment orders up to $n_{\mathrm{model}} = 4$ reads

$$\begin{bmatrix}B_{1,0}\\B_{0,1}\end{bmatrix} = \begin{bmatrix}0\\0\end{bmatrix}, \quad \begin{bmatrix}C_{2,0}\\C_{1,1}\\C_{0,2}\end{bmatrix} = \begin{bmatrix}E_{2,0}\\0\\E_{0,2} = E_{2,0} - \frac{E_{4,0}}{6} + \frac{E_{6,0}}{120} - \frac{E_{8,0}}{5040}\end{bmatrix}, \quad \begin{bmatrix}C_{3,0}\\C_{2,1}\\C_{1,2}\\C_{0,3}\end{bmatrix} = \begin{bmatrix}0\\0\\0\\0\end{bmatrix},$$

$$\begin{bmatrix}C_{4,0}\\C_{3,1}\\C_{2,2}\\C_{1,3}\\C_{0,4}\end{bmatrix} = \begin{bmatrix}E_{4,0}\\0\\E_{2,2} = \frac{E_{4,0}}{3} - \frac{E_{6,0}}{18} + \frac{E_{8,0}}{360} - \frac{E_{10,0}}{15120}\\0\\E_{0,4} = E_{4,0} - \frac{E_{6,0}}{6} - \frac{E_{4,2}}{2} + \frac{E_{8,0}}{120} + \frac{E_{6,2}}{40} - \frac{E_{10,0}}{5040} - \frac{E_{8,2}}{1680}\end{bmatrix}$$

C.4.2 Linearized Dynamics

The linearization of the nonlinear dynamics around the equilibrium of Section C.4.1 is presented for a stationary bucket. The nonlinear dynamics are calculated according to Section 4.6.1 with $\varphi_{\mathrm{R}} = 0$, $\hat{k} = 3$. The dynamics of moments up to the order $n = n_{\mathrm{model}} = 4$ are summarized in this section. The equilibrium values E_{n_x,n_y} are given in Section C.4.1 and the deviations from this equilibrium are $\Delta C_{n_x,n_y} = C_{n_x,n_y} - E_{n_x,n_y}$. For the basic moments $B_{1,0} = \Delta B_{1,0}$ and $B_{0,1} = \Delta B_{0,1}$ holds. The dynamics of the basic moments are

$$\frac{\Delta \dot{B}_{1,0}}{\omega_{\mathrm{syn}}} = -\Delta B_{0,1} \tag{C.1a}$$

$$\begin{aligned}
\frac{\Delta \dot{B}_{0,1}}{\omega_{\mathrm{syn}}} = &\left[1 - \frac{E_{2,0}}{2} + \frac{E_{4,0}}{24} - \frac{E_{6,0}}{720}\right]\left[\Delta B_{1,0} - u_\varphi\right] - \frac{1}{6}\Delta C_{3,0} + \\
&+ \frac{1}{120}\Delta C_{5,0} - \frac{1}{5040}\Delta C_{7,0}
\end{aligned} \tag{C.1b}$$

The dynamics of the central moments of order $n = 2$ are given by

$$\frac{\Delta\dot{C}_{2,0}}{\omega_{\text{syn}}} = -2\Delta C_{1,1} \tag{C.2a}$$

$$\frac{\Delta\dot{C}_{1,1}}{\omega_{\text{syn}}} = \Delta C_{2,0} - \Delta C_{0,2} - \frac{1}{6}\Delta C_{4,0} + \frac{1}{120}\Delta C_{6,0} - \frac{1}{5040}\Delta C_{8,0} + \\ + \left[E_{2,0} - \frac{E_{4,0}}{6} + \frac{E_{6,0}}{120} - \frac{E_{8,0}}{5040}\right] u_\epsilon \tag{C.2b}$$

$$\frac{\Delta\dot{C}_{0,2}}{\omega_{\text{syn}}} = 2\Delta C_{1,1} - \frac{1}{3}\Delta C_{3,1} + \frac{1}{60}\Delta C_{5,1} - \frac{1}{2520}\Delta C_{7,1} \tag{C.2c}$$

The dynamics of the central moments of order $n = 3$ read

$$\frac{\Delta\dot{C}_{3,0}}{\omega_{\text{syn}}} = -3\Delta C_{2,1}$$

$$\frac{\Delta\dot{C}_{2,1}}{\omega_{\text{syn}}} = \left[\frac{1}{2}\left[E_{2,0}^2 - E_{4,0}\right] + \frac{1}{24}\left[E_{6,0} - E_{2,0}E_{4,0}\right] + \frac{1}{720}\left[E_{2,0}E_{6,0} - E_{8,0}\right]\right] \cdot \\ \cdot \left[\Delta B_{1,0} - u_\varphi\right] + \left[1 + \frac{E_{2,0}}{6}\right]\Delta C_{3,0} - 2\Delta C_{1,2} - \left[\frac{1}{6} + \frac{E_{2,0}}{120}\right]\Delta C_{5,0} + \\ + \left[\frac{1}{120} + \frac{E_{2,0}}{5040}\right]\Delta C_{7,0} - \frac{1}{5040}\Delta C_{9,0}$$

$$\frac{\Delta\dot{C}_{1,2}}{\omega_{\text{syn}}} = 2\Delta C_{2,1} - \Delta C_{0,3} - \frac{1}{3}\Delta C_{4,1} + \frac{1}{60}\Delta C_{6,1} - \frac{1}{2520}\Delta C_{8,1}$$

$$\frac{\Delta\dot{C}_{0,3}}{\omega_{\text{syn}}} = \left[\frac{3}{2}\left[E_{2,0}E_{0,2} - E_{2,2}\right] + \frac{1}{8}\left[E_{4,2} - E_{0,2}E_{4,0}\right] + \frac{1}{240}\left[E_{0,2}E_{6,0} - E_{6,2}\right]\right] \cdot \\ \cdot \left[\Delta B_{1,0} - u_\varphi\right] + \frac{E_{0,2}}{2}\Delta C_{3,0} + 3\Delta C_{1,2} - \frac{E_{0,2}}{40}C_{5,0} - \frac{1}{2}\Delta C_{3,2} + \frac{1}{40}\Delta C_{5,2} + \\ + \frac{E_{0,2}}{1680}\Delta C_{7,0} - \frac{1}{1680}\Delta C_{7,2}$$

The dynamics of the central moments of order $n = 4$ are

$$\frac{\Delta\dot{C}_{4,0}}{\omega_{\text{syn}}} = -4\Delta C_{3,1}$$

$$\frac{\Delta\dot{C}_{3,1}}{\omega_{\text{syn}}} = \Delta C_{4,0} - 3\Delta C_{2,2} - \frac{1}{6}\Delta C_{6,0} + \frac{1}{120}\Delta C_{8,0} - \frac{1}{5040}\Delta C_{10,0} + \\ + \left[E_{4,0} - \frac{E_{6,0}}{6} + \frac{E_{8,0}}{120} - \frac{E_{10,0}}{5040}\right] u_\epsilon$$

$$\frac{\Delta\dot{C}_{2,2}}{\omega_{\text{syn}}} = 2\Delta C_{3,1} - 2\Delta C_{1,3} - \frac{1}{3}\Delta C_{5,1} + \frac{1}{60}\Delta C_{7,1}$$
$$\frac{\Delta\dot{C}_{1,3}}{\omega_{\text{syn}}} = 3\Delta C_{2,2} - \Delta C_{0,4} - \frac{1}{2}\Delta C_{4,2} + \frac{1}{40}\Delta C_{6,2} + \left[3E_{2,2} - \frac{E_{4,2}}{2} + \frac{E_{6,2}}{40} - \frac{E_{8,2}}{1680}\right] u_\epsilon$$
$$\frac{\Delta\dot{C}_{0,4}}{\omega_{\text{syn}}} = 4\Delta C_{1,3} - \frac{2}{3}\Delta C_{3,3} + \frac{1}{30}\Delta C_{5,3}$$

C.4.3 Models for Coherent Modes

In this section, $\hat{k} = 3$ and $n_{\text{model}} \in \{1,2,4\}$ were chosen to obtain transfer functions for the dipole and quadrupole mode in a nonlinear stationary bucket ($\varphi_{\text{R}} = 0$).

Mode $m = 1$ For the choice $\hat{k} = 3$, $n_{\text{model}} = 1$, the transfer function has the shape

$$G_1(s) = \frac{\Delta B_{1,0}(s)}{u_\varphi(s)} = \frac{b_1\omega_{\text{syn}}^2}{s^2 + a_1\omega_{\text{syn}}^2}. \tag{C.3}$$

For a uniform density and with Table C.2

$$a_1 = b_1 = 1 - \frac{E_{2,0}}{2} + \frac{E_{2,0}^2}{12} - \frac{E_{2,0}^3}{144}.$$

For a Gaussian density and with Table C.3

$$a_1 = 1 - \frac{5E_{2,0}}{8} + \frac{35E_{2,0}^2}{192} - \frac{35E_{2,0}^3}{1024}, \quad b_1 = 1 - \frac{E_{2,0}}{2} + \frac{E_{2,0}^2}{8} - \frac{E_{2,0}^3}{48}.$$

Mode $m = 2$ The transfer function of $m = 2$ is given by

$$G_2(s) = \frac{\Delta C_{2,0}(s)}{u_\epsilon(s)} = \frac{s}{s} \cdot \frac{b_2\omega_{\text{syn}}^2}{s^2 + a_2\omega_{\text{syn}}^2}.$$

For a uniform density, the columns for E_{n_x,n_y} and $\Delta C_{n_x,n_y}(r_2)$ of Table C.2 yield

$$E_{4,0} = 2E_{2,0}^2, \quad E_{6,0} = 5E_{2,0}^3, \quad E_{8,0} = 14E_{2,0}^4$$
$$\Delta C_{4,0} = 4E_{2,0}\Delta C_{2,0}, \quad \Delta C_{6,0} = 15E_{2,0}^2\Delta C_{2,0}, \quad \Delta C_{8,0} = 56E_{2,0}^3\Delta C_{2,0}$$
$$\Delta C_{3,1} = 2E_{2,0}\Delta C_{1,1}, \quad \Delta C_{5,1} = 5E_{2,0}^2\Delta C_{1,1}, \quad \Delta C_{7,1} = 14E_{2,0}^3\Delta C_{1,1}$$

This leads to

$$a_2 = 4\left[1 - \frac{E_{2,0}}{2} + \frac{E_{2,0}^2}{12} - \frac{E_{2,0}^3}{144}\right], \quad b_2 = -2E_{2,0}\left[1 - \frac{E_{2,0}}{3} + \frac{E_{2,0}^2}{24} - \frac{E_{2,0}^3}{360}\right]$$

For a Gaussian density, the columns for E_{n_x,n_y} and $\Delta C_{n_x,n_y}(r_2)$ of Table C.3 yield

$$\begin{aligned}
&E_{4,0} = 3E_{2,0}^2, \quad E_{6,0} = 15E_{2,0}^3, \quad E_{8,0} = 105E_{2,0}^4 \\
&\Delta C_{4,0} = 6E_{2,0}\Delta C_{2,0}, \quad \Delta C_{6,0} = 45E_{2,0}^2\Delta C_{2,0}, \quad \Delta C_{8,0} = 420E_{2,0}^3\Delta C_{2,0} \\
&\Delta C_{3,1} = 3E_{2,0}\Delta C_{1,1}, \quad \Delta C_{5,1} = 15E_{2,0}^2\Delta C_{1,1}, \quad \Delta C_{7,1} = 105E_{2,0}^3\Delta C_{1,1}
\end{aligned}$$

This leads to

$$a_2 = 4\left[1 - \frac{3E_{2,0}}{4} + \frac{E_{2,0}^2}{4} - \frac{5E_{2,0}^3}{96}\right], \quad b_2 = -2E_{2,0}\left[1 - \frac{E_{2,0}}{2} + \frac{E_{2,0}^2}{8} - \frac{E_{2,0}^3}{48}\right]$$

Modes $m \in \{1,2,3,4\}$ The dynamics of the moments of order $n_x + n_y \in \{1,3\}$ are

$$\Delta\dot{\boldsymbol{x}}_{\text{odd}} = \mathbf{A}_{\text{odd}}(E_{2,0})\Delta\boldsymbol{x}_{\text{odd}} + \boldsymbol{b}_{\text{odd}}(E_{2,0})u_2$$

with

$$\mathbf{A}_{\text{odd}} = \omega_{\text{syn}}\left[\begin{array}{cc|cccc} 0 & -1 & 0 & 0 & 0 & 0 \\ a_{2,1} & 0 & a_{2,3} & 0 & 0 & 0 \\ \hline 0 & 0 & 0 & -3 & 0 & 0 \\ a_{4,1} & 0 & a_{4,3} & 0 & -2 & 0 \\ 0 & a_{5,2} & 0 & a_{5,4} & 0 & -1 \\ a_{6,1} & 0 & a_{6,3} & 0 & a_{6,5} & 0 \end{array}\right], \quad \boldsymbol{b}_{\text{odd}} = \omega_{\text{syn}}\left[\begin{array}{c} 0 \\ b_2 \\ \hline 0 \\ b_4 \\ 0 \\ b_6 \end{array}\right].$$

For a uniform density, the entries are

$$\begin{aligned}
a_{2,1} &= 1 - \frac{1}{2}E_{2,0} + \frac{1}{12}E_{2,0}^2 - \frac{1}{144}E_{2,0}^3, \quad a_{4,1} = -\frac{1}{2}E_{2,0}^2 + \frac{1}{8}E_{2,0}^3 - \frac{1}{80}E_{2,0}^4 \\
a_{6,1} &= \frac{1}{2}E_{2,0}^2 - \frac{5}{24}E_{2,0}^3 + \frac{7}{120}E_{2,0}^4 - \frac{3}{320}E_{2,0}^5 + \frac{1}{1920}E_{2,0}^6, \quad a_{5,2} = 0 \\
a_{2,3} &= -\frac{1}{6} + \frac{1}{30}E_{2,0} - \frac{1}{240}E_{2,0}^2, \quad a_{4,3} = 1 - \frac{2}{3}E_{2,0} + \frac{2}{15}E_{2,0}^2 - \frac{1}{80}E_{2,0}^3 \\
a_{6,3} &= \frac{1}{2}E_{2,0} - \frac{7}{24}E_{2,0}^2 + \frac{3}{40}E_{2,0}^3 - \frac{3}{320}E_{2,0}^4 + \frac{1}{1920}E_{2,0}^5 \\
a_{5,4} &= 2 - E_{2,0} + \frac{3}{20}E_{2,0}^2 - \frac{1}{90}E_{2,0}^3, \quad a_{6,5} = 3 - \frac{1}{2}E_{2,0} + \frac{1}{40}E_{2,0}^2 \\
b_2 &= -1 + \frac{1}{2}E_{2,0} - \frac{1}{12}E_{2,0}^2, \quad b_4 = \frac{1}{2}E_{2,0}^2 - \frac{1}{8}E_{2,0}^3 + \frac{1}{80}E_{2,0}^4 \\
b_6 &= -\frac{1}{2}E_{2,0}^2 + \frac{5}{24}E_{2,0}^3 - \frac{7}{120}E_{2,0}^4 + \frac{3}{320}E_{2,0}^5 - \frac{1}{1920}E_{2,0}^6
\end{aligned}$$

For a Gaussian density, the entries are

$$a_{2,1} = 1 - \frac{1}{2}E_{2,0} + \frac{49}{384}E_{2,0}^2 - \frac{7}{320}E_{2,0}^3, \quad a_{4,1} = -\frac{101}{96}E_{2,0}^2 + \frac{1039}{1920}E_{2,0}^3 - \frac{857}{6144}E_{2,0}^4$$
$$a_{6,1} = -\frac{15}{32}E_{2,0}^2 + \frac{603}{640}E_{2,0}^3 - \frac{4707}{10240}E_{2,0}^4 + \frac{203}{4096}E_{2,0}^5 - \frac{483}{81920}E_{2,0}^6$$
$$a_{5,2} = -\frac{1}{48}E_{2,0}^2 + \frac{1}{80}E_{2,0}^3 - \frac{53}{15360}E_{2,0}^4$$
$$a_{2,3} = -\frac{1}{6} + \frac{7}{96}E_{2,0} - \frac{21}{1280}E_{2,0}^2, \quad a_{4,3} = 1 - \frac{31}{24}E_{2,0} + \frac{1183}{1920}E_{2,0}^2 - \frac{21}{128}E_{2,0}^3$$
$$a_{6,3} = \frac{1}{2}E_{2,0} - \frac{15}{32}E_{2,0}^2 + \frac{283}{1280}E_{2,0}^3 - \frac{133}{2560}E_{2,0}^4 + \frac{63}{10240}E_{2,0}^5$$
$$a_{5,4} = 2 - \frac{7}{4}E_{2,0} + \frac{189}{320}E_{2,0}^2 - \frac{77}{640}E_{2,0}^3, \quad a_{6,5} = 3 - \frac{7}{8}E_{2,0} + \frac{63}{640}E_{2,0}^2$$
$$b_2 = -1 + \frac{1}{2}E_{2,0} - \frac{1}{8}E_{2,0}^2, \quad b_4 = E_{2,0}^2 - \frac{1}{2}E_{2,0}^3 + \frac{1}{8}E_{2,0}^4, \quad b_6 = -\frac{1}{2}E_{2,0}^3 + \frac{1}{4}E_{2,0}^4$$

The dynamics of the moments of order $n_x + n_y \in \{2,4\}$ are

$$\Delta\dot{\boldsymbol{x}}_{\text{even}} = \mathbf{A}_{\text{even}}(E_{2,0})\Delta\boldsymbol{x}_{\text{even}} + \boldsymbol{b}_{\text{even}}(E_{2,0})u_1$$

with

$$\frac{\mathbf{A}_{\text{even}}}{\omega_{\text{syn}}} = \left[\begin{array}{ccc|ccccc} 0 & -2 & 0 & 0 & 0 & 0 & 0 & 0 \\ a_{2,1} & 0 & -1 & a_{2,4} & 0 & 0 & 0 & 0 \\ 0 & a_{3,2} & 0 & 0 & a_{3,5} & 0 & 0 & 0 \\ \hline 0 & 0 & 0 & 0 & -4 & 0 & 0 & 0 \\ a_{5,1} & 0 & 0 & a_{5,4} & 0 & -3 & 0 & 0 \\ 0 & a_{6,2} & 0 & 0 & a_{6,5} & 0 & -2 & 0 \\ a_{7,1} & 0 & 0 & 0 & 0 & a_{7,6} & 0 & -1 \\ 0 & a_{8,2} & 0 & 0 & a_{8,5} & 0 & 4 & 0 \end{array}\right], \quad \frac{\boldsymbol{b}_{\text{even}}}{\omega_{\text{syn}}} = \left[\begin{array}{c} 0 \\ b_2 \\ 0 \\ \hline 0 \\ b_5 \\ 0 \\ b_7 \\ 0 \end{array}\right].$$

For a uniform density, the entries are

$$a_{2,1} = 1 - \frac{3}{40}E_{2,0}^2 + \frac{1}{90}E_{2,0}^3, \quad a_{5,1} = \frac{3}{2}E_{2,0}^2 - \frac{7}{15}E_{2,0}^3 + \frac{3}{56}E_{2,0}^4$$
$$a_{7,1} = -\frac{1}{2}E_{2,0}^2 + \frac{4}{15}E_{2,0}^3 - \frac{13}{240}E_{2,0}^4 + \frac{1}{240}E_{2,0}^5, \quad a_{3,2} = 2 - \frac{1}{20}E_{2,0}^2 + \frac{1}{180}E_{2,0}^3$$
$$a_{6,2} = E_{2,0}^2 - \frac{7}{30}E_{2,0}^3, \quad a_{8,2} = -2E_{2,0}^2 + \frac{11}{15}E_{2,0}^3 - \frac{19}{180}E_{2,0}^4 + \frac{1}{360}E_{2,0}^5$$
$$a_{2,4} = -\frac{1}{6} + \frac{1}{20}E_{2,0} - \frac{1}{180}E_{2,0}^2, \quad a_{5,4} = 1 - E_{2,0} + \frac{7}{30}E_{2,0}^2 - \frac{1}{42}E_{2,0}^3$$

$$a_{3,5} = -\frac{1}{3} + \frac{1}{15}E_{2,0} - \frac{1}{180}E_{2,0}^2, \quad a_{6,5} = 2 - \frac{4}{3}E_{2,0} + \frac{7}{30}E_{2,0}^2$$
$$a_{8,5} = \frac{1}{15}E_{2,0}^2 - \frac{1}{45}E_{2,0}^3 + \frac{1}{360}E_{2,0}^4, \quad a_{7,6} = 3 - E_{2,0} + \frac{1}{10}E_{2,0}^2$$
$$b_2 = E_{2,0} - \frac{1}{3}E_{2,0}^2 + \frac{1}{24}E_{2,0}^3 - \frac{1}{360}E_{2,0}^4, \quad b_5 = 2E_{2,0}^2 - \frac{5}{6}E_{2,0}^3 + \frac{7}{60}E_{2,0}^4 - \frac{1}{120}E_{2,0}^5,$$
$$b_7 = 2E_{2,0}^2 - \frac{4}{3}E_{2,0}^3 + \frac{1}{3}E_{2,0}^4 - \frac{29}{720}E_{2,0}^5 + \frac{13}{4320}E_{2,0}^6 - \frac{1}{8640}E_{2,0}^7.$$

For a Gaussian density, the entries are

$$a_{2,1} = 1 - \frac{9}{40}E_{2,0}^2 + \frac{1}{12}E_{2,0}^3, \quad a_{5,1} = \frac{9}{2}E_{2,0}^2 - \frac{7}{2}E_{2,0}^3 + \frac{135}{112}E_{2,0}^4$$
$$a_{7,1} = -\frac{3}{2}E_{2,0}^2 + \frac{3}{2}E_{2,0}^3 - \frac{9}{16}E_{2,0}^4 + \frac{3}{32}E_{2,0}^5, \quad a_{3,2} = 2 - \frac{3}{20}E_{2,0}^2 + \frac{1}{24}E_{2,0}^3$$
$$a_{6,2} = 3E_{2,0}^2 - \frac{7}{4}E_{2,0}^3, \quad a_{8,2} = -6E_{2,0}^2 + \frac{7}{2}E_{2,0}^3 - E_{2,0}^4 + \frac{1}{16}E_{2,0}^5$$
$$a_{2,4} = -\frac{1}{6} + \frac{1}{10}E_{2,0} - \frac{1}{36}E_{2,0}^2, \quad a_{5,4} = 1 - 2E_{2,0} + \frac{7}{6}E_{2,0}^2 - \frac{5}{14}E_{2,0}^3$$
$$a_{3,5} = -\frac{1}{3} + \frac{2}{15}E_{2,0} - \frac{1}{36}E_{2,0}^2, \quad a_{6,5} = 2 - \frac{8}{3}E_{2,0} + \frac{7}{6}E_{2,0}^2$$
$$a_{8,5} = \frac{1}{3}E_{2,0}^2 - \frac{1}{6}E_{2,0}^3 + \frac{1}{24}E_{2,0}^4, \quad a_{7,6} = 3 - 2E_{2,0} + \frac{1}{2}E_{2,0}^2$$
$$b_2 = E_{2,0} - \frac{1}{2}E_{2,0}^2 + \frac{1}{8}E_{2,0}^3 - \frac{1}{48}E_{2,0}^4, \quad b_5 = 3E_{2,0}^2 - \frac{5}{2}E_{2,0}^3 + \frac{7}{8}E_{2,0}^4 - \frac{3}{16}E_{2,0}^5,$$
$$b_7 = 3E_{2,0}^2 - 4E_{2,0}^3 + 2E_{2,0}^4 - \frac{7}{16}E_{2,0}^5 + \frac{5}{64}E_{2,0}^6 - \frac{1}{128}E_{2,0}^7.$$

C.4.4 Models for Ellipsoidal Bunches

For bunches with an ellipsoidal shape, the linearized dynamics are given by

$$\Delta\dot{\boldsymbol{x}}_{\mathrm{ME}} = \begin{bmatrix} \Delta\dot{B}_{1,0} \\ \Delta\dot{B}_{0,1} \\ \Delta\dot{C}_{2,0} \\ \Delta\dot{C}_{1,1} \\ \Delta\dot{C}_{0,2} \end{bmatrix} = \omega_{\mathrm{syn}} \begin{bmatrix} -\Delta B_{0,1} \\ a_1\Delta B_{1,0} \\ -2\Delta C_{1,1} \\ a_2\Delta C_{2,0} - \Delta C_{0,2} \\ a_3\Delta C_{1,1} \end{bmatrix} + \omega_{\mathrm{syn}} \begin{bmatrix} 0 \\ -a_1 u_\varphi \\ 0 \\ b_1 u_\epsilon \\ 0 \end{bmatrix}.$$

The transfer functions of the basic and second order moments are

$$\frac{\Delta B_{1,0}(s)}{u_\varphi(s)} = \frac{a_1}{\frac{s^2}{\omega_{\mathrm{syn}}^2} + a_1}, \qquad \frac{\Delta C_{2,0}(s)}{u_\epsilon(s)} = \frac{s}{s}\frac{-2b_1}{\frac{s^2}{\omega_{\mathrm{syn}}^2} + 2a_2 + a_3}.$$

The calculation for an ellipsoidal bunch with a **uniform density** and with $\hat{k} = 6$ yields

$$
\begin{aligned}
a_1 &= 1 - \frac{E_{2,0}}{2} + \frac{E_{2,0}^2}{12} - \frac{E_{2,0}^3}{144} + \frac{E_{2,0}^4}{2880} - \frac{E_{2,0}^5}{86400} + \frac{E_{2,0}^6}{3628800} \\
b_1 &= E_{2,0} - \frac{E_{2,0}^2}{3} + \frac{E_{2,0}^3}{24} - \frac{E_{2,0}^4}{360} + \frac{E_{2,0}^5}{8640} - \frac{E_{2,0}^6}{302400} + \frac{E_{2,0}^7}{14515200} \\
a_2 &= 1 - \frac{2E_{2,0}}{3} + \frac{E_{2,0}^2}{8} - \frac{E_{2,0}^3}{90} + \frac{E_{2,0}^4}{1728} - \frac{E_{2,0}^5}{50400} + \frac{E_{2,0}^6}{2073600} \\
a_3 &= 2 - \frac{2E_{2,0}}{3} + \frac{E_{2,0}^2}{12} - \frac{E_{2,0}^3}{180} + \frac{E_{2,0}^4}{4320} - \frac{E_{2,0}^5}{151200} + \frac{E_{2,0}^6}{7257600} \\
2a_2 + a_3 &= 4a_1
\end{aligned}
$$

The calculation for an ellipsoidal bunch with a **Gaussian density** and with $\hat{k} = 6$ yields

$$
\begin{aligned}
a_1 &= 1 - \frac{E_{2,0}}{2} + \frac{E_{2,0}^2}{8} - \frac{E_{2,0}^3}{48} + \frac{E_{2,0}^4}{384} - \frac{E_{2,0}^5}{3840} + \frac{E_{2,0}^6}{46080} \\
b_1 &= E_{2,0} - \frac{E_{2,0}^2}{2} + \frac{E_{2,0}^3}{8} - \frac{E_{2,0}^4}{48} + \frac{E_{2,0}^5}{384} - \frac{E_{2,0}^6}{3840} + \frac{E_{2,0}^7}{46080} \\
a_2 &= 1 - E_{2,0} + \frac{3E_{2,0}^2}{8} - \frac{E_{2,0}^3}{12} + \frac{5E_{2,0}^4}{384} - \frac{E_{2,0}^5}{640} + \frac{7E_{2,0}^6}{46080} \\
a_3 &= 2 - E_{2,0} + \frac{E_{2,0}^2}{4} - \frac{E_{2,0}^3}{24} + \frac{E_{2,0}^4}{192} - \frac{E_{2,0}^5}{1920} + \frac{E_{2,0}^6}{23040} \\
2a_2 + a_3 &= 4\left[1 - \frac{3E_{2,0}}{4} + \frac{E_{2,0}^2}{4} - \frac{5E_{2,0}^3}{96} + \frac{E_{2,0}^4}{128} - \frac{7E_{2,0}^5}{7680} + \frac{E_{2,0}^6}{11520}\right]
\end{aligned}
$$

Bibliography

[1] FAIR facility for antiproton and ion research. http://www.fair-facility-for-antiproton-and-ion-research.org.

[2] M. Abramowitz and I.A. Stegun, editors. *Handbook of Mathematical Functions with Formulas, Graphs, and Mathematical Tables*. New York: Dover, 1972.

[3] W. Ackermann and T. Weiland. Efficient time integration for beam dynamics simulations based on the moment method. In *Proceedings of ICAP 2006, Chamonix, France*, 2006.

[4] W. Ackermann and T. Weiland. Flexible implementation of the ensemble model with arbitrary order of moments. *Nuclear Instruments & Methods in Physics Research A*, 558:274–276, 2006.

[5] W. Ackermann, M. Krasilnikov, T. Weiland, W. Beinhauer, H.-D. Gräf, and A. Richter. Simulation of particle dynamics in accelerators using the ensemble model. In *Proceedings of the 2003 Particle Accelerator Conference*, Portland, Oregon, 2003.

[6] J. Adamy. *Nichtlineare Regelungen*. Springer-Verlag Berlin Heidelberg, 2009.

[7] M. E. Angoletta, J. Bento, A. Blas, A. Findlay, P. Matuszkiewicz, A. Salom-Sarasqueta, and F. Pedersen. Beam tests of a new digital beam control system for the CERN LEIR accelerator. In *Proceedings of 2005 Particle Accelerator Conference*, pages 1649–1651, Knoxville, Tennessee, May 2005.

[8] K. J. Aström and R. M. Murray. *Feedback Systems: An Introduction for Scientists and Engineers*. Princeton University Press, 2008. URL `http://www.cds.caltech.edu/~murray/wiki/Main_Page`.

[9] K. J. Aström and B. Wittenmark. *Computer-Controlled Systems*. Prentice Hall, 1997.

[10] R. Bellman and K. L. Cooke. *Differential-Difference Equations*, volume 6 of *Mathematics in Science and Engineering*. Academic Press, New York, London, 1963.

[11] M. Berz and H. Wollnik. Simulation of intense particle beams with regularly distributed gaussian subbeams. *Nuclear Instruments and Methods in Physics Research*, A267:25–34, 1988.

[12] D. Boussard. Design of a ring RF system. Technical report, CERN SL, 1991.

[13] D. Boussard. Design of a ring RF system. In *Proc. of the 1991 CERN Accelerator School on RF Engineering for Particle Accelerators*, 1992.

[14] C. Bovet, R. Gouiran, I. Gumowski, and K.H. Reich. A selection of formulae and data useful for the design of a.g. synchrotrons. Technical report, CERN/MPS-SI/Int. DL/70/4, 23 April 1970.

[15] K. Burg, H. Haf, and F. Wille. *Partielle Differentialgleichungen*. B. G. Teubner Stuttgart, Leipzig, Wiesbaden, 3rd edition, 2004.

[16] G. Carron, H. Herr, G. Lebee, H. Koziol, F. Krienen, D. Möhl, G. Petrucci, C. Rubbia, F. Sacherer, B. Sadoulet, G. Stefanini, L. Thorndahl, S. Van der Meer, and T. Wikberg. Experiments on stochastic cooling in ice (initial cooling experiment). *IEEE Transactions on Nuclear Science*, NS-26(3):3455–3461, 1979.

[17] F. Caspers. Stochastic cooling. CERN/PS 96-03 (1996), Proceedings of the Workshop on Beam Crystallization and Related Topics, Erice, Nov. 1995.

[18] P. J. Channell. The moment approach to charged particle beam dynamics. *IEEE Transactions on Nuclear Science*, NS-30(4):2607–2609, August 1983.

[19] A. W. Chao. *Physics of Collective Beam Instabilities in High Energy Accelerators*. John Wiley & Sons, 1993.

[20] A. W. Chao and M. Tigner, editors. *Handbook of Accelerator Physics and Engineering*. World Scientific Pub. Co., 3rd printing edition, 2009.

[21] G. Chesi. LMI techniques for optimization over polynomials in control: a survey. *IEEE Transactions on Automatic Control*, 55(11):2500–2510, 2010.

[22] E. D. Courant and H. S. Snyder. Theory of the alternating-gradient synchrotron. *Annals of Physics*, 3(1):1–48, January 1958.

[23] R. Courant and D. Hilbert. *Methoden der Mathematischen Physik II:*. Springer-Verlag Berlin, Heidelberg, New York, 2nd edition, 1968.

[24] H. Damerau. *Creation and storage of long and flat bunches in the LHC*. PhD thesis, TU Darmstadt, 2005.

[25] G. Dome. Theory of RF acceleration. In *CAS - CERN Accelerator School: Accelerator Physics*, pages 110–158, Geneva, Switzerland, 16-27 Sep 1985.

[26] O. Föllinger. Zur Stabilität von Totzeitsystemen. *Regelungstechnik*, pages 145–149, 1967.

[27] O. Föllinger. *Regelungstechnik: Einführung in die Methoden und ihre Anwendung*. Hüthig Buch Verlag, Heidelberg, 1990.

[28] O. Föllinger. *Laplace- und Fourier-Transformation*. Heidelberg: Hüthig, 1990.

[29] S. Franke, W. Ackermann, and T. Weiland. A fast and universal Vlasov solver for beam dynamics simulations in 3D. In *Proceedings of ICAP 2009*, Oslo, 2009.

[30] J. Gareyte. Beam observation and the nature of instabilities. In R. G. Lerner, editor, *AIP Conference Proceedings 184, Vol. 1, Physics of Particle Accelerators*, pages pp.343–429, 1989.

[31] J. Gareyte. *Frontiers of Particle Beams: Intensity Limitations*, chapter Observation and Correction of Instabilities in Circular Accelerators, pages 134–167. Lecture Notes in Physics. Springer-Verlag, 1992.

[32] R. Gouiran. Fünf Protonensynchrotrons. *Philips Technische Rundschau*, 30(11/12):343–382, 1969/70.

[33] T. Gußner. *Reglerentwurf für nichtlineare Systeme mit Stellgrößenbeschränkungen*. PhD thesis, Technische Universität Darmstadt, 2011.

[34] T. Gußner and J. Adamy. Controller design for polynomial systems with input constraints. In *Joint 48th IEEE Conf. on Decision and Control and 28th Chinese Control Conference*, pages 6917–6922, Shanghai, P.R. China, Dec. 16-18 2009.

[35] H. H. Gutbrod. International facility for antiproton and ion research (FAIR) at GSI, darmstadt. *Nuclear Physics A*, 752:457c–469c, 2005.

[36] T. Gußner. Entwurf sättigender Regler für polynomiale Systeme mit Stellgrößenbeschränkung. *at - Automatisierungstechnik*, 2010.

[37] W. Hackbusch, H. R. Schwarz, and E. Zeidler. *Teubner-Taschenbuch der Mathematik*. B. G. Teubner Stuttgart, Leipzig, 1996.

[38] S. Hancock, M. Lindroos, E. McIntosh, and M. Metcalf. Tomographic measurements of longitudinal phase space density. *Computer Physics Communications*, 118:61–70, 1999.

[39] S. Hancock, M. Lindroos, and S. Koscielniak. Longitudinal phase space tomography with space charge. In *Proc. European Particle Accelerator Conference 2000*, Vienna, Austria, 2000.

[40] H. G. Hereward. Second order effects in beam control systems of particle accelerators. In *Proceedings of the 1961 International Conference on High Energy Accelerators*, pages 235–243, Brookhaven, 1961.

[41] H. G. Hereward. What are the equations for the phase oscillations in a synchrotron? Technical report, CERN, 1966.

[42] H. G. Hereward. Statistical phenomena - theory. Technical report, CERN, 1977.

[43] F. Hinterberger. *Physik der Teilchenbeschleuniger und Ionenoptik*. Springer-Verlag Berlin Heidelberg, 2008.

[44] A. Hofmann. Kinetic theory. Technical report, CAS - CERN Accelerator School: 5th Advanced Accelerator Physics Course, Rhodes, Greece, 20 Sep - 1 Oct 1993, pp. 259-274, 1995.

[45] A. Hofmann and F. Pedersen. Bunches with local elliptic energy distributions. *IEEE Transactions on Nuclear Science*, NS-26(3):3526–3528, 1979.

[46] M.-K. Hu. Visual pattern recognition by moment invariants. *IRE Transactions on Information Theory*, 8(2):179–187, 1962.

[47] T. Hu and Z. Lin. *Control Systems with Actuator Saturation*. Boston: Birkhäuser, 2001.

[48] P. Hülsmann, O. Boine-Frankenheim, H. Klingbeil, and G. Schreiber. Considerations concerning the RF system of the accelerator chain SIS12/18 - SIS100 for the FAIR-project at GSI. Technical report, GSI, 2004.

[49] A. Isidori. *Nonlinear Control Systems*. Springer-Verlag London Limited, 3rd edition, 1995.

[50] J. Johann. *Modulationsverfahren. Grundlagen analoger und digitaler Übertragungssysteme*. Springer-Verlag, 1992.

[51] K. Johnson. Effects of non-linearities on the phase-transition. In *Symposium du CERN sur les Accélérateurs de Haute Energie et la Physique des Mesons*, pages 106–111, Geneva, Switzerland, June 11-23 1956.

[52] T. F. Jordan. Steppingstones in hamiltonian dynamics. *American Journal of Physics*, 72(8): 1095, 2004.

[53] K.-D. Kammeyer and K. Kroschel. *Digitale Signalverarbeitung*. Vieweg+Teubner, 7 edition, 2009.

[54] W. H. Kegel. *Plasmaphysik. Eine Einführung*. Springer-Verlag Berlin Heidelberg, 1998.

[55] H. K. Khalil. *Nonlinear Systems*. Prentice Hall, Upper Saddle River, New Jersey 07458, 3rd edition, 2002.

[56] H. Klingbeil. Private communication.

[57] H. Klingbeil. Lecture: Acceleration of charged particles in electromagnetic fields. Technische Universität Darmstadt, 2009.

[58] H. Klingbeil. *Elektromagnetische Feldtheorie: Ein Lehr- und Übungsbuch*. Vieweg+Teubner, 2nd edition, 2010.

[59] H. Klingbeil, B. Zipfel, M. Kumm, and P. Moritz. A digital beam-phase control system for heavy-ion synchrotrons. *IEEE Transactions on Nuclear Science*, 54(6):2604–2610, December 2007.

[60] H. Klingbeil, D. Lens, M. Mehler, and B. Zipfel. Modeling longitudinal oscillations of bunched beams in synchrotrons. *arXiv:1011.3957v1 [physics.acc-ph]*, 17 Nov. 2010. URL `http://arxiv.org/abs/1011.3957`.

[61] S. Koscielniak. KAON factory PDS design notes: Detailed longitudinal phase-space matching. Technical Report TRI-DN-90-K160, TRIUMF, 26 Feb 1991.

[62] S. R. Koscielniak. The LONG1D simulation code. In *Proc. EPAC 1988, Rome, Italy, June*, volume 1, page 743, 1988.

[63] S. R. Koscielniak. LONG1D user's guide. Technical Report TRI-DN-97-12 v3.2, TRIUMF Vancouver, Canada, 2003.

[64] M. Krasilnikov. Space charge algorithm for the multi ensemble model. In *8th International Computational Accelerator Physics Conference ICAP*, St. Petersburg, Russia, 29 June - 2 Juli 2004.

[65] F. Kuypers. *Klassische Mechanik*. Wiley-VCH, 9th edition edition, 2010.

[66] H. G. Kwatny and G. L. Blankenship. *Nonlinear control and analytical mechanics*. Birkhäuser Boston, 2000.

[67] P. M. Lapostolle. Possible emittance increase through filamentation due to space charge in continuous beams. *IEEE Transactions on Nuclear Science*, NS-18(3):1101–1104, 1971.

[68] T. Lau. *Numerische Methoden zur Simulation teilchengenerierter Felder in der Beschleunigerphysik*. PhD thesis, TU Darmstadt, 2006.

[69] J. D. Lawson, P. M. Lapostolle, and R. L. Gluckstern. Emittance, entropy and information. *Particle Accelerators*, 5:61–65, 1973.

[70] S. Y. Lee. Single-particle dynamics at synchro-betatron coupling resonances. *Physical Review E*, 49:5706–5716, 1994.

[71] S. Y. Lee. *Accelerator Physics*. World Scientific Pub. Co., Singapore, 2004.

[72] D. Lens, H. Klingbeil, and J. Adamy. Analysis of several RF control loops using control theory methods. *GSI Scientific Report*, (FAIR-Accelerators-22):96, 2008.

[73] D. Lens, H. Klingbeil, and P. Hülsmann. Beam loading effects on the RF control loops of a double-harmonic cavity system for FAIR. In *Proceedings of the 2009 Particle Accelerator Conference*, Vancouver, Canada, 2009.

[74] D. Lens, J. Adamy, and H. Klingbeil. Modellierung und Regelung von HF-Systemen in Schwerionensynchrotrons. In *44. Regelungstechnisches Kolloquium*, Boppard, Germany, 2010.

[75] D. Lens, H. Klingbeil, T. Gußner, A. Popescu, and K. Groß. Damping of longitudinal modes in heavy-ion synchrotrons by rf-feedback. In *Proc. 2010 IEEE Multi-Conference on Systems and Control, 8.-10. September 2010*, Yokohama, Japan, 2010.

[76] D. Lens, J. Grieser, and H. Klingbeil. Longitudinal closed-loop beam control in heavy ion synchrotrons: Simulation methods and results. In *Proceedings of the International Conference on Simulation Technology SimTech*, Stuttgart, Germany, 14-17 June 2011.

[77] H. Lens. *Schnelle Regelung mit Ausgangsrückführung für Systeme mit Stellgrößenbeschränkungen*. PhD thesis, TU Darmstadt, 2009.

[78] H. Lens, J. Adamy, and D. Domont-Yankulova. A fast nonlinear control method for linear systems with input saturation. *Automatica*, 47:857–860, 2011.

[79] J. Lévine. *Analysis and control of nonlinear systems. A flatness-based approach*. Springer-Verlag Berlin Heidelberg, 2009.

[80] E. M. Lifschitz and L. P. Pitajewski. *Lehrbuch der Theoretischen Physik - Physikalische Kinetik*. Akademie Verlag, Berlin, 1990.

[81] A. Lindner. *Grundkurs Theoretische Physik*. B. G. Teubner, Stuttgart, 2nd edition, 1997.

[82] J. Löfberg. Yalmip: a toolbox for modeling and optimization in matlab. In *Proceedings 2004 IEEE International Symposium CACSD*, Taipei, September 2004.

[83] J. D. Logan. *An Introduction to Nonlinear Partial Differential Equations*. John Wiley & Sons, Inc., Hoboken, New Jersey, 2nd edition, 2008.

[84] J. Lunze. *Regelungstechnik 2: Mehrgrößensysteme, Digitale Regelung*, volume 3rd edition. Springer-Verlag Berlin Heidelberg, 2005.

[85] J. MacLachlan and J.-F. Ostiguy. Enhancements to the longitudinal dynamics code ESME. In *Proceedings of the 1997 Particle Accelerator Conference*, 1997.

[86] J. A. MacLachlan. Particle tracking in e - ϕ space as a design tool for cyclic accelerators. In *Proc. 1987 IEEE Particle Accelerator Conference*, pages 1087–1089, Washington D.C., 16–19 March 1987.

[87] J. A. MacLachlan. Fundamentals of particle tracking for the longitudinal projection of beam phasespace in synchrotrons. Technical Report FN-481, Fermi National Accelerator Laboratory, 1988.

[88] J. A. MacLachlan. Particle tracking in e-ϕ space for synchrotron design and diagnosis. Technical Report FNAL/C–92/333, Fermi National Accelerator Laboratory, 1992.

[89] J. A. MacLachlan and Z. Nazario. Scaling for faster macroparticle simulation in longitudinal multiparticle dynamics. *Physical Review Special Topics - Accelerators and Beams*, 3:114401, 2000.

[90] H. Mais. Some topics in beam dynamics of storage rings. Technical Report DESY 96–119, Deutsches Elektronen-Synchrotron DESY, Hamburg, June 1996.

[91] J. Marriner. Stochastic cooling overview. *Nuclear Instruments and Methods in Physics Research A*, 532:11–18, 2004.

[92] E. M. McMillan. The synchrotron - a proposed high energy particle accelerator. *Physical Review*, 68:143–145, 1945.

[93] M. Mehler. Longitudinal feedback system for FAIR, EU FP6 design study - final report, 2009.

[94] M. Mehler. Second intermediate report about the induction of sextupole modes. Internal report, GSI, 2010.

[95] M. Mehler, H. Klingbeil, M. Kumm, U. Laier, and K.-P. Ningel. The damping of longitudinal quadrupole oscillations at GSI. In *Proceedings of the 2009 Particle Accelerator Conference*, Vancouver, 2009.

[96] D. Möhl. The status of stochastic cooling. *Nuclear Instruments and Methods in Physics Research A*, 391:164–171, 1997.

[97] D. Möhl and A. M. Sessler. Beam cooling: principles and achievements. *Nuclear Instruments and Methods in Physics Research A*, 532:1–10, 2004.

[98] D. Möhl, G. Petrucci, L. Thorndahl, and S. van der Meer. Physics and technique of stochastic cooling. *Physics Reports*, 58(2):73–102, 1980.

[99] R. R. Mohler. *Bilinear Control Processes: With Applications to Engineering, Ecology, and Medicine*, volume 106 of *Mathematics in Science and Engineering*. Academic Press, 1973.

[100] K. Y. Ng. *Physics of Intensity Dependent Beam Instabilities*. World Scientific Publishing Co., 2006.

[101] H. Nijmeijer and A. van der Schaft. *Nonlinear Dynamical Control Systems*. Springer-Verlag, 1990.

[102] F. Nolden, I. Nesmiyan, and C. Pescke. On stochastic cooling of multi-component fragment beams. *Nuclear Instruments and Methods in Physics Research A*, 564:87–93, 2006.

[103] A. Novokhatski and T. Weiland. The model of ensembles for the beam dynamics simulation. In *Proceedings of the 1999 Particle Accelerator Conference, New York*, 1999.

[104] A. Papachristodoulou and S. Prajna. A tutorial on sum of squares techniques for system analysis. In *Proceedings 2005 IEEE American Control Conference*, Portland, Orgegon, June 2005.

[105] G. Papotti, T. Bohl, T. Linnecar, E. Shaposhnikova, and J. Tückmantel. Study of controlled longitudinal emittance blow-up for high intensity LHC beams in the CERN SPS. In *Proceedings of the 11th European Particle Accelerator Conference*, Genoa, Italy, June 23-27 2008.

[106] A. Papoulis. *Probability, random variables, and stochasic processes*. McGraw-Hill, fourth edition edition, 2002.

[107] F. Pedersen. RF cavity feedback. Technical report, SLAC, 1992.

[108] F. Pedersen. Multibunch instabilities. In M. Dienes, M. Month, and S. Turner, editors, *Frontiers of particle beams: Factories with e^+ e^- Rings (Lecture Notes in Physics)*. Springer, June 1992.

[109] F. Pedersen and F. Sacherer. Theory and performance of the longitudinal active damping system for the CERN PS booster. *IEEE Transactions on Nuclear Science*, 24:1296–1398, 1977.

[110] I. Percival and D. Richards. *Introduction to Dynamics*. Cambridge University Press, 1983.

[111] A. Popescu. Performance und Stabilität von Regelungen zur Dämpfung der longitudinalen Oszillationen in einem Schwerionensynchrotron. Master's thesis, TU Darmstadt, 2009.

[112] W. H. Press, S. A. Teukolsky, W. T. Vetterling, and B. P. Flannery. *Numerical Recipes in C++*. Cambridge University Press, 3rd edition, 2007.

[113] E. C. Raka. Damping bunch shape oscillations in the Brookhaven AGS. *IEEE Transactions on Nuclear Science*, 16(3):182–186, 1969.

[114] F. J. Sacherer. RMS envelope equations with space charge. *IEEE Transactions on Nuclear Science*, 18(3):1105–1107, 1971.

[115] F. J. Sacherer. A longitudinal stability criterion for bunched beams. In *Proceedings of the 1973 Particle Accelerator Conference, San Francisco, CA, March 5-7*, 1973.

[116] F. J. Sacherer. A longitudinal stability criterion for bunched beams. *IEEE Transactions on Nuclear Science*, NS-20:825, 1973.

[117] F. J. Sacherer. Bunch lengthening and microwave instability. *IEEE Transactions on Nuclear Science*, NS-24:1393–1395, 1977.

[118] C. Sakreida. Private communication.

[119] S. S. Sastry. *Nonlinear Systems: Analysis, Stability and Control*. Springer-Verlag New York, 1999.

[120] H. Schwarz. *Einführung in die Systemtheorie nichtlinearer Regelungen*. Shaker, 1999.

[121] R. H. Siemann. Bunched beam diagnostics. In R. G. Lerner, editor, *AIP Conference Proceedings 184, Vol. 1, Physics of Particle Accelerators*, pages 431–524, 1989.

[122] R. Sipahi, S. Niculescu, C. T. Abdallah, W. Michiels, and K. Gu. Stability and stabilization of systems with time delay. *IEEE Control Systems Magazine*, 31(1):38–65, 2011.

[123] J.-J. E. Slotine and W. Li. *Applied nonlinear control*. Prentice Hall, Englewood Cliffs, New Jersey 07632, 1991.

[124] E. D. Sontag. *Mathematical Control Theory: Deterministic Finite Dimensional Systems*. Textbooks in Applied Mathematics, Number 6. Springer-Verlag New York, 2nd edition, 1998.

[125] A. H. Sorensen. Liouville's theorem and emittance. In *In: CAS - CERN Accelerator School, third general accelerator physics course, Salamanca, Spain*, Sep. 19-30 1988.

[126] A. Sorenssen. Crossing the phase transition in strong-focusing proton synchrotrons. *Particle Accelerators*, 6:141–165, 1975.

[127] K. C. Toh, M. J. Todd, and R. H .Tütüncü. SDPT3–a MATLAB software package for semidefinite programming. *Optimization Methods and Software*, 11:545–581, 1999.

[128] U. Topcu, A. Packard, P. Seiler, and G. Balas. Help on SOS. *IEEE Control Systems Magazine*, 30(4):18–23, 2010.

[129] S. van der Meer. Stochastic cooling and the accumulation of antiprotons. *Review Modern Physics*, 57:689–697, 1985.

[130] S. van der Meer. An introduction to stochastic cooling. In *AIP Conference Proceedings*, volume 153, pages 1628–49, 1987.

[131] V. I. Veksler. *Proc. USSR Acad. Sci.*, 43:346, 1944.

[132] V. I. Veksler. A new method of acceleration of relativistic particles. *Journal of Physics UdSSR*, 9:153–158, 1945.

[133] K. Walton and J. E. Marshall. Direct method for TDS stability analysis. *IEE Proceedings*, 134, Pt. D(2):101–107, March 1987.

[134] M. Weiss. A short demonstration of Liouville's theorem. In *In: CAS - CERN Accelerator School: Accelerator Physics*, pages 162–163, Aarhus, Denmark, September 15-26 1986.

[135] E. W. Weisstein. Elliptic integral of the second kind. From MathWorld–A Wolfram Web Resource. http://mathworld.wolfram.com/EllipticIntegraloftheSecondKind.html, August 2010.

[136] H. Wiedemann. *Particle Accelerator Physics*. Springer, 2007.

[137] K. Wille. *Physik der Teilchenbeschleuniger und Synchrotronstrahlungsquellen*. B.G. Teubner, Stuttgart, 1992.

[138] Wolfram Research, Inc. *Mathematica Edition: Version 8.0*. Wolfram Research, Inc., Champaign, Illinois, 2010.

[139] B. Zotter. *Handbook of Accelerator Physics and Engineering*, chapter Vlasov and Fokker-Planck Equations, pages 131–132. World Scientific, Singapore, 1998.